CERAMICS DIVISION

MATERIALS SCIENCE AND ENGINEERING

University of Illinois

Urbana, Illinois

REPORT DOCUMENTATION PAGE

Form Approved
OMB No. 0704-0188

1. AGENCY USE ONLY (Leave blank)	2. REPORT DATE	3. REPORT TYPE AND DATES COVERED
		Final report for 3/01/89 - 12/31/92

4. TITLE AND SUBTITLE
"Transformation Toughening of Composite Ceramics"

5. FUNDING NUMBERS
G AFOSR-89-0300
61102F
2303/BS

6. AUTHOR(S)
Professor Waltraud M. Kriven

7. PERFORMING ORGANIZATION NAME(S) AND ADDRESS(ES)
Department of Materials Science and Engineering
University of Illinois at Urbana-Champaign
105 South Goodwin Avenue
Urbana, IL 61801

8. PERFORMING ORGANIZATION REPORT NUMBER
UILU-ENG-93-5100

9. SPONSORING/MONITORING AGENCY NAME(S) AND ADDRESS(ES)
Air Force Office of Scientific Research
Dr. Alexander Pechenik
Chemistry and Materials Science Directorate
AFOSR/NC, 110 Duncan Ave., Suite B 115
Bolling AFB, Washington, D.C. 20332-0001

10. SPONSORING/MONITORING AGENCY REPORT NUMBER
AFOSR-89-0300

11. SUPPLEMENTARY NOTES

12a. DISTRIBUTION/AVAILABILITY STATEMENT
Publically available
Approved for public release;
distribution unlimited.

12b. DISTRIBUTION CODE

13. ABSTRACT (Maximum 200 words)

A systematic investigation into some possible transformation tougheners alternative to zirconia (ZrO_2) has been conducted. Three systems have been focussed upon: dicalcium silicate (Ca_2SiO_4), dysprosia (Dy_2O_3) and nickel sulfide (NiS). Composites of Ca_2SiO_4 in calcium zirconate ($CaZrO_3$) or magnesia (MgO) or fine grained, single phase pure, and Ba-doped Ca_2SiO_4 were fabricated, microstructurally characterized and mechanically evaluated. Although surface grinding was able to stress-induce the transformation in Ca_2SiO_4, a crack tip propagating in the bulk was not. A comprehensive crystallographic study of the transformation mechanisms implied that compressive shear, rather than tensile stresses were required. The mechanism could not controllably be nucleated by a propagating crack. Spontaneous thermal transformation of Ca_2SiO_4 was too powerful for a confining matrix and tended to cause dusting. The kinetics and mechanism of the transformation in single phase Dy_2O_3 were studied and revealed that it only operated above 600°C. No transformation toughening in HIPPED SiC-Dy_2O_3 composites could be detected at room temperature. Microstructural studies of industrial NiS in glass composites found a correlation between transfomed NiS and deleterious fracture.

14. SUBJECT TERMS	15. NUMBER OF PAGES
Ceramic composites, transformation otughening, zirconia (ZrO_2), dicalcium silicate (Ca_2SiO_4), dysprosia (Dy_2O_3) nickel sulfide (NiS), processing, microstructure, mechanical properties.	350
	16. PRICE CODE

17. SECURITY CLASSIFICATION OF REPORT	18. SECURITY CLASSIFICATION OF THIS PAGE	19. SECURITY CLASSIFICATION OF ABSTRACT	20. LIMITATION OF ABSTRACT
Unclassified	Unclassified	Unclassified	UL

Report AFOSR - 89 - 0300

TRANSFORMATION TOUGHENING OF COMPOSITE CERAMICS

Professor Waltraud M. Kriven
Department of Materials Science and Engineering,
University of Illinois at Urbana-Champaign,
105 South Goodwin Ave.,
Urbana, IL 61801

July 7th 1993
Final Report for the Period March 1st 1989 to Sep 30th 1992, with a no-cost extension until Dec 31st 1992.

Prepared for: Air Force Office of Scientific Research,
Dr. Alexander Pechenik
Chemistry and Materials Science Directorate,
AFOSR/NC,
110 Duncan Ave., Suite B115,
Bolling Air Force Base,
Washington DC 20332-6600.

(a) OBJECTIVES OF RESEARCH EFFORT

Several new potential transformation tougheners to zirconia have been identified on the basis of crystallographic considerations and experimental observations. Examples can be found in ceramic, minerals, and components of glass and cement. The displacive transformations exhibit martensitic characteristics of dusting or self-disintegration, and a critical particle size effect operates. Table I summarizes the current list of known first order displacive transformations in ceramics. It is seen that most of the compounds have the non-perovskite structure and have large volume and/or unit cell shape changes which could have a profound effect on the mechanical properties of composites. The objectives of this research program were to examine, in a systematic way, the relative effects of volume change, X-ray unit cell shape change and the (martensitic) macroscopic shape chage of the mechanical properties of a composite ceramic system. This understanding should guide the design and fabrication of tough, structural ceramic composites.

(b) SUMMARY OF RESEARCH EFFORT

A systematic investigation into some possible transformation tougheners alternative to zirconia (ZrO_2) has been conducted. Three systems have been focussed upon: dicalcium silicate (Ca_2SiO_4), dysprosia (Dy_2O_3) and nickel sulfide (NiS). Compared to ZrO_2 whose martensitic transformation at 950°C is accompanied by a 4.9% volume increase (ΔV) at room temperature and a 9° unit cell shape change ($\Delta\beta$), Ca_2SiO_4 has a ΔV of +12% with $\Delta\beta$ of 4.6° at 490°C; Dy_2O_3 has a ΔV of 8% at 1850°C with $\Delta\beta$ of 10°; and NiS has a ΔV of 4% at 372°C. Composites of Ca_2SiO_4 in calcium zirconate ($CaZrO_3$) or magnesia (MgO) or fine grained, single phase pure and Ba-doped Ca_2SiO_4 were fabricated. The copmposites made were microstructurally characterized (by XRD, SEM, EM, EDS, HREM and HVEM) and mechanically evaluated in terms of toughness, strength and transformability.

Although surface grinding was able to stress-induce the monoclinic to orthorhombic transformation in Ca_2SiO_4, a crack tip propagating in the bulk was not. A comprehensive crystallographic study of the transformation mechanism in the context of the whole sequence of five transformations was done in a companion AFOSR URI program, and revealed the nature of the crystal structural stabilizing forces controlling the transformation. They implied that compressive shear, stress rather than tensile stresses were required, and it was

Table 1. Examples of First Order Displacive Transformations in Ceramics

Compound	Crystal Symmetries	Transformation Temperature (T_o on cooling)	Volume Change (ΔV)	Unit Cell Shape Change(°)
ZrO_2	tetragonal→ monoclinic	950	(+)4.9% (R.T.)	9
Ln_2O_3 (type)	monoclinic→ cubic	600–2200	(+)10%	10
Ca_2SiO_4 (K_2SO_4-type)	monoclinic→ orthorhombic	490	(+)12%	4.6
Sr_2SiO_4 (K_2SO_4-type)	orthorhombic→ monoclinic	90	0.2%	2
NiS	rhombohedral →hexagonal	379	(+)4%	—
$2Tb_2O_3.Al_2O_3$ (type)	orthorhombic→ monoclinic	1070	(+)0.67%	18.83
$PbTiO_3$	cubic→ tetragonal	445	(+)1%	0
$KNbO_3$	tetragonal→ orthorhombic	225	~0%	0
$LuBO_3$	hexagonal→ rhombohedral	1310	(+)8%	—
$MgSiO_3$ ($CaSiO_3$-type) ($FeSiO_3$-type)	orthorhombic → monoclinic	865	(-)5.5%	18.3
$YNbO_4$ ($LnNbO_4$-type)	tetragonal → monoclinic	900	(-) 1.8%	4.53
$LnBO_3$ (type)	hexagonal→ hexagonal	550–800	(-)8.2%	—

observed that the mechanism could not controllably be nucleated by a propagating crack. Spontaneous thermal transformation of Ca_2SiO_4 was too powerful for a confining matrix and caused dusting of specimens.

The kinetics and mechanisms of the monoclinic to cubic transformation in single phase Dy_2O_3 were studied and revealed that the transformation may operate, but only above 600°C. Room temperature measurements of strength and toughness of hot pressed and HIPPED Dy_2O_3 - SiC composites indicated that a 40% increase in toughening could be achieved, but by a crack deflection and crack bridging mechanism, rather than by transformation toughening. No high temperature toughening mechanisms have as yet been done in this system. Further work needs to be done to ascertain the value of the high atomic number lanthanide sesquioxides as high temperature transformation tougheners.

NiS-glass composites could not be fabricated with a sufficient NiS grain size. However, industrial composites were obtained and investigated. TEM /SEM and EDS analyses allowed the identification of untransformed NiS in unfractured glass and transformed NiS in fractured glass. This observation was consistent with the hypothesis that the transformation in NiS played a role in initiating fracture in tempered glass-containing nickel sulfide stones. Bulk processing of NiS in other sulfide matrices such as ZnS was found to be too difficult, since it involved control of sulfur partial pressures.

(c) PUBLICATIONS IN REFERREED JOURNALS

(In chronological order)

- "Preparation and Hydration Kinetics of Pure $CaAl_2O_4$," M. A. Gulgun, I. Nettleship, O. O. Popoola, W. M. Kriven and J. F. Young. In Advanced Cementitious Systems: Mechanisms and Properties, edited by F. P. Glasser, P. L. Pratt, T. O. Mason, J. F. Young and G. J. McCarthy. Mater. Res. Soc. Symp. Proc. **245**, 199-204, 1992.

- "Chemical Preparation and Phase Stability of Ca_2SiO_4 and Sr_2SiO_4 Powders," I. Nettleship, J. L. Shull Jr. and W. M. Kriven, J. European Ceramic Society, **11** 291-298 (1993).

- "Phase Transformations in Dicalcium Silicate. I: Fabrication and Phase Stability," I. Nettleship, K. G. Slavick, Y. J. Kim and W. M. Kriven, J. Am Ceram. Soc., **75** [9] pp 1-7 (1992).

- "Phase Transformations in Dicalcium Silicate. II: TEM Studies of Crystallography, Microstructures and Mechanisms," Y. J. Kim, I. Nettleship and W. M. Kriven, J. Am Ceram. Soc., **75** [9] pp 1-13 (1992).

- "Phase Transformations in Dicalcium Silicate. III: Effects of Barium on the Stability of Fine-grained α'_L and β," I. Nettleship, K. G. Slavick, Y. J. Kim and W. M. Kriven, J. Am Ceram. Soc., accepted.

- "Kinetics and Crystallography of the Monoclinic (B) to Cubic (C) Transformation in Dysprosia," O. Sudre, K. R. Venkatachari and W. M. Kriven. Proc. Vth Int'l Conf. on the Science and Technology of Zirconia. Technomic Publishing Company, in press (1993).

- "Preparation, Microstructure and Properties of Silicon Carbide - Dysprosia Composites," S. Kim and W. M. Kriven, J. Am. Ceram. Soc., in preparation.

- "Mechanical Properties and Microstructures of $CaZrO_3$-Ca_2SiO_4 Composites,"
T. I. Hou and W. M. Kriven, J. Am. Ceram. Soc., accepted.

- "The Monoclinic (B) to Cubic (C) Phase Transformation of Dysprosia (Dy_2O_3), Part I: Experimental Studies," O. Sudre, K. R. Venkatachari and W. M. Kriven, in preparation.

PUBLICATIONS IN UNREFEREED CONFERENCE PROCEEDINGS

- "Microstructural Characterization of Ca_2SiO_4 Particles in a $CaZrO_3$ and a MgO Matrix," Y.J. Kim, E.S. Mast, T.I. Hou, and W. M. Kriven. Electron Microscopy 1990, vol 4, pp 1050-1051. Proc.12th Int. Congr. for Electron Microscopy, Washington, Seattle, (1990). San Fransisco Press publishers.

- "TEM Characterization of a Modulated β Phase in Polycrystalline Dicalcium Silicate," Y.J. Kim, I. Nettleship and W.M. Kriven. Proc. 49th Annual Meeting of the Electron Microscopy Society of America (EMSA), San Jose, California (1991). G.W. Bailey editor, San Fransisco Press, pp 946-947.

- "Microstructural and Microchemical Characterization of Nickel Sulfide Inclusions in Plate Glass," J.J. Cooper, O.O. Popoola and W.M. Kriven. Proc. 49th Annual Meeting of the Electron Microscopy Society of America (EMSA), San Jose, California (1991). G.W. Bailey editor, San Fransisco Press, pp 962-963.

- "Effect of Dysprosia Dispersions on the Properties of Silicon Carbide Composites," S. Kim and W. M. Kriven. Proc. First Inter. Symp. on Science of Engineering Ceramics '91. Symposium held in Koda, Japan, Oct. 21-23 (1991). Edited by S. Kimura and K. Niihara, The Ceramic Society of Japan, Tokyo, (1991), pp 63-68.

- "TEM Characterization of the α′and β Phases in Polycrystalline Distrontium Silicate (Sr_2SiO_4)," Y. J. Kim, J. L. Shull and W. M. Kriven. Proc. 50th Annual Meeting of the Electron Microscopy Society of America (EMSA). Edited by G. W. Bailey, J. Bentley and J. A. Small, pp 354-355 (1992).

- "Characterisation of Nickel Sulphide Stones in Glass," J. J. Cooper, O. O. Popoola and W. M. Kriven. Proceedings of Austceram '92, International Ceramics Conference and Exhibition, held in Australia, August 16-24th 1992.Published by CSIRO, Melbourne, Australia.Vol 1, pp 186-191, (1992).

- "Microstructural Investigation of Fracture-Initiating Nickel Sulfide Inclusions in Glass," O. O. Popoola, J. J. Cooper and W. M. Kriven. Ceramic Science and Engineering Proceedings, **14** [3-4] 284-294 (1993).

(d) GRADUATE THESES SUBMITTED

"Control of β-Dicalcium Silicate Particle Size for Dispersion in a Magnesia Matrix" by Eric Sidney Mast.
M.S. thesis submitted December 1990.

"Preparation, Microstructure and Properties of Silicon Carbide - Dysprosia Composites" by Shin Kim.
Ph.D. thesis submitted June 1991.

"Preparation, Properties and Microstructures of Dicalcium Silicate-Calcium Zirconate Composites" by Tien -I Hou.
Ph.D. thesis submitted July 1991.

"Investigation of Nickel Sulfide (NiS) as a Possible Transformation Toughener,"
by Jemima Jane Cooper
M. S. thesis submitted June 1992.

"Mechanical Properties and Phase Stability of Dicalcium Silicates,"
by Kurt Gordon Slavick
M. S. thesis submitted August 1992.

UNDERGRADUATE THESES SUBMITTED

"Eutectic Sintering for Formation of Dicalcium Silicate in Magnesia"
Raymond Pilapil.
Senior Thesis submitted May 1991

"Doping, Phase Stability and Formation of Dicalcium Silicate,"
Kyle E. Eckman
Senior Thesis submitted August 1991

"Preparation of Dibarium Silicate Powders,"
Richard Russel
Senior Thesis submitted May 1992

POST DOCTORAL RESEARCH ASSOCIATES

Dr. Ian Nettleship, now an Assistant Professor in the Department of Materials Science and Engineering at the University of Pittsburgh, PA.

(e) INTERACTIONS CONFERENCE PRESENTATIONS

- "Processing and phase transformation of dysprosia in silicon carbide matrix," S. Kim* and W. M. Kriven. Abstract #[18-SI-89]. Presented at the 91st Annual Meeting of the American Ceramic Society, Indianapolis, April 23-27, 1989.

- "High temperature stability of mullite-cordierite composites in air," Tien-I Hou* and W. M. Kriven. Abstract #[8-SIP-89]. Presented at the 91st Annual Meeting of the American Ceramic Society, Indianapolis, April 23-27, 1989.

- "Sintering and microstructural development of dicalcium silicate in magnesia," E. S. Mast* and W. M. Kriven. Abstract #[7-SI-89]. Presented at the 91st Annual Meeting of the American Ceramic Society, Indianapolis, April 23-27, 1989.

- "Eutectic sintering for formation of dicalcium silicate in magnesia," E. S. Mast*, R. Pilapil and W. M. Kriven. Abstract #[43-BP-89]. Presented at the 91st Annual Meeting of the American Ceramic Society, Indianapolis, April 23-27, 1989.

- "Martensitic Transformations in Ceramics," W. M. Kriven.* Presented at the International Conference on Martensitic Transformations (ICOMAT-89), Sydney, Australia, July 3-7, (1989).

- "Investigations of the monoclinic (B) to cubic (C) transformation in the lanthanide sesquioxides," W. M. Kriven*, P. D. Jero, O. Sudre, and K. R. Venkatachari. Presented at the International Conference on Martensitic Transformations (ICOMAT89), Sydney, Australia, July 3-7, (1989).

- "Martensitic nucleation and transformation in $\beta \rightarrow \gamma$ dicalcium silicate," W. M. Kriven*, C. J. Chan and E. A. Barinek. Presented at the International Conference on Martensitic Transformations (ICOMAT-89), Sydney, Australia, July 3-7, (1989).

- "Preparation and Microstructure of Dispersed Dysprosia in Silicon Carbide Matrix," S. Kim* and W.M. Kriven,Abstract # [72-SIV-90]. Presented at the Annual Meeting of the American Ceramic Society, Dallas, Texas, April 22nd -26th 1990.

- "The Development of Dicalcium Silicate as a Transformation Toughener," W.M. Kriven* and E.A. Barinek, Abstract # [7-SVI-90]. Presented at the Annual Meeting of the American Ceramic Society, Dallas, Texas, April 22nd -26th 1990.

- "Processing and Mechanical Evaluation of Ca_2SiO_4-Transformation Toughened $CaZrO_3$ Composites," T.I. Hou * and W.M. Kriven, Abstract # [8-SVI-90]. Presented at the Annual Meeting of the American Ceramic Society, Dallas, Texas, April 22nd -26th 1990.

- "Retention of β Dicalcium-Silicate in a Magnesia Matrix," E.S. Mast*, I. Nettleship and W.M. Kriven, Abstract # [9-SVI-90]. Presented at the Annual Meeting of the American Ceramic Society, Dallas, Texas, April 22nd -26th 1990.

- "Microstructural Characterization of Ca_2SiO_4 Particles in a $CaZrO_3$ and an MgO Matrix," Y.J. Kim*, E.S. Mast, T.I. Hou, and W. M. Kriven. Presented at the Proc.12th Int. Congr. for Electron Microscopy, Washington, Seattle, Aug, (1990).

- "Mechanical Properties of β Dicalcium Silicate Polycrystals," K.G. Slavick*, I. Nettleship and W.M. Kriven.Presented at 93rd Annual Meeting of the

American Ceramic Society, held in Cincinnati, OH, April 28th-May 2nd 1991.

- "Mechanical Properties and Microstructures of $CaZrO_3$-Ca_2SiO_4 Composites," T. I Hou* and W.M. Kriven. Presented at 93rd Annual Meeting of the American Ceramic Society, to be held in Cincinnati, OH, April 28th-May 2nd 1991.

- "Preparation and Metastability of β Dicalium Silicate Polycrystals," I. Nettleship*, Y.J. Kim and W.M. Kriven. Presented at 93rd Annual Meeting of the American Ceramic Society, held in Cincinnati, OH, April 28th-May 2nd 1991.

- "Crystallography and Microstructure of Polycrystalline α'_L in β-Ca_2SiO_4," Y.J. Kim,* I. Nettleship and W.M. Kriven. Presented at 93rd Annual Meeting of the American Ceramic Society, held in Cincinnati, OH, April 28th-May 2nd 1991.

- "Microstructure and Microchemistry of Nickel Sulfide Inclusions in Plate Glass," J.J. Coooper*, O.O. Popoola and W.M. Kriven. Presented at 93rd Annual Meeting of the American Ceramic Society, held in Cincinnati, OH, April 28th-May 2nd 1991.

- "Microstructure and Properties of Silicon Carbide-Dysprosia Composites," S. Kim and W.M. Kriven*. Presented at 93rd Annual Meeting of the American Ceramic Society, held in Cincinnati, OH, April 28th-May 2nd 1991.

- "Preparation of Calcium Aluminate Powders Using a Sol-Gel Method," M.A. Gulgun*, O.O. Popoola, I. Nettleship and W.M. Kriven. Presented at 93rd Annual Meeting of the American Ceramic Society, held in Cincinnati, OH, April 28th-May 2nd 1991.

- "Microstructural and Microchemical Characterization of Nickel Sulfide Inclusions in Plate Glass," J.J. Cooper*, O.O. Popoola and W.M. Kriven.Presented at 49th Annual Meeting of the Electron Microscopy Society of America (EMSA), San Jose, California (1991).

- "Effect of Dysprosia Dispersions on the Properties of Silicon Carbide Composites," S. Kim* and W. M. Kriven. Proc. First Inter. Symp. on Science of Engineering Ceramics '91, pp 63-68 (1991). Symposium held in Koda, Aichi-Prefecture, Japan, Oct. 21-23 (1991).

- "Toughening Mechanisms in Non-Zirconia Composites," W. M. Kriven*. Invited Lecture, abstract # [42-C-92]. Presented at the Annual Meeting of the American Ceramic Society, April 12-16th, 1992 in Minneapolis, MN.

- "Stress-induced Phase Transformations in Polycrystalline Dicalcium Silicate," K. G. Slavick,* I. Nettleship and W. M. Kriven. Abstract # [43-C-92] presented at the Annual Meeting of the American Ceramic Society, April 12-16th, 1992 in Minneapolis, MN.

- Silicate," K. G. Slavick, I. Nettleship and W. M. Kriven. Abstract # [23-BP-92]. Presented at the Annual Meeting of the American Ceramic Society, April 12-16th, 1992 in Minneapolis, MN.

- "Microstructure and Phase Transformations of Nickel Sulfide Inclusions in Plate Glass," J. J. Cooper, O. O. Popoola and W. M. Kriven. Abstract # [27-BP-92].Presented at the Annual Meeting of the American Ceramic Society, April 12-16th, 1992 in Minneapolis, MN.

- "Characterisation of Nickel Sulphide Stones in Glass," J. J. Cooper, O. O. Popoola and W. M. Kriven. Presented at Austceram '92, International Ceramics Conference and Exhibition held in Australia, August 16-21st, 1992.

- Transformation in Dysprosia," O. Sudre, K. R. Venkatachari and W. M. Kriven. Presented at the Vth International Conference on the Science and Technology of Zirconia, held in Melbourne, August 16th-21st, 1992.

- "Phase Transformations and Fracture Associated with Nickel Sulfide Stones in Glass," W. M. Kriven*, J. J. Cooper and O. O. Popoola. Presented at 53rd Annual Conference on glass Problems, Nov 17-18th 1992, Ohio State University.

- "Transformation Mechanisms and Induced Fracture in Ceramics," W. M. Kriven*. Presented at the Materials Research Society, Spring Meeting, held in San Fransisco, California in April 16-18th 1993.

- "Transformation -Induced Fracture in Ceramic Composites," W. M. Kriven*. Invited talk, presented at the Annual Meeting of the American Ceramic Society, held in Cincinnati in April 18-22, 1993.

- "Synthesis of Silicate and Aluminate Powders by a Modified Pechini Process," M. A. Gulgun, C. M. Huang, D. H. Kuo, J. L. Shull*, K. G. Slavick, T. K Swanson,W. M. Kriven, I. Nettleship and R. Russel. Presented at the Annual Meeting of the American Ceramic Society, held in Cincinnati in April 18-22nd, 1993.

INVITED TALKS

- "SEM and TEM in Materials Science," W.M. Kriven. Invited lecture, American Chemical Society Annual Meeting, Tutorial Sessions in Materials Science, New York, NY, Aug 25th 1991.

- "On Phase Transformation Mechanisms in Dicalcium Silicate (Ca_2SiO_4)," Y.J. Kim and W. M. Kriven*. Invited lecture presented at the Fall meeting of the American Geolophysical Union held in San Fransisco, California, Dec 9-13th 1991.

- "Phase Transformations and Toughening Mechanisms in Composite Ceramics," W. M. Kriven. Invited lecture presented at the Materials Science and Engineering Departmental Colloquium, University of Illinois at Urbana-Champaign, on February 10th 1992.

- "Phase Transformations and Toughening Mechanisms in Composite Ceramics," W. M. Kriven. Invited lecture presented at the Materials Science and Engineering Departmental Seminar, Massachussetts Institute of Technology (MIT), on February 18th 1992.

- "Toughening Mechanisms in Non-Zirconia Composites," W. M. Kriven. Invited lecture presented at the Annual Meeting of the American Ceramic Society, April 12-16th, 1992 in Minneapolis, MN.

- "Phase Transformations and Toughening Mechanisms in Composite Ceramics," W. M. Kriven. Invited lecture presented at the Materials Science and Engineering Departmental Seminar, Illinois Institute of Technology (IIT), on April 30th 1992.

- "Transformation Mechanisms in Dicalcium Silicate and Distrontium Orthosilicates," Y. J. Kim, J.L. Shull, B. N. Sun and W. M. Kriven*. Presented at the International Conference on Martensitic Transformations (ICOMAT '92). Held in Monterey, CA, July 20-24th 1992.

- "Electron Microscopy Observations of Micromechanical Behavior in Ceramic Composites," W. M. Kriven. Invited seminar presented in the Materials Science and Engineering Laboratory, National Institute of Science and Technology (NIST), Gaithesburg, MD., per Dr. S. M. Wiederhorn. Held on Oct 29th 1992.

- "Phase Transformations in Ceramics," W. M. Kriven*. Invited talk, presented at the Microscopy Society of America (MSA) Annual Meeting, held in Cincinnati in Aug 1-6, 1993.

- "Twinning in Structural Ceramics," W. M. Kriven.* Invited talk to be presented at TMS Fall Meeting in Symposium on Twinning in Advanced Materials. To be held in Pittsburgh, PA, Oct 17-21, 1993.

- "Volume Changes During Transformation in Ceramics," W. M. Kriven.* Invited talk to be presented at TMS Fall Meeting in Symposium on Effect of Plastic Deformation on the Thermodynamics, Kinetics and Mechanisms of Phase Transformations,". To be held in Pittsburgh, PA, Oct 17-21, 1993.

- "Martensitic Transformations in Ceramics," W. M. Kriven.* Invited paper, to be presented at International Conference on Solid to Solid Phase Transformations in Inorganic Materials '94. to be held in Pittsburgh in July 17-22, 1994.

Journal of the European Ceramic Society **11** (1993) 291–298

Chemical Preparation and Phase Stability of Ca_2SiO_4 and Sr_2SiO_4 Powders

Ian Nettleship,* James L. Shull, Jr. & Waltraud M. Kriven

Department of Materials Science and Engineering, University of Illinois at Urbana-Champaign, Urbana, Illinois 61801, USA

(Received 29 January 1992; revised version received 23 June 1992; accepted 10 July 1992)

Abstract

A process has been developed to produce high surface area Ca_2SiO_4 and Sr_2SiO_4 powders using colloidal silica for the silicon precursor. This method was relatively straightforward and avoided the use of precipitation techniques and unstable alkoxides. Calcium carbonate and strontium carbonate were identified as intermediate compounds, and the silicates appeared to form by a low-temperature solid-state reaction. The effect of resin content and calcination conditions on the phase distribution and physical properties of the powders was examined. Finally, the sodium content of the colloidal silica was found to have a significant effect on the phase stability of β-Ca_2SiO_4 after calcination at 1400°C.

Es wurde ein Verfahren zur Herstellung von Ca_2SiO_4- und Sr_2SiO_4-Pulvern mit großer freier Oberfläche entwickelt. Als Silizium-haltiger Prekursor wurde Siliziumdioxid verwendet. Diese verhältnismäßig direkte Methode erspart die Anwendung von Ausscheidungstechniken und nicht stabiler Alkoxide. Kalziumkarbonat und Strontiumkarbonat konnten als intermediäre Verbindungen identifiziert werden. Die entsprechenden Silikate scheinen sich durch eine Festphasenreaktion bei tiefen Temperaturen zu bilden. Die Auswirkungen des Anteils an Binderharz und der Kalzinierungsbedingungen auf die Phasenverteilung und die physikalischen Eigenschaften der Pulver wurden genauer untersucht. Schließlich konnte gezeigt werden, daß der Natrium-Gehalt des kolloiden Siliziumdioxids einen beträchtlichen Einfluß auf die Stabilität der β-Ca_2SiO_4-Phase nach der Kalzinierung bei 1400°C ausübt.

Un procédé a été développé pour synthétiser des poudres de Ca_2SiO_4 et Sr_2SiO_4 présentant une surface spécifique élevée, avec de la silice colloïdale comme précurseur du silicium. Cette méthode est relativement directe et évite les techniques de précipitation et l'usage d'alcoolates instables. Les carbonates de calcium et de strontium ont été détectés en tant que composés transitoires et les silicates paraissent se former par réaction à l'état solide à basse température. Les auteurs rapportent l'influence de la teneur en résine et des conditions de calcination sur la distribution de phase et les propriétés physiques des poudres. Les résultats démontrent, enfin, que la stabilité de la phase β-Ca_2SiO_4 après calcination à 1400°C est influencée de façon significative par la teneur en sodium de la silice colloïdale.

1 Introduction

The polymorphism of dicalcium silicate (Ca_2SiO_4) has been well studied[1,2] because of the considerable importance of this compound in the cement and refractories industries. The currently accepted sequence of phase transformations is illustrated in Fig. 1. In most cases work on the material has been directed at avoiding the disruptive 12 vol.% expansion associated with the $\beta \rightarrow \gamma$ transformation, commonly referred to as 'dusting'. The α'_L- and β-phases are also important hydraulic phases in Portland cement, but the γ-phase is undesirable because it does not hydrate.

Dicalcium silicate powders have usually been fabricated by a high-temperature solid-state reaction between CaO and SiO_2. The kinetics of this reaction are slow, and temperatures of 1450°C and above are commonly used to drive the reaction to completion. The resulting powder is predominantly γ-phase after cooling to room temperature. Retention of the high-temperature polymorphs is achieved by the addition of stabilizing additives or impurities.[3]

The β-phase of Ca_2SiO_4 can also be retained after

* Present address: Department of Materials Science and Engineering, University of Pittsburgh, Pittsburgh, Pennsylvania 15261, USA.

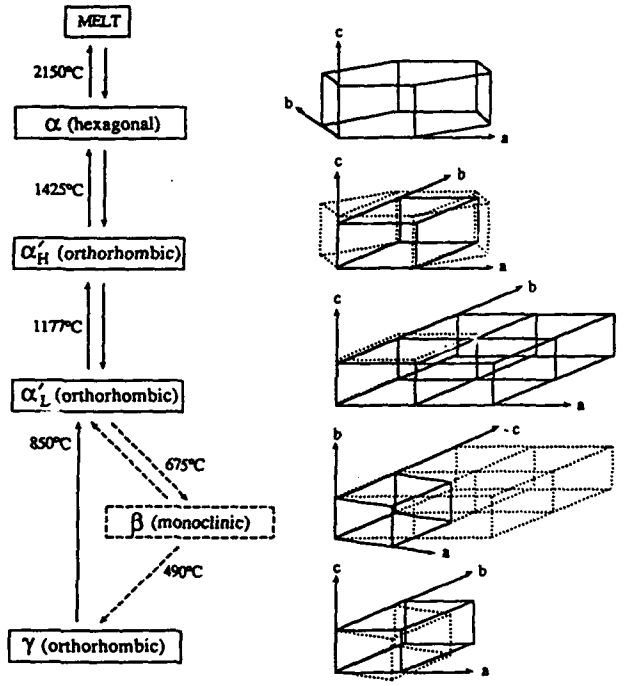

Fig. 1. The polymorphism of Ca_2SiO_4.

low-temperature heat treatment of γ-powders,[4] or by chemical preparation.[5] Both studies have linked the retention of the β-phase to a particle size effect on the $\beta \rightarrow \gamma$ transformation.

The chemical preparation route[5] involved either spray reacting or direct gelling of colloidal silica in the presence of $Ca(NO_3)_2$. This was an extension of the method used for the preparation of other silicates, as reviewed by Luth & Ingamells.[6] These chemical methods allowed preparation of β-Ca_2SiO_4 powders at temperatures as low as 750°C.[5] Powders of β-Ca_2SiO_4 have also been prepared by solid-state reaction of CaC_2O_4 and amorphous SiO_2 at 950°C in a CO_2 atmosphere.[7] The advantage of the latter method is that no corrosive salts, which produce acidic fumes on calcination, are used in the powder production. All the low-temperature methods already mentioned produced powders with higher surface areas than those produced by high-temperature calcination. Another advantage of the low-temperature routes is that the β-phase is retained and hence the powders are reactive in terms of their hydration behavior. Unfortunately, the nature of the chemical reactions that formed Ca_2SiO_4 has not been studied in detail and the physical properties, including the particle size, have not been fully reported, even though they are important to the hydration behavior.

Dicalcium silicate has recently been considered as a candidate for a possible alternative transformation toughener to zirconia.[8] This was based on the large volume change (12 vol.%) associated with the $\beta \rightarrow \gamma$ transformation. The desire to fabricate dense, polycrystalline Ca_2SiO_4 in order to study the transformation has also stimulated research into the preparation of high surface area Ca_2SiO_4 powders.

In comparison, Sr_2SiO_4 has been less well studied. The $\alpha' \rightarrow \beta$ transformation in this compound is structurally analogous to the $\alpha'_L \rightarrow \beta$ transformation in Ca_2SiO_4, but the transformation occurs at 90°C compared to 675°C for pure Ca_2SiO_4. This makes it easier to study the ferroelastic $\alpha' \rightarrow \beta$ type transformation in Sr_2SiO_4.[9,10] Consequently, fine Sr_2SiO_4 powders are required to process dense polycrystalline Sr_2SiO_4.

In this study a quick and comparatively easy method is reported for the chemical preparation of Ca_2SiO_4 and Sr_2SiO_4 powders. The method has previously been used to prepare Ca_2SiO_4 powders for incorporation into a calcium zirconate ($CaZrO_3$) matrix.[11] It involves a 'Pechini-type' process in which one of the constituents is colloidal. The effect of resin content and calcination conditions on the physical properties of the powder and the phase distribution are presented. The effect of the sodium content of the colloidal silica on the phase distribution of the Ca_2SiO_4 is also studied.

2 Experimental Procedures

A flow diagram detailing the preparation method is shown in Fig. 2. The resin content of the resulting gel is defined as follows:

$$\% \text{ resin content} = 100\, W_{resin}/(W_{oxide} + W_{resin})$$

where W_{oxide} is the weight of the oxide after calcination, calculated from the known weights of the precursors, and W_{resin} is the weight of resin added. In all cases the resin was composed of 60 wt% citric acid monohydrate and 40 wt% ethylene glycol.

Firstly, the calcium and strontium precursors, which were $Ca(NO_3)_2 \cdot 4H_2O$ and $Sr(NO_3)_2$ respectively, were assayed and stored in desiccators. The

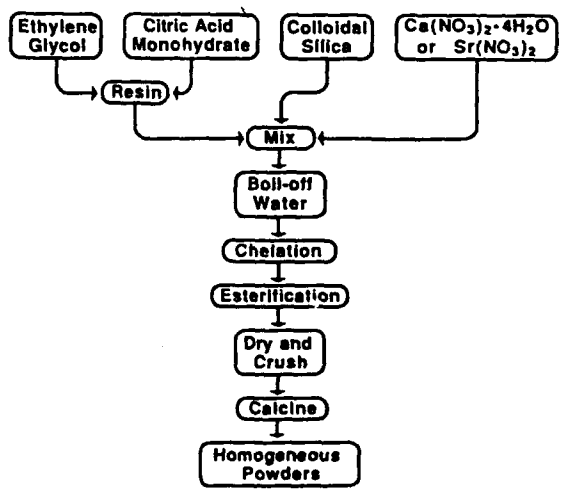

Fig. 2. Flow diagram showing the processing route for both Ca_2SiO_4 and Sr_2SiO_4 powders.

use of the hydrated nitrates, which can have variable moisture contents, did not affect the phase distributions obtained in the final powder. The required amount of the nitrate precursor was dissolved in water and then added to colloidal silica. In order to prevent flocculation of the silica, the pH of the colloidal silica was adjusted to below 1·5 with nitric acid prior to the addition of the nitrates. In this study, two colloidal silicas with different sodium contents were used. The first, which was designated Silica 1 (Ludox® SM, Du Pont Chemical Company), contained more sodium than the second, which was called Silica 2 (Ludox® AS-40, Du Pont Chemical Company). Silica 1 was used for all the Sr_2SiO_4 and Silica 2 was used for most of the Ca_2SiO_4 preparations. After the nitrate solutions and colloidal silica had been mixed, the resin was added and the mixture was heated. As the water boiled off, the gel formed without flocculation of the colloidal silica, and the viscosity increased. The remaining water then evaporated, expanding the gel into a foam. Finally the foam was dried and crushed before calcination at temperatures in the range 200°C to 1400°C.

Some of the crushed Ca_2SiO_4 gel was subjected to differential thermal analysis (DTA) and thermogravimetric analysis (TGA) while heating at 5°C/min, the same heating rate used for calcination. The phase distributions in the powders were evaluated by X-ray diffraction (XRD). This was after calcination for 1 min at temperatures in the range 200°C to 800°C and also after calcination for 1 h in the temperature range 800°C and 1400°C.

The effects of resin content and calcination conditions on the specific surface area and the particle size of the powders were determined by nitrogen adsorption (BET) and sedigraph techniques respectively. Some of the powders were also examined by SEM.

Finally, chemical analysis by plasma emission spectroscopy was performed on some Ca_2SiO_4 powders to check the calcium to silicon ratio, which was found to be in the range 2 to 2·1.

3 Results and Discussion

3.1 Phase development on calcination

Figure 3(a) shows the TGA results for a Ca_2SiO_4 gel containing 85% resin. The first major weight loss took place just above 250°C and could be correlated with the first low exothermic peak in the DTA curve of the same material, shown in Fig. 3(b). This was thought to be associated with the decomposition of the gel. The other major weight loss occurred at about 450°C and corresponded to a large exothermic DTA peak in Fig. 3(b). This was the stage at which the remainder of the gel decomposed and

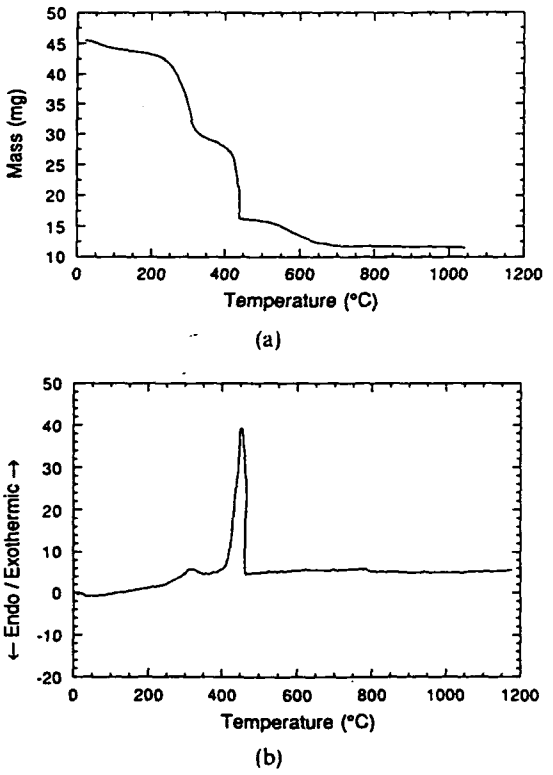

Fig. 3. (a) TGA and (b) DTA of a Ca_2SiO_4 gel containing 85% resin.

pyrolyzed. Further weight loss at higher temperatures was attributed to the removal of carbon formed during the pyrolysis. The thermal decomposition behavior of all the Ca_2SiO_4 and Sr_2SiO_4 gels in this study had the same characteristics as already described.

The phase distributions for the Ca_2SiO_4 gel containing 85% resin at different temperatures during the calcination are shown in Fig. 4(a). Each sample was heated at 5°C/min, held at the requisite temperature for 1 min and cooled. At temperatures below the pyrolysis stage the samples were X-ray amorphous, but after the pyrolysis at temperatures between 500°C and 650°C, the crystalline calcite phase of $CaCO_3$ could clearly be identified. As the temperature was increased, the amount of calcite appeared to diminish and the amount of Ca_2SiO_4 increased. By 700°C the sample was single phase α'_L-Ca_2SiO_4. When the calcination temperatures was increased to 800°C, the presence of β-Ca_2SiO_4 was observed. To further show that $CaCO_3$ was an intermediate compound, a sample of gel was calcined for 1 h at 600°C and then recalcined at 800°C. As can be seen in Fig. 4(b), after calcination at 600°C the only observable crystalline phase was $CaCO_3$, whereas after a second calcination at 800°C the sample was single phase β-Ca_2SiO_4. The exact nature of the reactions by which the $CaCO_3$ was removed and the Ca_2SiO_4 formed was unclear. Similar behavior was observed for the Sr_2SiO_4 gels with $SrCO_3$ being positively identified as an

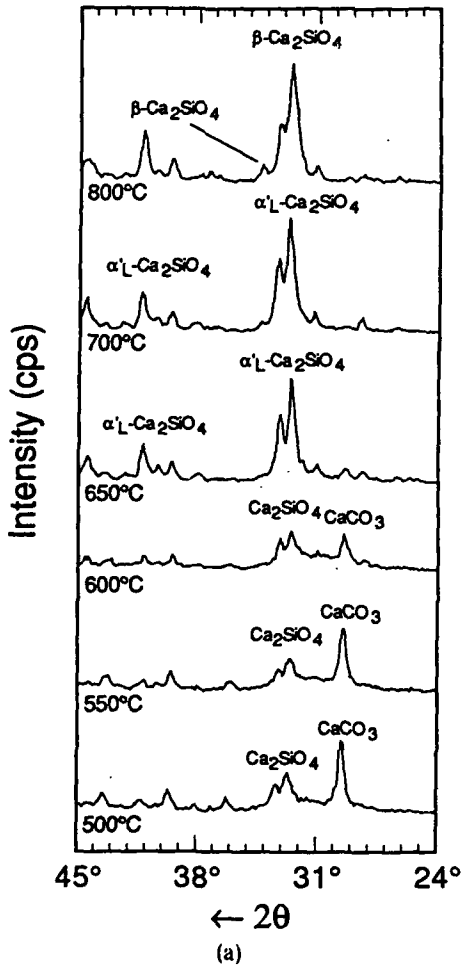

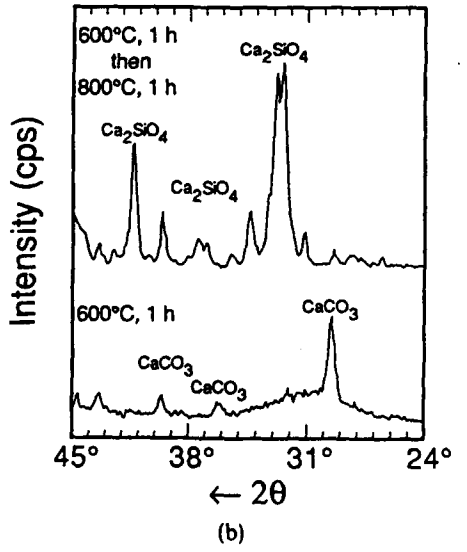

Fig. 4. (a) X-Ray diffraction traces showing the phase distribution in a Ca_2SiO_4 gel containing 85% resin, at different temperatures after the pyrolysis. Each sample was heated to temperature at 5°C/min and held at temperature for 1 min. (b) A comparison of X-ray diffraction traces of a Ca_2SiO_4 gel containing 85% resin, after calcination at 600°C for 1 h, and then after further calcination at 800°C for 1 h.

intermediate phase. Carbonates, specifically $BaCO_3$, have been identified during calcination of chemically derived powders in other studies.[12,13] They were intermediates in the formation of $BaTiO_3$, for example.

The phase distributions of Ca_2SiO_4 prepared with Silica 2 and calcined at high temperature are shown in Fig. 5(a). From 800°C to 1200°C the powders remained single phase β-Ca_2SiO_4, but the sample calcined at 1400°C showed single phase γ-Ca_2SiO_4. This could be attributed to enhanced grain growth at higher temperatures which decreased the stability of the β-phase. A particle size effect for this transformation in powders has been reported previously.[4,14-18]

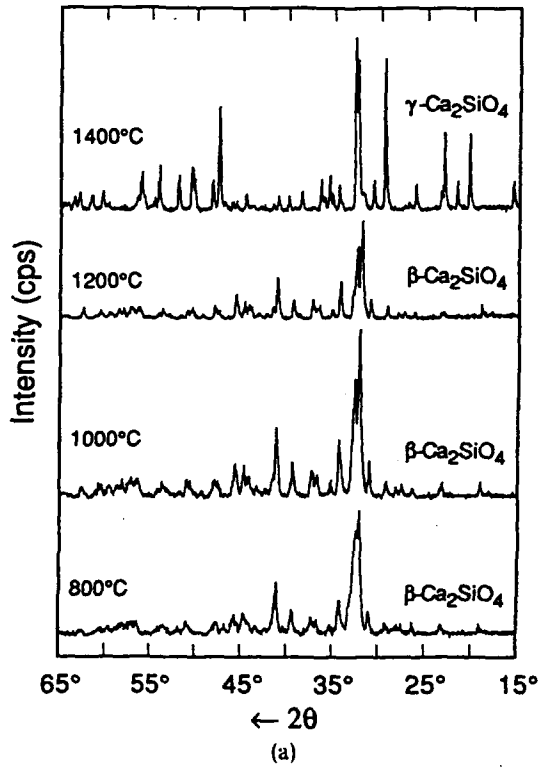

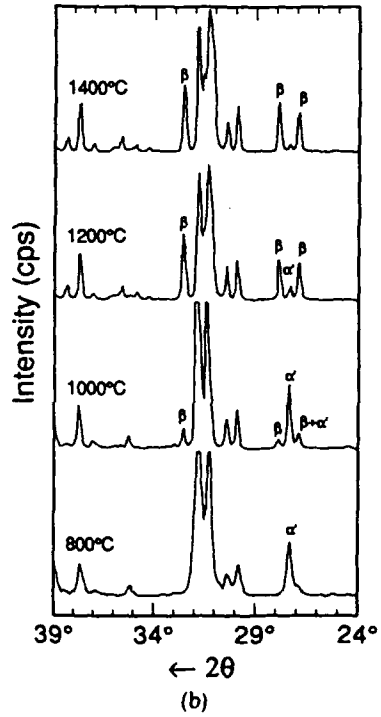

Fig. 5. X-Ray diffraction traces of (a) Ca_2SiO_4 (containing 85% resin) and (b) Sr_2SiO_4 (containing 90% resin) gels calcined for 1 h at temperatures in the range 800°C to 1400°C.

Figure 5(b) shows the development of the phase distribution for Sr_2SiO_4 prepared with Silica 1 and fired in the temperature range 800°C to 1400°C. The resin content was 90%. At 800°C the powder was single phase α' but as the temperature was increased β-phase was detected. The amount of β-phase increased with temperature until after 1400°C the sample was almost entirely β-phase.

The morphology of Sr_2SiO_4 powder calcined at 800°C for 1 h is shown in Fig. 6(a). The agglomerates were highly porous and comprised crystallites approximately 80 nm in size. Calcination at higher temperatures caused the agglomerates to densify and the crystallites to grow. Figure 6(b) shows powder calcined at 1400°C in which the agglomerates were dense and the grains were substantially larger than 1 μm. The SEM and X-ray diffraction results indicate a particle size dependence for the $\alpha' \rightarrow \beta$ transformation in Sr_2SiO_4.

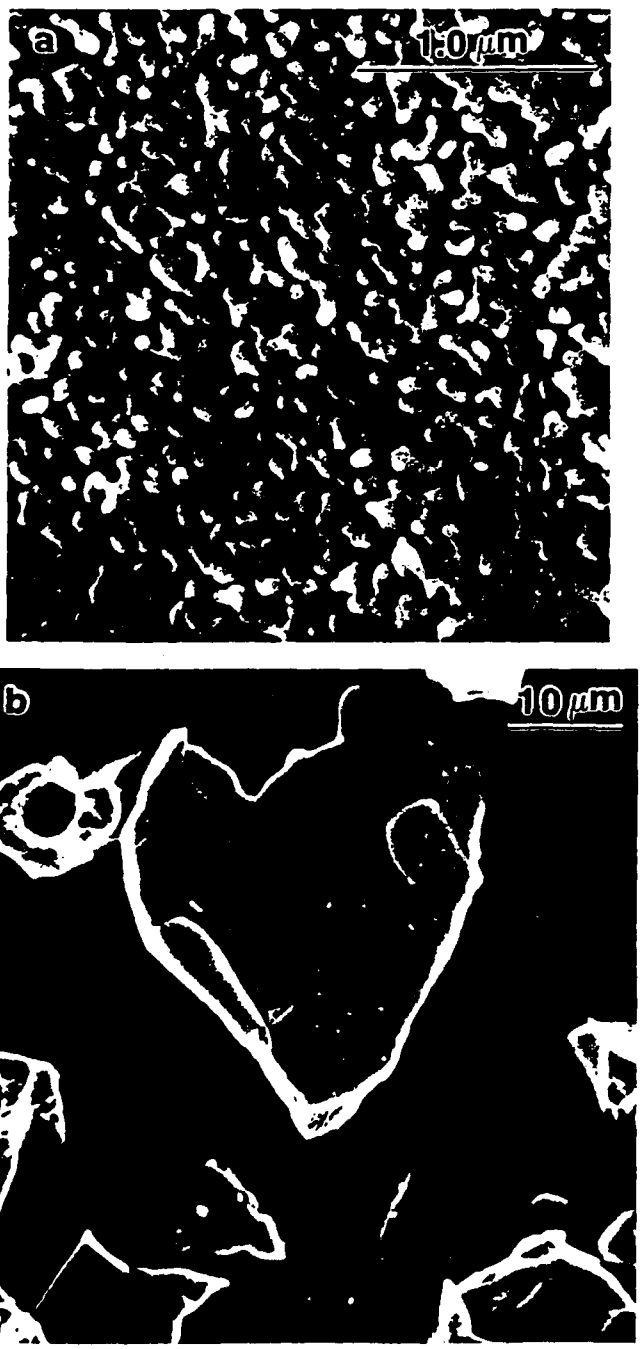

Fig. 6. SEM micrographs of Sr_2SiO_4 powder derived from a gel containing 90% resin calcined at (a) 800°C for 1 h (the individual crystallites have sintered together into highly porous agglomerates), and (b) 1400°C for 1 h (the agglomerates have fully sintered).

3.2 Effect of resin content

It is well known that the resin content can have an effect on the physical characteristics of powders produced by the Pechini process.[19] Hence the effect of resin content on the powders was investigated in this study. Resin contents from 50% to 93% were investigated and found to have no effect on the phase distribution in Ca_2SiO_4 for a specific calcination condition. In contrast, the resin content did affect the phase distributions in the Sr_2SiO_4 powders. Lower resin contents (50% and 70%) produced significant amounts of $SrCO_3$ or SrO along with $SrSiO_3$ after calcination at 800°C and 1000°C. This was attributed to strontium nitrate observed in the dried gels by X-ray analysis.

The presence of $Sr(NO_3)_2$ in the dried gels was attributed to incomplete chelation of the strontium ions during heating of the mixture and consequent precipitation of the nitrate. However, at the high resin contents required to obtain high surface area, this behavior was not observed.

Figure 7 shows DTA traces for Sr_2SiO_4 gels with different resin contents. It can be seen that those gels which contained crystalline $Sr(NO_3)_2$ (50% and 70% resin) clearly exhibited a broad endotherm at approximately 650°C, which could be linked to the melting and decomposition of $Sr(NO_3)_2$. Such segregation would be a source of chemical inhomo-

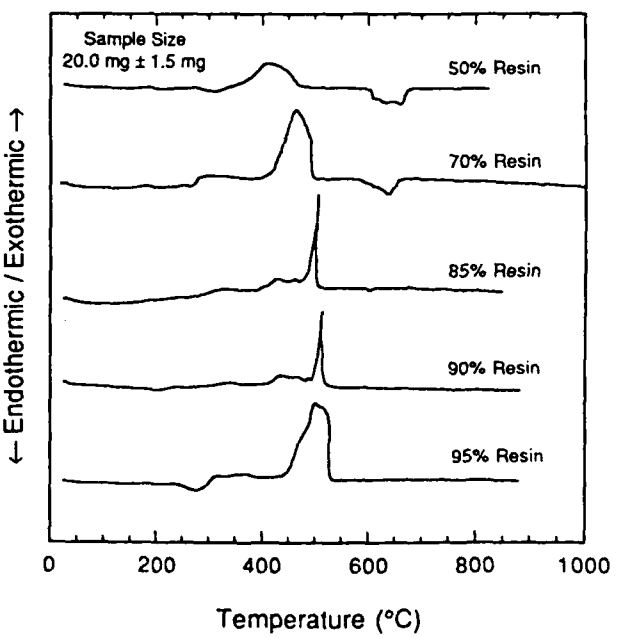

Fig. 7. DTA of Sr_2SiO_4 gels containing different resin contents.

geneity that could lead to the formation of SrO during calcination. It may also have been responsible for the retention of the $SrCO_3$ intermediate at temperatures above 700°C. In order to avoid reprecipitation of $Sr(NO_3)_2$ in the gels during drying, resin contents of 90% or above were used in the preparation of Sr_2SiO_4.

The physical characteristics of the powder were also affected by the resin content of the gel. Figure 8(a) shows the surface area of Ca_2SiO_4 powder as a function of calcination temperature for different resin contents. Above 1000°C, the resin content did not appear to have any significant effects on the surface areas of the powders. However, at lower temperatures the situation was very different. After calcination at 800°C the 85% and 93% resin contents showed the highest surface areas ($\sim 17\,m^2/g$), while the gels made without resin by direct casting of the colloidal silica in the presence of $Ca(NO_3)_2 . 4H_2O$ had the lowest surface area ($6\,m^2/g$). This increase in surface area with resin content was attributed to the extensive internal porosity seen in the powders made using high resin contents (Fig. 6(a)). When the calcination temperature was increased, sintering and grain growth of the powder agglomerates reduced the internal porosity (Fig. 6(b)) and led to lower specific surface areas.

Figure 8(b) displays the effect of resin content on the surface area of Sr_2SiO_4 powders. As was the case with Ca_2SiO_4, gels with higher resin contents produced powders with higher surface areas. This plot clearly showed that resin contents above 85% must be employed to produce high surface area powders.

The particle size of the powders was also affected by resin content. The results of different resin contents for Sr_2SiO_4 powders calcined at 800°C are shown in Fig. 9(a). The 50% and 70% resin contents gave powders with large median values of 20 μm and 11 μm respectively. Further increases in the resin content shifted the distributions to smaller particle sizes. The median value for 85% resin was about 6 μm and the largest particles in the distribution were approximately 20 μm. This trend to smaller sizes may have been due to the more violent pyrolysis in gels containing higher resin contents, leading to smaller, highly porous agglomerates. The highest resin contents used, including 90% and 95%, gave powders with the lowest median particle sizes. However, the largest particles in the distributions were of a similar size to the largest particles in the powders made from gels with 70% resin. Interestingly, both of the higher resin contents give bimodal distributions and 40% of the powder was submi-

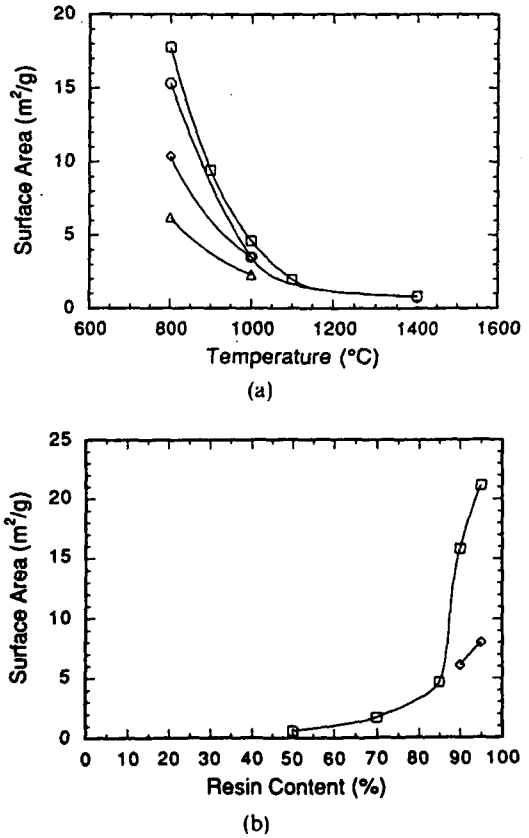

Fig. 8. (a) Surface areas of Ca_2SiO_4 powders containing different resin contents and calcined in the temperature range 800°C to 1400°C. (△) 0%, (◇) 50%, (□) 85%, and (○) 93% resin. (b) Effect of resin content on the surface area of Sr_2SiO_4 powders calcined at (□) 800°C and (◇) 1000°C for one hour.

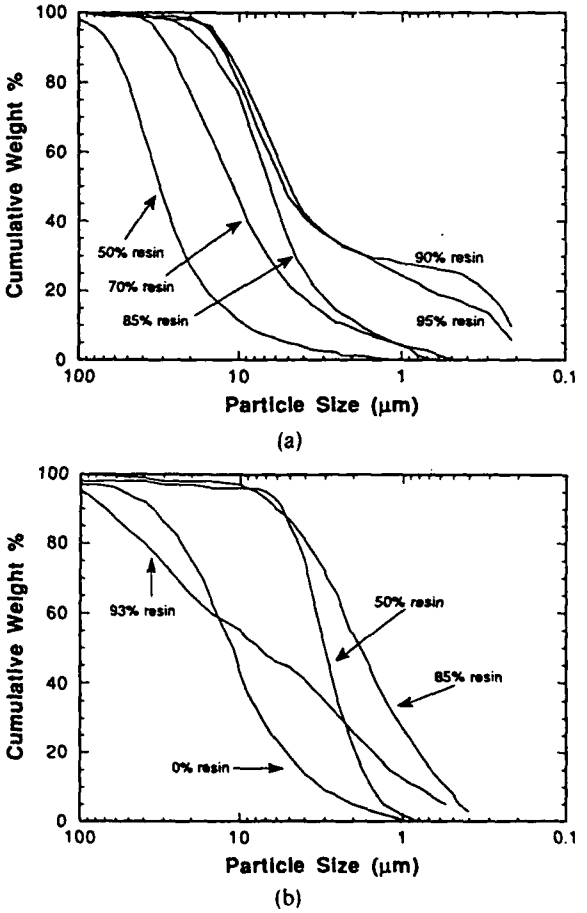

Fig. 9. Effect of resin content on particle size distribution of (a) Sr_2SiO_4 and (b) Ca_2SiO_4 powders calcined at 800°C for one hour.

cron. This biomodal characteristic was reproducible although difficult to explain.

Figure 9(b) shows the effect of resin content on the particle size of the Ca_2SiO_4 powders. The trend with resin content was not as systematic as in the Sr_2SiO_4 powders. With no resin, the distribution was wide. The 50% resin sample had a narrow distribution, between 10 μm and 1 μm with a median of approximately 2 μm. This was in contrast to the trend in Fig. 9(a), but may be explained by the fact that during calcination, the Ca_2SiO_4 gel with this resin content exploded at about 200°C. This was thought to be a consequence of the sudden and violent release of moisture, leading to smaller particles. When the resin content was increased to 85%, the particle size distribution shifted to smaller particle sizes. For this powder, the large particles were about 6 μm in size but there was also approximately 30% of submicron powder. Further increase in the resin content to 93% gave a very wide particle size distribution from submicron to 100 μm. This contrasted with the results for Sr_2SiO_4 using similar resin contents. In this case interagglomerate sintering was thought to have taken place during pyrolysis and calcination.

3.3 Effect of sodium on the phase distribution in dicalcium silicate powders

The phase distributions in Ca_2SiO_4 powders prepared with Silica 1 and Silica 2 were markedly different after calcination for 1 h at 1400°C. This was attributed to the difference in sodium content, since sodium is known to be a stabilizer for β-Ca_2SiO_4.[20] Calculation showed that Silica 2 would give Ca_2SiO_4 with 0·14 wt% Na_2O and Silica 1 would give Ca_2SiO_4 with 0·67 wt% Na_2O. Sodium was added in preparations of Ca_2SiO_4 with Silica 2 in the form of $NaNO_3$ dissolved with the $Ca(NO_3)_2.4H_2O$. In this way, powders containing up to 1 wt% Na_2O were prepared, and calcined at temperatures ranging from 800°C to 1500°C. The results of the phase analysis are shown in Table 1. All the powders exhibited β-phase after calcination at temperatures below 1400°C. However, after calcination at 1400°C, samples containing less than 0·5 wt% Na_2O transformed to γ-phase on cooling, while the other compositions remained β-phase.

Table 1. Phase distributions of Ca_2SiO_4 powders with different sodium contents, calcined for 1 h at various temperatures

Na_2O (wt%)	800°C	1000°C	1200°C	1400°C
0·14 (Silica 2)	β	β	β	γ
0·27	β	β	β	γ
0·41	—	—	β	γ
0·54	—	—	β	β
0·67 (Silica 1)	β	β	β	β
1·0	—	β	β	β

Consequently, there was evidence to suggest that the difference in phase distribution for samples prepared with Silica 1 and Silica 2 was due to the sodium content of these colloidal silica precursors.

4 Summary

A quick and relatively simple method for the preparation of both Ca_2SiO_4 and Sr_2SiO_4 powders of high surface area has been developed. The method avoided the use of unstable alkoxides and precipitation techniques. The powders so produced were very porous and friable and could easily be milled into submicron particle sizes.

The development of single phase powders at 700°C or above appeared to involve the formation of $CaCO_3$ or $SrCO_3$ as intermediate compounds. The desired silicate then developed by a low-temperature solid-state reaction between 500°C and 700°C. When the temperature was increased in this range, the silicate developed and the carbonates disappeared. The exact nature of the reaction was unknown.

Single phase powders of α'_L-, β- and γ-Ca_2SiO_4 could easily be produced by this route. The method has also been used to prepare single phase α'-powders of Sr_2SiO_4 for the first time.

The physical characteristics of the powders could be controlled by the resin content of the gel and the calcination conditions. In the case of Sr_2SiO_4, the resin content was also used to control chemical inhomogeneity caused by the reprecipitation of $Sr(NO_3)_2$ during drying of the gel. The effect of resin content on surface area was generally the same for both systems, but there were marked differences in how the resin content affected the particle size distributions.

Finally, the difference in the phase distributions observed in the Ca_2SiO_4 powders prepared with Silica 1 and Silica 2 was attributed to the difference in the sodium content of these colloidal silicas.

Acknowledgements

The authors wish to thank Mr Kyle E. Eckmann for help in preparing some of the dicalcium silicate and some of the X-ray analyses. This project was funded by the US Air Force Office of Scientific Research under grants AFOSR-89-0300 and URI AFOSR-90-0174. James L. Shull, Jr was supported by a US National Science Foundation Graduate Fellowship. The authors would also like to thank the Du Pont Chemical Company for supplying the colloidal silica used in this study. Use of the electron microscope facilities at the Center for Electron Microscopy at

UIUC is gratefully acknowledged. The plasma emission spectroscopy was performed by the staff of the Microanalytical Laboratory in the School of Chemical Sciences at UIUC.

References

1. Schwiete, H. E., Kronert, W. & Deckert, K., Existence range and stabilization of high temperature modification of dicalcium silicate. *Zement Kalk Gips*, **9** (1968) 359–66.
2. Midgley, H., The polymorphism of calcium orthosilicate. In *6th International Congress on the Chemistry of Cements*, Moscow, Suppl. Paper I, 1974, pp. 1–16.
3. Pritts, I. M. & Daugherty, K. E., The effect of stabilizing agents on the hydration rate of β-C_2S. *Cement Concrete Res.*, **6** (1976) 783–96.
4. Chan, C. J., Kriven, W. M. & Young, J. F., Physical stabilization of the β to γ transformation in dicalcium silicate. *J. Am. Ceram. Soc.*, **75** (1992) 1621–27.
5. Roy, D. M. & Oyfesobi, S. O., Preparation of very reactive Ca_2SiO_4 powder. *J. Am. Ceram. Soc. Discussion and Notes*, **60** (1977) 178–80.
6. Luth, W. C. & Ingamells, C. O., Gel preparation of starting materials for hydrothermal experimentation. *Am. Mineral.*, **50** (1965) 255–8.
7. Kralj, D., Matkovic, B., Trojko, R., Young, J. F. & Chan, C. J., Preparation of dicalcium silicate at 950°C. *J. Am. Ceram. Soc.*, **69** (1986) C170–C172.
8. Kriven, W. M., Possible alternative transformation toughening to zirconia: Crystallographic aspects. *J. Am. Ceram. Soc.*, **71** (1988) 1021–30.
9. Catti, M., Gazzoni, G., Ivaldi, G. & Zanini, G., The $\beta \leftrightarrow \alpha'$ phase transition of Sr_2SiO_4. I: Order–disorder in the structure of the α' form at 383 K. *Acta Cryst.*, **B39** (1983) 674–9.
10. Catti, M. & Gazzoni, G., The $\beta \leftrightarrow \alpha'$ phase transition of Sr_2SiO_4. II: X-Ray and optical study, and ferroelasticity of the β form. *Acta Cryst.*, **B39** (1983) 679–84.
11. Hou, T. I. & Kriven, W. M., Mechanical properties and microstructures of $CaZrO_3$–Ca_2SiO_4 composites. *J. Am. Ceram. Soc.*, in press.
12. Chaput, I. F. & Boilet, J. P., Chemically derived barium titanate gels and ceramics. In *High Tech Ceramics, Materials Monograph*, Vol. 36(B), ed. P. Vincenzini. Elsevier, 1987, pp. 1459–68.
13. Phule, P. P. & Risbud, S. H., Sol–gel synthesis and characterization of $BaTi_4O_9$ and $BaTiO_3$ powders. In *Materials Research Society Symposium Proceedings*, Vol. 121, *Better Ceramics through Chemistry III*, ed. C. J. Brinker, D. E. Clark & D. R. Ulrich. Materials Research Society, Pittsburgh, USA, 1988, pp. 275–80.
14. Chromy, S., The inversion of the $\beta \rightarrow \gamma$ modification of dicalcium silicate. *Zement Kalk Gips*, **23** (1970) 382–9 (in German).
15. Gawlicki, M. & Nocon-Wczelik, W., Influence of thermal treatment on the transition of $\beta \rightarrow C_2S$. In *Proceedings of the 7th International Symposium on Chemistry of Cements*, Vol. II, Paris, 1980, pp. 161–5 (in French).
16. Shibata, S., Kishi, K., Asaga, K. & Daimon, M., Effect of thermal history on $\beta \rightarrow \gamma$ transformation of pure Ca_2SiO_4. *Yogyo-Kyokai-Shi.*, **91** (1983) 497–502 (in Japanese).
17. Gawlicki, M., The role of thermal treatment on dicalcium silicate polymorphic transitions. In *Proceedings of the 14th Conference on Silicate Industry and Silicate Science III*. Budapest, Hungary, 1985, pp. 67–73.
18. Kriven, W. M., Chan, C. J. & Barinek, E. A., The particle size effect of dicalcium silicate in a calcium zirconate matrix. In *Advances in Ceramics*, Vol. 24, *Science and Technology of Zirconia III*, ed. S. Somiya, N. Yamamoto & H. Yanagida. American Ceramic Society, Westerville, OH, 1988, pp. 145–55.
19. Lessing, P. A., Mixed-cation oxide powders via polymeric precursors. *Am. Ceram. Bull.*, **68** (1989) 1002–7.
20. Ghosh, S., Rao, P., Paul, A. K. & Raina, K., Review: The chemistry of dicalcium silicate mineral. *J. Mat. Sci.*, **14** (1979) 1554–66.

PREPARATION AND HYDRATION KINETICS OF PURE $CaAl_2O_4$

M. A. Gulgun, O. O. Popoola, I. Nettleship, W. M. Kriven and J. F. Young,
Department of Materials Science and Engineering, University of Illinois at Urbana-Champaign, Urbana, IL 61801.

ABSTRACT

Single phase, pure monocalcium aluminate ($CaAl_2O_4$) powders are chemically synthesized at temperatures as low as 900°C. The powders have a specific surface area of approximately 10 m^2/g. The hydration kinetics of $CaAl_2O_4$ and the morphology of the hydrates are analyzed using electron microscopy techniques.

INTRODUCTION

Monocalcium aluminate ($CaAl_2O_4$, CA) and calcium dialuminate ($CaAl_4O_7$, CA_2) are the two major phases present in high alumina cements which are used in macro-defect free cement composites. However, monocalcium aluminate is primarily responsible for the characteristic hydration behavior (i.e. early strength development) of this kind of chemically bonded ceramic. In addition, $CaAl_2O_4$ has important refractory and infrared optical applications depending on its crystallinity.

In general, monocalcium aluminate powders are produced by high temperature solid state reactions between calcia, or calcium carbonate, and alumina powder. The extent of the reaction depends on the particle size, surface area and the mixing of the reactant powders, and usually requires temperatures in excess of 1400° C. Typically, powders produced by this method have a surface area of 0.235m^2/g to 0.56 m^2/g [1,2]. X-ray amorphous, high specific surface area calcium aluminate powder has been chemically prepared by Uberoi and Risbud [3] using aluminum di-sec-butoxide acetoacetate esterchelate and calcium nitrate precursors. Roy et al.[4] reported an evaporative decomposition of solution technique to produce CA powders at 900°C from nitrate precursors of calcium and aluminum.

The hydration behavior of calcium aluminate powders prepared by conventional high temperature synthesis techniques have been studied in the temperature range 4°C to 40°C using calorimetric analysis [1,2], solution chemistry [1,5], X-ray diffraction [2,6], and analytical electron microscopy [6]. At temperatures up to 30°C, an $Al(OH)_3$ gel and a so-called " *intrusion hydrated layer* " of thickness 12 nm were observed to form on CA particles [1]. Upon the destruction of this hydration layer, nuclei of crystalline products form and hydration proceeds by a dissolution-precipitation mechanism. Percival et al. [5] studied the precipitation of CAH_{10} ($CaO{\cdot}Al_2O_3{\cdot}10H_2O$) from supersaturated calcium aluminate solution at 21°C, and found that the amounts of calcia and alumina in solution determine which of the hydrate phases will precipitate. High concentrations of ions in the solution yielded C_2AH_8 ($2CaO{\cdot}Al_2O_3{\cdot}8H_2O$), CAH_{10} and $Al(OH)_3$, whereas lower concentrations precluded CAH_{10} precipitation. The hydration behavior of $Ca_3Al_2O_6$ (C_3A) in aqueous suspension (w/c = ~50) has been studied by Breval [6]. The products formed from the hydration of C_3A are the same as those formed during the hydration of CA, except that the formation of $Al(OH)_3$ was not reported for C_3A.

The aim of this communication is to describe a chemical preparation route for single phase $CaAl_2O_4$. Powders with various degrees of crystallinity, particle sizes, and specific surface area are produced and fully characterized. The hydration behavior of these powders and sintered pellets is reported.

Mat. Res. Soc. Symp. Proc. Vol. 245. ©1992 Materials Research Society

EXPERIMENTAL PROCEDURES

Powder preparation

The powders in this study were prepared in a similar way to those produced by Uberoi and Risbud [4] except that the precursors were $Ca(NO_3)_2 \cdot 4H_2O$ and $Al(NO_3)_3 \cdot 9H_2O$.

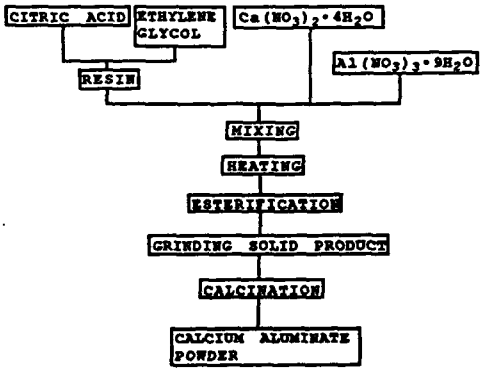

Fig. 1. Flow chart of the method used to prepare the powders

Fig.1 shows the "Pechini type" preparation route [7]. This method avoids the problems arising from the solubility of hydroxides during coprecipitation, and the use of unstable alkoxide precursors. The precursors were dissolved in 200ml of deionized water and then resin was added. The resin was composed of 60 wt% citric acid monohydrate dissolved in 40wt% ethylene glycol. The resultant mixture was heated until it boiled dry and foamed. Then the aerated gel was dried and crushed before calcining it on a platinum sheet in air. For each mixture the resin content of the gel is defined as:

$$100(w_{resin}/[w_{resin}+w_{oxide}]) \quad (1)$$

where w_{oxide} is the weight of the resulting oxides calculated from the known weight of precursors used and w_{resin} is the weight of the resin. Although complicated, this definition avoids the problems of determining both the moisture content of the gel prior to calcination and the yield of the processing.

Pyrolysis of the crushed gels was monitored by DTA and the phase distribution was analyzed by X - ray diffraction, both prior to and after calcination, at temperatures ranging from 200°C to 1400°C. The effect of resin content and calcination conditions on surface area and particle size distribution were studied using BET and sedigraph techniques. The carbon content of selected powders fired at 800°C, 900°C, and 1000°C was studied before and after an Ar^+ sputtering treatment by Auger Electron Spectroscopy (AES). Finally, the crystallinity, chemistry and morphology of the powders were observed using scanning and transmission electron microscopes (SEM, EDS, TEM).

The powder calcined at 900°C for 3 hours was milled in alcohol with a high purity zirconia ball for 72 hours. Submicon particles were classified by sedimentation in propan-2-ol. Some of the submicron powder was die pressed into bars, isostatically pressed to a pressure of 170MPa and fired in air for 1 hour at 1355°C. The density of the bars was determined to be 98.9% of the theoretical density using the Archimedes method and kerosene. SEM studies showed that the surface was devoid of porosity. The average grain size was 2μm. No grain boundary phase was detected.

Hydration

Hydration experiments at 5°C, 24°C, and 40°C were carried out for various times with submicron powders, powders with a wide particle size distribution, and sintered bars. The anomalous hydration behavior at 28°C was purposely avoided. CO_2-free deionized water was used in all experiments. Experiments were performed in closed HDPE bottles in which the void space was filled with argon. For each temperature regime the deionized water was thermally equilibrated for 1 day before the experiments were commenced. The bars were 2.6x2.5x2.0 mm^3. Powder hydration took place in a suspension made up of 0.4 g of powder in 15 ml of water. To stop hydration each bar was taken out of the water at the specified time, washed twice with acetone and then stored under acetone until it was examined. This was carried out

within 24 hours for most of the samples. For the powders, sampling was done by withdrawing small amounts of hydrated powder from the solution. The powder was both washed and stored in acetone. The hydrate morphology was observed with an ISI DS 130 SEM with EDS attachment operated at 10 kV. Selected powders were studied using X-ray diffraction In cases where no distinct X-ray peaks were observed, morphologies reported in the literature were used to identify the phases present.

RESULTS and DISCUSSION:

Powder Preparation

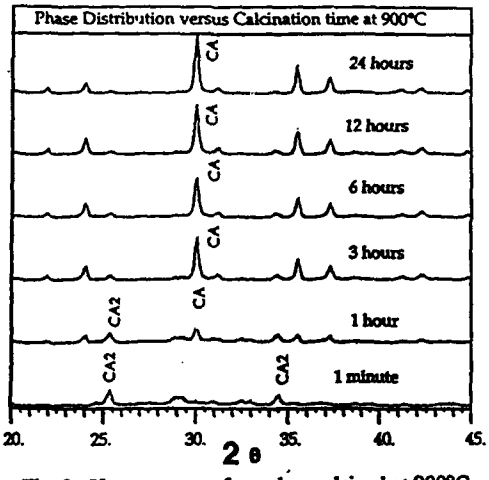

Fig. 2. X-ray spectra of powders calcined at 900°C for various calcination times.

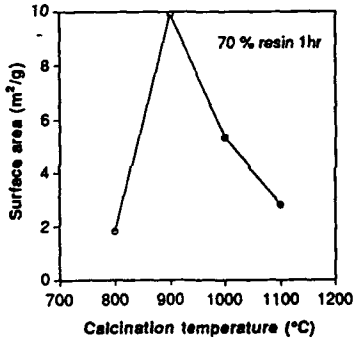

Fig. 3 The effect of firing temperature on the specific surface area of powders made from 70% resin content precursor.

Phase distribution.: The phase distributions in the powders were analyzed for different calcination conditions, as a function of resin content of the gel. For powders calcined at 900°C or higher for 3 hours, the amount of resin in the starting solution had no significant effect on the distribution of phases. In contrast, the calcination temperature, as well as firing time, determined the phases in the final product. Powders calcined at 900°C initially exhibit only CA_2 peaks when X-rayed. As the calcination time was increased CA peaks started to develop. After 3 hrs calcination at 900°C the CA_2 peaks were hardly detectable and the X-ray spectra consisted mainly of CA peaks (Fig. 2). This result is consistent with the formation kinetics of calcium aluminates proposed by Singh et al.[8]. The powders fired at 800°C appeared to be X-ray amorphous. However, TEM analysis of powders prepared from chlorine precursors revealed the powders to be microcrystalline.

Particle size: The effect of calcination temperature on the particle size was as expected, i.e. increased temperature caused agglomeration. *Resin content did affected the particle size* distribution. Powders prepared from highest and lowest resin content precursors, i. e. 92.5% and 50%, respectively, both gave a median particle size of 25 μm ESD (equivalent spherical diameter), whereas the powders from 85% and 70% resin content precursors showed a median particle size of ~8μm. The gels with low resin content (50%) gave large, relatively dense particles because the pyrolysis did not disrupt the gel. When the resin content is as high as 92% the exotherm associated with the pyrolysis is very high, as determined by DTA, and the agglomerates are larger due to partial sintering.

Specific surface area: The surface area of the monophase CA powders is very sensitive to both the firing conditions and the composition of the starting gel. As the calcination temperature was increased one would expect that coarsening and densification would lead to a

reduction in surface area. In contrast, the powders with the lowest surface area were the ones calcined at 800°C (the lowest temperature employed) (Fig.3). This powder was visibly black, and AES analysis showed a strong carbon peak which was absent for powders calcined at higher temperatures. Successive sputtering between AES runs revealed the residual carbon to be on the surface. This surface carbon probably closed off the internal porosity in the powder agglomerates which led to low surface area measurements. When the calcination temperature was increased to 900°C the carbon was removed, exposing more internal porosity which led to a specific surface area of about 10 m^2/g. This value is 40 times larger than the specific surface area of CA powders prepared by high temperature reactions [1,2]. At higher temperatures densification and coarsening of crystallites in the powder caused a decrease in surface area.

Hydration

The hydration rate tended to increase with temperature. Figure 4 shows the SEM micrographs of surfaces hydrated at 5°C. Submicron powder surfaces were covered by a gel after one hour of hydration. Agglomeration was observed, with the gel interconnecting individual particles at 24 hours. After 7 days, the hydration product morphology consisted of intersecting hexagonal plates. X-ray analysis showed them to be CAH_{10}. In the case of powder with a wide particle size distribution, the first indication of a reaction taking place was observed after only 3 hours and a product with a "pincushion"-like morphology was formed after 24 hours. Again CAH_{10} was observed after 7 days of hydration. On the sintered bar surfaces a porous layer approximately 10 μm thick was observed after 3 hours. EDS analysis of this layer showed only an aluminum peak, indicating that the layer was most likely $Al(OH)_3$ (AH_3). After 24 hours, this cover layer was extensively cracked, and a leached macroporous

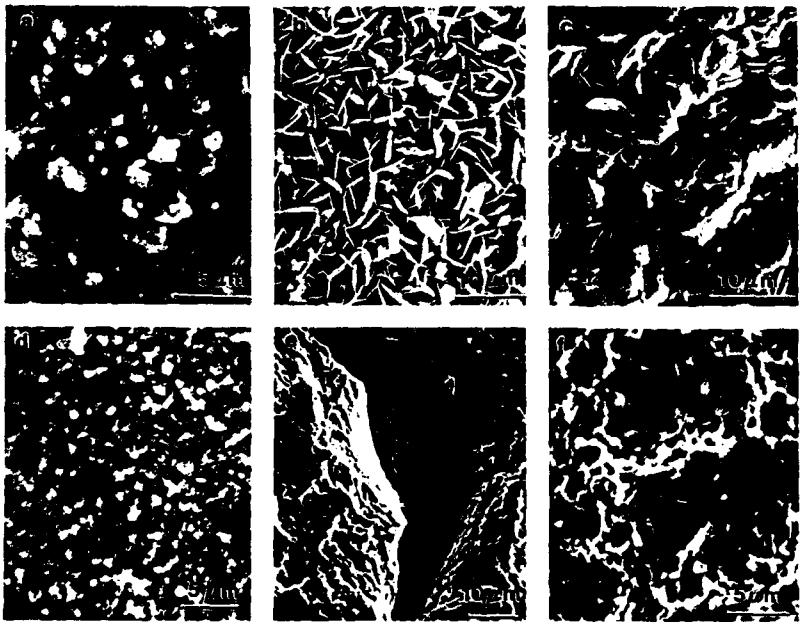

Fig. 4. Surface hydrated at 5°C: (a) submicron powder after 1 hour is covered with a thin gel, (b) after 7 days intersecting hexagonal plates of CAH_{10} form, (c) powder with a wide particle size distribution after 7 days dissolution of plates at the edges, (d) bar with a gel layer formed on the surface after 10 min., (e) thick layer formed on the surface of the bar after 3 hours, (f) leached surface under the thick layer after 7 days.

underlying surface was revealed. Following 7 days of hydration some spherical outgrowths were observed.

At 24°C, the first indication of a reaction was observed after 10 min. in a powder with a wide particle size distribution and after 1 hour in the submicron powder. The growth of C_2AH_8 and C_4AH_{19} ($4CaO.Al_2O_3.19H_2O$) occured predominantly as parallel stacks of hexagonal plates (Fig.5a). Figure 5b revealed growth of hexagonal plates parallel to the c-axis of the crystal. After 7 days of hydration dissolution was observed at plate edges and there was an increase in the amount of the featureless deposit formed in powder specimens. The bar surface revealed the same features as described for the surface of the bars hydrated at 5°C. It appeared that the rate of reaction was increased at 24°C. After 7 days the cracked surface showed hexagonal plates of C_2AH_8 forming underneath the cover layer. One cracked spherical crust also revealed hexagonal prisms growing inside the hollow spheres. Although the identification of these prisms has not yet been accomplished, their morphology indicated that the crystal probably had a low c/a lattice parameter ratio. No cubic phase was observed.

At 40°C, hydration proceeded in a similar way but at a faster rate than at 24°C (Fig. 6). The first cubic products in the form of trapezohedrons were observed on powder surfaces after 4 days of hydration. Few spherical features were also observed in the hydrated submicron powder. Fig. 6b shows them to be hollow, with hexagonal flakes growing inside them.

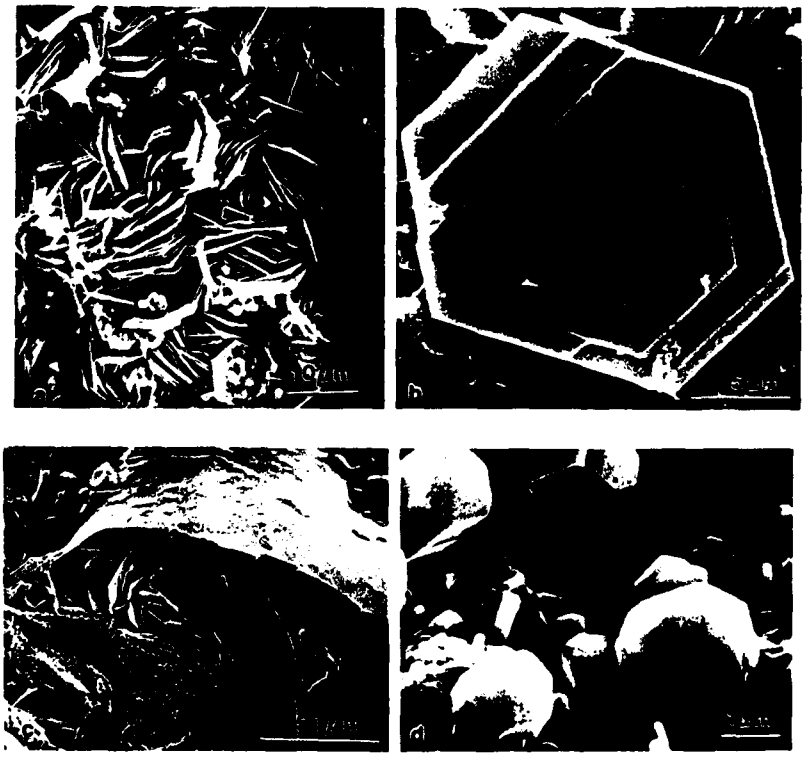

Fig. 5. Surfaces hydrated at 24 °C: Powders with wide particle size distribution after 7 days (a) showing parallel stacks of C_2AH_8, (b) hexagonal plate growing parallel to its c-axis, (c) bar after 7 days with hexagonal plates growing underneath the cover layer, (d) hexagonal prisms growing on bars after 7 days.

After 24 hours of hydration at 40°C the cover layer on the surface of the bars was made up of tightly spaced needles. EDS analysis of this layer gave only the aluminum peak. It appears that the AH_3 amorphous layer crystallized in spherulitic morphology. Figure 6c shows that hexagonal plates grew out from the inside of the hollow spheres. The restricted occurrence of the hexagonal plates only inside these balls or underneath a cover layer, suggested that the concentration of calcium and aluminum ions in solution under the crust may have reached the solubility limit of C_2AH_8 locally to allow its precipitation.

Fig. 6. Surfaces hydrated at 40°C: (a) submicron powder showing cubic crystals of C_3AH_6 and hexagonal plates growing out of (b) and underneath the spherical crust (c).

CONCLUSIONS

The main conclusions of this investigation are as follows:

1. High purity, high specific surface area, monophase, highly reactive $CaAl_2O_4$ (CA) powders have been chemically synthesized using a sol-gel method.
2. At low temperatures, a gel forming on the surface of the sintered bars and submicron particles apparently slows down further reaction of the underlying surface. The thickness of this protective layer reaches ~ 10 µm at 5°C after three hours of hydration, which is significantly thicker than previously reported.
3. The temperature at which the hydration is carried out seems to affect the reaction rate of monocalcium aluminate (CA) in aqueous suspension, which is in accord with the dissolution-precipitation mechanism proposed for the hydrate formation and conversion reactions.

ACKNOWLEDGEMENTS.

This work was supported by the Center for Cement Composite Materials. Dr. Nettleship's work was supported by AFOSR - 89 - 0300.

REFERENCES:

1. K. Fujii, W. Kondo, and H. Ueno, *J. Am. Ceram. Soc.*, **69** (4), 361 (1986).
2. R. N. Edmonds and A. J. Majumdar, *Cement and Concrete Research*, **18**, 311 (1988).
3. M. Uberoi, S.H. Risbud, *J. Am. Ceram. Soc.*, **73**, 1768 (1990).
4. D.M. Roy, R.R. Neurgaonkar, T. P. O'Holleran, and R. Roy, *Bull. Am. Ceram. Soc.*, **56**, 1023, (1977).
5. A. Percival, F.G. Buttler, and H.F.W. Taylor, *Proc. IV th Int.. Symp. on the Chem. of Cem.*, Washington, D.C., Paper III-S5, 277 (1960).
6. E. Breval, *Cement and Concrete Res arch*, **6**, 129 (1976).
7. P.A. Lessing, *Am. Ceram. Soc. Bull.*, **68**, 1002 (1989).
8. V.K. Singh, M.M. Ali, and U.K. Mandal, J. Am. Ceram. Soc., **73**, 872, (1990).

journal

Reprinted from the Journal of the American Ceramic Society, Vol. 75, No. 9, September 1992

J. Am. Ceram. Soc., 75 [9] 2400–406 (1992)

Phase Transformations in Dicalcium Silicate: I, Fabrication and Phase Stability of Fine-Grained β Phase

Ian Nettleship,*,† Kurt G. Slavick,* Youn Joong Kim,* and Waltraud M. Kriven*

Department of Materials Science and Engineering, University of Illinois at Urbana-Champaign, Urbana, Illinois 61801

Fine-grained β-Ca_2SiO_4 containing small amounts of sodium was fabricated as an analogue to tetragonal zirconia polycrystals (TZP) in order to study the stress-induced β→γ transformation. This avoided the problems associated with the fabrication and evaluation of composites containing β-Ca_2SiO_4. The microstructure of dense β-Ca_2SiO_4 exhibited severe intergranular strains and twin-terminating microcracks as seen by TEM. The β-phase twin widths were quantitatively correlated with grain sizes giving an average ratio of 0.04. Stress-induced transformation was observed on ground surfaces but not on fracture surfaces. The stress–strain behavior and the mechanical properties were consistent with stress-induced microcracking and microcrack coalescence. The elastic modulus of fully dense β phase was estimated to be 123 GPa.

I. Introduction

DICALCIUM SILICATE (Ca_2SiO_4) and its polymorphism have been the subject of many studies over the past 50 years or so. It is currently accepted that there are five polymorphs of Ca_2SiO_4 that can exist at atmospheric pressure: α, α'_H, α'_L, β, and γ.[1,2] The sequence of phase transformations and the transformation temperatures are shown in Fig. 1. Ca_2SiO_4 is of considerable importance to both refractory and cement technologies. In most cases there is a need to avoid the disruptive 12 vol% increase associated with the β→γ transformation. This is commonly called "dusting," and Ca_2SiO_4 has been known to degrade refractory materials in which it is a contaminant. In the cement industry, Ca_2SiO_4 is the second most important hydrating phase in portland cement and is considered to be responsible for latter-stage hardening. The γ phase does not hydrate, and, hence, the more reactive high-temperature polymorphs need to be stabilized to room temperature in cement powders. This is commonly done by the incorporation of well-known stabilizing additives such as Na_2O, Al_2O_3, K_2O, and $BaSO_4$.[3]

Ca_2SiO_4 has also been reported as a potential transformation toughener based on the large volume change associated with the β→γ transformation,[4] and some attempts have been made to toughen ceramic matrices by the incorporation of β-Ca_2SiO_4.[5–9] However, direct proof of stress-induced transformation during fracture remains elusive, even though some toughness enhancement has been observed. Most of the toughness increase has been attributed to crack deflection and microcracking.[7]

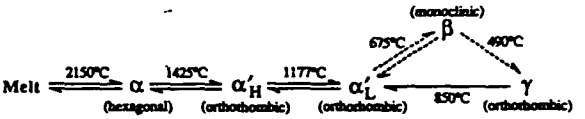

Fig. 1. Polymorphism of Ca_2SiO_4.

There have been many problems associated with the use of composites containing Ca_2SiO_4 in the study of the β→γ transformation. The main difficulty has been the processing of Ca_2SiO_4 in chemically compatible matrices such as MgO[8] and calcium zirconate ($CaZrO_3$).[7,9] Little is known about the preparation of such composites. Usually, the composites have been fabricated with only 10 to 20 vol% Ca_2SiO_4 in analogy to zirconia toughened alumina (ZTA), and this has unfortunate consequences when one attempts to study transformation toughening. The low content of transformable phase inhibits the detection of product phase by XRD after grinding and fracture. This is especially true if the transformation causes the Ca_2SiO_4 to debond from the matrix and fall out. This also causes problems for TEM study since the debonded γ-Ca_2SiO_4 grains tend to be removed during specimen preparation.

The interpretation of the microstructure–property relationships of Ca_2SiO_4-containing composites in terms of transformation toughening and stress-induced transformation is also difficult. The composite properties and microstructure show evidence of a complex combination of mechanisms,[7] and the relative importance of each mechanism cannot be precisely determined.

In this study, a single-phase, polycrystalline β-Ca_2SiO_4 material was developed in order to study the stress-induced β→γ transformation in more detail. Dense, fine-grained β-Ca_2SiO_4 was fabricated as an analogue to tetragonal zirconia polycrystals (TZP) using chemically prepared powders containing small amounts of sodium. The mechanical properties were evaluated, but the main purpose of the work was to observe evidence for stress-induced transformation on fracture and grinding.

A significant way in which the β→γ transformation in Ca_2SiO_4 differs from the tetragonal (*t*) to monoclinic (*m*) transformation in zirconia is its irreversible nature, due to the fact that the β phase is a high-pressure phase that has no thermodynamic stability at atmospheric pressure.[10]

The companion study[11] examined the microstructures and crystallography of Ca_2SiO_4 in a variety of composites and single-phase materials in order to develop a structural interpretation of the stability of the polymorphs. This is considered to be very important with regard to explaining the transformability of the β phase sintered in different phase fields and, hence, the properties of Ca_2SiO_4 containing ceramics.

II. Experimental Procedure

The Ca_2SiO_4 powders were prepared by a "Pechini method" modified to use a silica sol (Ludox SM, Dupont Chemical Co., Wilmington, DE) as a precursor.[7] The details of the preparation

M. P. Harmer—contributing editor

Manuscript No. 196054. Received January 13, 1992; approved May 11, 1992.
Presented at the 93rd Annual Meeting of the American Ceramic Society, Cincinnati, OH, April 29 to May 2, 1991 (Basic Science Division, Paper Nos. 121-B-91 and 114-B-91).
Supported by the U.S. Air Force Office of Scientific Research under Grant No. AFOSR-89-0300.
*Member, American Ceramic Society.
†Present address: Department of Materials Science and Engineering, University of Pittsburgh, Pittsburgh, PA 15261.

method have been reported elsewhere.[12] In this study the silica sol contained some sodium so that the final Ca_2SiO_4 powder was calculated to contain 0.7 wt% Na_2O. Chemical analysis of some powders calcined at 800°C showed the Ca/Si ratio to be in the range 2.0 to 2.1. The resulting powders were calcined at temperatures in the range 800° to 1500°C.

The preparation of the dense material involved sedimentation classification of powders that had been calcined at 800°C for 1 h and milled in 2-propanol with high-purity zirconia balls (Union Process, Akron, OH). The sedimentation was also conducted in 2-propanol because of the moisture sensitivity of β-Ca_2SiO_4. The submicrometer powder thus obtained was pressed into bars or pellets, isostatically pressed at 170 MPa, and fired in air in the temperature range 1300° to 1500°C. A 700°C annealing treatment was incorporated into the cooling schedule to relieve stresses built up during cooling from the firing temperature. This was done for all the specimens in this study including the powders. Without this step the sintered specimens were quite unstable and dusted over a period of few days.[8]

Changes in the phase distributions of the powders and the dense material were determined qualitatively by direct comparison of XRD traces. The complexity of the XRD traces of the β and γ phases and the extensive peak overlap made phase distribution determination by comparison of integrated intensities of single peaks inaccurate.

The density of the sintered materials was measured by the Archimedes technique in kerosene. The strength of the materials was measured by four-point bending of at least five specimens, and the stress–strain behavior of certain bars was monitored by strain gauges (Model HBM 0.6/120 LY 11, Omega Engineering, Stamford, CT) mounted on the tensile surfaces until fracture. Bars were polished to a 1-μm finish prior to testing. The elastic moduli were measured using the pulse-echo method (NDT-150, Nortec Corp., Kennewick, WA), and the hardness was evaluated by Vickers indentation (Zwick 3212, Mark V Laboratories, East Granby, CT). No attempt was made to measure toughness because of the crack size dependence for polycrystalline ceramics.

Some specimens were examined by SEM (Model ISI-130, International Scientific Instruments, Santa Clara, CA), and the grain size was measured by the linear intercept method on micrographs of polished surfaces after thermal etching at 1300°C for 15 min. The grain size results were directly expressed as the average intercept length, and at least 400 intercepts were used. It was thought to be inappropriate to multiply the average intercept length by a constant because of the assumptions that had to be made in choosing a value. Finally, TEM (Model 600, Hitachi Instruments, Conroe, TX) was conducted on samples prepared by ion milling of thin sections.

III. Results

(1) Phase Distribution in the Calcined Powders

Figure 2 shows the phase distributions in the Ca_2SiO_4 powders after calcination at different temperatures ranging from 800° to 1500°C. After calcination for 1 h at low temperature, the powder was crystalline and consisted entirely of β phase. Low-temperature preparation routes used in other studies also produced β-phase powders.[13,14] When the calcination temperature was increased to 1400°C, the powder remained predominantly β phase on cooling to room temperature. In contrast, the powders fired at 1500°C exhibited considerably more γ phase.

(2) Fabrication and Phase Distribution of Dense, Polycrystalline Ca_2SiO_4

The powder produced by calcination at 800°C for 1 h was chosen to make dense material. Figure 3(A) shows the relative densities of samples heated to 1400°C at 5°C/min and fired for different times. The materials had completed most of the sintering after the first 3 h. Figure 3(B) shows the grain size of the same materials as a function of time. After 1 h at 1400°C, the grain size was about 1 μm and the material was 90% dense, but, when the firing time was increased to 12 h, the material approached 99% density while the grain size was only 2 μm. This showed that grain growth in the dense material was quite slow. In all the materials studied, the grain morphology was equiaxed and uniform.

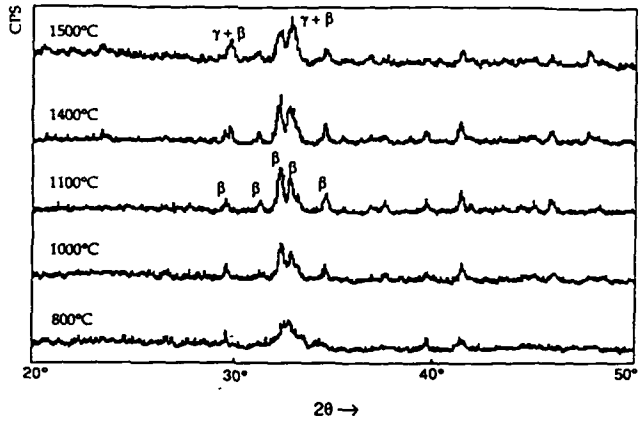

Fig. 2. XRD phase distribution in powders calcined in the temperature range 800° to 1500°C for 1 h.

The phase distribution on the sintered surfaces of the ceramics fired at 1400°C is shown in Fig. 4(A). After 1 h, the surface was predominantly β phase although some α_L' phase did appear to be present. As the firing time increased, the amount of α_L' decreased until, after 12 h, the material was single-phase β. It

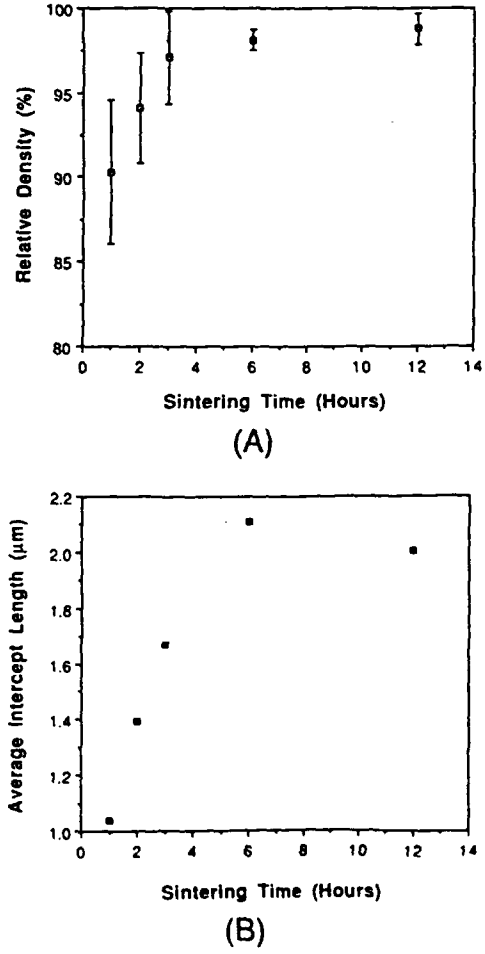

Fig. 3. (A) Relative density versus time for samples fired at 1400°C. (B) Grain size (average intercept length) as a function of sintering time at 1400°C, taken from SEM micrographs.

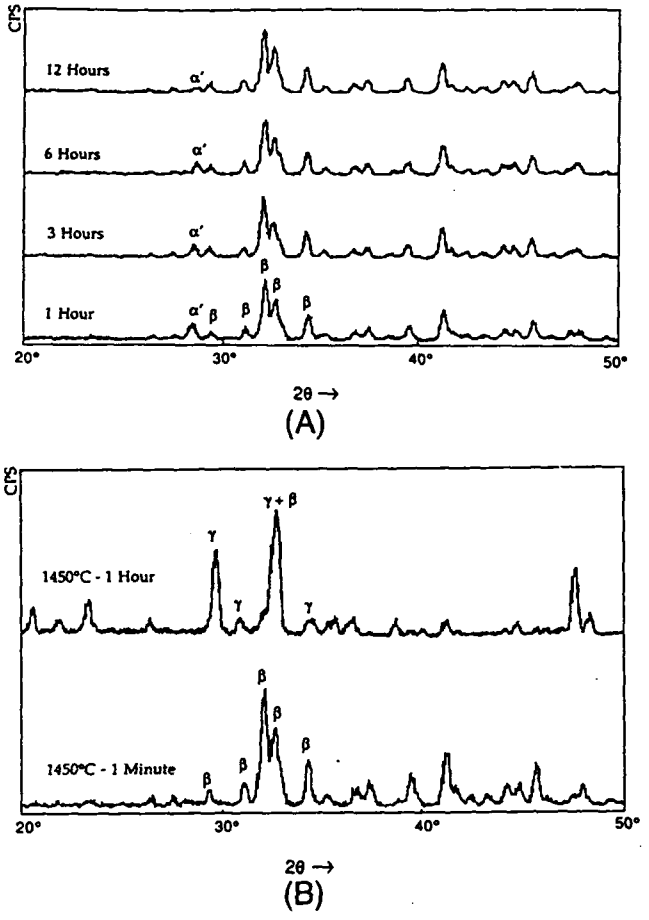

Fig. 4. (A) XRD phase distributions on sintered surfaces after firing at 1400°C. (B) XRD phase distributions on sintered surfaces after firing at 1450°C.

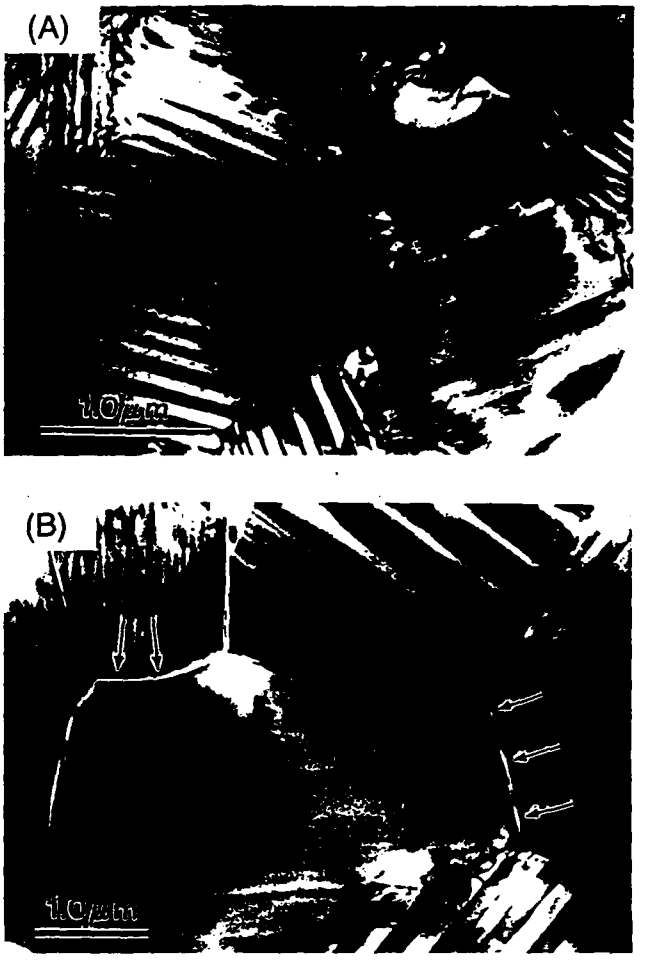

Fig. 5. (A) TEM micrograph of β-Ca_2SiO_4 fired at 1400°C for 1 h, showing intergranular strains. (B) TEM micrograph of β-Ca_2SiO_4 fired at 1400°C for 6 h, showing intergranular strains, twin-terminating microcracks, and coalesced microcracks (arrowed).

is thought that grain growth caused a decrease in the amount of the α_L' phase that was consistent with a particle size effect on the stability of the α_L' phase. When the sintering time was increased above 6 h, the frequency with which samples dusted because of β→γ transformation on cooling increased. Despite this result, some samples survived for all the times used, which extended to 72 h. These undusted samples showed no γ phase on the sintered surface.

When the compacts were fired at 1450°C, the behavior was very different. Figure 4(B) shows the phase distributions for materials fired for 1 min and for 1 h. After only 1 min at 1450°C, XRD analysis of the sintered surface of the pellet showed the material to be entirely β phase, but after 1 h the surface of the sample dusted, and the dust contained mainly γ phase.

(3) Microstructure of Dense, Polycrystalline β Phase

Figure 5(A) shows a TEM micrograph of material fired at 1400°C for 1 h. The grains were β phase twinned by the α_L'→β transformation.[15] Each grain usually contained just one type of twin that extended all the way across the grain. There did not seem to be any grain-boundary phase, although large strains were observed where twin terminations of adjacent grains met across grain boundaries. Despite the high strain, there appeared to be only twin-terminating microcracks at grain boundaries.[16] Grain growth during annealing at 1400°C had a considerable effect on the microstructure. Figure 5(B) shows the general features of the microstructure after firing for 6 h. Some grain boundaries still showed the accumulation of strain without significant cracking. However, other boundaries (arrowed) showed evidence that some cracks had coalesced and extended over more than one facet length. It is not certain whether the extended microcracks were instrinsic to the material or if they were stress induced during preparation of the TEM specimens.

After the preparation of TEM specimens, most of the grains were retained as the β phase. However, sometimes a grain that had transformed to the γ phase was observed (e.g., Fig. 13 in Ref. 11). The grain was untwinned, as previously noted in cement clinkers by Groves.[17] Large cracks appeared to have initiated at the transformed grain and extended into the surrounding microstructure, without causing the surrounding grains to transform.

TEM experiments were also conducted to measure the twin width as a function of grain size for the β phase. For 100 grains, the average twin width and average grain cross section were measured. Although the grain cross section in the plane of the TEM specimen was not a strict measure of grain size, Fig. 6(A) did show a linear relationship between twin width and grain cross section. Although there was scatter in the data, a least-squares fit gave a slope of 0.037.

A similar experiment was conducted by Chan.[18] The specimens were $CaZrO_3$–30 wt% Ca_2SiO_4 composites hot-pressed at 1450°C for 15 min and annealed at 1400°C. The results presented in Fig. 6(B) showed a similar scatter, and the gradient of the plot was 0.045. Hence, despite the difference in the processing conditions, the relationship between twin width and grain size for β-Ca_2SiO_4 in Chan's study closely paralleled the results of this study. Both gave plots with a gradient close to 0.04.

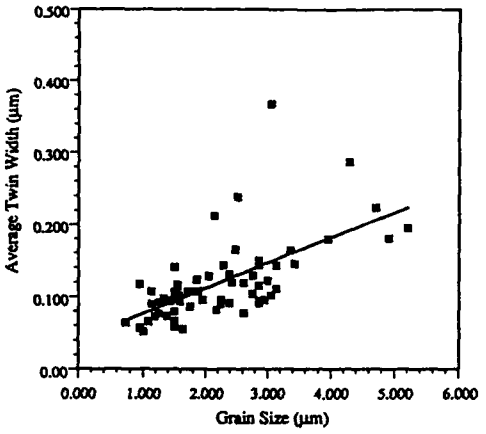

(A)

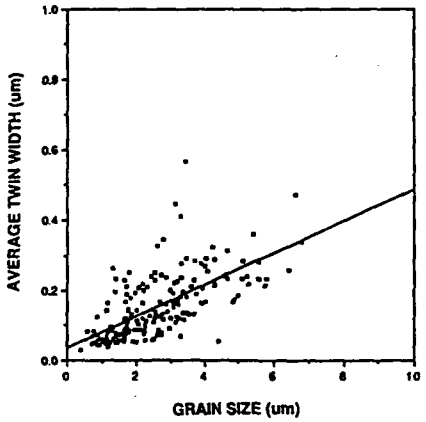

(B)

Fig. 6. (A) Plot showing average twin widths of β-Ca_2SiO_4 as a function of grain size, as measured by TEM. (B) Plot of average twin widths as a function of grain size for hot-pressed and annealed samples of $CaZrO_3$–30 wt% CA_2SiO_4 composites, as measured by TEM (after Chan[18]).

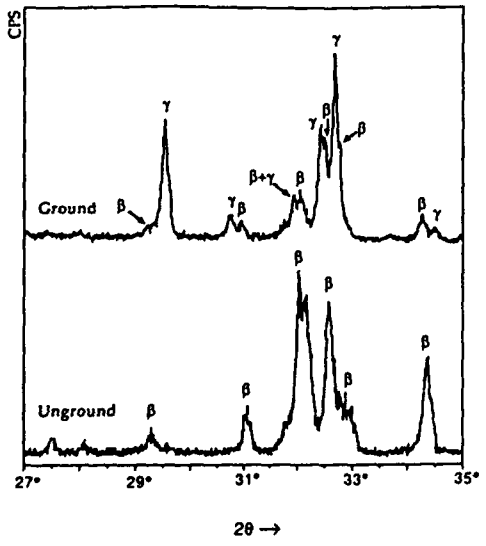

Fig. 7. XRD phase distribution of Ca_2SiO_4 fired at 1400°C for 6 h, before and after grinding.

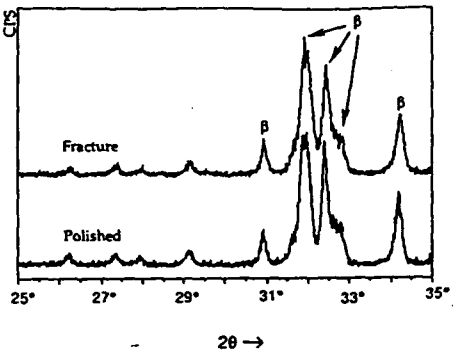

Fig. 8. Comparison of the XRD phase distributions on the polished surface before testing and on the fracture surface. Sample was fired at 1400°C for 3 h.

(4) Transformability of Polycrystalline β Phase

Quenching the polycrystalline materials into liquid nitrogen did not induce the transformation. However, severe grinding of the materials fired at 1400°C for times ranging from 1 to 12 h produced evidence of some β→γ transformation (Fig. 7). Irrespective of sintering time, transformation occurred on grinding of some samples fired at 1400°C. This behavior was unpredictable and could not be related to any grain size effects.

Transformation during the application of stress in bending was studied by comparing the phase distributions before and after fracture and also by observing stress–strain behavior. Figure 8 compares the phase distribution of a polished surface and a fracture surface of Ca_2SiO_4 fired at 1400°C for 3 h. No evidence of γ phase was found on either surface. The stress–strain behavior prior to fracture for materials fired at 1400°C is shown in Fig. 9. Deviation from linearity suggested stress-induced effects, such as stress-induced transformation,[19] which is common in some TZPs. In this study, strain gauges were attached to the tensile surfaces of Ca_2SiO_4 bars tested in four-point bending. Figure 9 shows that the stress–strain curves were perfectly linear until fracture for a fine-grained Ce-TZP sample, whereas all of the β-Ca_2SiO_4 samples deviated from linearity. The fact that the behavior of the zirconia sample was perfectly linear implied that the nonlinearity observed for the Ca_2SiO_4 specimens was not related to slippage of the specimens or of the test fixture. The deviation from linearity was particularly noticeable for the sample fired for 12 h. Some specimens were also unloaded and reloaded before they fractured, and they exhibited small permanent strains of approximately 0.005%.

(5) Mechanical Properties of Polycrystalline β Phase

The strength of the materials fired at 1400°C is shown in Fig. 10. Obviously the values were low, and, although the average strength value appeared to increase with sintering time, the trend was not significant, given the size of the error bars. Low values and high scatter occurred despite the fact that all the bars

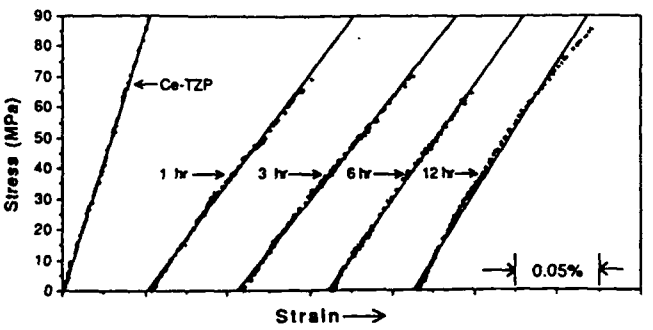

Fig. 9. Stress–strain curves for β-Ca_2SiO_4 fired at 1400°C compared to a fine-grained Ce-TZP.

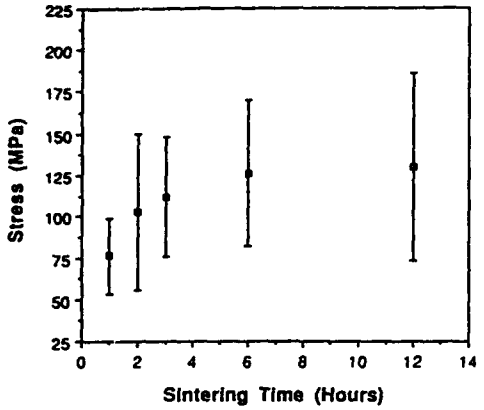

Fig. 10. Fracture stress versus sintering time for β-Ca_2SiO_4 fired at 1400°C.

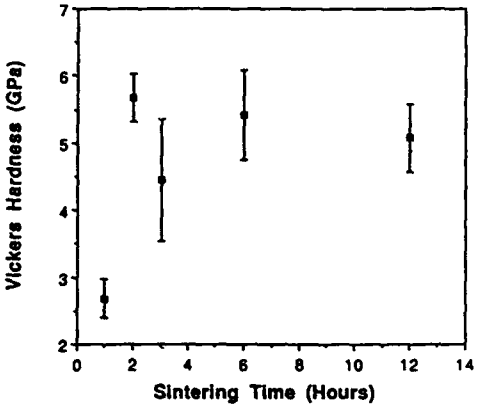

Fig. 12. Hardness of β-Ca_2SiO_4 as a function of sintering time for samples fired at 1400°C.

were polished to a 1-μm finish prior to testing. It proved to be very difficult to prepare specimens fired for 6 h or longer because the samples would dust due to the β→γ transformation prior to, during, or after machining. Indeed, the survival rate of these specimens was low and unpredictable, which suggested some increased transformability with increased sintering time.

The elastic moduli of materials fired at 1400°C also increased with sintering time. This was consistent with the increase in density on sintering for longer times. Figure 11 shows a least-squares fit to the modulus as a function of porosity using the following relationship:[20]

$$E = E_0(1 - 1.9P + 0.9P^2) \quad (1)$$

where E is Young's modulus and P is the fractional porosity. This assumes spherical pores, which was appropriate for this case because the porosity removed during sintering for the first 12 h was equiaxed. The fit was not good, but it did allow an estimate of 123 GPa for elastic modulus (E_0) of fully dense β-Ca_2SiO_4.

Figure 12 shows the hardness of these materials, which also increased with increased sintering time.

IV. Discussion

(1) Phase Distribution in the Powders

Many studies have been conducted on the effect of thermal treatment on the stability of β phase at room temperature.[21–25] Usually the Ca_2SiO_4 powders used in such studies were prepared by repeated solid-state reaction at high temperature and transformation to γ phase occurred on cooling to room temperature. Further study,[6,22–26] suggested that there was a particle size effect controlling the β→γ transformation. The results of the present study, showing that powders fired at higher temperatures (>1400°C) produced more γ phase, were consistent with such an effect. The sodium content also affected the phase distribution in powders prepared by this method and fired above 1200°C.[12]

Unfortunately, the situation could be further complicated by the cooling-rate dependence of the phase distribution for materials fired above 1400°C in the α-phase field. Powders cooled slowly tended to favor γ phase, and this result was reflected in the phase distribution in the sample fired at 1500°C in this study. Fast cooling rates gave β phase.[6,23–29] This was thought to be due to retention of the "herringbone" structures caused by the α→α_H' transformation and an inferred reduction in effective particle size.[6,24] The particle size could also be reduced by periodic microcracking across the β twins, which was thought to be caused by accumulation of strain from the α→α_H' transformation.[24,28] However, the cooling rates from the α region in this study were slow compared with those required to retain the β phase; therefore, γ phase resulted.

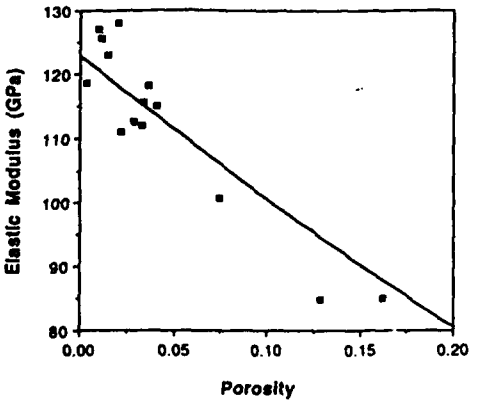

Fig. 11. Elastic moduli as a function of porosity for β-Ca_2SiO_4 fired at 1400°C.

(2) Phase Distribution and Microstructure of Dense Ca_2SiO_4

At first, it was surprising that the materials could be fired for long periods at 1400°C without transforming to the γ phase. However, if a particle size effect existed, as suggested by previous studies, then it must be kept in mind that the grain size only increased from 1 to 2 μm during the first 12 h. Estimates of the critical particle size in both powders and dense material from previous studies varied by over an order of magnitude from 0.3 μm [23,26] to 7 μm.[25] This was primarily due to the fact that the β phase was twinned, and some studies associated the critical particle size with the twin width, whereas the larger estimate was based on the grain size. The twinning made the choice of a microstructural feature in the definition of critical particle size ambiguous. Indeed, Kriven *et al.*[6] pointed out that the particle size effect may depend on grain size, twin width, twin length, or critical volume determined from twin length and twin width.

Figures 6(A) and (B) show a similar relationship between twin width and grain size for β-Ca_2SiO_4 in two independent studies. Extrapolation of the data in both studies indicated that a twin width of 0.3 μm corresponded to a grain size of approximately 7 μm. Hence, the previously quoted critical particle sizes based on twin width and grain size could be consistent since a β-Ca_2SiO_4 grain of 7 μm would correspond to twins 0.3 μm in width. The grain sizes and twin widths measured in this study were below the critical values discussed above, which was consistent with the lack of transformation to the γ phase.

The dusting of samples fired at 1450°C leads one to suspect that firing in the α region above 1425°C had some effect on the stability of the β phase. Significant amounts of γ phase did not appear in the powders or the sintered material until they were fired in the α region. Similar behavior has been observed in previous studies[22,23] and has been attributed to rapid grain growth above 1425°C. This caused the grain size to exceed the critical particle size for the β→γ transformation. Unfortunately, many of these studies used excess silica or calcia, which are known to result in a grain-boundary phase.[29] Hence, controlled grain growth studies are required to determine if materials fired in the α region grow more rapidly than for those fired in the α_H' region. Unfortunately, the dusting behavior of samples in this study prevented such an experiment because the lath morphology of the γ phase destroyed individual grains, making it impossible to distinguish the grain structure.

Another possible reason for the enhanced transformability of materials fired in the α region may be seen in the microstructure of composites.[11] These exhibited relatively more intergranular strain than those fired in the α_L' region, as seen by TEM. There was also an increase in the dislocation content. These features might be expected to destabilize the β phase relative to the γ phase.

The observations in this study only supported the contention that β-phase materials fired in the α region were more transformable. They did not provide any evidence that would distinguish the relative importance of the arguments based on grain growth versus accumulated intragranular strain.

(3) Transformability of β-Ca_2SiO_4

The effects of microstructural variables, such as grain size, on transformability have been difficult to establish, even for dense, single-phase materials fired at 1400°C. The study of stress-induced surface transformation by grinding was hard to interpret. In general, it was difficult to induce transformation, and high grinding loads were required. However, when transformation did take place, the resulting damage caused the surface of the specimen to dust. There was no correlation between sintering time and the extent of grinding-induced transformation or the frequency with which grinding caused the surface of the specimens, sintered for the same time, to dust. This apparently random behavior was inconsistent with the idea of a critical particle size. It was thought that there may be some other microstructural features that had more influence on the transformability of these single-phase materials during grinding experiments. One such feature is the severe residual intergranular strain accumulated at the grain boundaries due to the twinning accompanying the $\alpha_L' \rightarrow \beta$ transformation.

Quenching and fracture did not induce transformation in any of the samples produced in this study. This was consistent with the nature of the β→γ transformation. The β phase is metastable at atmospheric pressure,[10] and the transformation is thought to be inhibited by a high kinetic barrier that is a common characteristic of irreversible phase transformations.[30] In this case the high kinetic barrier could have been due to bond breaking and large volume change associated with the β→γ transformation.

The lack of evidence for the stress-induced β→γ transformation on fracture suggested that the observed deviation from linearity in stress–strain behavior must have been due to other stress-induced effects. Nucleation and propagation of microcracks similar to those observed in Fig. 5(B) may have been reponsible. This would account for the observations and seems quite reasonable given the large amounts of residual strain observed at the grain boundaries. It was also possible that stress-induced transformation took place during fracture, and the γ phase thus formed was debonded and fell out of all the fracture surfaces prior to examination by X-ray analysis. However, this was thought to be unlikely.

(4) Mechanical Properties of β-Ca_2SiO_4

The results suggested that the elastic moduli and hardness were controlled by the porosity as final-stage sintering continued to occur in materials fired in the first 6 h at 1400°C. This is somewhat different from the conclusion that one would arrive at by examining the TEM micrographs. These micrographs showed an increasing incidence of microcracking and microcrack coalescence as the sintering time was increased. Such cracking would be expected to cause a decrease in elastic modulus and hardness, which is contrary to the results. This could be explained if most of the microcracking and microcrack coalescence was stress-induced during TEM sample preparation and not present in the as-sintered material. It was also consistent with the nonlinearity of the stress–strain behavior prior to fracture, which was attributed to stress-induced microcracking and microcrack coalescence during loading.

The low strength results and the large scatter in the values could also be attributed to the high residual strain in the materials and the resulting stress-induced microcracking coalescence, which was thought to occur both during machining and in loading prior to failure.

V. Conclusion

In contrast to Ca_2SiO_4 produced from mixed oxide powders, the β phase was obtained in chemically prepared powders after calcination at 800°C and remained stable at room temperature even when prepared by prolonged heat treatment at 1400°C. Polycrystalline β-Ca_2SiO_4 was fabricated from such powders containing small quantities of sodium and fired to high density at 1400°C for times up to 72 h.

The dense material was predominantly β phase with some small amounts of α_L' phase, which disappeared at the longer sintering times. As the sintering time was increased above 6 h, the frequency with which samples dusted due to the β→γ transformation increased. TEM observation showed that microstructures of dense β-Ca_2SiO_4 fired at 1400°C exhibited severe intergranular strains and twin-terminating microcracks. The β-phase twin widths were quantitatively correlated with grain sizes giving an average ratio close to 0.04. A similar result was achieved in a previous study of β-Ca_2SiO_4 in a $CaZrO_3$ matrix.[18]

When the sintering temperature was increased to 1450°C, the pellets dusted on cooling after sintering for times as short as 1 h. This indicated a difference in the room-temperature stability of the β phase for materials fired in the α region.

Quenching and fracture was found to be unable to induce the β→γ transformation in dense β-Ca_2SiO_4 fired at 1400°C. This was thought to be consistent with the nature of the transformation and the concept of a high kinetic barrier. In contrast, surface transformation could be stress-induced by grinding with high loads, which commonly caused the surface of the specimen to dust. The transformability on grinding could not be correlated with a grain size effect, and it was thought that other microstructural features may have dominated the transformation behavior in these materials. The high intergranular strain accumulated at grain boundaries may have been responsible.

Careful study of the stress–strain behavior showed deviation from linearity before fracture, and it was concluded that a stress-induced phenomenon could be occurring. In the absence of evidence for stress-induced transformation, the nonlinearity was attributed to stress-induced microcracking and microcrack coalescence. This was also thought to be caused by the high residual strain at grain boundaries associated with twin formation on the $\alpha_L' \rightarrow \beta$ transformation.

The mechanical strength of the polycrystalline β phase was low, and this was consistent with the proposed stress-induced microcracking and microcrack coalescence. The increase in elastic modulus and hardness values with sintering time was consistent with the effects of porosity as the relative density rose from 90% to 99% over the first 12 h at 1400°C.

Acknowledgments: The authors would like to thank Dr. Peter Kurath of the Materials Engineering Research Laboratory, University of Illinois at Urbana-Champaign (UIUC), for assistance with the strain gauge measurements. Use of the electron microscope facilities at the Center for Microanalysis of Materials in the Materials Research Laboratory and the Center for Electron Microscopy, both at UIUC, are gratefully acknowledged.

References

[1]H. E. Schwiete, W. Kronert, and K. Deckert, "Existence Range and Stabilization of High-Temperature Modification of Dicalcium Silicate," *Zem.-Kalk-Gips*, **9**, 359–66 (1968).

[2]H. Midgley, "The Polymorphism of Calcium Orthosilicate"; pp. 1–16 in *6th International Congress on the Chemistry of Cement*, Supplement Paper I (Moscow, 1974). Stroizdat, Moscow, USSR, 1974.

[3]I. M. Pritts and K. E. Daugherty, "The Effect of Stabilizing Agents on the Hydration Rate of β-C_2S," *Cem. Concr. Res.*, **6**, 783–96 (1976).

[4]W. M. Kriven, "Possible Alternative Transformation Toughening to Zirconia: Crystallographic Aspects," *J. Am. Ceram. Soc.*, 71 [12] 1021–30 (1988).

[5]J. S. Moya, P. Pena, and S. De Aza, "Transformation Toughening in Composites Containing Dicalcium Silicate," *J. Am. Ceram. Soc.*, **68** [9] C-259–C-262 (1985).

[6]W. M. Kriven, C. J. Chan, and E. A. Barinek, "The Particle Size Effect of Dicalcium Silicate in a Calcium Zirconate Matrix"; pp. 145–55 in Advances in Ceramics, Vol. 24A, *Science and Technology of Zirconia III*. Edited by S. Sōmiya, N. Yamamoto, and H. Yanagida. American Ceramic Society, Westerville, OH, 1988.

[7]T. I. Hou and W. M. Kriven," Mechanical Properties and Microstructures of $CaZrO_3$–Ca_2SiO_4 Composites," to be published in *J. Am. Ceram. Soc.*

[8]E. S. Mast, "Development and Possible Use of Dicalcium Silicate in the Transformation Toughening of Magnesia"; M.S. Thesis. University of Illinois at Urbana-Champaign, 1991.

[9]E. A. Barinek, "The Development of Dicalcium Silicate as a Transformation Toughener"; M.S. Thesis. University of Illinois at Urbana-Champaign, 1988.

[10]F. Hanic, J. Kamard, J. Stracesky, and I. Kapralik, "The *p–T* Diagram of Ca_2SiO_4," *Br. Ceram. Trans. J.*, **86**, 194–98 (1987).

[11]Y. J. Kim, I. Nettleship, and W. M. Kriven, "Phase Transformations in Dicalcium Silicate: II, TEM Studies of Crystallography, Microstructures, and Transformation Mechanisms," *J. Am. Ceram. Soc.*, 75 [9] 2407–19 (1992).

[12]I. Nettleship, J. L. Shull, Jr., and W. M. Kriven, "Preparation and Phase Stability of Ca_2SiO_4 and Sr_2SiO_4 Powders," *J. Eur. Ceram. Soc.*, in press.

[13]D. M. Roy and S. O. Oyefesobi, "Preparation of Very Reactive Ca_2SiO_4 Powders," *J. Am. Ceram. Soc.*, **60** [3–4] 178–80 (1977).

[14]D. Kralj, B. Matkovic, R. Trojko, J. F. Young, and C. J. Chan, "Preparation of Dicalcium Silicate at 950°C," *J. Am. Ceram. Soc.*, **69** [8] C-170–C-172 (1986).

[15]C. M. Midgley, "The Crystal Structure of β-Dicalcium Silicate," *Acta Crystallogr.*, **5**, 307–12 (1952).

[16]Y. Fu, A. G. Evans, and W. M. Kriven, "Microcrack Nucleation in Ceramics Subject to a Phase Transformation," *J. Am. Ceram. Soc.*, **67** [9] 626–30 (1984).

[17]G. W. Groves, "Phase Transformations in Dicalcium Silicate," *J. Mater. Sci.*, **18**, 1615–24 (1983).

[18]C. J. Chan, "Effect of Phase Transformations, Chemical Doping, and Matrix Constraint on the Microstructural Development of Dicalcium Silicate"; Ph.D. Thesis. University of Illinois at Urbana-Champaign, 1989.

[19]P. E. Reyes-Morel and I-W. Chen, "Transformation Plasticity of CeO_2-Stabilized Tetragonal Zirconia Polycrystals: I, Stress Assistance and Autocatalysis," *J. Am. Ceram. Soc.*, **71** [5] 343–53 (1988).

[20]J. K. MacKenzie, "The Elastic Constants of a Solid Containing Spherical Holes," *Proc. Phys. Soc. London*, **B63**, 2–11 (1950).

[21]V. I. Korneev and E. B. Bygalina, "Thermal Stability of β-$2CaO{\cdot}SiO_2$"; pp. 285–88 in *Proceedings of the 5th International Symposium on Chemistry of Cements*, Vol. 1 (Tokyo, Japan, 1968). Cement Association of Japan, Tokyo, Japan, 1969.

[22]S. Chromy, "The Inversion of the β→γ Modification of Dicalcium Silicate" (in Ger.), *Zem. Kalk-Gips*, **23**, 382–89 (1970).

[23]M. Gawlicki and W. Nocon-Wczelik, "Influence of Thermal Treatment on the Transition of β→γ C_2S" (in Fr.); pp. 161–65 in *Proceedings of the 7th International Symposium on Chemistry of Cements*, Vol II (Paris, France). Editions Septima, Paris, France, 1980.

[24]C. J. Chan, W. M. Kriven, and J. F. Young, "Physical Stabilization of the β to γ Transformation in Dicalcium Silicate," *J. Am. Ceram. Soc.*, 75 [6] 1621–27 (1992).

[25]S. Shibata, K. Kishi, K. Asaga, and M. Daimon, "Effect of Thermal History on β→γ Transformation of Pure Ca_2SiO_4" (in Jpn.), *Yogyo Kyokaishi*, **91**, 497–502 (1983).

[26]M. Gawlicki, "The Role of Thermal Treatment on Dicalcium Silicate Polymorphic Transitions"; pp. 67–73 in *Proceedings of the 14th Conference on Silicate Industry and Silicate Science, III* (Budapest, Hungary). OMIKK-Technoinform, Budapest, Hungary, 1985.

[27]G. W. Groves, "Twinning in β-Dicalcium Silicate," *Cem. Concr. Res.*, **12**, 619–24 (1982).

[28]C. J. Chan, W. M. Kriven, and J. F. Young, "Microstructure Characterization of Non-Stoichiometric Dicalcium Silicates Doped with Aluminum Oxide"; pp.452–53 in *Proceedings of the 44th Annual Meeting of the Electron Microscopy Society of America* (Albuquerque, NM, 1986). San Francisco, CA, 1986.

[29]C. J. Chan, W. M. Kriven, and J. F. Young, "Analytical Electron Microscopic Studies of Doped Dicalcium Silicate," *J. Am. Ceram. Soc.*, **71**, 713–19 (1988).

[30]C. N. R. Rao and K. J. Rao, *Phase Transformations in Solids—An Approach to the Study of Chemistry and Physics of Solids*; Ch. 2. McGraw-Hill, New York, 1978. □

journal

Reprinted from the Journal of the American Ceramic Society, Vol. 75, No. 9, September 1992

J. Am. Ceram. Soc., 75 [9] 2407–19 (1992)

Phase Transformations in Dicalcium Silicate: II, TEM Studies of Crystallography, Microstructure, and Mechanisms

Youn Joong Kim,* Ian Nettleship,*,† and Waltraud M. Kriven*

Department of Materials Science and Engineering, University of Illinois at Urbana-Champaign, Urbana, Illinois 61801

The crystallography, microstructures, and phase transformation mechanisms in dicalcium silicate (Ca_2SiO_4) were studied by TEM. Three types of superlattice structures were observed in the α_L' and β phases. Almost all β grains were twinned and strained. Symmetry-related domain structures inherited from previous high-temperature transformations were observed in β grains. Both the $\alpha \rightarrow \alpha_H'$ and $\alpha_L' \rightarrow \beta$ transformations were considered to be ferroelastic, and spontaneous strains were calculated. In terms of the crystal structures, the major driving force for the $\beta \rightarrow \gamma$ transformation is proposed to be strains and cation charge repulsions in the β structure. This mechanism can be displacive, but it needs to overcome a comparatively high energy barrier.

I. Introduction

DICALCIUM SILICATE (Ca_2SiO_4) is a major component of portland cement that has been studied for a long time. However, considerable confusion and lack of understanding exist in the literature regarding the crystal structures and microstructures as well as transformation behavior between its polymorphs. As an orthosilicate, Ca_2SiO_4 has an unusually large number of polymorphs, viz., α, α_H', α_L', β, and γ. For comparison, olivine (Mg_2SiO_4), a typical orthosilicate mineral, has only one stable phase (the orthorhombic γ phase) throughout the entire temperature range, from room temperature to the melting point. Most microstructural studies of Ca_2SiO_4 have been limited to the stabilized β and α_L' phases, because of the difficulty in retaining solid samples of the other phases at room temperature. The dusting effect due to a large volume increase accompanying the $\beta \rightarrow \gamma$ transformation has been observed, but the transformation mechanism itself is poorly understood.

There are many different reports on the polymorphism, microstructures, and phase transformations in Ca_2SiO_4,[1] possibly due to (i) different macrostructures and microstructures of the starting materials, such as different grain sizes;[2,3] (ii) different chemistry of the starting materials, especially the presence of impurities;[4] and (iii) different processing conditions, in particular, cooling kinetics.[3] Nevertheless, five polymorphs of pure Ca_2SiO_4 have been widely observed, including the metastable, high-pressure β phase. Table I lists crystallographic data of each polymorph from the literature.[5–16] Several different choices of crystallographic axes have been used in describing these polymorphs, especially the orthorhombic structures. As a working model for this study, one space group is chosen for each polymorph, and these polymorphs are correlated to one another. Figure 1 schematically displays the geometries of these polymorphs and the reported lattice correspondences among them. Figure 1 shows the interchange of *b* and *c* axes between the two orthorhombic phases (α_L' and γ) and the monoclinic β phase. Since the *b* axis of the β phase is the highest symmetry axis in conventional crystallographic notation, which corresponds to the *c* axes of the other phases, there is actually no switching of axes by the transformation in this system.

The following points summarize some of the current problems in the crystal structures and microstructures that are relevant to this study:

(1) The crystal structure of α has not yet been firmly determined. Three space groups for the structure have been suggested: $P6_3/mmc$,[6] $P6_3mc$,[17] or $P\bar{3}m1$.[5]

(2) No report of a structural refinement of α_H' exists, but a space group of *Pmcn* has been assigned[5] based on high-temperature powder XRD data.

(3) Two superlattice models have been proposed for the α_L' structure referring to the α_H' lattice: (i) doubling of the *a* and *b* axes ($\times 2a, 2b$-type) with a space group *Pmcn*[5] and (ii) tripling of the *c* axis ($\times 3c$-type) with a space group $P2_1cn$.[11]

(4) Two different twinning modes of β-Ca_2SiO_4 have been reported: (i) both {100}-type and {001}-type twinning[18] or (ii) only {100}-type twinning.[13,19]

(5) The suggested transformation mechanisms among the polymorphs are generally (i) a semireconstructive mechanism between α and α_H';[17] (ii) an order–disorder transformation mechanism between α_H' and α_L';[17] (iii) a displacive, possibly martensitic mechanism between α_L' and β;[17,20] and (iv) a reconstructive[17] or displacive[21] mechanism for $\beta \rightarrow \gamma$.

The objective of this study is to address the above-listed problems through an in-depth TEM characterization of various Ca_2SiO_4 samples. The approach is to understand these problems as a part of the entire sequence of phase transformations in the Ca_2SiO_4 system. A special intention is to understand the $\beta \rightarrow \gamma$ transformation in terms of crystal structures and the mechanisms involved. It is an unusual, low- to high-symmetry transformation accompanied by a large volume increase (~12%) on cooling.

II. Experimental Methods

Three groups of samples were studied: (i) pellets of fine-grained, single-phase Ca_2SiO_4, sintered between 1300° and 1450°C for 1 min to 12 h;[22] (ii) pellets of Ca_2SiO_4, doped with 1 to 5 mol% Ba_2SiO_4 and sintered between 1300° and 1400°C for 1 to 3 h;[23] and (iii) composites of Ca_2SiO_4 (15 vol%) in an MgO matrix, sintered at 1600°C for 3 h,[24] and composites of Ca_2SiO_4 (10 vol%) in a $CaZrO_3$ matrix, sintered at 1600°C for 2 h.[25]

All pellets were examined by TEM (Model EM-430 (300 kV), Philips Instruments, Inc., Mahwah, NJ; Model EM-420 (120 kV), Philips Instruments, Inc., with EDS Model EDAX-9900, EDAX International, Inc., Prairie View, IL; Model EM-400T (120 kV), Philips Instruments, Inc.; and Model 600 (100 kV), Hitachi Instruments, Inc., Conroe, TX,

M. P. Harmer—contributing editor

Manuscript No. 196055. Received January 13, 1992; approved May 11, 1992.
Presented at the 93rd Annual Meeting of the American Ceramic Society, Cincinnati, OH, April 29 to May 2, 1991 (Basic Science Division, Paper Nos. 122-B-91 and 123-B-91). Also presented at Fall Symposium of the American Ceramic Society, Marco Island, FL, October 15–18, 1991 (Basic Science Division, Paper No. 10-BP-91F).
Supported by the U.S. Air Force Office of Scientific Research through a URI Grant No. AFOSR-90-0174.
*Member, The American Ceramic Society
†Present address: Department of Materials Science and Engineering, University of Pittsburgh, Pittsburgh, PA 15261.

Table I. Crystallographic Data from the Literature for Ca_2SiO_4 Polymorphs

Polymorph (crystal system)[a]	Space group	Lattice parameters[†]				T_{rxn} (°C)[‡]	Sample[§]	Reference
		a (Å)	b (Å)	c (Å)	β (deg)			
α	$P\bar{3}m1$	5.526		7.307		1500	Powder	5
	$P6_3/mmc$	5.579		7.150		RT	Single xl[a]	6
α_H'	$Pmcn$	5.593	9.535	6.860		1250	Powder	5
	$Pnma$	6.748	5.494	9.261		1330	Powder	7
	?	11.227	6.865	19.110		1270	Powder	8
	$Pcmn$	9.49	5.59	6.85		1200	Powder	9
α_L'	$Pmcn$	11.184	18.952	6.837		1000	Powder	5
	?	11.207	6.849	18.952		1020	Powder	8
		11.150	6.820	18.822		770		
	$Pcmn$	9.48	5.59	20.49		1000	Powder	9
		9.41	5.53	20.43		800		
	$Pmcn$?	5.48	9.27	20.40		RT	Powder[b]	10
	$P2_1cn$	5.566	9.355	20.569		RT	Single xl[c]	11
	$Pna2_1$	20.863	9.500	5.601		RT	Single xl[c]	12
β	$P2_1/n$	5.554	6.813	9.421	93.60	650	Powder	5
		5.506	6.749	9.304	94.62	RT		
	?	5.544	6.802	9.419	93.28	720	Powder	8
		5.512	6.752	9.294	93.34	RT		
	$P2_1/n$	5.502	6.745	9.297	94.59	RT	Single xl	13
γ	$Pcmn$	5.085	6.773	11.237		RT	Powder	5
	$Pbnm$	5.091	11.371	6.78		RT	Single xl	14
	$Pbnm$	5.078	11.225	6.760		RT	Single xl	15
	$Pbnm$	5.081	11.224	6.778		RT	Single xl	16

[a] α is hexagonal, α_H', α_L', and γ are orthorhombic and β is monoclinic. [†] 1 Å = 10^{-1} nm [‡] RT is room temperature. [§] xl is crystal, a is barium-stabilized Ca_2SiO_4, b is $Na_2P_2O_7$-stabilized Ca_2SiO_4, and c is strontium-stabilized Ca_2SiO_4.

with EDS Model TN-5500, Tracor Northern Co., Middletown, WI) to study the crystal structures, microstructures, and microchemistry. Ion-thinned foils (Model 600 dual ion miller, Gatan, Inc., Pleasanton, CA) were prepared from all specimens for TEM observation.

III. Results

(1) Overview

Of the five polymorphs of Ca_2SiO_4, α_L', β, and γ were studied by TEM. The two types of superlattice for α_L' were both present: (i) the $\times 2a,2b$-type in composites of $Ca_2SiO_4/CaZrO_3$ and (ii) the $\times 3c$-type in Ba_2SiO_4-doped Ca_2SiO_4 samples. Twinned β grains were found throughout the samples, but all showed a superlattice structure that was not previously reported. Transformed γ grains retained in single-phase Ca_2SiO_4 samples showed the known γ crystal structure. Interfaces of α_L'/β, untwinned-β/twinned-β, and β/γ phases were identified and studied to establish lattice correspondences.

Untwinned, euhedral α_L' grains were found in Ba_2SiO_4-doped samples. In single-phase Ca_2SiO_4, twinned β grains were mostly euhedral, but their grain boundaries were highly strained. Most β grains showed {100} twinning, but some clearly showed {001} twinning. Two twinned domains coexisted in some β grains. Microcracks tended to develop along grain boundaries as the grain size increased at longer sintering times. β grains in composites sintered in the α region were also twinned. They were more elongated and strained as compared to those in the single-phase Ca_2SiO_4. High concentrations of defects and numerous microcracks were observed. In addition, symmetry-related domain structures of β grains were often observed. Large cracks were frequently present around the transformed γ grains. Whereas β grains were mostly twinned, γ grains were untwinned and strain-free, but the latter usually contained some planar defects.

(2) Crystallography

(A) α_L' Phase: Remnants of the untwinned α_L' phase surrounded by the twinned β domains were occasionally observed in composites of $Ca_2SiO_4/CaZrO_3$. Figure 2 illustrates one of

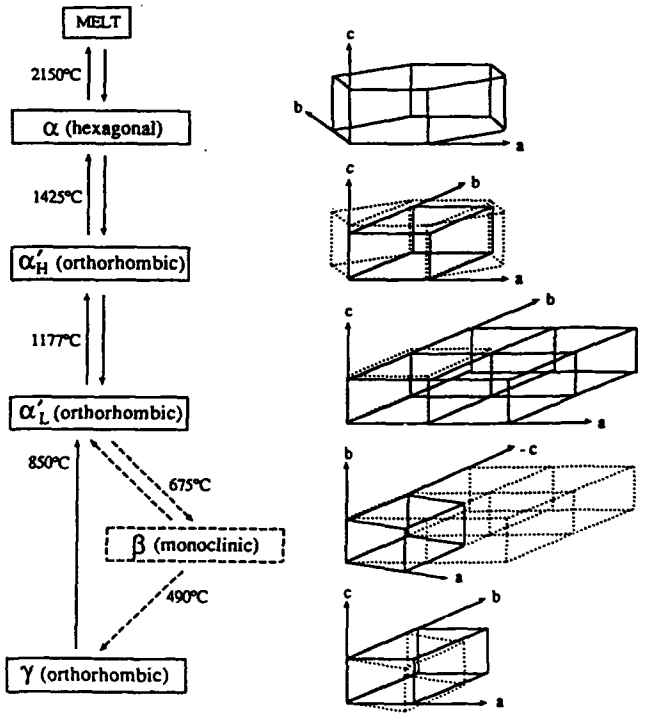

Fig. 1. Schematic diagram of the geometries and lattice correspondences for the five Ca_2SiO_4 polymorphs, including the metastable β phase.

these microstructures. The $[001]_{\alpha_L'}$ SADP indicated the presence of the $\times 2a,2b$-type superlattice of α_L'. Doubling of the {100} and {010} planes was evident by comparison with the corresponding $[010]_\beta$ SADP. By tilting the specimen along the b axis of α_L', only a doubling of the {100} planes was detected. This was clearly displayed in the $[014]_{\alpha_L'}$ SADP compared to the corresponding $[021]_\beta$ SADP. The surrounding β domains were

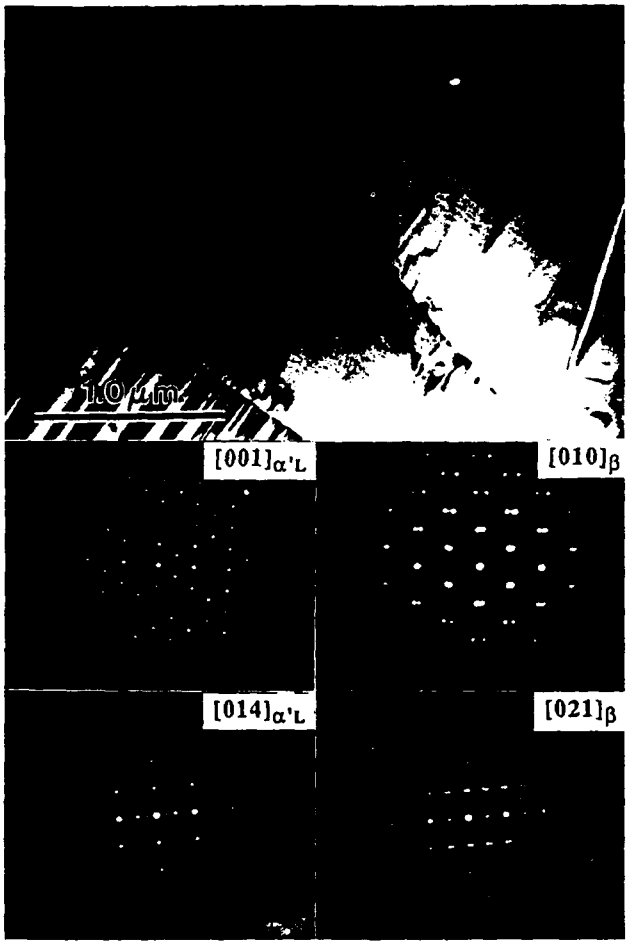

Fig. 2. Interfaces between the untwinned α_L' and the twinned β domains and the corresponding SADPs: $[001]_{\alpha_L'}$ vs $[010]_\beta$ and $[014]_{\alpha_L'}$ vs $[021]_\beta$ (from a $Ca_2SiO_4/CaZrO_3$ composite sintered at 1600°C for 2 h).

symmetrically related by a 120° rotation. These domain microstructures are explained in the next section.

SADPs from untwinned α_L' grains of a Ba_2SiO_4-doped specimen showed another type of superlattice reflections. In Fig. 3, the $[100]_{\alpha_L'}$ SADP clearly displayed a tripling of the {001} planes, that is, the $\times 3c$-type α_L' superlattice. These superlattice reflections were shown whenever the $\{001\}_{\alpha_L'}$ planes were in the reflecting condition, such as in the $[120]_{\alpha_L'}$. The $[001]_{\alpha_L'}$ SADP indicated the absence of the $\times 2a,2b$-type superlattice in this specimen.

(B) β Phase: The superlattice structure of β phase was totally unexpected, not only because it had not been reported before, but also because the β phase had been most extensively studied in the Ca_2SiO_4 system. β grains from all the available samples observed, however, showed superlattice reflections. In contrast to the superlattice reflections of α_L'—which were evident in SADPs of the principal zone axes, such as $[001]_{\alpha_L'}$ or $[100]_{\alpha_L'}$—those of β did not appear in SADPs of the principal zone axes, such as $[100]_\beta$, $[010]_\beta$, or $[001]_\beta$. However, when the specimens were tilted to intersect either the $\{10\bar{3}\}_\beta$ or $\{103\}_\beta$ planes, such as the $[311]_\beta$ or $[\bar{3}11]_\beta$ orientations, superlattice reflections were visible at the 1/3 positions along the $\{10\bar{3}\}_\beta^*$ or $\{103\}_\beta^*$ directions. Figure 4 displays the six major orientations showing these superlattice reflections.

(C) γ Phase: Solid samples of γ phase were normally not retainable because of the shattering effect of the large volume increase accompanying the β→γ transformation. However, a few transformed γ grains were retained among the β grains in some single-phase Ca_2SiO_4 samples. The SADPs from the γ

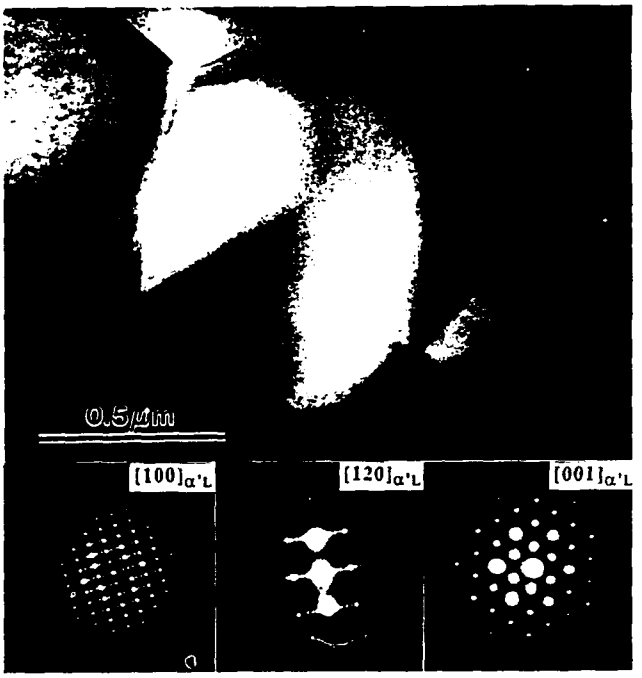

Fig. 3. Untwinned euhedral α_L' grains and the SADPs of the $\times 3c$-type α_L' superlattice: [100], [120], and [001] (from a Ba_2SiO_4-doped (5 mol%) Ca_2SiO_4 sample sintered at 1300°C for 3 h).

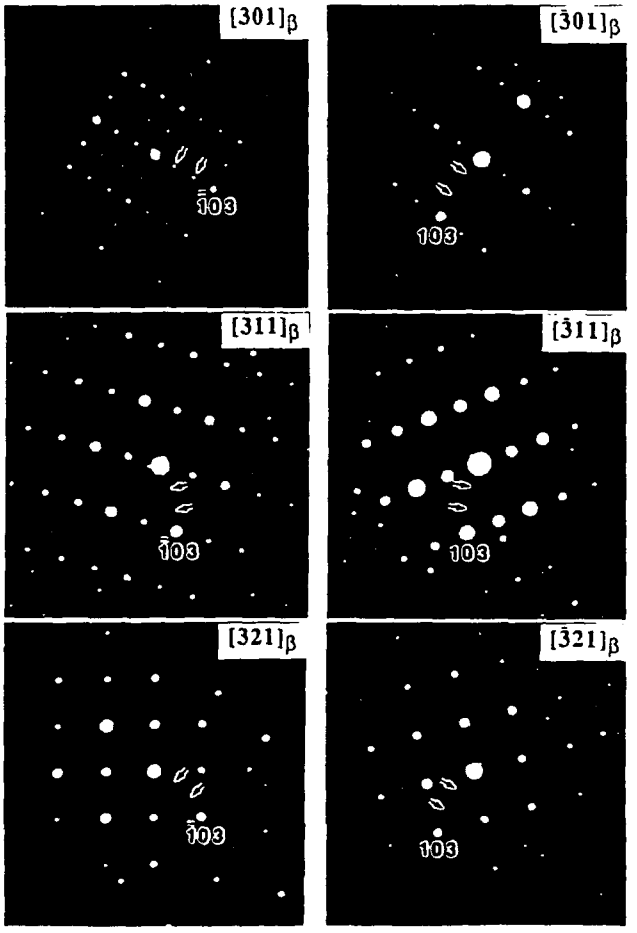

Fig. 4. [301]–[311]–[321] and $[\bar{3}0\bar{1}]$–$[\bar{3}11]$–$[\bar{3}21]$ SADPs of the β phase showing a tripling of both (10$\bar{3}$) and (103) planes (arrowed).

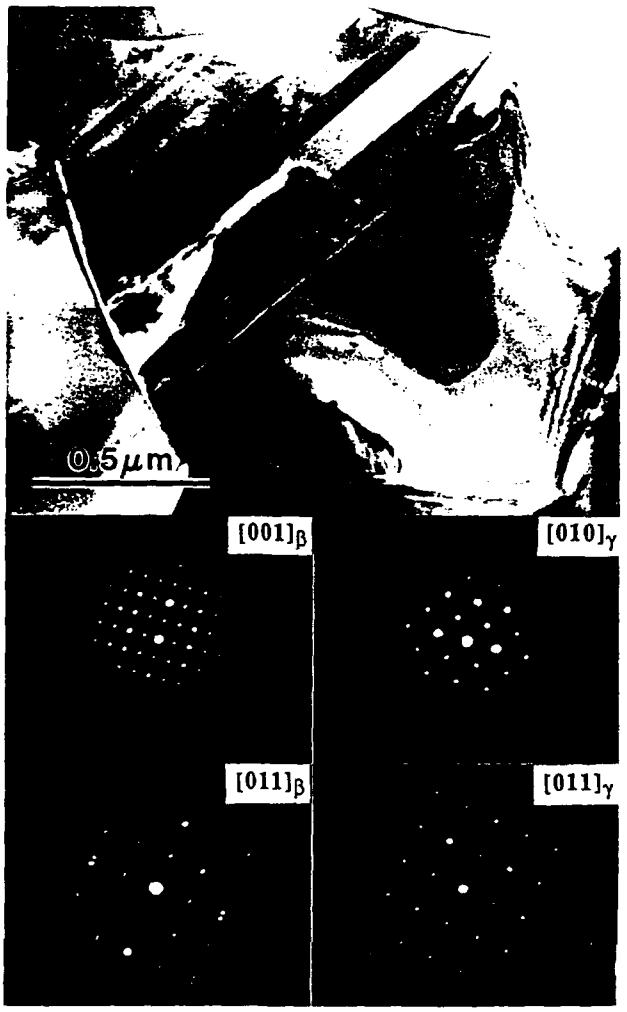

Fig. 5. Interface between the β phase and the transformed γ phase and the corresponding SADPs in two different orientations: $[001]_\beta$ vs $[010]_\gamma$ and $[011]_\beta$ vs $[0\bar{1}1]_\gamma$.

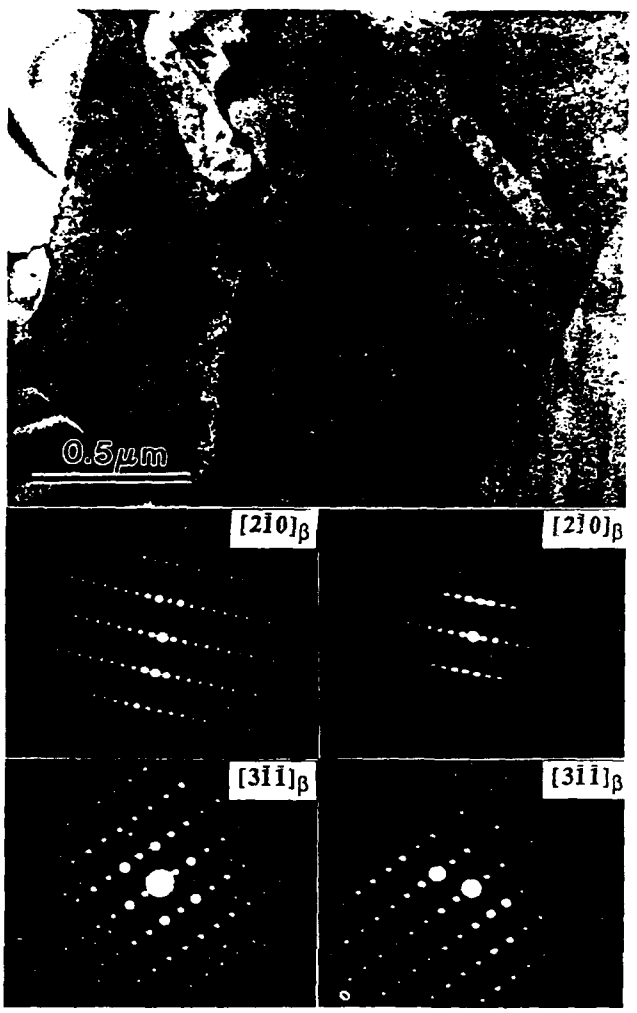

Fig. 6. Interface between the untwinned β phase and the (001)-twinned β phase. Corresponding $[2\bar{1}0]$ and $[3\bar{1}\bar{1}]$ SADPs are shown.

grains were consistent with the reported structure and the XRD results. Occasionally, the transformed γ phase and the untransferred β phase coexisted in a single grain, as shown in Fig. 5. The SADPs from these two parts showed the orientation relationship between the two phases to be $[001]_\beta \| [010]_\gamma$. The $[011]_\beta$ SADP obtained by tilting the same grain closely resembled the $[011]_\gamma$ SADP, except for the additional $\{100\}_\beta$-type twinned reflections.

(D) Interfaces and Lattice Correspondences: The interfaces between α_L' ($\times 2a, 2b$) and β were sharp and straight, as shown in Fig. 2, and not noticeably strained or cracked. The following relationship was observed:

$$[001]_{\alpha_L'} \| [010]_\beta \text{ such that } (020)_{\alpha_L'} \| (00\bar{2})_\beta \text{ and } (200)_{\alpha_L'} \| (200)_\beta$$

As a result, a possible lattice correspondence could be

$$a_{\alpha_L'} \| a_\beta^*,\ b_{\alpha_L'} \| -c_\beta, \text{ and } c_{\alpha_L'} \| b_\beta$$

which agreed with previous single-crystal X-ray precession work.[26]

The interfaces between β and γ were also sharp but always showed some microcracks. The interface shown in Fig. 5 has the following relationship:

$$[001]_\beta \| [010]_\gamma \text{ such that } (010)_\beta \| (00\bar{2})_\gamma \text{ and } (100)_\beta \| (200)_\gamma$$

This result gave rise to a possible lattice correspondence:

$$a_\beta^* \| a_\gamma,\ b_\beta \| -c_\gamma, \text{ and } c_\beta \| b_\gamma$$

which also agreed with previous single-crystal X-ray precession work.[26]

The untwinned β phase had not been previously reported. However, several β grains containing an untwinned portion and a twinned portion were observed in this study. Figure 6 illustrates one such grain, in which both portions had similar orientations. As shown in the $[2\bar{1}0]_\beta$ SADP, the twinned portion typically had the {001}-type twinning instead of the more popular {100}-type twinning. The $[3\bar{1}\bar{1}]_\beta$ SADPs from both portions also showed the previously mentioned superlattice reflections.

(3) Microstructures

(A) α_L' Phase: The euhedral α_L' grains observed in 5-mol%-Ba_2SiO_4-doped samples (sintered at 1300°C for 3 h) were not twinned. Grain boundaries were well-defined and strain-free (Fig. 3). No apparent grain-boundary phases were noticed. EDS analyses showed barium peaks within grains, indicating that barium was in solid solution.

(B) β Phase: In single-phase Ca_2SiO_4, almost all euhedral β grains were twinned, and their grain boundaries were highly strained (Fig. 7(A)). Grain growth on longer sintering times gave rise to a development of microcracks along the grain boundaries (Fig. 7(B)). Both twin types, {100} and {001}, were observed, but the {100}-type was observed more frequently.

To study the relative populations of the two main twin types occurring in β, 100 grains were randomly chosen from various samples and examined by TEM. Grain sizes and average twin widths were also measured and correlated. The results showed that 87 grains were {100} twinned, and 13 grains were {001}

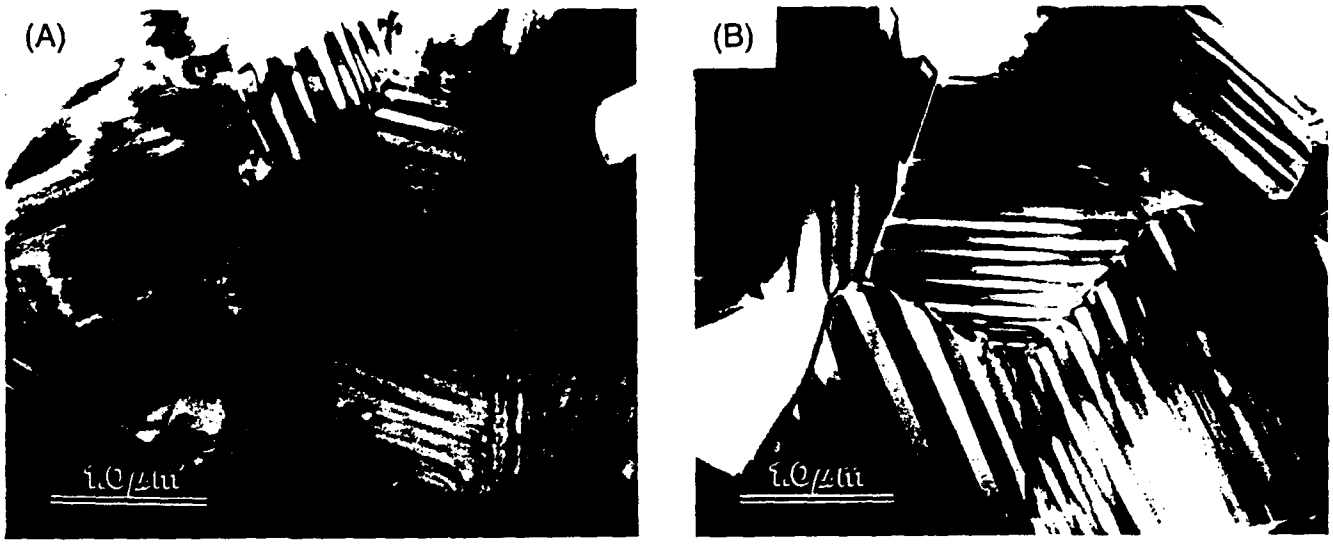

Fig. 7. Twinned euhedral β grains showing strains and microcracks along grain boundaries (from single-phase Ca_2SiO_4 samples sintered at 1400°C for (A) 1 and (B) 3 h).

twinned. The twin widths correlated positively with the grain sizes. For the same grain size, the twin width of the {001}-type was generally a little larger than that of the {100}-type (Fig. 8).

Several β grains from the pure Ca_2SiO_4, which experienced the $\alpha_L' \rightarrow \beta$ transformation, showed domain structures of the two twin types. Figure 9 shows a single grain composed of the two twin types that had the same [010] orientation. Twin lamellae at the interface terminated in wedges.

Samples from the composites that experienced the $\alpha \rightarrow \alpha_H'$ transformation displayed another type of domain structure of twinned β. Figure 10 shows a typical domain structure where three domains had the same [010] orientation but were related to one another by 120° rotations. Each domain was {100}-twinned and its twin lamellae were matched with the lamellae of the adjacent domains. The domain boundaries, however, were rather curved.

Euhedral β grains in single-phase Ca_2SiO_4 were internally strained and sometimes showed streaking in the SADPs. In composites, twinned β grains were more elongated and more internally strained. Figure 11 displays the internal strain of a β grain in one such composite that gave rise to two-directional streaking in the [010] SADP, both parallel and perpendicular to {200}*. Because of this internal strain, the grains were so unstable under the electron beam that amorphous ring patterns were rapidly produced (e.g., Fig. 10). Whereas the Ca_2SiO_4/MgO composites contained a higher concentration of defects, such as dislocations with β grains, the Ca_2SiO_4/$CaZrO_3$ composites contained numerous microcracks, both within and around β grains (Fig. 12).

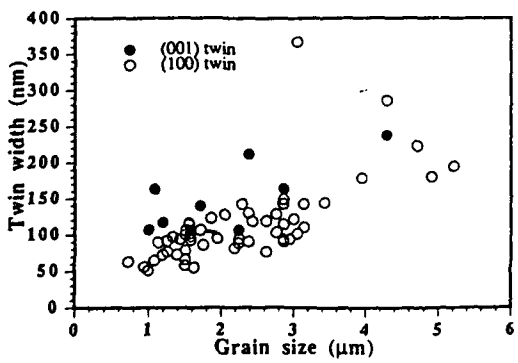

Fig. 8. Plot of grain sizes versus twin widths measured from β grains of various samples ((○) {100}-twinned grains and (●) {001}-twinned grains).

(C) γ Phase: Frequently, γ grains in single-phase Ca_2SiO_4 were surrounded by large microcracks because of the large volume increase of the $\beta \rightarrow \gamma$ transformation (Fig. 13). Twinning in β grains disappeared during this transformation. γ grains usually showed a clear appearance without strain contrast and produced sharp SADPs. However, the γ grains contained some planar defects. These planar defects were possibly related to the previous twins in the β structure. Figure 14(A) shows apparent similarity between twin planes of the untransformed β part and a planar defect of the transformed γ part in a single grain. Figure 14(B) also indicates that twin lamellae in one grain tended to match across the neighboring grains (arrowed). The complex shapes and fringe patterns of planar defects in Fig. 14(C) suggested that the nature of the defect was related to faults formed by the detwinning process during the $\beta \rightarrow \gamma$ transformation.

IV. Discussion

(1) Crystallography

(A) α_L' Phase: This study has shown that two superlattices of α_L' are present independently. This is contrary to the previous suggestion that the high-temperature X-ray diffractograms of α_L' could be indexed in two ways, i.e., based either on the $\times 2a,2b$-type cell or on the $\times 3c$-type cell.[9,21] Calcium displacements have been suggested to be a possible origin for the $\times 2a,2b$-type superlattice.[5] The $\times 3c$-type superlattice in α_L' has been attributed to tilting or rotation of SiO_4 tetrahedra.[9] It is still uncertain as to whether there is any relationship between these superlattice types and their chemistry. However, this study and previous reports show some tendency for the $\times 2a,2b$-type in purer Ca_2SiO_4 and for the $\times 3c$-type in doped Ca_2SiO_4.

(B) β Phase: A tripling of both $\{10\bar{3}\}$ and {103} planes in β could have originated from the tripling of the *a* axis. Figure 15(A) shows this geometrical relationship. Since the $\alpha_L' \rightarrow \beta$ transformation involved the interchange of *b* and *c* axes, the superlattice structure occurring in β was not the same type as that occurring in α_L'. Considering that all of the solid samples studied should have experienced the $\alpha_L' \rightarrow \beta$ transformation, this superlattice may have originated from another unreported type of superlattice in α_L', i.e., the $\times 3a$-type. Alternatively, it could have formed during the $\alpha_L' \rightarrow \beta$ transformation.

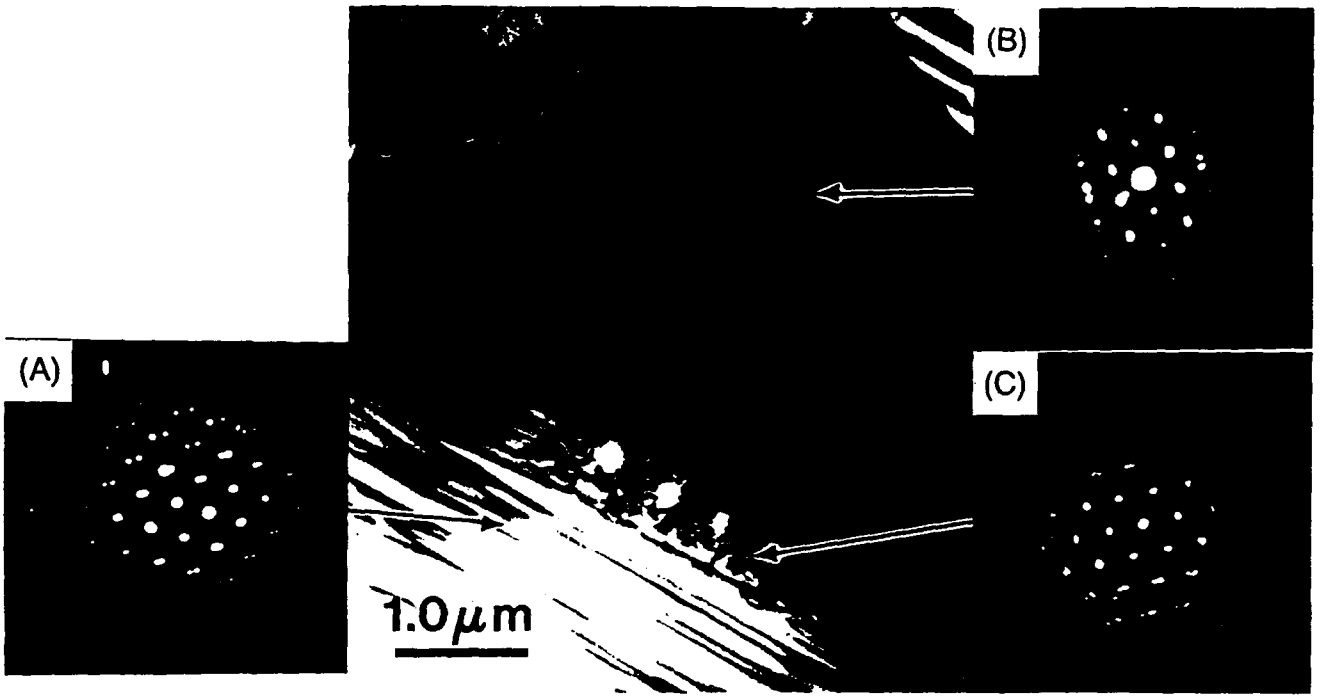

Fig. 9. Two twin domains of the β grains and SADPs from (A) (100)-twinned domain, (B) (001)-twinned domain, and (C) interface (from a single-phase Ca_2SiO_4 sample sintered at 1400°C for 12 h).

The (010) projection of the β structure in Fig. 15(B) displayed $\{10\bar{3}\}$ and $\{103\}$ planes, which may have been responsible for the superlattice reflections. In fact, both planes were closely related to the arrangements of silicon in SiO_4 tetrahedra and adjacent calcium. Being analogous to the $\times 3c$-type of α_L', systematic tilting of SiO_4 tetrahedra along the direction perpendicular to $\{10\bar{3}\}$ or $\{103\}$ planes may have been an origin of this threefold modulation. The lack of superlattice reflections along the a^* direction was possibly related to the predominant {100} twinning or to systematic absences.

(C) γ Phase: The crystal structure of γ was well established. The diffraction data obtained from the γ phase correspond well to previous reports. No superlattice reflections were observed in γ-Ca_2SiO_4.

(2) Microstructures

(A) Intergranular Strains in β: The intergranular strains observed in single-phase β-Ca_2SiO_4 could be attributed to an anisotropic and large thermal expansion. From the lattice parameter data[5] given in Table I, the calculated thermal expansion coefficients of the β-Ca_2SiO_4 are

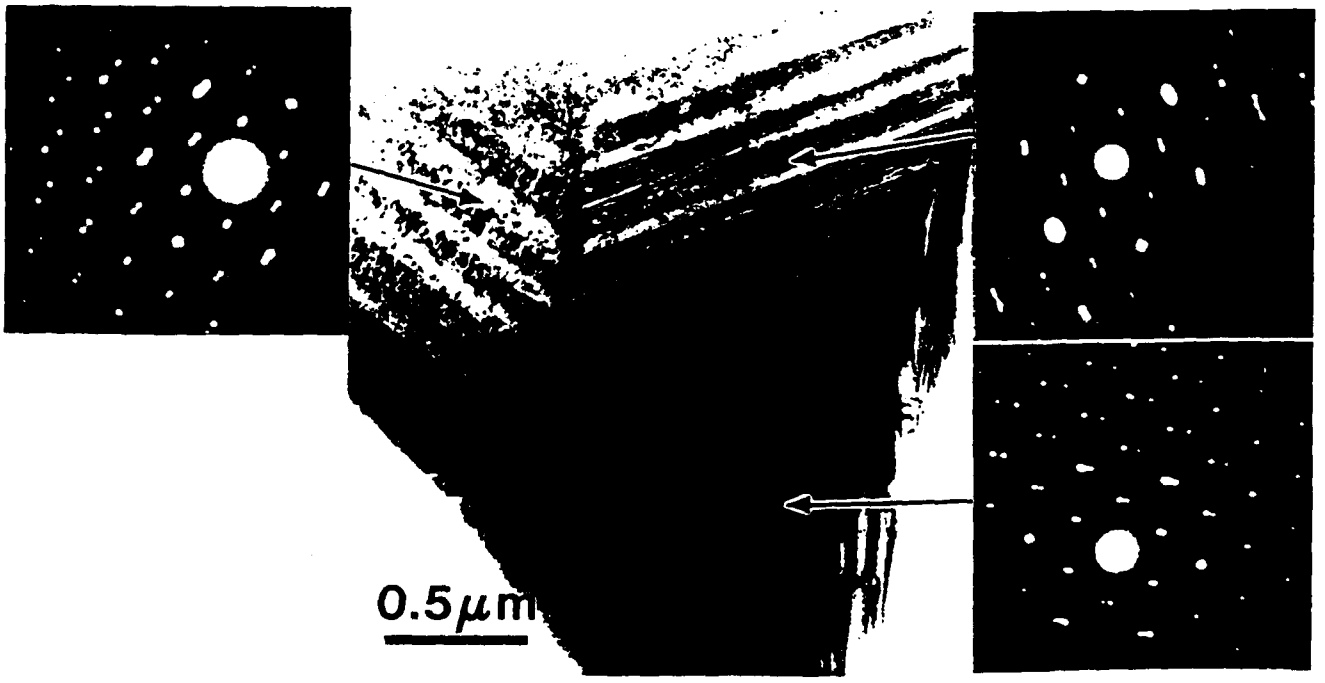

Fig. 10. Three domains related by 120° rotation along the *b* axis of β (from a Ca_2SiO_4/MgO composite sintered at 1600°C for 3 h).

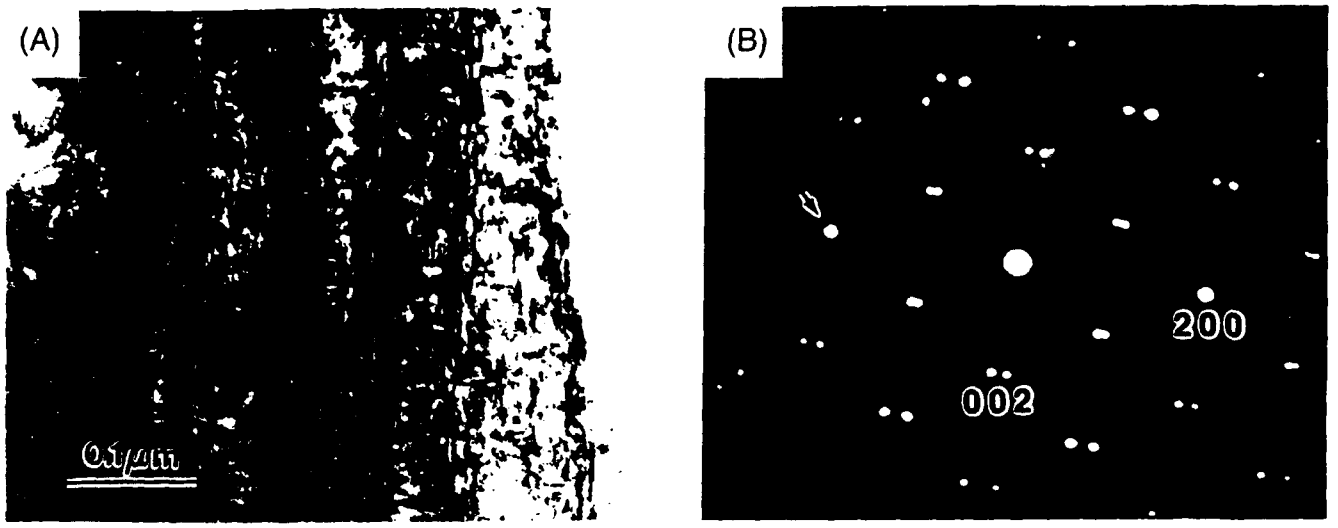

Fig. 11. (A) Strained and twinned β grain and (B) corresponding SADP showing two-directional streaking (arrow), both parallel and perpendicular to (200)* (from a Ca_2SiO_4/MgO composite sintered at 1600°C for 3 h).

$\alpha_a = 13.9 \times 10^{-6}\ °C^{-1}$
$\alpha_b = 15.2 \times 10^{-6}\ °C^{-1}$
$\alpha_c = 20.1 \times 10^{-6}\ °C^{-1}$
α_l (average) $= 16.4 \times 10^{-6}\ °C^{-1}$
$\alpha_v = 51.8 \times 10^{-6}\ °C^{-1}$

This α_l value corresponds to the linear thermal expansivity of CaO_x polyhedra ($\sim 15 \times 10^{-6}\ °C^{-1}$).[27] Since strains were accumulated as the grains grew, microcracks could easily be generated to release the strains. The intragranular strains were possibly related to the spontaneous strains produced by the ferroelastic transformations, which are discussed in the next section.

(B) Domain Structures in β: The domain structures observed in β grains of single-phase Ca_2SiO_4 (Fig. 9) were probably related to the $\alpha_L' \rightarrow \beta$ transformation. The symmetry elements in α′ ({100}- and {001}-mirror planes in this case) were replaced by twin elements in β. Domain structures observed in β grains of composites (Fig. 10) could have been formed during the $\alpha \rightarrow \alpha_H'$ (hexagonal→orthorhombic) transformation, when a symmetry element (three-fold rotation) was lost, producing three symmetry-related domains, as proposed by Groves.[19] All domains later experienced the $\alpha_L' \rightarrow \beta$ transformation, producing $\{100\}_\beta$ twins within each domain. Figure 16 summarizes possible configurations of domain formations resulting from $\alpha \rightarrow \alpha_H'$ and $\alpha_L' \rightarrow \beta$ transformations. Figure 16(B) shows that there could be two possible shear mechanisms, i.e., shearing along the a_α· direction or along the b_α· direction.

Based on lattice parameter data,[5] the strain tensor components (ε_{ij}) of the transforms can be calculated as follows:[28]

$$\varepsilon_{ij} = \begin{bmatrix} 0.012 & 0 & 0 \\ 0 & 0.002 & 0 \\ 0 & 0 & -0.058 \end{bmatrix} \quad \text{for } \alpha \rightarrow \alpha_H'$$

$$\varepsilon_{ij} = \begin{bmatrix} 0.0010 & 0 & -0.0317 \\ 0 & 0.0012 & 0 \\ -0.0317 & 0 & -0.0067 \end{bmatrix}$$

for $\alpha_L' \rightarrow \beta$ by $[a_\alpha\cdot]$ shearing

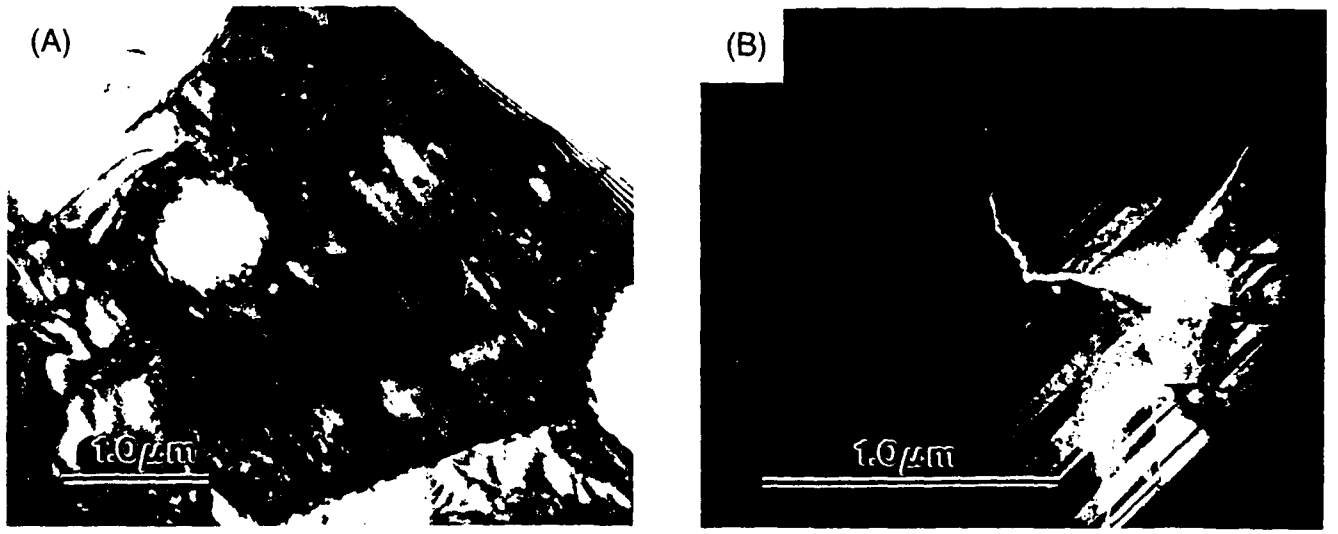

Fig. 12. (A) High concentrations of defects in β grains of the Ca_2SiO_4/MgO composite. (B) Microcracks in β grains of the Ca_2SiO_4/$CaZrO_3$ composite.

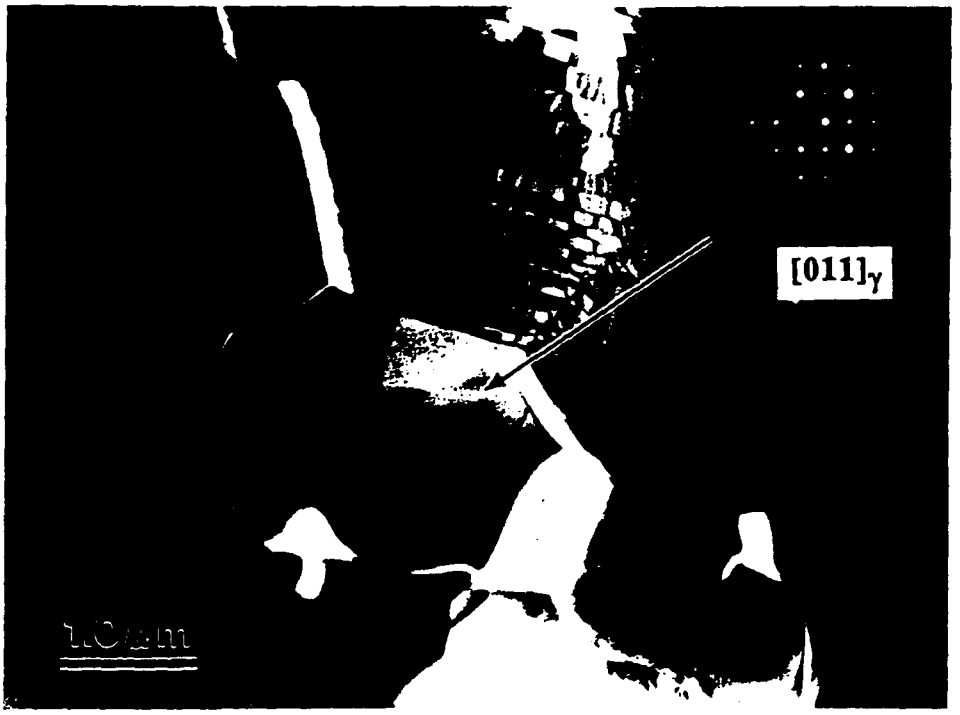

Fig. 13. Transformed γ grain retained in β grains. Large cracks generated during the β→γ transformation (from single-phase Ca_2SiO_4 sample sintered at 1400°C for 3 h).

Fig. 14. (A) Planar defects developed in γ grains of single-phase Ca_2SiO_4 samples. Note the resemblance between the defect in transformed γ part and twin planes of the untransformed β part. (B) Twin lamellae in one grain tend to match those of the neighboring grain (arrows). (C) A magnified image of planar defect in (B) showing complicated fringe pattern.

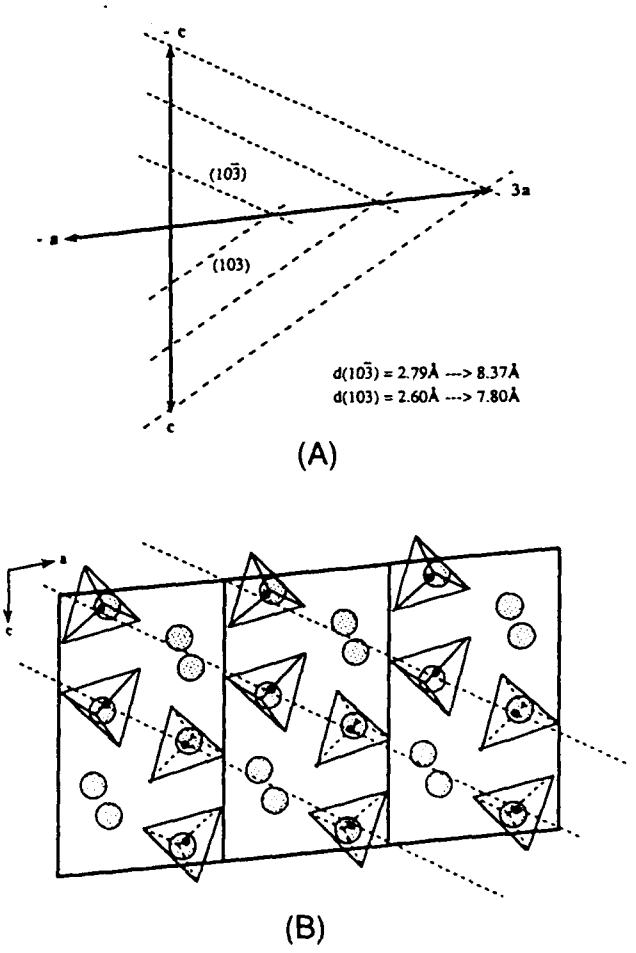

Fig. 15. (A) Geometrical explanation showing that the tripling of (10$\bar{3}$) and (103) planes may be due to the tripling of *a* axis of the β lattice. (B) (010) projection of the β structure showing {10$\bar{3}$} planes that may be responsible for the modulation in the structure.

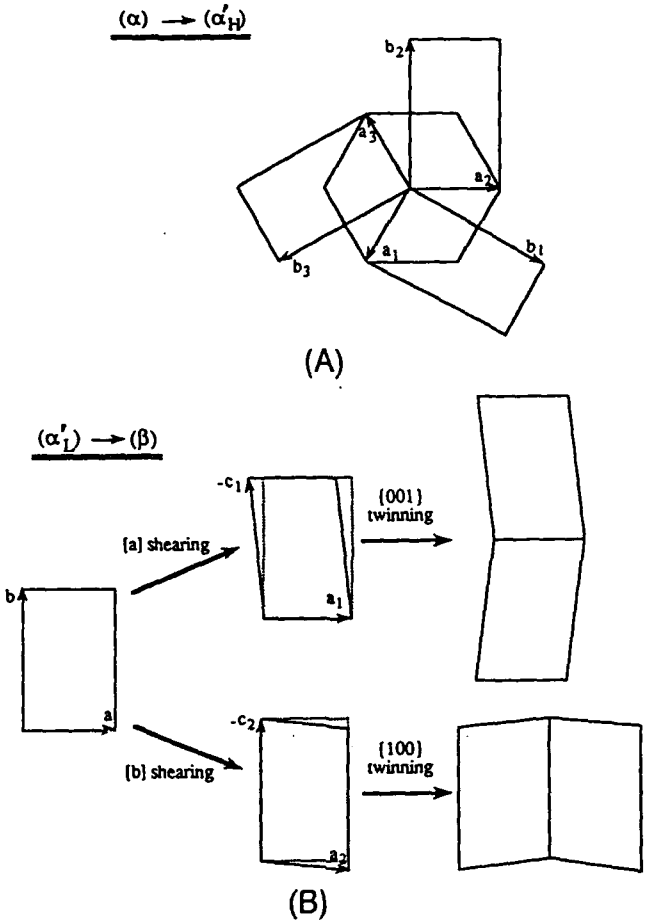

Fig. 16. Schematic drawing of possible domains formed during the α→β transformation: (A) α→α'H transformation and (B) α'L→β transformation.

$$\varepsilon_{ij} = \begin{bmatrix} 0.0087 & 0 & -0.0314 \\ 0 & 0.0012 & 0 \\ -0.0314 & 0 & -0.0030 \end{bmatrix}$$

for α'L→β by [$b_{\alpha'}$] shearing

(C) Twinning in β: The twins observed in β grains belonged to the type of "twinning by reticular pseudomerohedry."[29] The predominent population of {100} twins over {001} twins in β grains was related to (i) shearing during the α'L→β (orthorhombic→monoclinic) transformation and (ii) formation of twins after the shearing. The shear-strain components ($\varepsilon_{13} = \varepsilon_{31}$) for the α'L→β transformation indicated that the [$a_{\alpha'}$] shearing mechanism was slightly lower energy than the [$b_{\alpha'}$] shearing mechanism. To release the strains, twin formation would be energetically favorable. As shown in Fig. 16(B), $\{001\}_\beta$ twinning would be a natural consequence of the [$a_{\alpha'}$] shearing, whereas the [$b_{\alpha'}$] shearing would lead to $\{100\}_\beta$ twinning. The coexistence of the untwinned and the twinned part (mainly {001}-type) in β grains (Fig. 6) supported this sequential development of twinned structures. It also suggested that the formation of the $\{001\}_\beta$ twin was energetically more difficult compared with that of the $\{100\}_\beta$ twin. A wider twin width of the $\{001\}_\beta$ twin for the same grain size (Fig. 8) suggested that the twin boundary energy of the $\{001\}_\beta$ twin was higher than that of the $\{100\}_\beta$ twin.[30]

(3) Phase Transformations

(A) Molar Volume Changes: Ca_2SiO_4 experienced considerable volume changes throughout the phase transformations. Referring to the lattice parameter data[5] in Table I and to some extrapolations to account for thermal expansions, a volume shrinkage of ~4.4% was estimated for the α→α'H transformation (at ~1425°C). In the α' region, the volume change was small and steady, involving a ~3.3% shrinkage from 1425° to 650°C. The α'L→β transformation (at ~650°C) was accompanied by a small volume shrinkage of 0.4%. If the β phase was to be retained down to room temperature, it would experience a significant amount of volume shrinkage (~3.1%). Therefore, the total volume decrease from α (at 1425°C) to β (at room temperature) was estimated to be as much as ~11.2%, which was unusually large for ceramic materials. In some sense, then, the large volume increase of ~12.3% during the β→γ transformation at room temperature could be a recovery process for the volume shrinkages accumulated on cooling from the α phase at 1425°C.

(B) Symmetry Changes and Ferroelastic Transformations: From a symmetry point of view,[31] a ferroic transformation requires a group–subgroup symmetry relationship between the parent phase and the product phase. In addition, there should be a change of crystal system between the two phases to satisfy the criteria for a ferroelastic transformation.

Even though no direct studies of the α structure have been made to date, it is possible to deduce the symmetry of α from the data obtained in this study. Combining the established symmetry of β ($P2_1/n$; point group $2/m$) with the observed symmetry-related domain structures (threefold rotations along the *b* axis of β), a possible symmetry element along the *c* axis of α may be $6/m$. Since twin-related domain structures in β may be a result of the loss of previous mirror planes ({100} and {001} planes) during the α'L→β transformation, the point group of the α'-type structure (α'L or α'H, or both) is assumed to be *mmm*. In this case, a probable symmetry for the α phase may be $6/mmm$ as a point group and $P6_3/mmc$ as a space group. Actually, the most reliable structural studies of A_2BX_4-type compounds shows a space group of $P6_3/mmc$. This includes K_2SO_4[32] and Na_2SO_4,[33] which are believed to be isostructural with α-Ca_2SiO_4. Space group $P6_3/mmc$ is the highest possible symmetry (prototype) for A_2BX_4 polymorphs. This requires orientational disorder of the BX_4 tetrahedra along the *c* axis, which results in an additional mirror plane perpendicular to the axis.

If the α phase of Ca_2SiO_4 has a point symmetry of $6/mmm$ (hexagonal) and the α'H phase has a point symmetry of *mmm* (orthorhombic), the α→α'H transformation can be classified as ferroelastic, belonging to an Aizu species[34] $6/mmmFmmm$. In the case of K_2SO_4 and K_2SeO_4, this ferroelastic transformation has been directly proved to exist by movement of domain boundaries under an external stress.[35] A measure of ferroelasticity is usually expressed in terms of spontaneous strain (ε_s). Utilizing formulas given by Aizu,[36] the spontaneous strain generated by the α→α'H (pseudoorthorhombic→orthorhombic) transformation could be approximated as

$$\varepsilon_S^2 = \left[\frac{1}{2}(\varepsilon_{11} - \varepsilon_{22})\right]^2 + \left[\frac{1}{2}(\varepsilon_{22} - \varepsilon_{33})\right]^2 + \left[\frac{1}{2}(\varepsilon_{33} - \varepsilon_{11})\right]^2$$

Following this equation, $\varepsilon_S \approx 0.046$, which is quite a large value.

If the α'H→α'L transformation were a disorder–order transformation without change of symmetry, the α'L→β (orthorhombic (*mmm*)→monoclinic ($2/m$)) transformation would also be ferroelastic, belonging to an Aizu species[34] $mmmF2/m$. ε_S for $mmmF2/m$ is simply expressed as[36]

$$\varepsilon_S = \sqrt{2}\,|\varepsilon_{13}|$$

Then, $\varepsilon_S \approx 0.044$, which is again quite a large value. The ferroelastic nature of the α'→β transformation has also been reported for Sr_2SiO_4, with $\varepsilon_S = 0.033$.[37] Shift of domain walls caused by a lateral stress has been observed in twinned β-Sr_2SiO_4 crystals.

(C) Crystal Structure Changes: From a crystal structural point of view, the Ca_2SiO_4 structure is remarkably flexible to endure the large strains produced by the phase transformations.

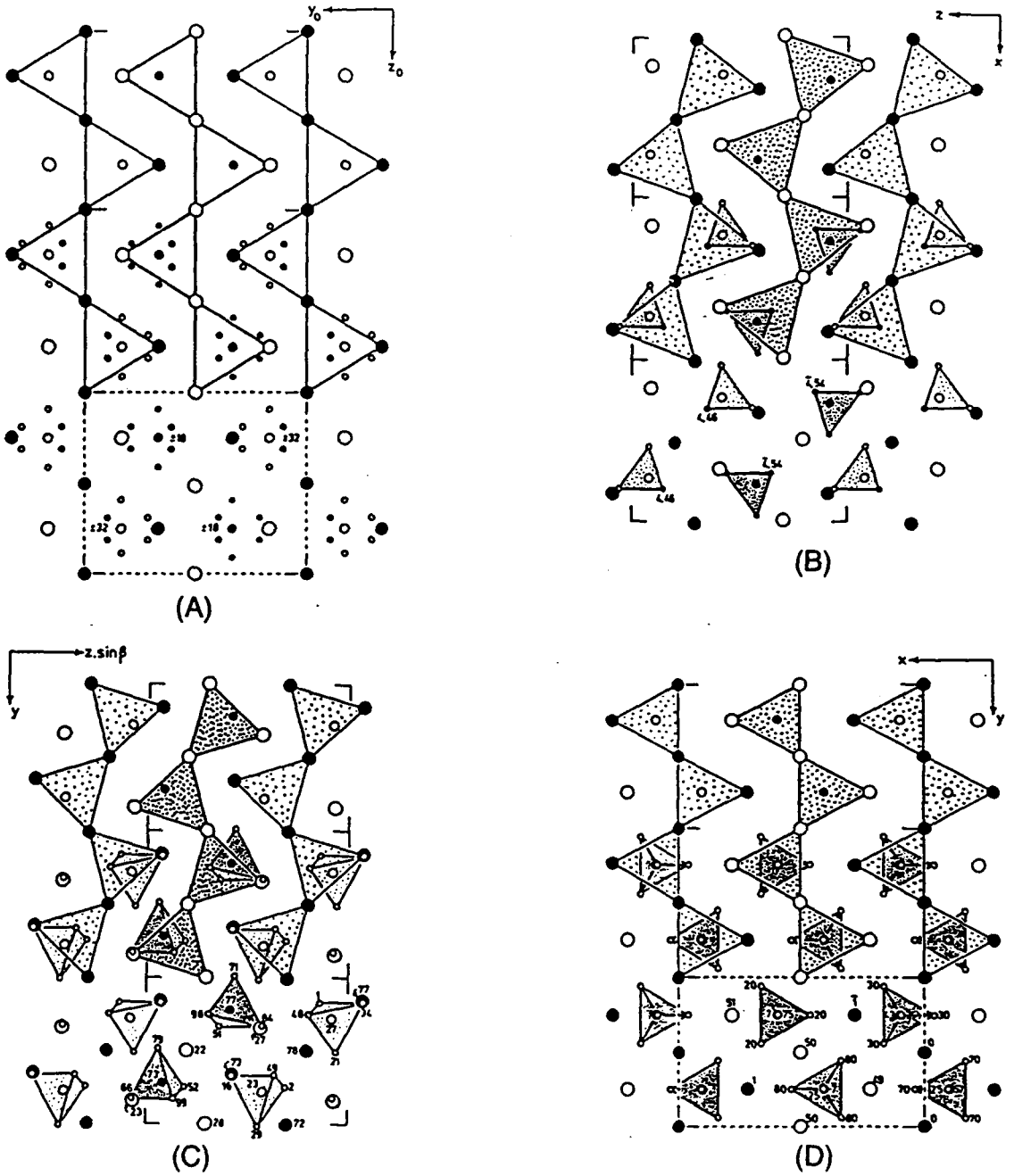

Fig. 17. Schematic projection of (A) α structure (from K_2SO_4), (B) α′ structure (from K_2SO_4), (C) β structure of Ca_2SiO_4, and (D) γ-structure of Ca_2SiO_4. Cation (Ca^{2+}) arrangements are emphasized. (After O'Keeffe and Hyde.[38])

One possible reason for this flexibility is that the structure is an inhomogeneous mixture of relatively large, but loosely-bonded CaO_n polyhedra and small, but rigid, SiO_4 tetrahedra. Furthermore, in this orthosilicate, the SiO_4 tetrahedra are not linked to one another and can easily be moved.

Figure 17 displays essential features of the sequence of Ca_2SiO_4 crystal structures in terms of the cation arrangements,[21,38] rather than the conventional view of an oxygen framework stuffed with cations. All the polymorphs of Ca_2SiO_4 have similar arrangements based on the Ca_2Si alloy structure.[38] They consist of regular, edge-linked trigonal prisms of calcium atoms with SiO_4 tetrahedra in the center. Although edge-linked calcium prisms have a linear arrangement in the α and γ structures, they have a kinked arrangement in the α′ and β structures. During the α→α′ transformation, collapse of the CaO_n polyhedra results in kinking of the calcium-prism arrangements and movement of SiO_4 tetrahedra to new positions. Subsequent tilting of the SiO_4 tetrahedra is a major change in the structure during the α′→β transformation. The kinked arrangement of the calcium prisms is straightened by the β→γ transformation.

From structural refinement data of Ca_2SiO_4, the cation–anion bond lengths and the nearest cation–cation bond distances have been calculated (Table II). Note that, while there are minor changes of Si–O bond lengths throughout the transformations, the changes of Ca–O bond lengths are significant. On cooling, the CaO_n polyhedra rapidly collapse because of the diminishing of the effective calcium vibration. The neighboring SiO_4 tetrahedra adjust their positions with respect to the CaO_n.

Comparison of the nearest bond distances between cations shows that the β structure has the shortest bond distances for both Ca–Ca and Si–Ca. Referring to ambient pressure data for nonbonded radii of silicon and calcium,[39] the ideal Ca–Ca distance is ~3.40 Å and the ideal Si–Ca distance is ~3.23 Å (1 Å = 10^{-1} nm). This means that the shortest Si–Ca bond distance in β (~2.97 Å) is too short to maintain the stability of the structure at ambient pressure. As a consequence, strong repulsive

Table II. Average Bond Lengths of Si–O and Ca–O and the Shortest Bond Distances between Silicon and Calcium Atoms for Ca_2SiO_4 Polymorphs

Polymorph	Bond length (Å)*					
	Si–O	Ca–O	Ca–Ca	Si–Ca	Si–Si	Reference
α	1.81(?)†	2.70(?)†	3.49	3.12	4.81	6
α_L'	1.63	2.63	3.48	3.13	4.39	11
β	1.63	2.50	3.43	2.97	4.11	13
γ	1.64	2.38	3.39	3.67	4.09	16

*1 Å = 10^{-1} nm. †Because of the uncertainty of one oxygen position (O(2)), these data may have significant errors.

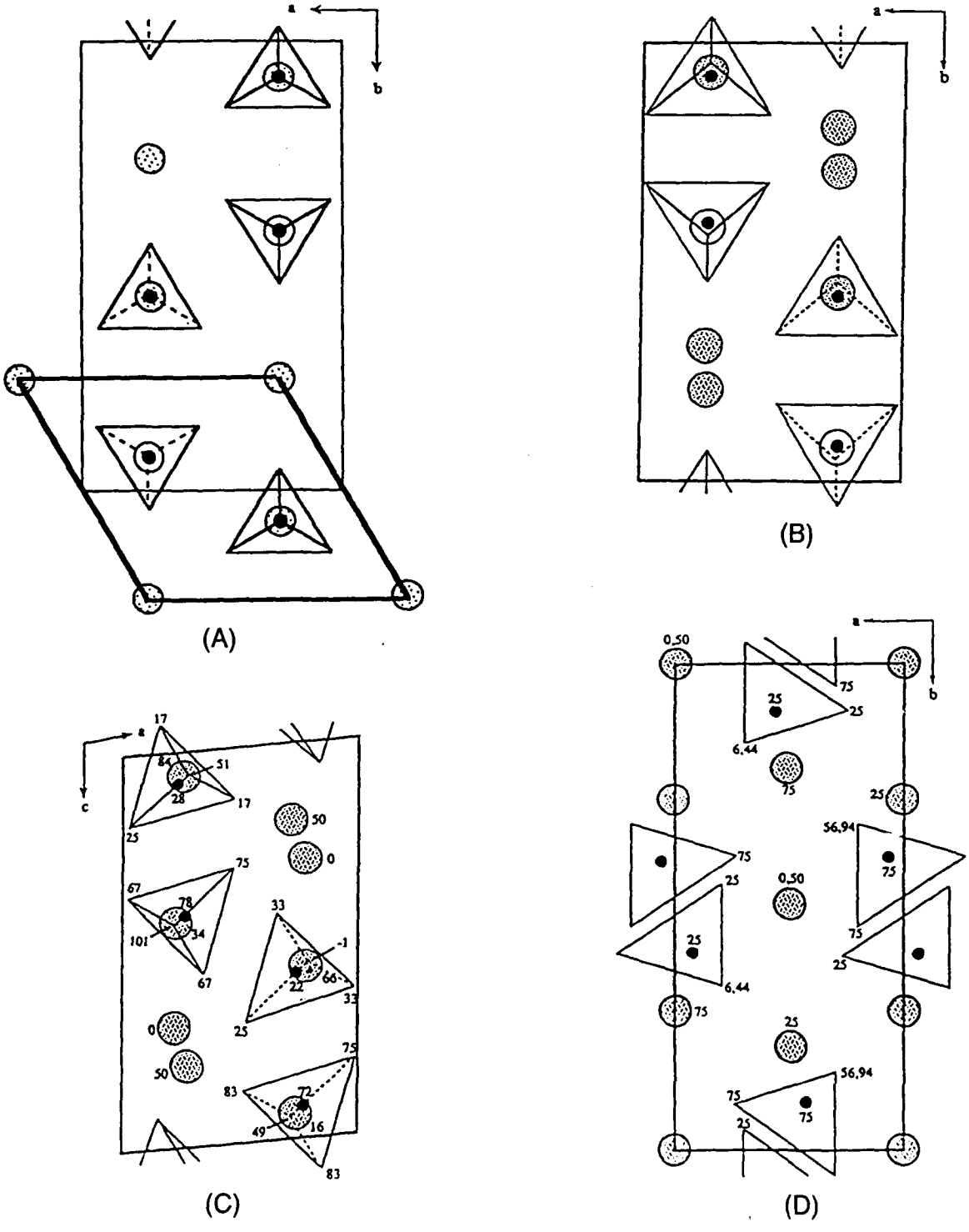

Fig. 18. Conventional projections of Ca_2SiO_4: (A) α structure, (B) α′ structure, (C) β structure, and (D) γ structure.

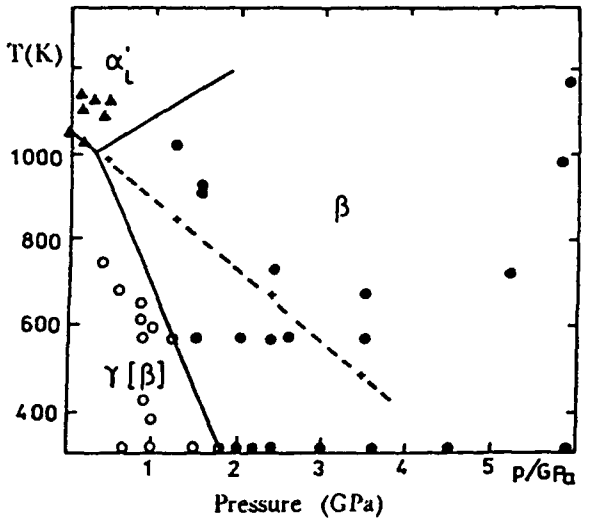

Fig. 19. *p–T* diagram of Ca_2SiO_4 determined by DTA, X-ray, and optical measurements. Metastable form is designated in square brackets. (After Hanic *et al.*[40])

forces are expected to be developed in the β structure. The modulated structures observed in both α′ and β may be related to some effective ways of calcium and SiO_4 arrangements to relieve such electrostatic repulsions between them.

Conventional projections of the Ca_2SiO_4 polymorphs in Fig. 18 illustrate that all of the α, α′, and β structures show close association of silicon atoms in SiO_4 tetrahedra with adjacent calcium atoms. However, in the γ structure, the silicon and calcium atoms are no longer closely associated because of large displacements of both the SiO_4 and calcium by the β→γ transformation. The displacements are not a simple shuffling movement of atoms, but involve a considerable amount of SiO_4 rotation. All major movements occur along the *b* axis of the γ structure. Compared with the α structure in a different projection (Figs. 17 (A) and (D)), the γ structure has silicon in a more balanced but distant position with respect to calcium. In other respects, the major configurations of both structures are very similar.

(D) Stability of β *Structure and* β→γ *Transformation:* From the crystal structure point of view discussed in the previous section, the β structure is expected to be unstable at ambient pressure because of the cation charge repulsions. As shown in Fig. 19, however, this structure has been reported to be more stable than both the γ structure and the α_L' structure at very high pressures.[40] For example, at 675°C, which is suggested to be the transformation temperature of α_L'→β, the β structure may be more stable than the γ structure only above 1 GPa. In this case, it is difficult to understand why the β phase always intervenes between α_L' and γ on cooling at ambient pressure. This observation implies that the structure should be in a highly stressed condition on cooling. One possible reason may be the influence of the spontaneous strain generated during the ferroelastic α_L'→β transformation. That is, the β structure is more suitable for accommodating the strain than the γ structure for certain temperature ranges. In this respect, the metastable β structure is inherently strained. This may be a reason why all the β grains observed in this study show intragranular strains.

Since the α→α_H' transformation also appeared to be ferroelastic, the β grains that experienced both α→α_H' and α_L'→β transformations should have a higher internal strain than the β grains that only experienced the α_L'→β transformation. This built-in strain may be a reason why (i) solid pellets of single-phase Ca_2SiO_4, which were sintered above the α→α_H' transformation temperature, could not be retained intact[22] and (ii) β grains in composites sintered above the α→α_H' transformation temperature showed higher intragranular strains, as well as a high concentration of defects and microcracks.

These large, built-in strains in the β structure and strong repulsive forces between silicon and calcium may be a possible reason why the β→γ transformation can occur instantaneously, despite the fact that the transformation necessarily involves the breaking of some oxygen bonds in the β structure. It suggests a reexamination of Buerger's classification[41] of displacive versus reconstructive transformation mechanisms. The higher symmetry and larger volume of the transformed γ phase are, therefore, probably related to the process of straightening of the β lattice to release strains and maximization of the volume to reduce charge repulsions.

V. Conclusion

From TEM studies of the Ca_2SiO_4 system, three types of superlattice structures were observed: (i) $\times 2a,2b$-type in α_L'; (ii) $\times 3c$-type in α_L'; and (iii) $\times 3a$-type in β. Almost all β grains were twinned and strained. Microcracks tended to develop along grain boundaries as the grain size increased. Some transformed γ grains coexisted with β grains, producing large intergranular microcracks. γ grains were strain free, but detwinning-related planar defects were usually present. The $\{100\}_\beta$ twinning occurred more favorably than did $\{001\}_\beta$ twinning. Two types of symmetry-related domain structures were observed in β grains: (i) two twin-related domains for samples that experienced the α_L'→β transformation and (ii) three 120° rotation-related domains for samples that experienced the α→α_H' transformation.

Based on symmetry considerations, both α→α_H' and α_L'→β appeared to be ferroelastic transformations. The α_L'→β transformation could be achieved by shearing along the a_α direction or along the b_α direction leading to $\{001\}_\beta$ or $\{100\}_\beta$ twinning, respectively. The β-Ca_2SiO_4 structure resulting from this sequence of ferroelastic transformations was inherently strained. This strained β structure was not stable at ambient pressure because of the strong electrostatic charge repulsions between silicon and calcium, which were too close to each other. In terms of the crystal structure, the major driving forces for the β→γ transformation, therefore, are considered to be the release of strains and charge repulsions in the β structure. The higher symmetry and larger volume of the transformed γ phase are probably related to the process of straightening of the β lattice to release strains and maximizing of the volume to reduce repulsions. The β→γ tranformation can be displacive in the sense of its instantaneous reaction, but needs to overcome a comparatively high energy barrier due to the breaking of some oxygen bonds in the β structure.

Acknowledgments: Dr. T. I. Hou and Mr. E. Mast are thanked for fabricating the composite samples used in this study. We acknowledge valuable discussions with Prof. A. H. Heuer of Case Western Reserve University. Use of the electron microscopy facilities at the Center for Microanalysis of Materials in the Materials Research Laboratory and at the Center for Electron Microscopy, both at the University of Illinois at Champaign-Urbana, is gratefully acknowledged.

References

[1]W. M. Kriven, "Possible Transformation Toughening Alternative to Zirconia: Crystallographic Aspects," *J. Am. Ceram. Soc.*, 71, 1021–30 (1988).

[2]W. M. Kriven, C. J. Chan, and E. A. Barinek, "The Particle-Size Effect of Dicalcium Silicate in a Calcium Zirconate Matrix"; pp. 145–55 in Advances in Ceramics, Vol. 24A, *Science and Technology of Zirconia III*. Edited by S. Sōmiya, N. Yamamoto, and H. Yanagida. American Ceramic Society, Westerville, OH, 1988.

[3]C. J. Chan, W. M. Kriven, and J. F. Young, "Physical Stabilization of the β to γ Transformation in Dicalcium Silicate," *J. Am. Ceram. Soc.*, 75 [6] 1621–27 (1992).

[4]C. J. Chan, W. M. Kriven, and J. F. Young, "Analytical Electron Microscopic Studies of Doped Dicalcium Silicate," *J. Am. Ceram. Soc.*, 71, 713–19 (1988).

[5]M. Regourd, M. Bigare, J. Forest, and A. Guinier, "Synthesis and Crystallographic Investigation of Some Belites"; pp. 44–48 in *Proceedings of the 5th International Symposium on the Chemistry of Cement*, Part I, Supplement Paper I-10 (Tokyo, Japan, 1968). Cement Association of Japan, Tokyo, Japan, 1969.

[6]S. Udagawa, K. Urabe, and T. Yano, "The Crystal Structure of α-Ca_2SiO_4," (in Jpn.), *Cem. Assoc. Jpn. Rev., Gen Meet., Tech. Sess.*, **31**, 26–29 (1977).

[7]G. Yamaguchi, Y. Ono, S. Kawamura, and Y. Soda, "Synthesis of the Modifications of Ca_2SiO_4 and the Determination of Their Powder X-ray Diffraction Patterns" (in Jpn.), *J. Ceram. Assoc. Jpn.*, **71**, 21–26 (1963).

[8]P. Barnes, C. H. Fentimen, and J. W. Jeffery, "Structurally Related Dicalcium Silicate Phases," *Acta Crystallogr., Sect. A: Cryst. Phys., Diffr., Theor. Gen. Crystallogr.*, **36**, 353–56 (1980).

[9]H. Saalfeld, "X-ray Investigation of Single Crystals of β-Ca_2SiO_4 (Larnite) at High Temperatures," *Am. Mineral.*, **60**, 824–27 (1975).

[10]I. Jelenic and A. Bezjak, "Electron Diffraction Evidence for Superstructures in α′-Modification of Dicalcium Silicate," *Cem. Concr. Res.*, **12**, 785–88 (1982).

[11]S. Udagawa, K. Urabe, T. Yano, K. Takada, and M. Natsume, "Studies on the Dusting of Ca_2SiO_4—The Crystal Structure of α_L'-Ca_2SiO_4" (in Jpn.), *Cem. Assoc. Jpn. Rev., Gen. Meet., Tech. Sess.*, **33**, 35–38 (1979).

[12]A. M. Il'inets and M. Ya. Bikbau, "Structural Mechanism of Polymorphic Transitions of Dicalcium Silicate, Ca_2SiO_4. Part II: Refinement of Crystal Structure of High-Temperature α_L' Modification of Dicalcium Silicate, Ca_2SiO_4," *Sov. Phys.—Crystallogr. (Engl. Transl.)*, **35**, 54–56 (1990).

[13]K. H. Jost, B. Ziemer, and R. Seydel, "Redetermination of the Structure of β-Dicalcium Silicate," *Acta Crystallogr., Sect. B: Struct. Crystallogr. Cryst. Chem.*, **33**, 1696–700 (1977).

[14]D. K. Smith, A. Majumdar, and F. Ordway, "The Crystal Structure of γ-Dicalcium Silicate," *Acta Crystallogr.*, **18**, 787–95 (1965).

[15]R. Czaya, "Refinement of the Structure of γ-Ca_2SiO_4," *Acta Crystallogr., Sect. B: Struct. Crystallogr. Cryst. Chem.*, **27**, 848–49 (1971).

[16]S. Udagawa, K. Urabe, M. Natsume, and T. Yano, "Refinement of the Crystal Structure of γ-Ca_2SiO_4," *Cem. Concr. Res.*, **10**, 139–44 (1980).

[17]W. Eysel and T. Hahn, "Polymorphism and Solid Solution of Ca_2GeO_4 and Ca_2SiO_4," *Z. Kristallogr.*, **131**, 322–41 (1970).

[18]C. M. Midgley, "The Crystal Structure of β-Dicalcium Silicate," *Acta Crystallogr.*, **5**, 307–12 (1952).

[19]G. W. Groves, "Twinning in β-Dicalcium Silicate," *Cem. Concr. Res.*, **12**, 619–24 (1982).

[20]G. W. Groves, "Portland Cement Clinker Viewed by Transmission Electron Microscopy," *J. Mater. Sci.*, **16**, 1063–70 (1981).

[21]J. Barbier and B. G. Hyde, "The Structures of the Polymorphs of Dicalcium Silicate, Ca_2SiO_4," *Acta Crystallogr., Sect. B: Struct. Sci.*, **41**, 383–90 (1985).

[22]I. Nettleship, K. Slavick, Y. J. Kim, and W. M. Kriven, "Phase Transformations in Dicalcium Silicate: I, Fabrication and Phase Stability of Fine-Grained β-Phase," *J. Am. Ceram. Soc.*, **75** [9] 2400–406 (1992).

[23]I. Nettleship, K. Slavick, Y. J. Kim, and W. M. Kriven, "Phase Transformations in Dicalcium Silicate: III, The Effects of Barium on the Stability of Fine-Grained α_L' and β"; unpublished work.

[24]E. S. Mast, "Development and Possible Use of Dicalcium Silicate in the Transformation Toughening of Magnesia"; M.S. Thesis, University of Illinois at Urbana-Champaign, 1990.

[25]T. I. Hou and W. M. Kriven, "Processing, Microstructures, and Mechanical Properties of Dicalcium Silicate–Calcium Zirconate Composites," to be published in *J. Am. Ceram. Soc.*

[26]S. Udagawa, K. Urabe, T. Yano, and M. Natsume, "Studies on the Phase Transitions of Ca_2SiO_4 by X-ray Single-Crystal Camera with a High-Temperature Apparatus" (in Jpn.), *J. Ceram. Assoc. Jpn.*, **88**, 285–91 (1980).

[27]R. M. Hazen and L. W. Finger, *Comparative Crystal Chemistry*; pp. 115–46. Wiley, New York, 1982.

[28]J. L. Schlenker, G. V. Gibbs, and M. B. Boison, "Strain-Tensor Component Expressed in Terms of Lattice Parameters," *Acta Crystallogr., Sect. A: Cryst. Phys., Diffr., Theor. Gen. Crystallogr.*, **34**, 52–54 (1978).

[29]J. W. Cahn, "Twinned Crystal," *Adv. Phys.*, **3**, 363–445 (1954).

[30]T. Roy and T. E. Mitchell, "Twin Boundary Energies in $YBa_2Cu_3O_{7-\delta}$ and La_2CuO_4," *Philos. Mag. A*, **63**, 225–32 (1991).

[31]V. K. Wadhawan, "Ferroelasticity and Related Properties of Crystals," *Phase Transitions*, **3**, 3–103 (1982).

[32]M. Miyake, H. Morikawa, and S.-I. Iwai, "Structural Reinvestigation of the High-Temperature Form of K_2SO_4," *Acta Crystallogr., Sect. B: Struct. Crystallogr. Cryst. Chem.*, **36**, 532–36 (1980).

[33]W. Eysel, H. H. Hofer, K. L. Keester, and Th. Hahn, "Crystal Chemistry and Structure of Na_2SO_4(I) and Its Solid Solutions," *Acta Crystallogr., Sect. B: Struct. Sci.*, **41**, 5–11 (1985).

[34]K. Aizu, "Possible Species of Ferromagnetic, Ferroelectric, and Ferroelastic Crystals," *Phys. Rev. B: Solid State*, **2**, 754–72 (1970).

[35]S. Shiozaki, A. Sawada, Y. Ishibashi, and Y. Takagi, "Hexagonal–Orthorhombic Phase Transition and Ferroelasticity in K_2SO_4 and K_2SeO_4," *J. Phys. Soc. Jpn.*, **43**, 1314–19 (1977).

[36]K. Aizu, "Determination of the State Parameters and Formulation of Spontaneous Strain for Ferroelastics," *J. Phys. Soc. Jpn.*, **28**, 706–16 (1970).

[37]M. Catti and G. Gazzoni, "The β ↔ α′ Phase Transition of Sr_2SiO_4. II. X-ray and Optical Study, and Ferroelasticity of the β Form," *Acta Crystallogr. Sect. B: Struct. Sci.*, **39**, 679–84 (1983).

[38]M. O'Keeffe and B. G. Hyde, "An Alternative Approach to Nonmolecular Crystal Structures with Emphasis on the Arrangements of Cations," *Struct. Bonding (Berlin)*, **61**, 77–144 (1985).

[39]M. O'Keeffe and B. G. Hyde, "The Role of Nonbonded Forces in Crystals"; pp. 227–54 in *Structure and Bonding in Crystals*, Vol. 1. Edited by M. O'Keeffe and A. Navrotsky. Academic Press, New York, 1981.

[40]F. Hanic, J. Kamarad, J. Stracelsky, and I. Kapralik, "The *p–T* Diagram of Ca_2SiO_4," *Br. Ceram. Trans. J.*, **86**, 194–98 (1987).

[41]M. J. Buerger, "Phase Transformations," *Sov. Phys.—Crystallogr. (Engl. Transl.)*, **16**, 959–68 (1972). □

Phase Transformations in Dicalcium Silicate. III: Effects of Barium on the Stability of Fine-Grained α'_L and β Phases

Ian Nettleship*†, Kurt G. Slavick *§, Youn Joong Kim*,

and Waltraud M. Kriven*.

Department of Materials Science and Engineering,

University of Illinois at Urbana-Champaign,

Urbana, IL 61801.

(For submission to Journal of the American Ceramic Society)

Presented at 94th Annual Meeting of the American Ceramic Society, Minneapolis, April 13-April 16, 1992. Paper number 43-C-92 in the Engineering Ceramics Division.

Supported by the Air Force Office of Scientific Research through a grant, number

AFOSR - 89 - 0300.

* Member, The American Ceramic Society.

† Present Address: Department of Materials Science and Engineering, University of Pittsburgh, Pittsburgh, PA 15261.

§ Present Address: Allied Signal Ceramic Components, 2525 W. 190th Street, Torrance, CA 90509-2960.

Abstract

Fine grained materials containing both α'_L-Ca_2SiO_4 and β-Ca_2SiO_4 were fabricated as an analog to tetragonal zirconia polycrystals (TZP) with the use of barium to stabilize the high temperature polymorphs of Ca_2SiO_4.

The microstructure of dense α'_L-Ca_2SiO_4 exhibited none of the twinning or residual strain previously observed in fine grained β-Ca_2SiO_4 and there was no evidence of barium rich grain boundary phases. Materials fired in the α region exhibited large grain sizes. Stress-induced $\alpha'_L \rightarrow \beta$ transformation was observed on ground surfaces but not on fracture surfaces.

Key Words: [dicalcium silicate, Ca_2SiO_4, phase transformations, barium doping, mechanical properties]

I. Introduction

The polymorphism of dicalcium silicate (Ca_2SiO_4) has been well studied and the currently accepted polymorphic sequence at atmospheric pressure[1,2] is shown in Fig. 1. The 12 vol% expansion on cooling through the $\beta \rightarrow \gamma$ transformation can cause fracture in refractories in which Ca_2SiO_4 is a contaminant. This phenomenon is widely known as "dusting". The transformations are also important in the cement industry because β phase is an important hydraulic constituent of cement responsible for final stage hardening. In contrast, γ phase does not hydrate and consequently the $\beta \rightarrow \gamma$ transformation is undesirable in cement powders. A considerable amount of work has been done in order to establish the effect of chemical additives on the stability of the β phase and other high temperature polymorphs.

The additives that stabilize the high temperature polymorphs are well known in the cement industry.[3,4] There have even been some studies that have attempted to predict the effect of additives on the basis of ionic size and valency of the cation.[3,5] However these studies paid little or no attention to the microstructure and experimental verification of the additive levels in solid solution. Chan et al.[6] performed one of the few analytical TEM studies of the microstructures of doped Ca_2SiO_4 to elucidate the effects of additives. The dopants were Al_2O_3 and K_2O and different Ca_2SiO_4 stoichiometries were also studied. The results were a dramatic illustration of the potential for chemical heterogeneity in this system when mixed oxide processing is used. Most of the additives were concentrated in extensive amounts of amorphous grain boundary phase. The authors also studied the effect of non-stoichiometry and showed that when the CaO/SiO_2 ratio was changed for the precursor oxides, the actual ratio in the final Ca_2SiO_4 grains remained as 2. Hence, the study of dopants and non-

stoichiometry without detailed microstructural characterization can be ambiguous and even contradictory.

Similarly, there have been too few studies of the effects of firing in different phase fields on the room temperature stability of the β phase. Most of the solid state reactions used to prepare pure Ca_2SiO_4 were conducted at 1450°C, which is in the α phase field, and the product at room temperature was γ phase. Some studies have looked at the effect of low temperature preparation or low temperature annealing on phase stability because it appeared that powders calcined or annealed in the α'_L region gave β phase at room temperatures.[7-12] For chemically prepared powders synthesized at low temperature, the crystallites in the powder were very small (< 1μm) and the retention of the β phase was attributed to a particle size effect.[7,8] The effect of low temperature annealing could be due to the β→γ transformation because the repeated dusting during the cooling cycle would reduce the particle size. Consequently, β phase would be stable after reheating if the new particle size was below the critical value.[9,11] Cooling from the α region also affected the phase distribution, in that rapid quenching stabilized the β phase at room temperature.[9,11,13,14] This is thought to be due to the retention of the domain "herringbone" structures inside the grains and an inferred reduction in the particle size.[13,14]

Dicalcium silicate has also been identified as a potential transformation toughener[15] and toughening has been observed when β-Ca_2SiO_4 was incorporated into chemically compatible matrices.[16,17] However there is some doubt as to whether the toughening is transformation toughening,[17] and a single phase material was developed to study this point.[18]

In this work the effect of barium on the stability of the α'_L and β phases was examined. Materials were fabricated in the Ca_2SiO_4-Ba_2SiO_4 pseudo-binary system[19,20] with compositions ranging from Ca_2SiO_4 to 95 mol% Ca_2SiO_4-5

mol% Ba_2SiO_4 (Fig. 2). The phase stability in the powders and the solid material was studied in the context of the microstructure and polymorphism.

The addition of different amounts of barium provided the means by which materials could be fired in the α and α'_H regions under the same conditions of temperature and time. This is important in determining the factors responsible for the increase in the transformability of β phase materials fired in the α region. Two explanations have been proposed based on either grain growth or strain accumulation.[18,21] One aim of this study was to observe the grain size of materials fired in the α region in comparison with those fired in the α'_H region.

Finally, since fine grained polycrystalline α'_L materials could be processed by the addition of barium, experiments were performed to study the stress-induced $\alpha'_L \rightarrow \beta$ transformation.

II. Experimental Procedure

The powders were chemically prepared using the same "Pechini type process" that has been used to prepare both Ca_2SiO_4 and Sr_2SiO_4.[8] The precursors were $Ca(NO_3)_2.4H_2O$, $Ba(CH_3CO_2)_2$ and colloidal silica*. In this study the silica sol contained some sodium such that the final Ca_2SiO_4 powder was calculated to contain 0.7 weight % Na_2O. Powders were calcined at temperatures in the range 800°C and 1400°C for 1 hour.

The preparation route for the dense material was the same as that previously used for polycrystalline Ca_2SiO_4[18] and involved sedimentation

---

* Ludox SM, Dupont Chemical Company, Wilmington, Delaware.

classification of powders which had been calcined at 800°C for 1 hour and milled in propan-2-ol with high purity zirconia balls. The submicron powder thus obtained was pressed into bars or pellets, isostatically pressed at 170 MPa and fired in air at 1300°C and 1400°C to achieve dense materials. A 700°C annealing treatment for 4.5 hours was incorporated into the cooling schedule in order to relieve stresses built up during cooling from the firing temperature. This was done for all the specimens in this study including the powders. Without this annealing step some samples would dust over a period of a few days.(22)

X-ray analyses of the phase distributions were conducted on the powders and the fired ceramic. The phase distributions were also studied after grinding and fracture. Semi-quantitative analysis using integrated intensity measurements from single peaks was difficult because of the complexity of the diffraction patterns and the extensive peak overlap for the α'_L and β phases in this system. Hence direct comparison of the X-ray traces was used to obtain a qualitative indication of the changes in phase distribution.

The strength was evaluated using 4 point bending on at least 5 bars polished to a 1μm finish. The elastic modulus was evaluated using the pulse-echo method¶. No attempt was made to measure toughness.

SEM# was conducted on fracture surfaces and polished surfaces. Grain size was determined by the linear intercept method on SEM micrographs of polished surfaces after thermal etching at 1300°C for 15 minutes. At least 400 intercepts were used and the average intercept length was used directly as a measure of grain size. Microstructures of representative samples were examined by TEM** of ion-milled thin sections.

¶ NDT-150, Nortec Corporation, Kennewick, WA.

Model ISI-130, International Scientific Instruments, Santa Clara, CA.

** Model 600, Hitatchi Instruments, Conroe, TX.

III. Results

(1) Phase Stability in the Powders

Powders containing 1, 2, 3, 4 and 5 mol% Ba_2SiO_4 were calcined for 1 hour at different temperatures ranging from 800°C to 1400°C. The powders calcined at 800°C were crystalline and the lack of the $(103)_\beta$ peak suggested that they were α'_L phase, although it was very difficult to distinguish between the α'_L and β phase because of peak broadening. Fig. 3 compares the phase distribution in the powders fired at 1300°C for 1 hour. After this treatment it was somewhat easier to use the $(103)_\beta$ peak to show the presence of the β phase. The powders containing higher barium contents (4 and 5 mol% Ba_2SiO_4) were α'_L, while those of lower barium content contained increasing amounts of β phase. Hence, barium addition stabilized the high temperature polymorphs which was consistent with previous studies that have shown similar effects with the addition of $BaSO_4$.[23] The results after calcination at 1400°C, displayed in Fig. 4, were quite different. Although the lower barium contents gave β phase, the higher barium contents gave γ phase at room temperature. For powders calcined at 1400°C, barium addition appeared, at first sight, to destabilize the high temperature polymorphs. The sample containing 5 mol% Ba_2SiO_4 was 100% γ phase at room temperature.

(2) Phase Distributions and Microstructures of the Dense Ceramics

Dense, fine grained materials were fired at 1400°C and 1300°C. Fig. 5 is a TEM micrograph of the microstructure of the 5 mol% Ba_2SiO_4 material fired at 1300°C for 3 hours. The grains were equiaxed and there was no observable barium rich grain boundary phase such as that observed in studies of similar materials prepared by mixed oxide techniques.(24) The grains were α'_L phase and they did not contain any of the barium rich precipitates found in a previous TEM study.(24) The microstructure was relatively free from the intergranular strain observed in the twinned β phase.(18)

Most of these materials were two phase mixtures of α'_L and β, in which both phases presumably had the same composition. Since it is difficult to prepare the pure phases with the same composition it was not possible to calculate theoretical densities of the samples from measured lattice parameters. However, it is thought that the materials fired at 1300°C for 12 hours and 1400°C for 1 hour were close to full density.

Fig. 6 displays a comparison of the X-ray traces of the sintered surfaces of materials containing different barium contents fired at 1300°C for 12 hours. The lack of the $(103)_\beta$ peak suggested that the 5 mol% Ba_2SiO_4 specimens were single phase α'_L after firing at 1300°C for 12 hours. Reducing the barium content had a marked effect on the phase distribution. Both the 3 mol% Ba_2SiO_4 and 1 mol% Ba_2SiO_4 material contained much more β phase. When fired at 1400°C for just 1 hour the 5 mol% Ba_2SiO_4 material contained mainly α'_L phase, as shown in Fig. 7. When the barium content was decreased the materials contained more β phase.

The effect of barium content on the grain size of materials fired at 1300°C for 12 hours and 1400°C for 1 hour is shown in Fig. 8. After firing at 1300°C for 12 hours, materials with compositions ranging from 1 mol% Ba_2SiO_4 to 5 mol% Ba_2SiO_4 had similar grain sizes. The average intercept length only varied

more β phase on the sintered surface than the sample fired at 1300°C, but grinding appeared to cause an observable increase in the amount of β phase. This was also attributed to stress induced transformation.

The observation of transformation on fracture is of key importance to proving stress induced transformation and hence the potential for transformation toughening. The polished surfaces and fracture surfaces of different specimens were compared in order to observe stress induced transformation on fracture. The material containing 5 mol% Ba_2SiO_4 fired for 12 hours at 1300°C was composed of α'_L phase and the fracture surface also showed single phase α'_L. Hence there was no evidence of transformation on fracture. A similar result was found for the same material fired at 1400°C for 1 hour. Although this particular material was a mixture of α'_L and β phases there was no observable difference between the phase distributions on the polished surface and the fracture surface.

The stress-strain behavior of 5 mol% Ba_2SiO_4 materials fired at 1300°C for 12 hours was also examined during four point bending. The strain on the tensile surface was measured using strain gages. This was undertaken to observe evidence of deviations from elasticity due to stress induced phase transformations in α'_L-Ca_2SiO_4, as in the previous study on fine grained β phase.[18] However, the behavior was perfectly linear and hence there was no evidence of stress induced $\alpha'_L \rightarrow \beta$ transformation on fracture.

(4) Mechanical Properties of the Dense Ceramics

The strength of materials fired at 1300°C for 12 hours and 1400°C for 1 hour are shown in Fig. 10. In general, the values were slightly higher than those achieved for the polycrystalline β phase material.[18] The trend in the results for the elastic modulus with barium content for materials fired at 1300°C for 12 hours and 1400°C for 1 hour are given in Fig. 11. In both cases there was a decrease in elastic modulus with increasing barium content.

VI. Discussion

(1) Phase Stability in the Powders

The results for calcination at 1300°C and 1400°C which are shown in Fig. 3 and Fig. 4 appear to be contradictory. Increasing the barium content at 1300°C increased the amount of the α'_L phase at room temperature, whereas increasing the barium content at 1400°C increased the amount of γ phase. The effect of barium addition in powders calcined at 1300°C was consistent with the idea of barium as a stabilizer for the high temperature phases of Ca_2SiO_4.[19,20,23,24] However, barium addition appeared to decrease the stability of the high temperature phases of powders calcined at 1400°C. The explanation for the apparent contradiction may be related to the effect of firing in the α region on the stability of the β phase, as proposed in the previous work.[18] The Ca_2SiO_4-Ba_2SiO_4 pseudo-binary phase diagram of Fig. 2[19,20] indicates that small additions of barium can dramatically lower the $\alpha \rightarrow \alpha'_H$ temperature. For pure Ca_2SiO_4 this transformation occurred at 1425°C but when 5 mol% Ba_2SiO_4 was added, the transformation temperature was depressed to 1325°C. Hence the materials containing more than 2 mol% Ba_2SiO_4, which contained γ phase at room temperature, were probably in the α region during firing at 1400°C. In the previous study of barium-free Ca_2SiO_4,[18] both powders and pellets were fired in the α region and contained γ phase at room temperature. The exact reasons for this were not known but it has been proposed that enhanced grain growth in the α region or strain accumulation and defects generated by both the $\alpha \rightarrow \alpha'_H$ and $\alpha'_L \rightarrow \beta$ transformations on cooling may be responsible.[18] This point will be discussed further in the next section which is concerned with the dense materials.

(2) Phase Distributions and Microstructures of the Dense Ceramics

Dense materials fired at 1300°C for 12 hours appeared, from analysis of the phase distributions on the sintered surfaces, to be composed of mixtures of α'_L and β. The amount of α'_L phase increased with increasing barium content, until by 5 mol% Ba_2SiO_4 the material was practically single phase α'_L. The trend in α'_L content with barium content was similar to the trend observed for powders fired at 1300°C for 1 hour. Since the grain size of the dense ceramics fired at 1300°C for 12 hours was similar for all barium compositions, the interpretation was not complicated by a grain size effect. The trend in phase content was consistent with the effect of barium as a stabilizer for the high temperature polymorphs.

The materials fired at 1400°C for 1 hour were also mixtures of α'_L and β. The only specimens that exhibited large amounts of α'_L phase were those containing 5 mol% Ba_2SiO_4. Unlike the powders fired at 1400°C for 1 hour, the dense materials did not show any evidence of γ phase.

The results also showed an effect of barium on the grain size for materials fired at 1400°C. This made the interpretation of the phase distributions on the sintered surfaces difficult because of a possible grain size effect on stability of the high temperature polymorphs as well as the effect of the stabilizer content. The discontinuity in grain size displayed in Fig. 7 is coincident with the expected composition of the closely spaced α to $\alpha+\alpha'_H$ and $\alpha+\alpha'_H$ to α'_H phase boundaries at 1400°C, as seen in Fig. 2.[19,20] Hence the materials containing more than 2 mol% Ba_2SiO_4, which have larger grain sizes, were thought to have been in the α region during firing. This suggested that materials fired in the α region had higher grain growth rates and larger grains, which was in agreement with previous qualitative results in cement clinkers[9,10]. The variation in grain size did not seem to control the stability of the high temperature polymorphs in the dense material. The intrinsic effect of the increased stabilizer content may have been responsible for the increase in α'_L phase in 5 mol% Ba_2SiO_4 fired at 1400°C despite the fact that the grain size was much larger than for samples containing 1 mol% Ba_2SiO_4 and 2 mol% Ba_2SiO_4.

Unfortunately, the results of this study were unable to clearly isolate the cause of the increase in transformability associated with materials fired in the α region in this study and the previous study.[18] In the previous study two reasons were suggested.[18] The first involved the possibility of relative rapid grain growth in materials fired in the α region and a consequent particle size effect. The grain size results for this study were consistent with rapid grain growth in the α region but the phase distributions in the dense material were not consistent with the idea of a consequent particle size effect. Despite this, such an argument could explain the phase distribution in the powders in this study and the phase distributions observed in powders and dense materials in the previous study.[18] The second argument was based on strain accumulation associated with cooling through the $\alpha \rightarrow \alpha'_H$ and $\alpha'_L \rightarrow \beta$ transformations, which could decrease the stability of β phase.[18] Indeed, increased strain accumulation has been observed by TEM in the structure of materials which have experienced both these transformations.[21] This argument, though, was difficult to prove experimentally.

(3) Transformability of the α'_L Phase

The results of grinding of 5 mol% Ba_2SiO_4 fired at 1300°C for 12 hours are displayed in Fig. 9. They showed clear evidence of stress induced $\alpha'_L \rightarrow \beta$ surface transformation. The other materials fired at 1300°C for 12 hours and all the materials fired at 1400°C for 1 hour contained significant quantities of β phase on the sintered surfaces and there was less stress-induced transformation on grinding. There was no evidence of stress-induced transformation on fracture for any of the materials examined so its unlikely that the transformation toughening mechanism could be achieved. It is difficult to speculate on the reasons why grinding stress-induced the $\alpha'_L \rightarrow \beta$ transformation but fracture did not. One could suggest that the high levels of stress associated with grinding could have been responsible. Alternatively, the high number

of defects generated by the grinding process[25] could help nucleate the transformation in the surface.

(4) Mechanical Properties of the Dense Ceramics

In general the strengths of the α'_L materials were only slightly higher than those of the fully dense β phase materials measured in the previous study.[18] This was despite the fact that the β phase was heavily twinned and exhibited high residual strain in the microstructure.[21] One would expect this microstructure to be more susceptible to microcracking and lead to lower strength values.

The materials with higher barium contents had lower Young's moduli and they also contained more α'_L phase. Since no microcracks were observed during TEM examination of α'_L materials (Fig. 5), the results could be explained if the elastic moduli of the α'_L phase was lower than that of the β phase.

V. Conclusion

The addition of barium to Ca_2SiO_4 powders resulted in greater stability of the α'_L phase as reported in previous studies.[19,20,23,24] However, when the powders were fired above 1300°C, increasing the barium content resulted in increasing amounts of γ phase. Dense polycrystalline materials have been fabricated and the material containing 5 mol% Ba_2SiO_4 was single phase α'_L when fired at 1300°C for 12 hours. There was no significant grain boundary phase and the microstructure was relatively free from strain compared to polycrystalline β phase material.[18] When the barium content was reduced, the materials became two phase

and contained more β phase. This was also true for materials with the same composition fired at 1400°C.

The stress induced $\alpha'_L \rightarrow \beta$ transformation ha^ been observed on grinding for materials fired at both 1300°C and 1400°C, but there was no evidence of transformation on fracture. The mechanical strength of the α'_L phase was slightly greater than the β phase[18] and the elastic modulus of the α'_L phase appeared to be lower than that of the β phase.

VI. Acknowledgments

The authors would like to thank Ms. Theresa Swanson for preparing some of the powders used in this study. Use of the electron microscope facilities at the Center for Microanalysis of Materials in the Materials Research Laboratory at UIUC are gratefully acknowledged.

VII. References

[1]H.E. Schweite, W. Konert and K. Deckert, "Existence Range and Stabilization of High Temperature Modification of Dicalcium Silicate," *Zement Kalk Gips* ., 9 359-366 (1968).

[2]H. Midgley, "The Polymorphism of Calcium Orthosilicate," pp. 1-16 in *6th International Congress on the Chemistry of Cement*, Supplemental Paper I (Moscow 1974), 1974.

[3]I.M. Pritt and K.E. Daugherty, "The Effect of Stabilizing Agents on the Hydration of β -C_2S," *Cement and Concrete Research* 6 783-796 (1976).

[4]B. Matkovic, "Doped Dicalcium Silicates," *God. Jugosl. Cent. Kristalogr.* (Annual Review of Yugoslav Center of Crystallography) **17** 67-88 Zagreb (1982).

[5]A. Derdacka - Grzymek, "Polymorphic Phase Changes of Dicalcium Silicate," (In Polish) *Pol. Akad. Nauk. Kom. Krakowie, Ceram.*, **29** 1-40 (1978).

[6]C. J. Chan, W. M. Kriven and J.F. Young, "Analytical Electron Microscopic Studies of Doped Dicalcium Silicate," *J. Am. Ceram. Soc.*, **71** [9] 713-719 (1988).

[7]D.M. Roy and S. O. Oyefesobi, "Preparation of Very Reactive Ca_2SiO_4 Powder," *J. Am. Ceram. Soc. Discussion and Notes.*, **60** [3-4] 178-180 (1977).

[8]I. Nettleship, J.L. Shull Jr. and W.M. Kriven, "Preparation and Phase Stability of Ca_2SiO_4 and Sr_2SiO_4 Powders," *J. European Ceram. Soc.*, **11** 291-298 (1993).

[9]M. Gawlicki and W. Nocon-Wczelik, " Influence of Thermal Treatment on the Transition of $\beta \rightarrow \gamma$ C_2S," (In French), *Proceedings of the 7th International Symposium on Chemistry of Cements, Vol II*, pp 161-165, Paris, (1980).

[10]S. Chomy, " The Inversion of the $\beta \rightarrow \gamma$ modifications in Dicalcium Silicate,"(in German) *Zement. Kalk. Gips.*, **23** 382-389 (1970).

[11]S. Shibata, K. Kishi, K. Asaga and M. Daimon, "Effect of Thermal History on $\beta \rightarrow \gamma$ Transformation of Pure Ca_2SiO_4," (in Japanese), *Yogyo Kyokai - Shi* **91** 497-502 (1983).

[12]D. Kralj, B. Matkovic, R. Trojko, J.F. Young and C.J. Chan, "Preparation of Dicalcium Silicate at 950°C," *J. Am. Ceram. Soc.* **69** [8] C-170-C-172 (1988).

[13]W.M. Kriven, C.J. Chan and E.A. Barinek, "The Particle Size Effect of Dicalcium Silicate in a Calcium Zirconate Matrix,"; pp. 145-155 in Advances in Ceramics, Vol. 24, Science and Technology of Zirconia III, Edited by S. Somiya, N. Yamamoto and H. Yanagida. American Ceramic Society, Westerville, OH, (1988).

[14]C.J. Chan, W.M. Kriven, and J.F. Young, "Physical Stabilization of the β to γ Transformation in Dicalcium Silicate," *J. Am. Ceram. Soc.*, **75** [6] 1621-11627 (1992).

[15]W.M. Kriven, "Possible Alternative Transformation Toughening to Zirconia: Crystallographic Aspects" *J. Am. Ceram. Soc.*, **71** [12] 1021-1030 (1988).

[16]J.S. Moya, P. Pena and S. de Aza, "Transformation Toughening in Composites containing Dicalcium Silicate," *J. Am. Ceram. Soc.*, **68** [9] C-259-C-262 (1985).

[17]T. I. Hou and W.M. Kriven, "Mechanical Properties and Microstructure of Ca_2SiO_4-$CaZrO_3$ Composites," *J. Am. Ceram. Soc.*, in press (1993).

[18]I. Nettleship, K.G. Slavick, Y.J. Kim and W.M. Kriven, "Phase Transformations in Dicalcium Silicate. I: "Fabrication and Phase Stability of Fine-Grained β Phase," *J. Am. Ceram. Soc.*, **75** [9] 2400-2406 (1992).

[19]B. Matkovic, S. Popovic and B. Grzeta, "Phases in the System Ca_2SiO_4 - Ba_2SiO_4," *J. Am. Ceram. Soc.*, **69** [2] 132-134 (1986).

[20]J. G. Thompson, R.L. Withers and B.G. Hyde, "Further Considerations of Phases in the System Ca_2SiO_4 - Ba_2SiO_4," *J. Am. Ceram. Soc.*, **70** [12] C-383–C-386 (1987).

[21]Y.J. Kim, I. Nettleship and W.M. Kriven, "Phase Transformations in Dicalcium Silicate. II: TEM Studies of Crystallography, Microstructures and Transformation Mechanisms," *J. Am. Ceram. Soc.*, **75** [9] 2407-2419 (1992).

[22]E.S. Mast, "Development and Possible Use of Dicalcium Silicate in the Transformation Toughening of Magnesia," M.S. Thesis, University of Illinois at Urbana-Champaign, (1991).

[23]B. Matkovic, V. Carin, T. Gacesa, R. Halle, I. Jelenic, and J.F. Young, "Influence of $BaSO_4$ on the Formation and Hydration Properties of Calcium Silicates I: Doped Dicalcium Silicates," *Am. Ceram. Bull.*, **60** [8] 825-829 (1981).

[24]A. Ghose, S. Chopra and J.F. Young, "Microstructural Characterization of Doped Dicalcium Silicate Polymorphs," *J. Mat. Sci.*, **18** 2905-2914 (1983).

[(25)]M.V. Swain and R.H.J. Hannink, "Metastability of the Martensitic Transformation in a 12 mol.% Ceria-Zirconia Alloy II: Grinding Studies," *J. Am. Ceram. Soc.*, **72** [8] 1358-64 (1989).

Figure captions

Fig. 1. Polymorphism of Ca_2SiO_4

Fig. 2. The Ca_2SiO_4 - Ba_2SiO_4 pseudo-binary phase diagram. After Thomson et al.[20]

Fig. 3. The XRD phase distributions in powders with different barium contents after calcination at 1300°C for 1 hour.

Fig. 4. The XRD phase distributions in powders with different barium contents after calcination at 1400°C for 1 hour.

Fig. 5. A TEM micrograph of 95 mol% Ca_2SiO_4 - 5 mol% Ba_2SiO_4 fired at 1300°C for 3 hours showing single phase α'_L. The microstructue was relatively free from the intergranular strain and microcracking associated with the twinned β phase.

Fig. 6. The XRD phase distributions of sintered surfaces of samples containing different barium contents fired at 1300°C for 12 hours.

Fig. 7. The XRD phase distributions of sintered surfaces of samples containing different barium contents fired at 1400°C for 1 hour.

Fig. 8. A plot of the effect of barium content on grain size (average intercept length) for materials fired at 1300°C for 12 hours and 1400°C for 1 hour.

Fig. 9. A comparison of XRD plots of sintered and ground surfaces for 5 mol% Ba_2SiO_4 sintered at 1300°C for 12 hours and 1400°C for 1 hour, respectively.

Fig. 10. The fracture strength of materials fired at 1300°C for 12 hours, and 1400°C for 1 hour, as a function of barium content.

Fig. 11. The elastic modulus as a function of barium content for materials fired at 1300°C for 12 hours and 1400°C for 1 hour, respectively.

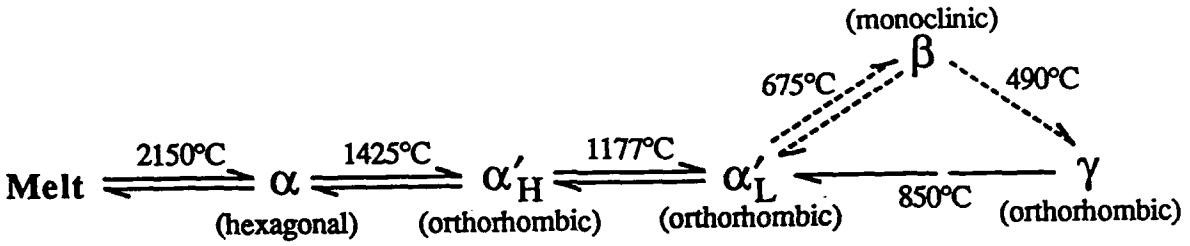

Fig. 1. Polymorphism of Ca_2SiO_4

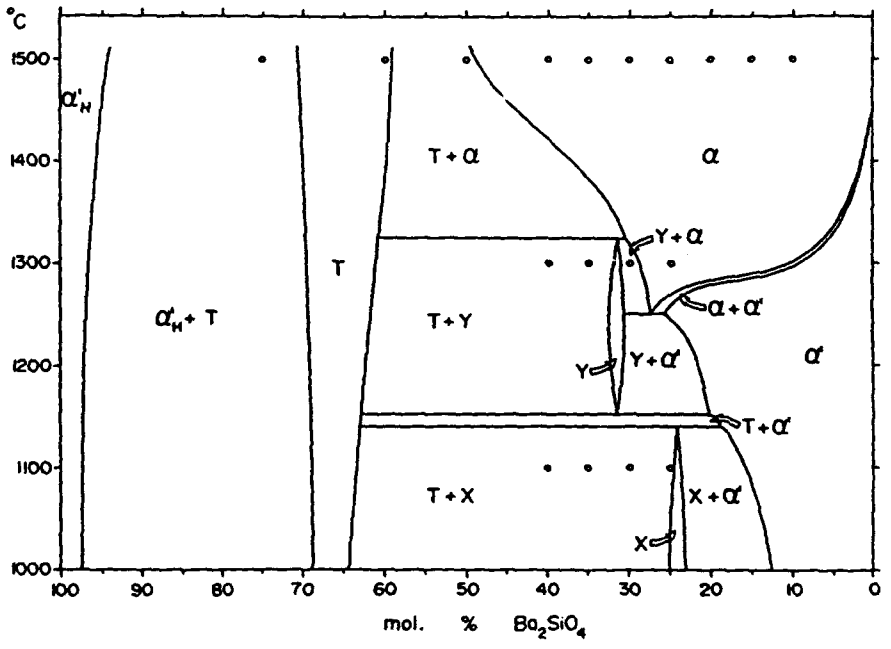

Fig. 2. The Ca_2SiO_4 - Ba_2SiO_4 pseudo-binary phase diagram. After Thomson et al.(20)

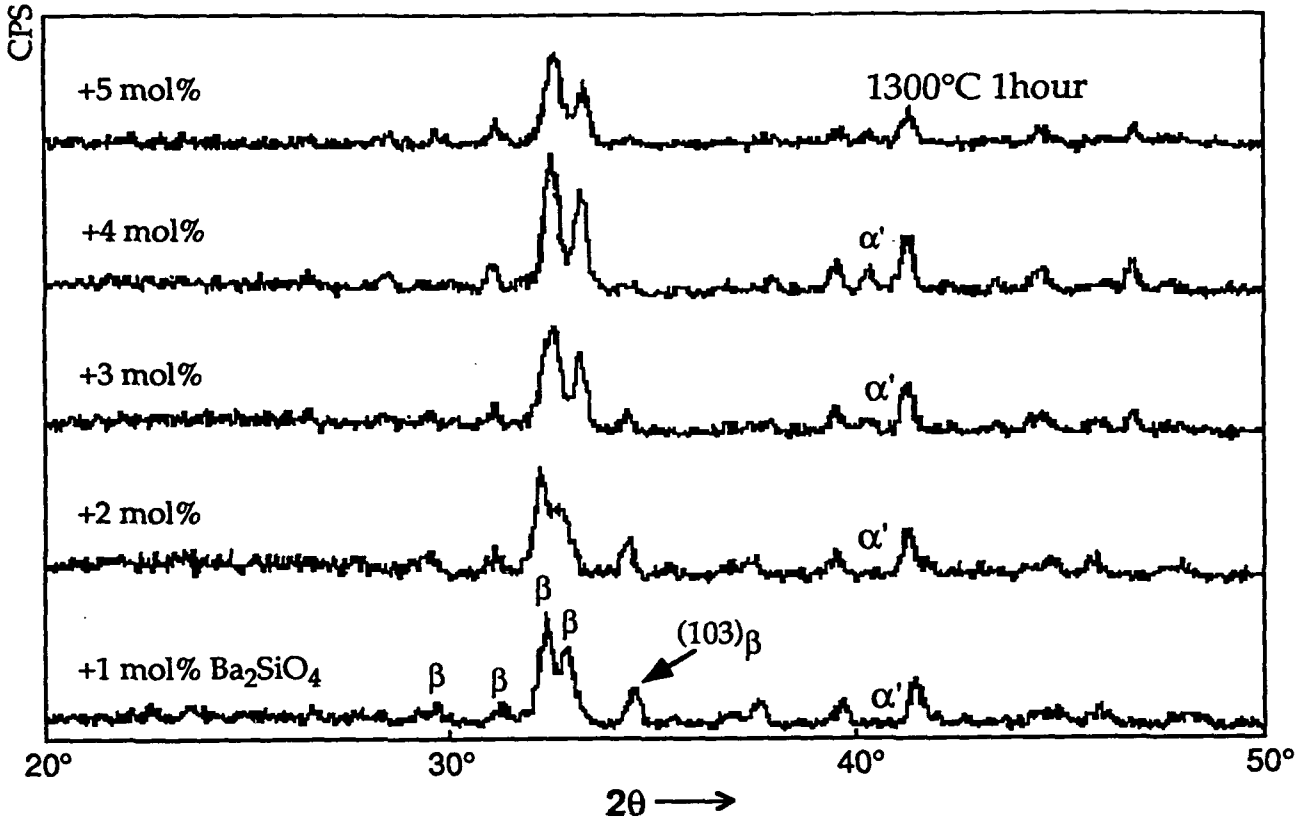
CPS
+5 mol%
1300°C 1hour
+4 mol%
α'
+3 mol%
α'
+2 mol%
α'
β
β
(103)β
+1 mol% Ba2SiO4
β
β
α'
20°
30°
40°
50°
2θ ⟶

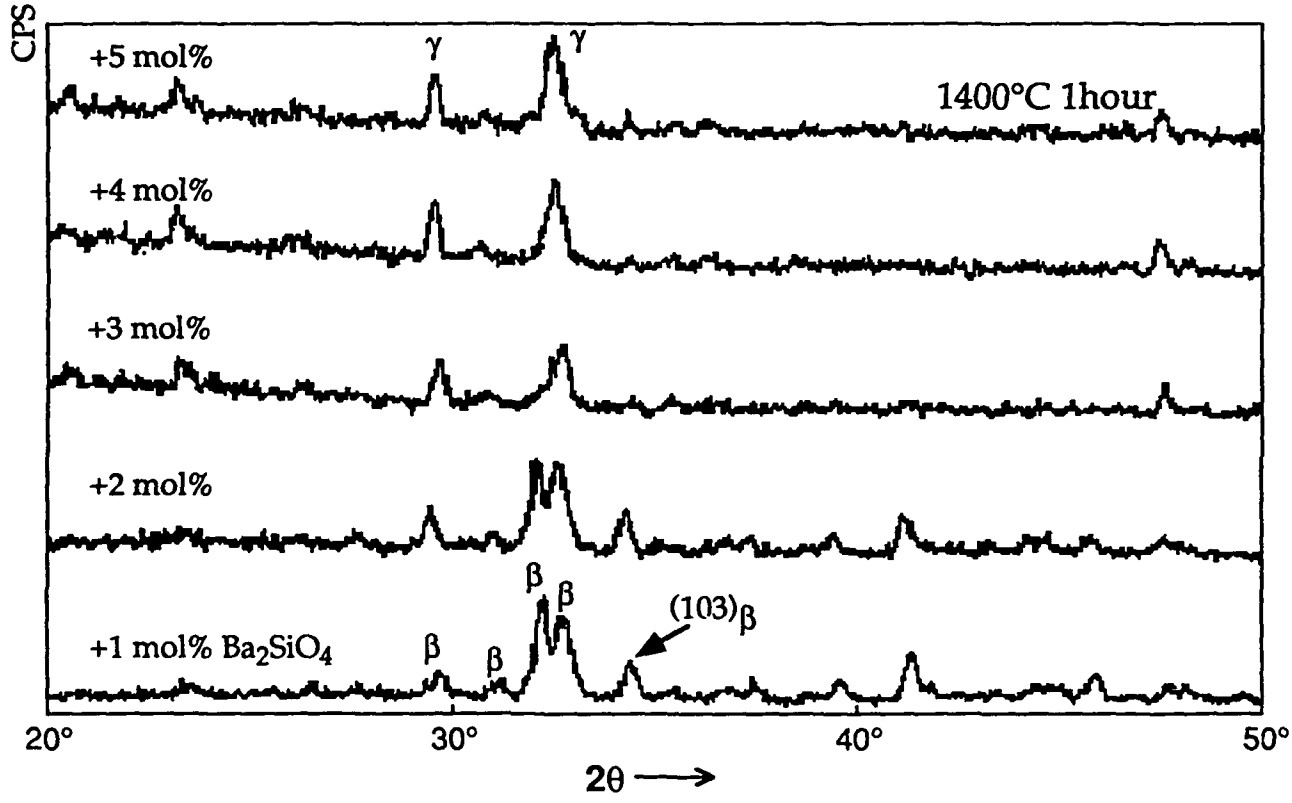
CPS
+5 mol%
γ
γ
1400°C 1hour
+4 mol%
+3 mol%
+2 mol%
β
β
(103)β
+1 mol% Ba2SiO4
β
β
20°
30°
40°
50°
2θ

Fig. 5

~~Fig. 6.~~ A TEM micrograph of 95 mol% Ca_2SiO_4 - 5 mol% Ba_2SiO_4 fired at 1300°C for 3 hours showing single phase α'_L. The microstructue was relatively free from the intergranular strain and microcracking associated with the twinned β phase.

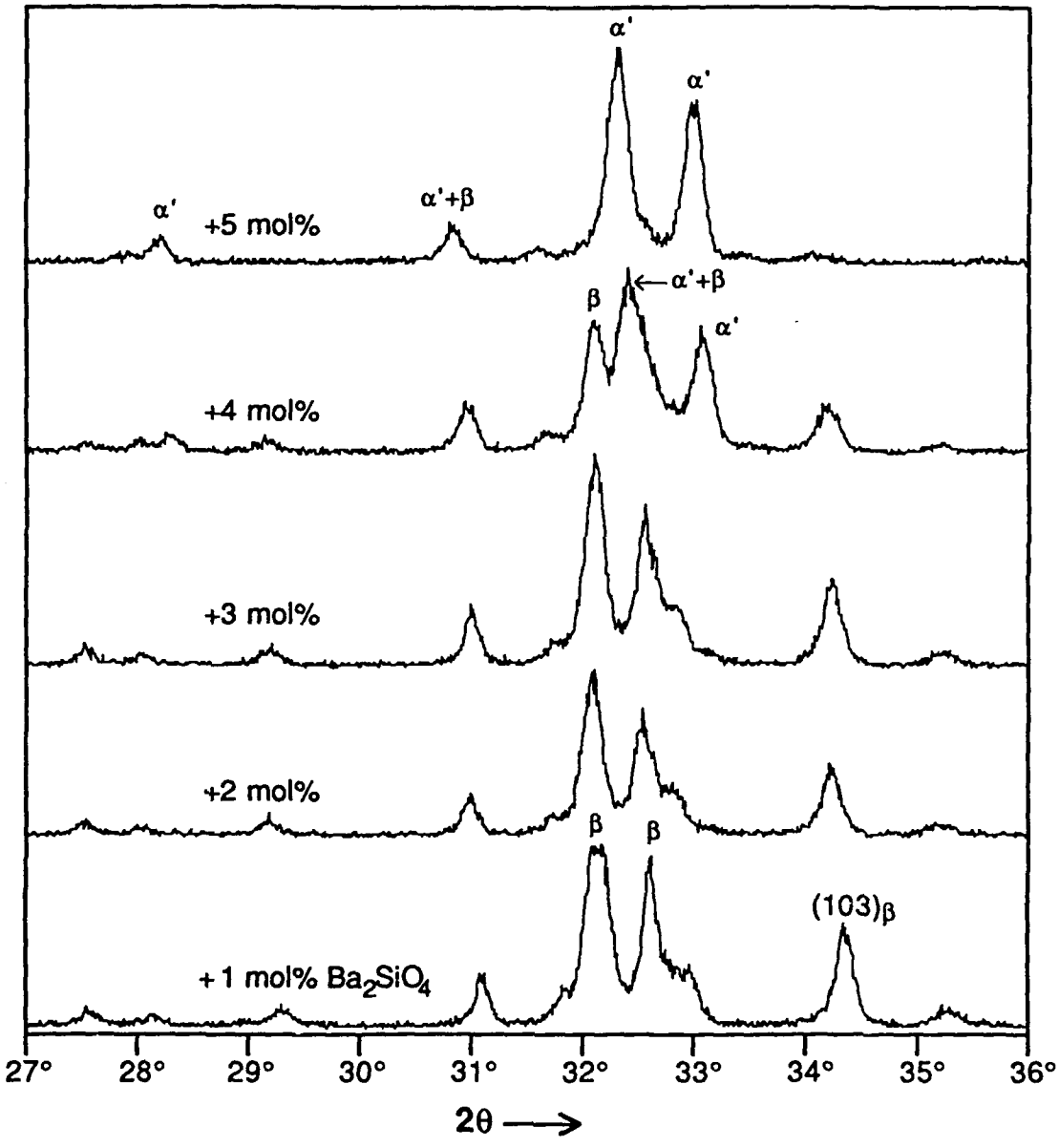
α'
α'
α'
α'+β
+5 mol%
β
←α'+β
α'
+4 mol%
+3 mol%
+2 mol%
β
β
(103)β
+1 mol% Ba2SiO4
27°
28°
29°
30°
31°
32°
33°
34°
35°
36°
2θ ⟶

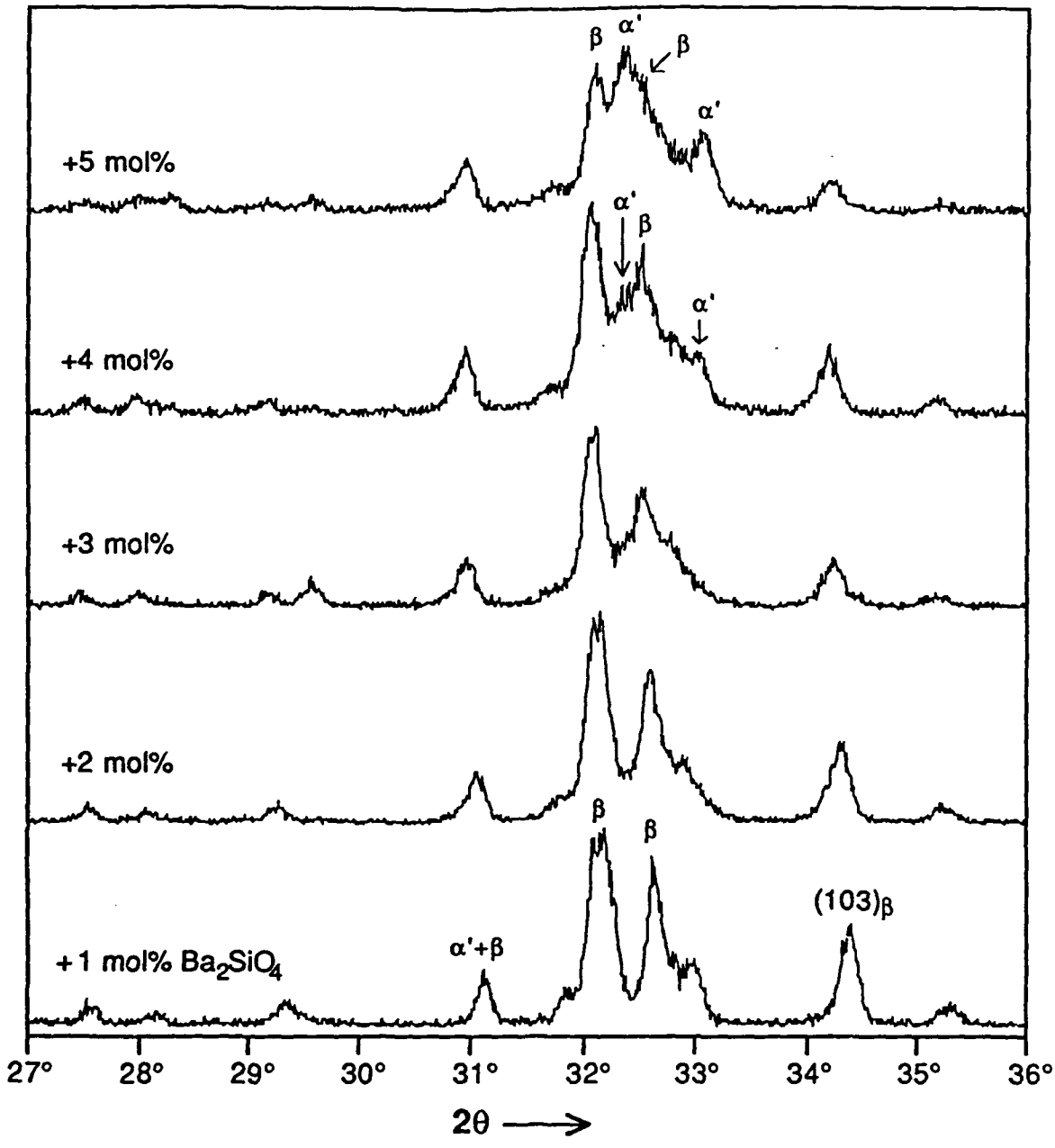
β
α'
β
α'
+5 mol%
α'
β
α'
+4 mol%
+3 mol%
+2 mol%
β
β
(103)β
α'+β
+1 mol% Ba2SiO4
27°
28°
29°
30°
31°
32°
33°
34°
35°
36°
2θ

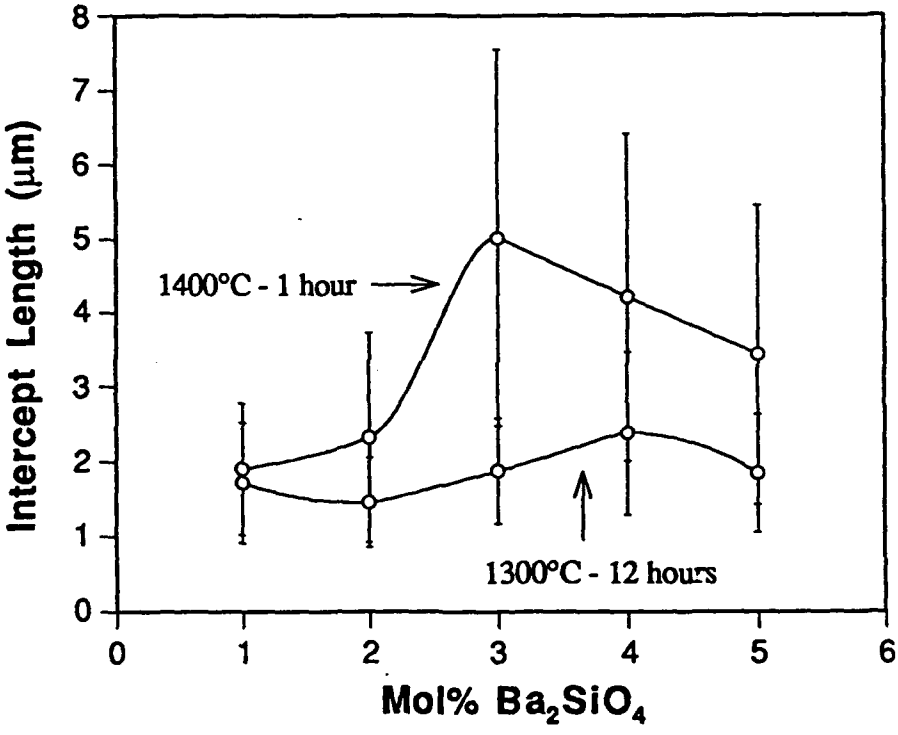
Intercept Length (μm)
8
7
6
5
4
3
2
1
0
1400°C - 1 hour
1300°C - 12 hours
0
1
2
3
4
5
6
Mol% Ba_2SiO_4

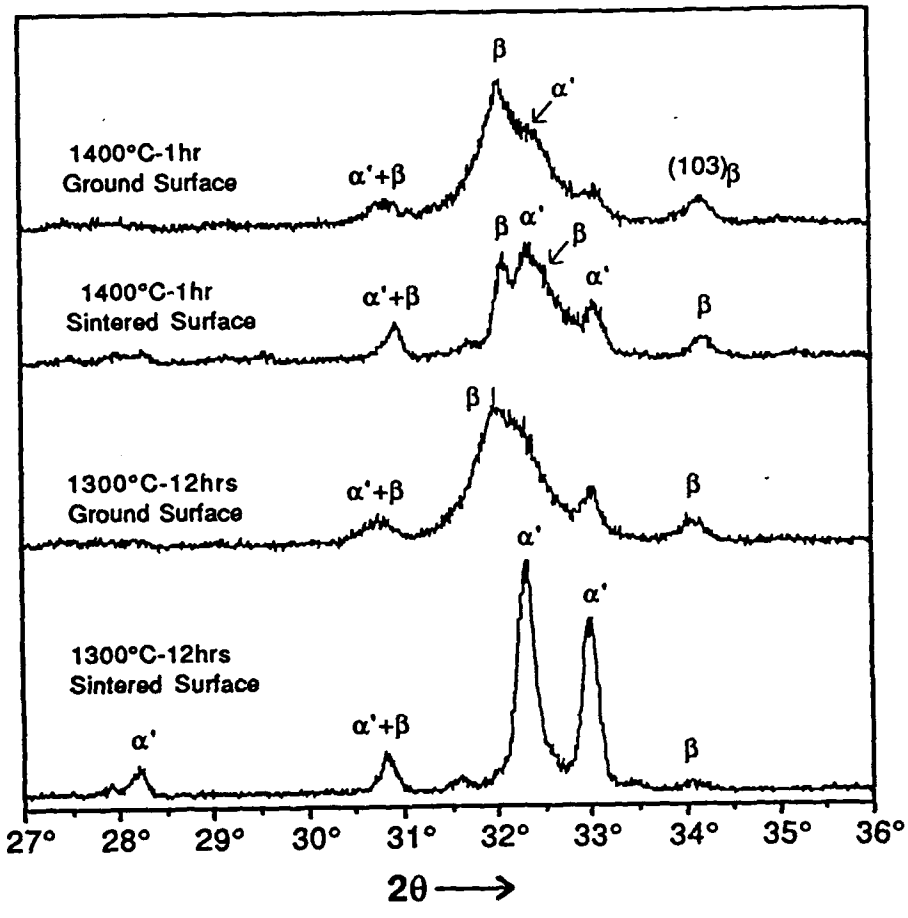
1400°C-1hr
Ground Surface
α'+β
β
α'
(103)β
1400°C-1hr
Sintered Surface
α'+β
β
α'
β
α'
β
1300°C-12hrs
Ground Surface
α'+β
β
β
1300°C-12hrs
Sintered Surface
α'
α'+β
α'
α'
β
27°
28°
29°
30°
31°
32°
33°
34°
35°
36°
2θ ⟶

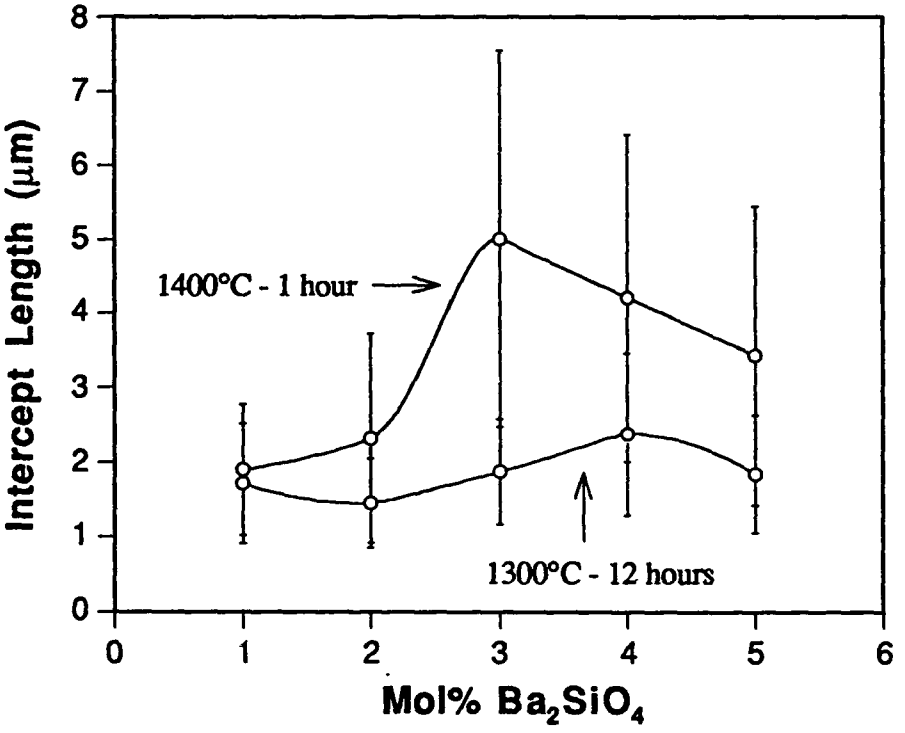
Intercept Length (μm)
0
1
2
3
4
5
6
7
8
1400°C - 1 hour
1300°C - 12 hours
0
1
2
3
4
5
6
Mol% Ba_2SiO_4

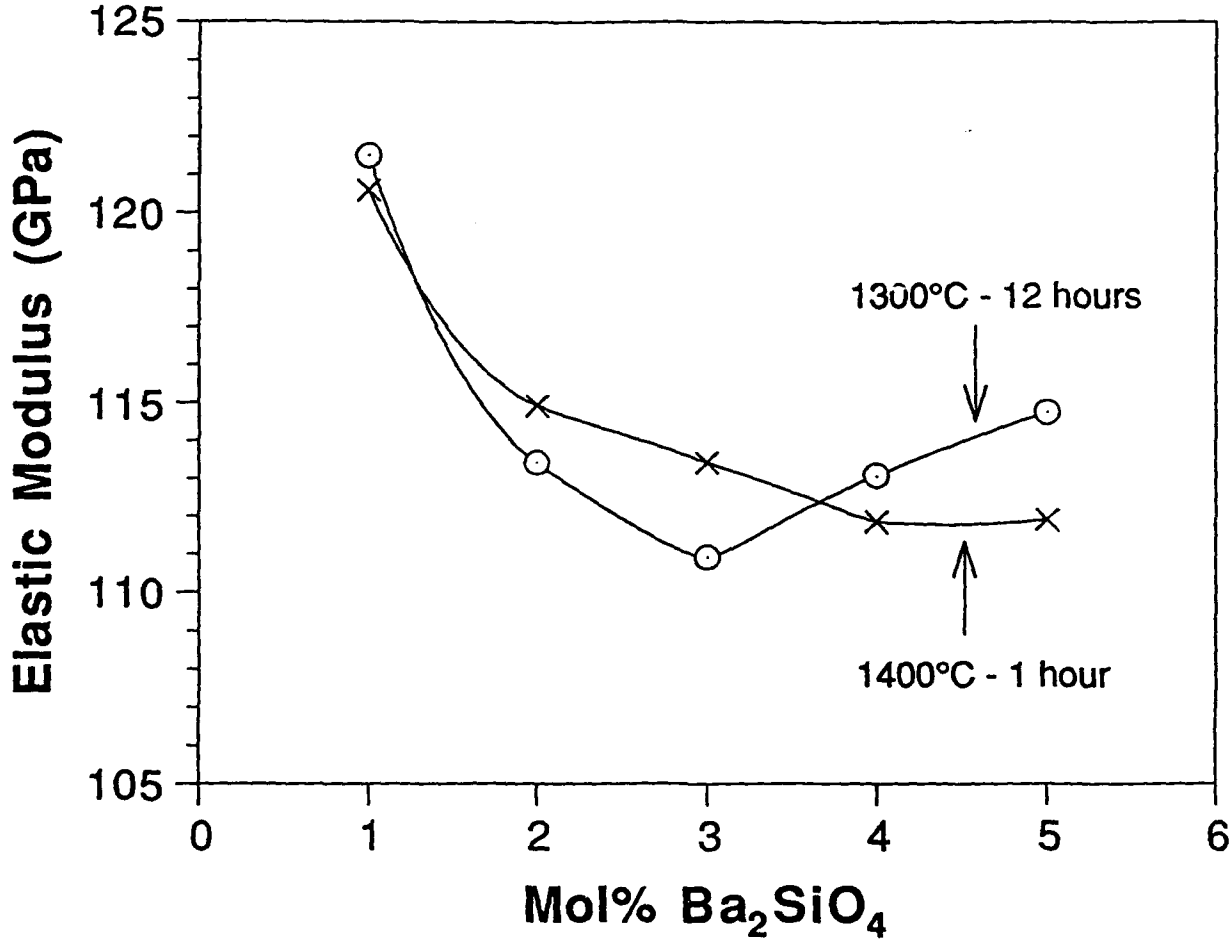

Fig. 11

~~Fig. (12).~~ The elastic modulus as a function of barium content for materials fired at 1300°C for 12 hours and 1400°C for 1 hour, respectively.

Fig. 11

Kinetics and Crystallography of the Monoclinic (B) to Cubic (C) Transformation in Dysprosia (Dy_2O_3)

O. Sudre, K.R. Venkatachari and W.M. Kriven

Department of Materials Science and Engineering,
Universty of Illinois at Urbana-Champaign,
Urbana, IL 61801, USA.

Manuscript number (MS 04)

ABSTRACT

The large volume change (≈8%) and the fast kinetics of the monoclinic (B) to cubic (C) transformation at 1950°C in dysprosia (Dy_2O_3) causes shattering of ceramic bodies on cooling. This behavior is analogous to that of zirconia with its tetragonal (t) to monoclinic (m) transformation. Dysprosia was thus considered as a potential transformation toughener for high temperature applications.

A laser-melting/roller-quenching technique was used to stabilize the high temperature monoclinic phase down to room temperature. The kinetics of the transformation back to the cubic phase through annealing heat treatments was followed by TGA, X-ray diffraction and electron microscopy techniques. A crystallographic model involving a shear mechanism was proposed.

INTRODUCTION

The first example of high-toughness ceramics relied upon the tetragonal (t) to monoclinic (m) phase transformation occurring in zirconia. The increase in fracture resistance was associated with the crystal volume expansion and shear deformation occurring in the vicinity of the crack tip. However, this toughening effect appears limited to low temperature applications, Therefore, other potential transformation tougheners have been proposed for high temperature applications [1]. The lanthanide sesquioxides (Ln_2O_3) appeared promising for further investigation.

Of particular interest, the monoclinic (B) to cubic (C) phase transformation of dysprosia (Dy_2O_3) occurs with a large positive volume expansion causing shattering upon cooling. The transformation temperature has been reported at around 1950°C which, in one hand, offers a greater potential for high temperature toughening, but on the other hand, makes it a challenging material to study by conventional techniques. Studies on the different polymorphs of the rare-earth

---

O. Sudre,[¥] K. R. Venkatachari[#] and W. M. Kriven
Department of Materials Science and Engineering, University of Illinois at Urbana-Champaign, Urbana, Illinois, 61801, USA.
[¥] Now at: ONERA Direction des Matériaux B.P.72, 92322 Châtillon Cedex, France.
[#] Now at Institute of Materials Processing, Michigan Technical University, Houghton, MI 49931.

sesquioxides has been extensive but results on their transformations were often inconsistent and led to many interpretations [2]. The polymorphs are as follows [3], where H is a hexagonal phase:

$$\text{Melt} \xrightarrow{2360^\circ C} H \xrightarrow{2175^\circ C} B \underset{1950^\circ C}{\overset{1860^\circ C}{\rightleftharpoons}} C \qquad [1]$$

Many different factors appeared to affect the stabilization of the monoclinic (B) phase and the B to C transformation, such as, pressure, stress state produced by grinding, some chemical impurities and/or additions, or even oxygen deficiency and cooling rate [2]. Possible surface anisotropy and particle size effects could also stabilize the high temperature monoclinic (B) phase. These various factors also influenced the transformation back to the cubic stable phase. In addition, the crystallographic mechanism for the transformation has not been worked out, but it has been postulated to involve some type of diffusion mechanism in the case of gadolinia [4].

In order to assess the potential use of dysprosia as a transformation toughener, further characterizations of this transformation are presented. This study was primarily focussed on the kinetics of the monoclinic to cubic transformation and on a crystallographic model compatible with experimental observations.

EXPERIMENTAL

The retention of the monoclinic phase was performed using a laser-melting/roller quenching technique. Bars of pure dysprosia powder were uniaxially compacted and the tip of the bars was melted using a laser beam (T_m = 2400°C). Once the droplet of liquid reached a critical size, it fell between two counter-spinning titanium rollers that were kept in contact. The liquid was therefore quenched and laminated as flakes. The quenching rate of this technique is thought to be of the order of 10^7°C/s. The resulting material was polycrystalline, monoclinic dysprosia. A similar technique applied to zirconia and hafnia was not able to retain the high temperature tetragonal phase.

The flakes were subsequently characterized as a function of annealing temperature. Techniques used included differential thermal analysis and thermogravimetry, quantitative X-ray diffraction, and electron microscopy . The quantitative analysis of the phase transformation from the monoclinic to the cubic phase was performed using integrated peaks (two for the cubic phase and six for the monoclinic phase) in the 25°-35° range and a calibration curve. The latter was produced using crushed monoclinic flakes and as-received cubic powder or flakes fully transformed to the cubic phase by heat treatment.

The flakes were up-quenched to different annealing temperatures and quenched back in air to room temperature. The quantity of monoclinic phase remaining was then determined by X-ray diffraction. The results were analysed using an Avrami-type equation [5,6]:

$$f(t)= k \exp(-kt^n) \quad [2]$$

where f(t) is the fraction of the monoclinic phase left untransformed after a time t, n is the kinetic law constant, also called the order of the transformation. This constant is related to the nucleation and growth mechanism of a cubic nucleus in the monoclinic matrix. The other constant, k, carries the thermal activation of the transformation through the relation:

$$k=k_0 \exp(-E_a/RT) \quad [3]$$

where E_a is the activation energy and k_0 is a constant.

RESULTS

The laser-melting/roller-quenching technique produced yellowish flakes, 1 to 3 cm^2 in size and 40 to 100 mm thick. The technique was difficult to control which resulted in a variable batch to batch flake size. Chemical analysis showed that they were 99.9% dysprosia. On the other hand, zirconia, hafnia or gadolinia produced in the same conditions resulted in white flakes.

The fast quenching rate effectively retained the high-temperature monoclinic phase of dysprosia down to room temperature. However, the strongest peak of the cubic phase corresponding to the $(222)_C$ plane could be detected by X-ray diffraction which may indicate the presence of a few percent of that phase. It was nevertheless neglected in the analysis. A preferred orientation of the $(20\bar{1})_B$ plane of the monoclinic phase relative to the flake surface was also observed and, therefore, the flakes were slightly crushed before heat treatments. The microstructural observations of the as-quenched flakes revealed a lot of surface features reminiscent of the solidification history of the material. In a number of locations, the grains were revealed and the grain size was estimated by computerized trace analysis to be about 2.4 μm. Observations by transmission electron microscopy showed different types of defects within the grains such as dislocations, low angle grain boundaries and twins. Some of the dislocations were mobile under the electron beam.

The transformation of the flakes from the monoclinic to cubic phase was solely obtained through annealing heat treatments. Grinding or undercooling in liquid nitrogen did not appear to trigger the transformation. Annealing experiments performed in air, nitrogen, in a vacuum furnace or in the hot-stage of a transmission electron microscope always resulted in the transformation of the monoclinic phase to the cubic phase. The thermogravimetric analysis under argon indicated a slight weight gain of about 0.325% as shown in figure 1. The weight gain occurred in two steps: below 600°C, the weight increased slowly, whereas it was more rapid above 600°C. This gain was accompanied by a change of coloration of the flakes from yellow-brown to grey. This result could originate from a partial recovering of the stoichiometry of dysprosia. With this hypothesis, the initial composition of the flakes would be Dy_2O_{3-x}, x=0.075. At the end of this thermal analysis to 1000°C, the monoclinic phase had fully transformed to the cubic phase. T.E.M. observations indicated that most microstructural defects were annealed out at 400-500°C. However, around 600°C, the large volume expansion of the transformation

caused cracking and shattering of the flakes. This was observed by S.E.M (figure 2a) and on the hot stage of a high voltage electron microscope (figure 2b). However, no characterisitic peak could be detected by differential thermal analysis.

The kinetic study further characterized the transformation. The quantitative X-ray analysis using the experimental monoclinic/cubic calibration curve provided data that could be fitted to the Avrami equation. Linear regression for different annealing temperatures provided a value of n, the order of the transformation, as a function of the temperature (figure 3a). In addition, two activation energies could be deduced from the data (figure 3b). Below 600°C, the transformation appears sluggish with a high order, n, and a high activation energy of 396 kJ/mole. However, above 600°C, the order of the transformation dropped towards zero and the activation energy was reduced to 30 kJ/mole.

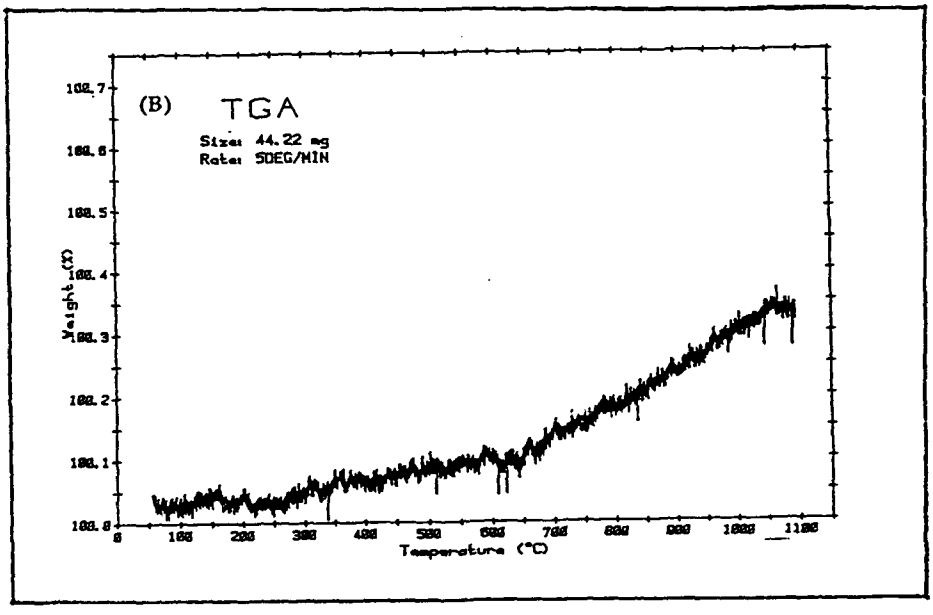

Figure 1. Thermogravimetric analysis of B-Dy_2O_3

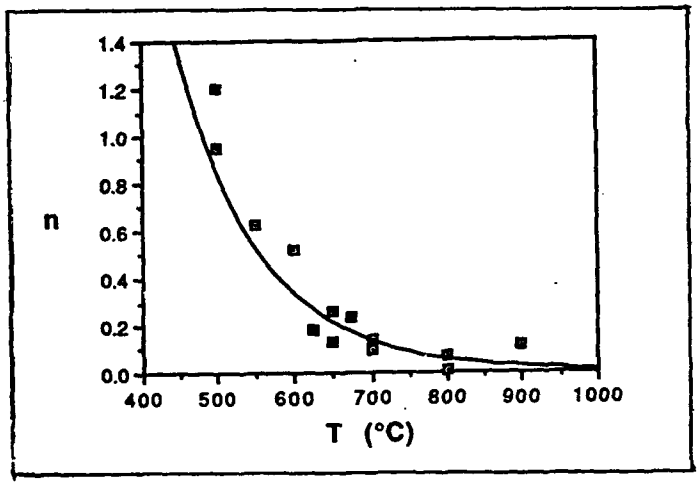

Figure 2(a). Kinetic study yielding the order of the transformation

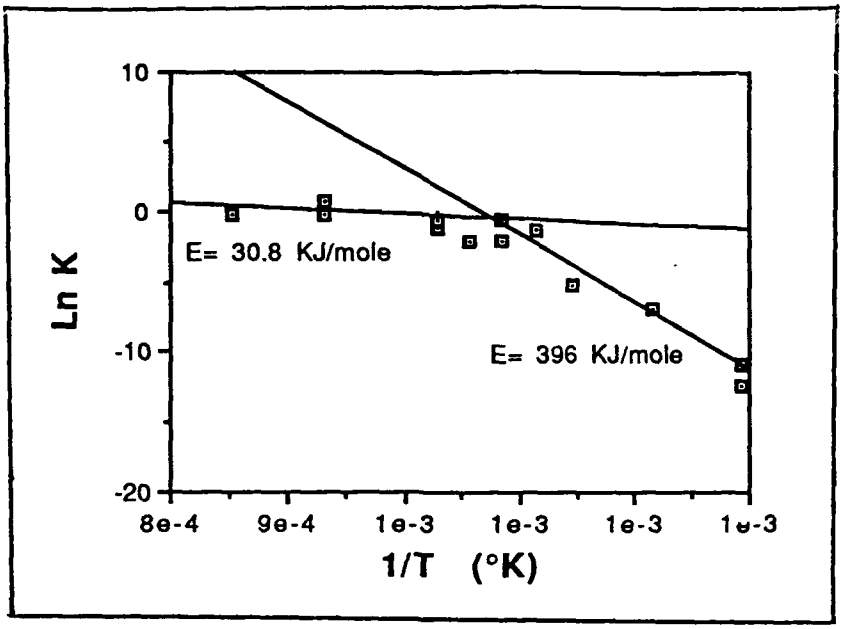

Figure 2(b). Kinetic study yielding activation energy as a function of temperature.

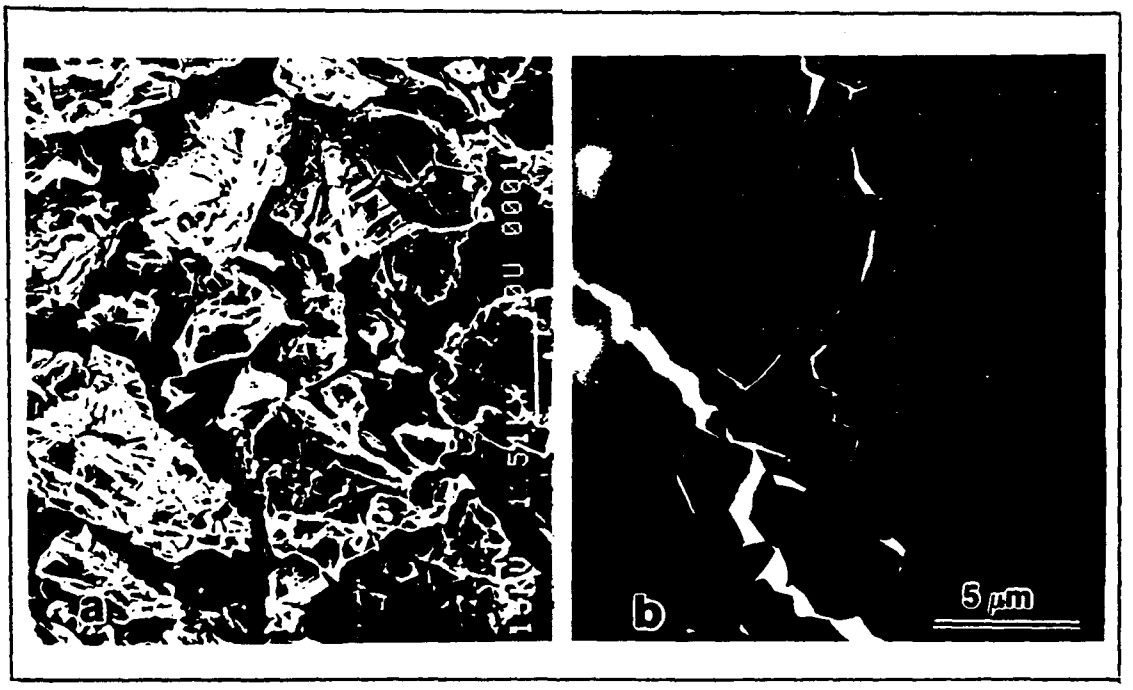

Figure 3(a). SEM micrograph of grains produced after annealing of a monoclinic flake and (b) H.V.E.M. micrograph of cracks in a flake at 600°C.

CRYSTALLOGRAPHIC MODEL

Parallel to the experimental work, a theoretical approach was adopted as it could provide additional insights into the experimental work. Most descriptions of the polymorphs of the rare-earth oxides are based on a (OLn_4) tetrahedral unit. [7] Even though the individual phases are well described by various packings of this structural unit, the transformation itself is more controversial. In the present work, a simple representation of the correspondence between the monoclinic (B) and the cubic (C) phases is proposed.

A complete description of the two crystal phases has been presented elsewhere [7]. The cubic structure is based on an oxygen-deficient fluorite structure, whereas the monoclinic structure is often described as a layered structure. In these two structures, the $(111)_C$ and $(20\bar{1})_B$ planes are often found in the literature in epitaxial relations [8,9]. In addition, the cation sublattice is almost identical in these two planes. A second relationship is found by noticing that the motif in the $(010)_B$ plane of the monoclinic phase (figure 4 a) can be derived from three motifs of each of the four types of $(110)_C$ planes of the cubic phase (figure 4 b). From these two observations, it was possible to establish a lattice correspondence shown in figure 5 which can be formalized mathematically by the following relation, where (x,y,z) are the coordinates of a direction in the respective structures.

$$\begin{pmatrix} xC \\ yC \\ zC \end{pmatrix} = \begin{pmatrix} 3/4 & -1/4 & 0 \\ 3/4 & 1/4 & 0 \\ -1/4 & 0 & 1 \end{pmatrix} \begin{pmatrix} xB \\ yB \\ zB \end{pmatrix} \qquad [4]$$

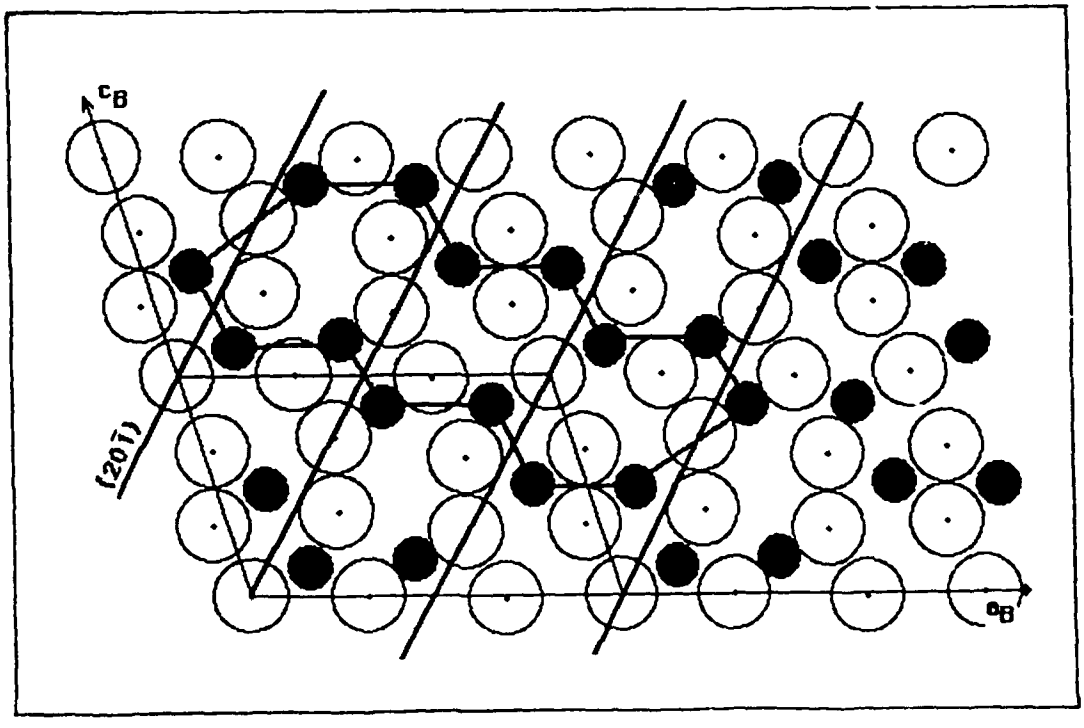

Figure 4(a). The $(010)_B$ plane with the corresponding motif.

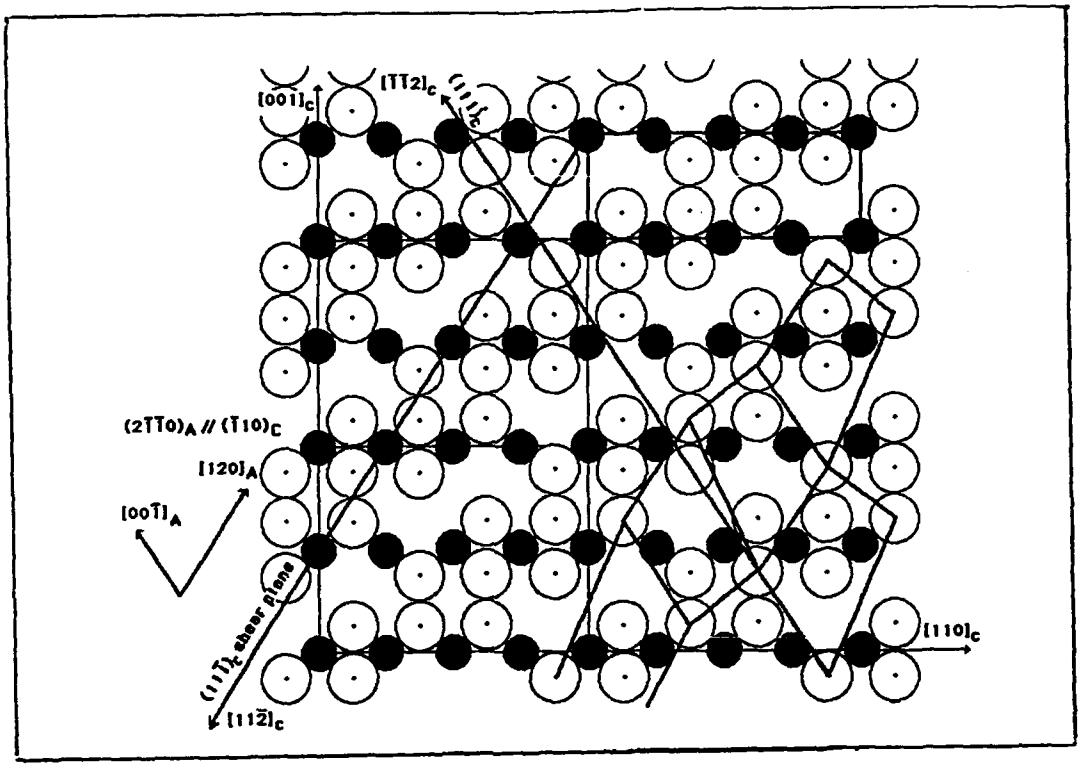

Figure 4(b). One of the four $(110)_C$ planes with major directions and three outlined motifs.

Futhermore, a phase transformation mechanism could also be proposed. The transformation is believed to occur via a shear deformation of the lattice in the $(20\bar{1})_B$ layer plane along the $1/3[\bar{1}0\bar{2}]_B$ direction. During this large shear deformation, a one to one relation exists between the atoms of the $(010)_B$ and the $(110)_C$ planes. The cation sublattice is simply sheared whereas some shuffling of the oxygen atoms is required within the motifs. Additional calculations using an approach developed for martensitic transformations [10], indicated that the change in volume ($\Delta V/V = 8.5\%$) and strain energy (=0.3687) involved during the B to C transformation at room temperature are very large (2 to 3 times larger than those of zirconia).

DISCUSSION

The laser-melting/roller-quenching technique was effective in retaining the high temperature phase of Dy_2O_3 unlike that of ZrO_2 and HfO_2. Several factors may have produced this difference. Assuming that the crystallization of the different materials was done in their respective high-temperature phase fields, the stabilization of monoclinc (B) dysprosia implied that additional stabilizing effects are present in dysprosia compared to the two others. These effects are of several types. First, the monoclinic phase appears to be non-stochiometric, based upon the weight gain on annealing and the change in color from yellowish to white. The nonstoichiometry may partly reduce the free-energy of the phase such as twins or

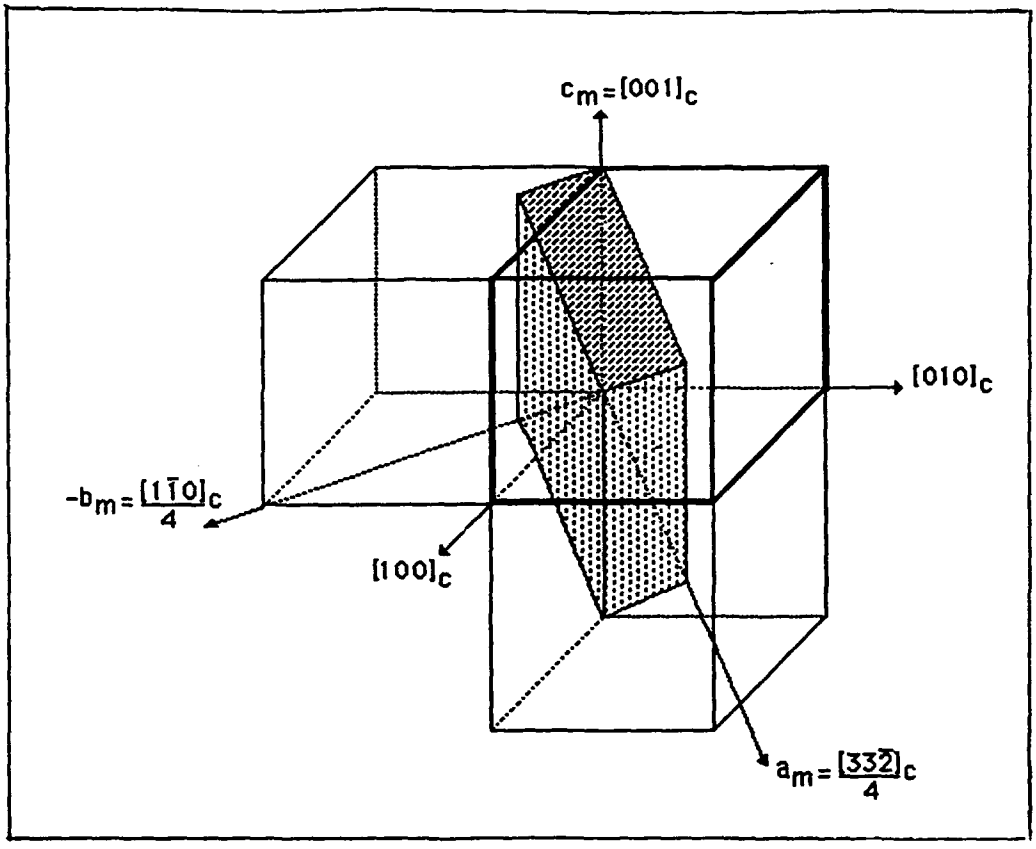

Figure 5. Lattice correspondence between cubic (C) and monoclinic (B) phases.

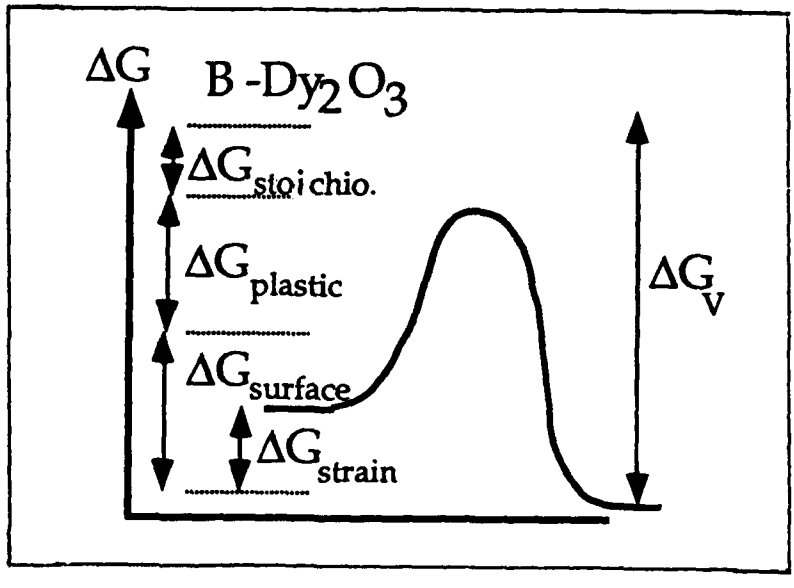

Figure 6. Schematic of the free-energy contributions to the stabilization of the monoclinic phase.

dislocations which could produce an additional free-energy reduction. Annealing of the phase was correlated with the transformation back to the stable cubic phase. Second, the mechanical action of the rollers may have been sufficient to trigger the transformation of ZrO_2 and HfO_2. Conversely, the monoclinic structure of the rare-earth oxides being rather plastic, the material may have relieved the mechanical strain of the roller action by deformation via twinning or dislocation activation. Finally, the preferred orientation of the surface of the flakes relative to the $(20\bar{1})_B$ plane may also produce a stabilizing effect. All these different factors may well have produced sufficient free energy gain to stabilize the monoclinic phase as depicted schematically in figure 6.

The characterization was completed with the kinetic study. The analysis of the data using an Avrami-type equation showed that the order of the transformation falls off to zero with increasing temperature, and that the activation energy is largely reduced above 600°C. Even though these results are difficult to interpret since nucleation and growth arguments have to be accounted for, a comparison with the transformation kinetic studies on zirconia [6] shows both a similar fall-off of the kinetic law exponent with temperature below 0.5 and similar activation energies.

In addition, the crystallographic model proposed a lattice correspondence between the two phases based on similar motifs between planes of the two structures. The resulting transformation mechanisms involving a large shear deformation of the cation lattice with some local shuffling of the oxygen atoms appears compatible with the other experimental observations. First, the large strain energy necessary for the transformation could explain the high stability of the monoclinic structure. Second, the B to C transformation occurs from a low symmetry structure to a high symmetry structure, which is rather uncommon. Therefore, a cooperative nucleation and growth at the atomic scale in different planes of the monoclinic structure is necessary to form a critical nucleus.

CONCLUSION

The present investigation attempted to shed some light on the monoclinic (B) to cubic (C) phase transformation of dysprosia. The study was successful in retaining the monoclinic phase and transforming it back to the cubic phase through annealing heat treatments. Both a two-step weight gain and two-step transformation kinetics were observed with a transformation temperature of 600°C. However, these observations are insufficient to fully characterize the transformation. A crystallographic model which involved a large shear deformation of the lattice and a local shuffling of oxygens, was also proposed. Further investigations on this transformation are required to settle the question on the possible use of this transformation for toughening of bulk structural ceramics.

ACKNOWLEDGEMENTS

This work was supported by the U.S. Air Force Office of Scientific Research under Grant number AFOSR 85-0242. Use of the facilities in the Center for Microanalysis of Materials at UIUC is acknowledged.

REFERENCES

1. Kriven, W.M., 1988. "On Possible Transformation Toughened Alternative to Zirconia: Crystallographic Aspects." J. Amer. Ceram. Soc., 71 [12]: 1021-1030.

2. Sudre, O., 1988. "Investigations of the Monoclinic (B) to Cubic (C) Transformation of Dysprosium Sesquioxide." M.S. Thesis, University of Illinois at Urbana-Champaign, Illinois, USA.

3. Foex, M. et Traverse, J.P., 1966. "Remarques sur les Cristallines Présentées à Hautes Températures par les Sesquioxides de Terres Rares." Rev. Int. Hautes Temp. et Réfract., 3: 429-453.

4. Stecura, S., 1965. "Crystallographic Modifications of Phase Transformation Rates of Five Rare-earth Sesquioxides." U.S. Bureau of Mines Report 6616.

5. Rao, C.N.R., and Rao, K.J., 1967. "Phase Transformations in Solids" in Progress in Solid State Chemistry 4, H. Reiss, ed., Thousand Oaks, California, USA: Pergamon Press, pp 131-185.

6. Whitney, E.D., 1965. "Kinetics and Mechanism of the Transition of Metastable Tetragonal to Monoclinic Zirconia." Trans. Farad. Soc., 61 [9]:1991-2000.

7. Caro, P.E., 1968. "OM_4 Tetrahedra Linkages and the Cationic Group $(MO)_n^{n+}$ in the Rare-Earth Oxides and Oxysalts." J. Less Common Metals, 16:367-377.

8. Caro, P.E., Schiffmacher, G., Boulesteix, C., Loir, Ch., and Portier, R.., 1974. "Defects and Impurities Influences on the Phase Transformations in the Rare-Earth Oxides." in Defects and Transport in Oxides, M.S. Seltzer and R.I. Jaffee, eds., Columbus and Salt Fork, Ohio, USA: Plenum Press, pp 519-535.

9. Michel, D., Rouaux, Y. and Perez Y Jorba, 1980. "Ceramic Eutectics in the ZrO_2-Ln_2O_3 (Ln: Lanthanide): Unindirectional Solidification, Microstructural and Crystallographic Characterization." J. Mater. Sci., 15:61-66.

10. Bowles, J.S. and MacKenzie, J.K., 1954. "The Crystallography of Martensite Transformation I." Acta Met., 2 [1]:129-137.

G. W. Bailey, Editor, Proceedings of the 49th Annual Meeting of the Electron Microscopy Society of America
 Published by San Francisco Press, Inc., Box 6800, San Francisco, CA 94101-6800, USA

MICROSTRUCTURAL AND MICROCHEMICAL CHARACTERIZATION OF NICKEL SULFIDE INCLUSIONS IN PLATE GLASS

J. Cooper, O. Popoola and W. M. Kriven

Department of Materials Science and Engineering, University of Illinois at Urbana-Champaign, Urbana, IL 61801

Nickel sulfide inclusions have been implicated in the spontaneous fracture of large windows of tempered plate glass.[1,2,3,4] Two alternative explanations for the fracture-initiating behaviour of these inclusions have been proposed: (1) the volume increase which accompanies the α to β phase transformation in stoichiometric NiS [5], and (2) the thermal expansion mismatch between the nickel sulfide phases and the glass matrix.[6] The microstructure and microchemistry of the small inclusions (80 to 250 μm spheres), needed to determine the cause of fracture, have not been well characterized hitherto. The aim of this communication is to report a detailed TEM and EDS study of the inclusions.

An inclusion (~100 μm) recovered from the fracture surface of a failed window (ICI House, Melbourne) was embedded in an epoxy mixture. Thin sections (~900 Å thick) were cut by ultramicrotomy following the method described in ref. 7. TEM and EDS were performed using a Philips EM 420 operated at 120 keV.

An optical micrograph of an inclusion in bulk glass, taken under polarized light, (Fig. 1) shows the associated strain field. The firm adherence of the particle to the glass fracture surface is illustrated in Fig. 2. A low magnification TEM image of the ultramicrotomed sections (Fig. 3) reveals that extensive mechanical damage occurred during specimen preparation. A small region analyzed as $Ni_{50}S_{50}$ contained twins (Fig. 4). These twins were believed to be deformation twins produced during ultramicrotomy. Figure 5 shows the frequency distribution of various nickel sulfide compositions found by EDS analysis. Very few stoichiometric NiS regions were found. The particle was composed mostly of untwinned nickel-rich phases.

The nickel sulfide particle studied was polycrystalline and contained predominantly Ni-rich phases. This is in agreement with the results of ref. 6 and supports the conclusion that the cause of fracture is the thermal expansion mismatch between nickel sulfide compounds and glass. The volume increase (~4%) which would result from the α to β transformation (if any) of the small regions of NiS would be easily accomodated by the surrounding ductile nickel rich phases.

References

1. E. R. Ballantyne, CSIRO Division of Building Research Report, Melbourne, (1961).
2. H. Tabuchi, 10th International Congress on Glass, Ceram. Soc. of Japan. Kyoto, Japan, (1974) July, 3-54.
3. C. C. Hsiao, Fracture 1977, ICF4, Waterloo, Canada, Volume 3, 985.
4. R. C. Bradt, Alfred University Fractography Conference, (1986) August.
5. M. V. Swain, *J. Mat. Sci.*, (1981) 16, 151.
6. St. Gobain Glass Industries, France. Internal Report.
7. O. Popoola, W. K. Kriven and J. F. Young, Ultramicrotomy (in press).

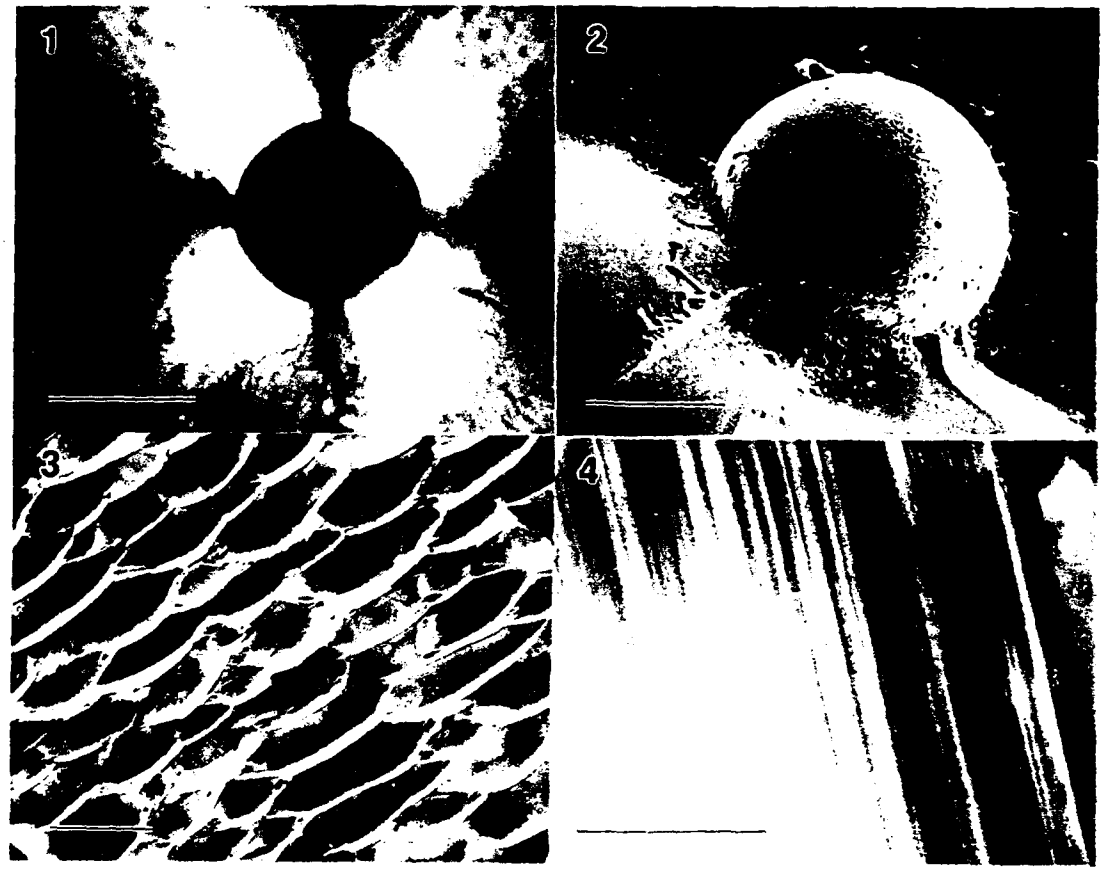

FIG. 1.--Optical micrograph showing nickel sulfide inclusion in plate glass. Note strain field. Bar = 100 μm.

FIG. 2.--SEM micrograph of inclusion adhering to glass fracture surface. Bar = 100 μm.

FIG. 3.--Ultramicrotomed sections showing "slivered" structure. Bar = 1μm.

FIG. 4.--Deformation twins produced by ultramicrotomy. Bar = 0.05 μm.

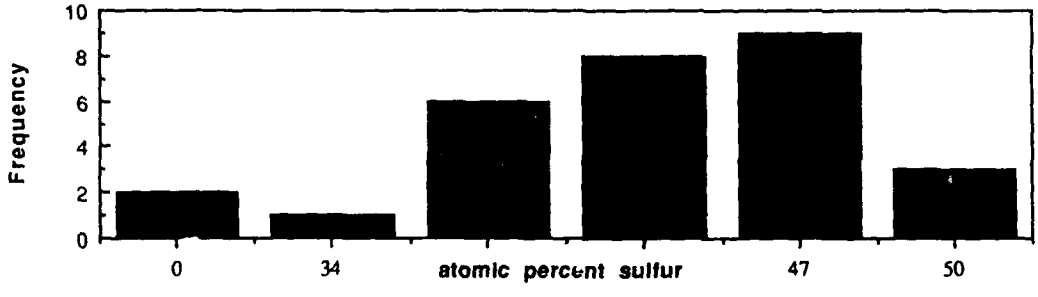

FIG. 5.--Frequency distribution of EDS analyses.

EFFECT OF DYSPROSIA DISPERSIONS ON THE PROPERTIES OF SILICON CARBIDE COMPOSITES

Shin Kim and Waltraud M. Kriven
Department of Materials Science and Engineering
University of Illinois at Urbana-Champaign, Urbana, IL 61801

Reprinted from Proceedings of the 1st International Symposium on the Science of Engineering Ceramics, October 21-23, 1991, Koda, Japan, Edited by S. Kimura and K. Niihara, The Ceramic Society of Japan, Tokyo, 1991, pp.63-68.

EFFECT OF DYSPROSIA DISPERSIONS ON THE PROPERTIES OF SILICON CARBIDE COMPOSITES

Shin Kim* and Waltraud M. Kriven
Department of Materials Science and Engineering
University of Illinois at Urbana-Champaign, Urbana, IL 61801

ABSTRACT

Composites of silicon carbide with 10% to 15 vol% dysprosia (Dy_2O_3) were fabricated by hot pressing. The effects of Dy_2O_3 dispersions on the physical and mechanical properties of the composites were investigated. Elastic moduli, hardness, fracture toughness and flexural strengths of the composites were evaluated. With the dispersion of 10% to 15 vol% Dy_2O_3 in SiC matrix, the fracture toughness increased by ≈ 40%. The increased fracture toughness was due to crack deflection in conjunction with crack-interface grain bridging and was not related to a phase transformation of Dy_2O_3 in the matrix.

INTRODUCTION

Silicon carbide is a promising material because of its excellent chemical and physical properties. However, its full potential has not been realized partially due to its tendency towards brittle behavior. In SiC composites, particulate toughening of SiC has been realized by incorporating second phase particles like TiB_2 (1) or TiC (2). Dysprosia (Dy_2O_3), one of the lanthanide sesquioxides, has high temperature thermodynamic stability and low volatility. The lanthanide sesquioxides have been proposed as potential high temperature transformation tougheners (3). On cooling, dysprosia (Dy_2O_3) transforms from monoclinic (B) to cubic (C) symmetry with an 8% volume increase at about 1850 °C. The nature of the transformation appears to be displacive and possibly martensitic, like that of zirconia (4).

An investigation of the lanthanide sesquioxides as transformation toughening agents (4) showed an increase in toughness by dispersing Tb_2O_3 into an MgO matrix. It was attributed to the B to C transformation at temperatures ≥ 1075°C. No previous work was conducted, however, to disperse Dy_2O_3 into a ceramic matrix in order to investigate its effect on the toughness of a composite.

In the present work, composites of silicon carbides with 10% to 15 vol% dysprosia were fabricated and the effects of dispersed dysprosia in SiC matrix on the physical and mechanical properties of the composites were evaluated. Possible toughening mechanisms were studied.

* Now at the Ceramic Materials Laboratory, Korea Institute of Machinery and Metals, Changwon, Korea.

MATERIALS AND METHODS

Fabrication of Composites

Plasma synthesized β-silicon carbide powders (0.5 μm particle size; designated AL) and commercial α-SiC powders (Grade A10, Herman C. Starck Inc.; designated ST) were used. Dy_2O_3 powders with 99.9% purity had an average particle size of ≈ 2 μm. Amorphous boron and carbon (as polyphenylene resin) were used in some composites as sintering additives. Most SiC - Dy_2O_3 powders were attrition milled in methanol for 1h using SiC balls as grinding media. The powder compacts were hot pressed at 2000 - 2050°C for 30 min to 1 h with an applied pressure of 28 MPa. A post densification hot isostatic pressing treatment was conducted at 2000°C for 1 h for some materials in an effort to increase the density of the composites. For selected specimens, attempts were made to retain the high temperature form of Dy_2O_3 in a SiC matrix by rapid cooling from the monoclinic phase region. Samples were heated up to 2050°C in a controlled atmosphere furnace which was capable of very rapid heating and cooling.

Characterization and Mechanical Property Evaluation

Elastic moduli were determined by the ultrasonic pulse-echo technique. Vickers indentation hardness was determined using a commercial microhardness tester at loads below the threshold for cracking. Fracture strength was measured in four-point flexure on bars ground to a 600 grit finish with bevelled edges. The inner and outer span lengths for the flexure tests were 10.5 mm and 19 mm, respectively. The crosshead speed was 0.5 mm/min. Fracture toughness was measured in three-point flexure on notched bars or by the Vickers microindentation technique depending on the specimen size. The notch depth was kept to about 40 % of the bar depth. The equation proposed by Anstis et al.(5) was used to calculate the Vickers indentation fracture toughness. The H/E ratio was obtained by the Knoop indentiation method (6) and by the calculation of the H/E ratio from direct measurements of both the Vickers hardness and the Young's modulus.

RESULTS AND DISCUSSION

Table 1 shows the densities of the composites after hot pressing. All SiC - Dy_2O_3 composites always contained cubic (C) Dy_2O_3 in SiC matrices. After the rapid cooling heat treatment from the monoclinic phase region, it was possible to retain monoclinic Dy_2O_3 in a SiC matrix. Table 2 lists the elastic properties of selected materials. The dispersion of Dy_2O_3 into a SiC matrix caused the Young's moduli to decrease because of the low modulus of Dy_2O_3. Addition of 10 vol% Dy_2O_3 caused the Young's modulus to decrease by ≈ 10 to 14 % and addition of 15 vol% Dy_2O_3 resulted in ≈ 12 to 15 % decreases in the Young's modulus. Notice, however, that the Dy_2O_3 - dispersed composites contained more porosity than those densified without Dy_2O_3 additions. Therefore, the zero porosity values of the composites could be higher than those reported here. There was no dramatic decrease in the moduli values observed in microcracked materials such as Al_2O_3 - ZrO_2 composite, indirectly proving that there was no formation of microcracks in the composites. The slightly increased moduli (≈ 3 to 4%) of post-densification hot isostatically pressed composites were due to the reduced porosity by the hot isostatic pressing treatment.
The Vickers hardness and indentation fracture toughness of AL SiC materials are shown in Table 3. An increase of fracture toughness by ≈ 40% was observed when 15 vol % Dy_2O_3 was added to SiC. The rapidly cooled material (monoclinic Dy_2O_3 in SiC matrix) exhibited the same fracture toughness as the as-hot pressed material (cubic Dy_2O_3 in SiC matrix). This suggested that the toughening mechanism in this particular composite was not related to a martensitic phase transformation of the Dy_2O_3 phase in the composite. The use of different methods for the determination of the H / E ratio caused relatively small differences in the indentation toughness values. The flexural strength (MOR) and notched beam fracture

Table 1. Densities of hot pressed SiC materials

ID No.	Specimen†	Densification	Density (g/cm^3)	%TD*
001	ST α-SiC	HP 2050°C/30 min (1% B and 1% C)	3.16	98.6%
012	ST α10D	HP 2050°C/30 min (0.5% C)	3.53	96.2%
012.5	ST α10D	HP followed by HIP 2000°C/1h	3.55	96.7%
013	ST α10D	HP 2050°C/30 min with 1%C	3.52	96.0%
013.5	ST α10D	HP followed by HIP 2000°C/1h	3.56	97.1%
104	AL β-SiC	HP 2000°C/1h	3.16	98.4%
104.5	AL β-SiC	HP followed by HIP at 2000°C/1h	3.19	99.4%
105	AL β15D	HP 2000°C/1h	3.53	90.4%
105.5	AL β15D	HP followed by HIP at 2000°C	3.57	91.7%

† α10D = α-SiC -10 vol% Dy_2O_3; β15D = β-SiC -15 vol% Dy_2O_3
* % TD = % of the theoretical density

Table 2. Elastic properties of SiC materials

ID No.	Specimen	Young's Modulus (GPa)	Shear Modulus (GPa)	Poisson's Ratio
001	ST α-SiC	458	193	0.18
012.5	ST α10D (0.5%C)	391	166	0.18
013.5	ST α10D (1% C)	411	160	0.29
104	AL β-SiC	414	178	0.17
104.5	AL β-SiC HIP treated	426	180	0.18
105	AL 15D	348	143	0.21
105.5	AL 15D HIP treated	361	153	0.18

Table 3. Vickers hardness and indentation fracture toughness of AL SiC materials

ID No.	Material	Vickers Hardness (GPa)	H / E Method*	H / E Ratio	Vickers load (N)	K_{IC} ($MPa\sqrt{m}$)
104	AL β-SiC	28.4 ± 0.5	Indep*	0.0686	20	3.16 ± 0.18
104	AL β-SiC		Knoop	0.0901	20	2.76 ± 0.16
105	AL β15D	22.6 ± 1.8	Indep*	0.0670	20	4.26 ± 0.32
105	AL β15D		Knoop	0.0699	20	4.17 ± 0.31
105	AL β15D		Indep*	0.0670	30	4.13 ± 0.22
105	AL β15D		Knoop	0.0699	30	4.04 ± 0.22
105.2	AL 15D-rapid cooled from 1950°C		Knoop	0.083	20	4.08 ± 0.81

* Indep = Calculated from independent measurements of Vickers hardness and Young's modulus

toughness of ST SiC composites are shown in Table 4. An increase of ≈ 38% in fracture toughness was observed. The flexural strengths of both materials were almost the same. The crack-propagation profiles produced by the Vickers indentation are shown in Figs. 1 and 2. The crack paths were nearly straight with negligible deflection in SiC hot pressed without Dy_2O_3 additions. The cracks propagated in a transgranular mode. With the dispersion of Dy_2O_3, the crack propagation profiles showed more crack deflection. Often the cracks cut through the Dy_2O_3 particles. The average SiC grain size of AL SiC was ≈ 2.2 μm and that of ST α-SiC was ≈ 5.7 μm while SiC grains in the composites had a grain size ≤ 3 μm. In ST α10D, cracks propagated mainly by an intergranular mode, whereas in AL β15D the cracks propagated predominantly in a transgranular mode. Fig. 3 shows the fracture surfaces of ST materials. The fracture surface of SiC hot pressed without Dy_2O_3 additions was rather smooth compared with the fracture surface of SiC - Dy_2O_3 composite which showed rougher surface with more deflection. Notice also the fine scale of the microstructure of the composite compared with SiC hot pressed without Dy_2O_3 additions. Fig. 4 (a) shows a grain along the crack path which could have served as a physical contact restraint to increase the crack resistance of the composite. Fig. 4 (b) shows a possible site for bridges across the crack interface.

The similar flexural strengths of Dy_2O_3 dispersed composite compared with SiC hot pressed without Dy_2O_3 additions could be due to the smaller grain size of SiC in the composite. In SiC - Dy_2O_3 composites, the addition of Dy_2O_3 inhibited the grain growth of the SiC in the composite. The liquid phase present during hot pressing separated the grains to prevent them from growing during the coalescence stage of densification. In spite of the lower strength of Dy_2O_3, the addition of Dy_2O_3 contributed to the finer SiC grains which contributed to the strengthening of the composite.

Table 4. Flexural strength and notched beam fracture toughness of ST SiC materials

ID No.	Material	Flexural strength (MPa)	K_{IC} (MPa$\sqrt{m}$)
001	ST α-SiC	387 ± 53 (6)*	4.0 ± 0.8 (5)
013.5	ST α10D	379 ± 18 (6)	5.5 ± 0.6 (7)

* The numbers in parentheses represent the number of specimens tested.

(a) (b)

Fig. 1. Vickers indentation crack propagations in AL SiC materials.
(a) AL β-SiC (specimen 104) (b) AL β15D (specimen 105).

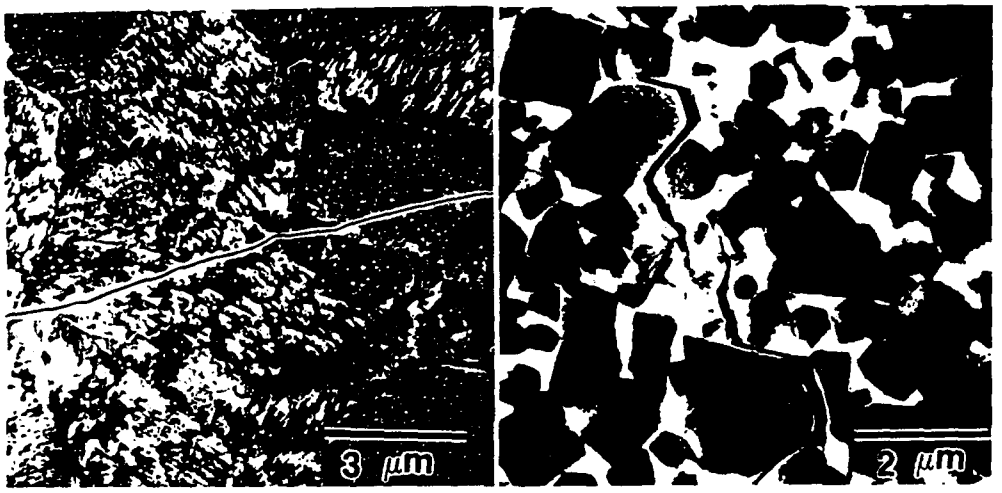

(a) (b)

Fig. 2. Vickers indentation crack propagations in ST SiC materials.
(a) ST α-SiC (specimen 001) (b) ST α10D (specimen 013.5)

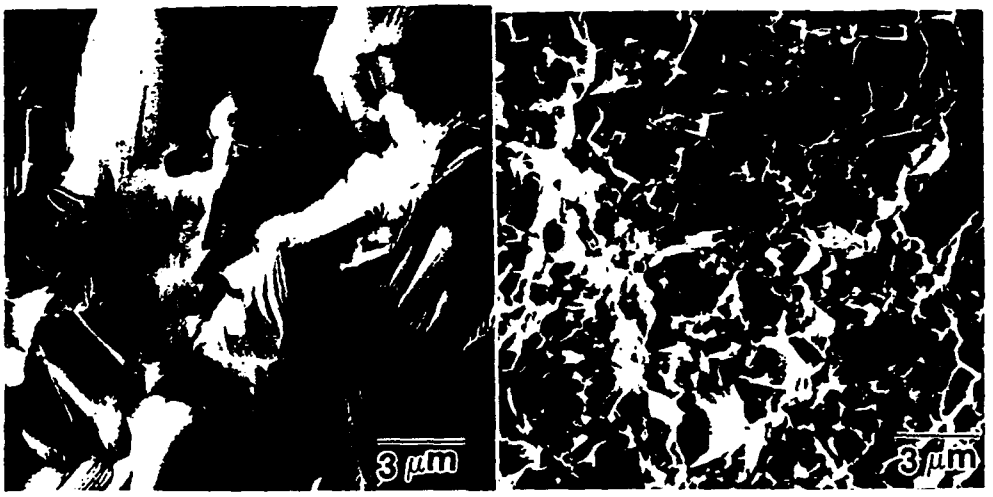

(a) (b)

Fig. 3. Fracture surfaces of hot pressed composites. (a) hot pressed ST α-SiC (specimen 001) (b) hot pressed ST α10D (specimen 013.5).

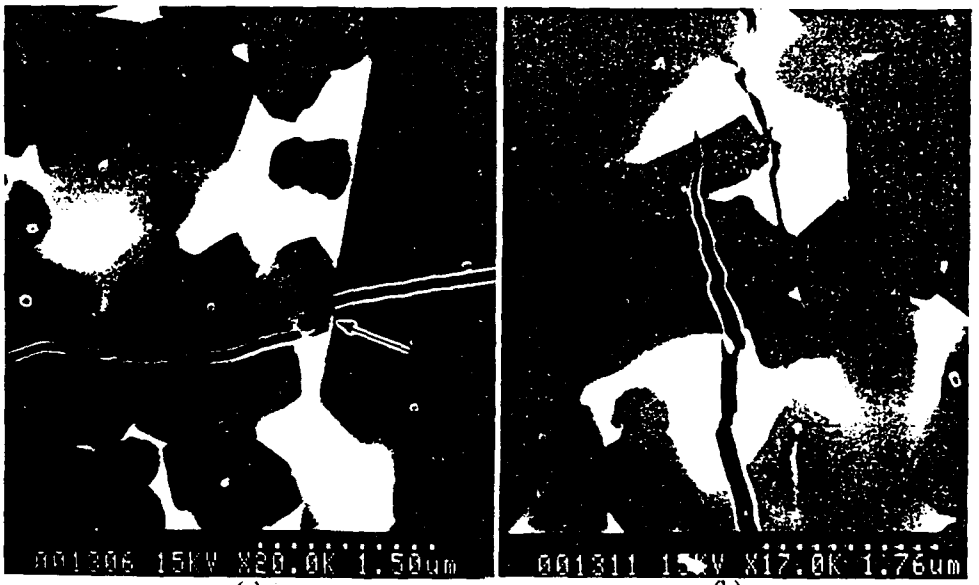

(a) (b)

Fig. 4. Scanning electron micrograph of (a) an indentation crack showing frictional interlocking at a grain bridging site and (b) a segmented fracture trace and the possible bridging site behind the tip of an extended crack (specimen 105).

CONCLUSIONS

The fracture toughness of Dy_2O_3 - dispersed SiC composites increased by ≈ 40% and the flexural strength was similar to that of unreinforced SiC. Hot pressed SiC without Dy_2O_3 additions showed typical brittle crack propagation behavior with a planar crack path throughout propagation. It appeared from examination of crack propagation behavior and fracture surfaces that the possible toughening mechanisms in the Dy_2O_3 - dispersed SiC composites could be crack deflection in conjunction with crack-interface grain bridging.

REFERENCES

1) C. H. McMurtry, W. D. G. Boecker, S. G. Seshadri, J. S. Zanghi, and J. Garnier, "Microstructure and Material Properties of SiC-TiB_2 Particulate Composites," *Am. Ceram. Soc. Bull.*, **66**, [2] 325-29 (1987).
2) G. C. Wei and P. E. Becher, "Improvements in Mechanical Properties in SiC by the Addition of TiC Particles," *J. Am. Ceram. Soc.*, **67**, [8] 571-574 (1984).
3) W. M. Kriven, "Martensitic Toughening of Ceramics," *J. Mater. Sci. & Eng. A*, **A 127**, [2] 249-255 (1990).
4) P. Jero, "Investigation of the lanthanide Sesquioxides as High Temperature Transformation Toughening Agents"; Ph. D. Thesis. University of Illinois, Urbana, IL, 1988.
5) G. R. Anstis, P. Chantikul, B. R. Lawn, and D. B. Marshall, "A Critical Evaluation of Indentation Techniques for Measuring Fracture Toughness: I, Direct Crack Measurements," *J. Am. Ceram. Soc.*, **64**, [9] 533-38 (1981).
6) D. B. Marshall, T. Noma, and A. G. Evans, "A Simple Method for Determining Elastic-Modulus- to-Hardness Ratios using Knoop Indentation Measurements," *J. Am. Ceram. Soc*, **65**, [10] c-175-c-176 (1982)

TEM CHARACTERIZATION OF THE α' AND β PHASES IN POLYCRYSTALLINE DISTRONTIUM SILICATE (Sr_2SiO_4)

Y. J. Kim, J. L. Shull and W. M. Kriven

Department of Materials Science and Engineering, University of Illinois at Urbana-Champaign, Urbana, IL 61801

Two polymorphs, α' and β, are known to be major phases in pure distrontium silicate (Sr_2SiO_4) at atmospheric pressure.[1] Fully dense pellets were fabricated by sintering chemically prepared powders in the temperature range of 900° to 1400°C for 1 to 5 hours. Their phases and microstructures were studied by TEM. At lower sintering temperatures such as 900°C, the major phase was orthorhombic α' (space group, *Pmnb*). The euhedral α' grains had a size of about 1 μm diameter (Fig. 1a). As the sintering temperature increased, the amount of monoclinic β phase (space group, $P2_1/n$) tended to increase. These β grains were usually irregular and twinned on $\{100\}_\beta$ or $\{001\}_\beta$ planes. Concentration of the electron beam on the grains gave rise to a disappearence of twins (Fig. 1b).

SADP's from the α' grains showed an incommensurate modulation along the $\underline{b}^*$ direction. In the $[001]_{\alpha'}$ orientation, the modulation was almost commensurate, with satellite reflections located at ~1/3 of the principal reflections (Fig. 2a). When the specimen was tilted to the $[102]_{\alpha'}$ orientation, the number of satellite reflections increased (Fig. 2b). This modulation could be interpreted in several different ways, one of which suggested that the satellite reflections around $\{0k0\}$ were extinct, when k is even, in the $[001]_{\alpha'}$ orientation. In this case the modulation vector, **q**, would be about 0.3 $\underline{b}^*$. A previous study reported $\mathbf{q} = 0.303 \pm 0.005\ \underline{b}^*$.[2] SADP's from the twinned β grains also showed a similar incommensurate modulation along the $\underline{b}^*$ direction. Fig. 3a shows the $[100]_\beta$ SADP, which is almost identical to the $[001]_{\alpha'}$ SADP except for the appearance of $\{010\}_\beta$ principal reflections in the former. The $[110]_\beta$ SADP of the same area (Fig. 3b) did not display any modulations, but $\{001\}_\beta$ twinned reflections were observed (arrowed). Because of complications and variations of the modulated structures of both the α' and β phases in samples processed under different conditions, further study is needed, particularly in conjunction with the transformation mechanism between the α' and β phases.

References

1. M. Catti *et al.*, Acta Cryst. (1983) B39, 674.
2. R. L. Wither *et al.*, J. Physics (1987) C20, 1653.
3. This research was supported by Air Force Office of Scientific Research through a URI Grant AFOSR-90-0174.

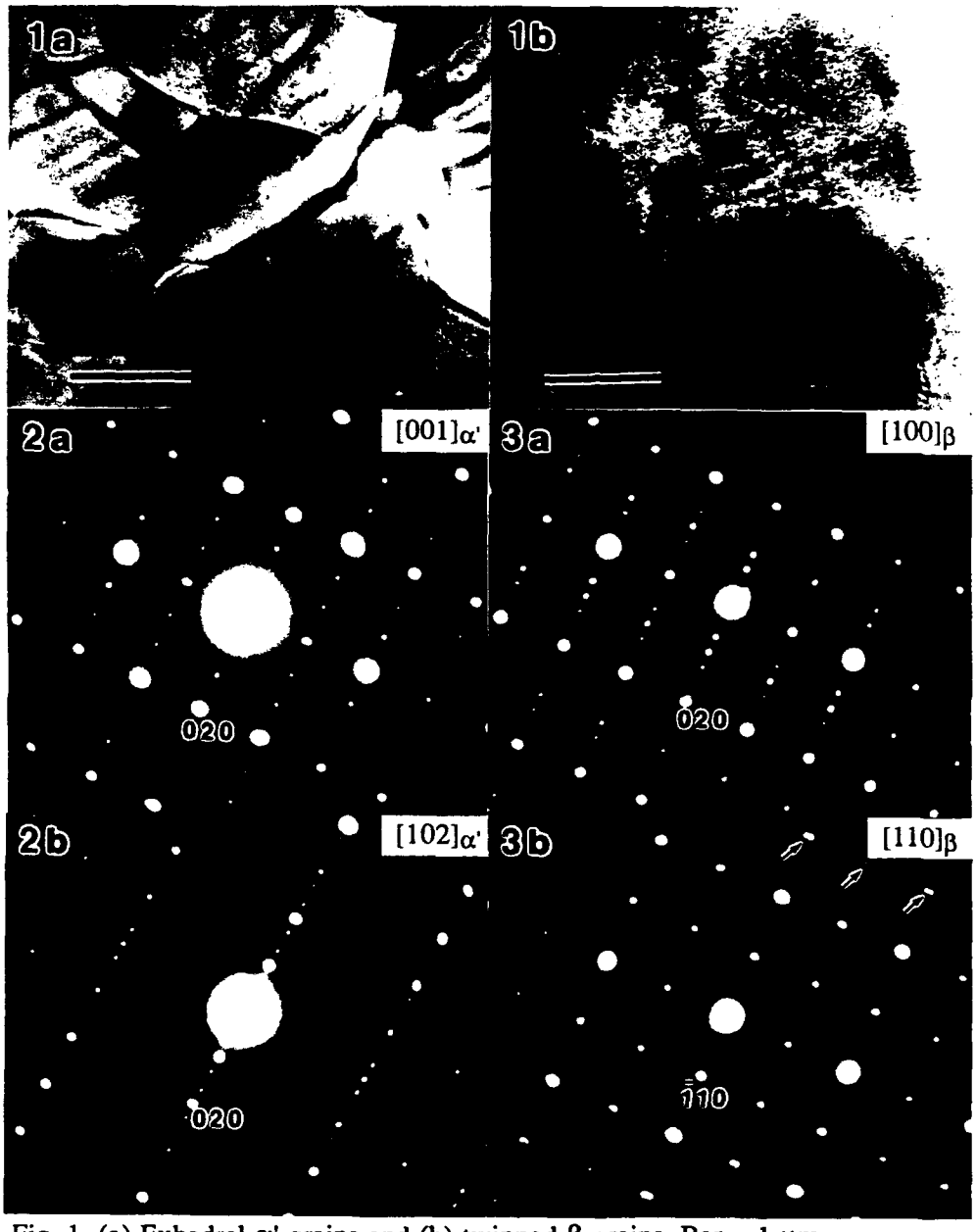

Fig. 1. (a) Euhedral α' grains and (b) twinned β grains. Bar = 1 μm.
Fig. 2. SADP's from an α' grain showing an incommensurate modulation: (a) $[001]_{\alpha'}$ and (b) $[102]_{\alpha'}$
Fig. 3. SADP's from a twinned β grain: (a) $[100]_{\beta}$ showing an incommensurate modulation and (b) $[110]_{\beta}$ with $\{001\}_{\beta}$ twinned reflections (arrowed).

CHARACTERISATION OF NICKEL SULPHIDE STONES IN GLASS

J.J. Cooper, O.O. Popoola and W.M. Kriven
University of Illinois at Urbana-Champaign
Department of Materials Science and Engineering
105 South Goodwin Ave, Urbana, IL. 61801, USA

INTRODUCTION

The small stones of nickel sulphide found at the fracture origins of broken plate glass have been the subject of a number of studies concerned with analysing and preventing failure of windows. Work has concentrated on determining the composition and origin of the particles [1,2,3,4] and on analysing the stress fields of particles in tempered plate glass [5,6,7,8].

The small size of the stones, typically ~120 μm in diameter, has limited the methods available for characterising them. Using scanning electron microscopy (SEM) and energy dispersive spectroscopy (EDS), Bradt [5] found them to be composed of nickel and sulphur and noted that it was probable that the stones were polycrystalline and not single phase. Hsiao [7] examined a small stone from a fracture surface and identified both α-NiS and β-NiS by X-ray diffraction, and similar findings were reported by Ballantyne [9]. A study of sulphide inclusions in plate glass by electron probe microanalysis (EPMA) [1] identified sulphide stones of various compositions, including Ni_3S_2 and $Ni_{1-x}S$. The α-$Ni_{1-x}S$ inclusions were found to have partially reverted to β-$Ni_{1-x}S$ after a period of 18 months. A compositional profile of the $Ni_{1-x}S$ inclusions [1] found them to be very homogeneous, though Ni-poor just at the glass contact. This is consistent with the work of Wagner [2], who reported that during glass manufacture the nickel sulphide particles may be partially dissolved by the oxide glass, leading to relative sulphur enrichment of the $Ni_{1-x}S$ as NiO is formed and dissolved according to the chemical reaction:

$$2Ni_{1-x}S + 3/2\,O_2 \rightarrow NiO + Ni_{1-2x}S + SO_2$$

Two alternative explanations for the fracture-initiating behaviour of the nickel sulphide stones have been proposed. Many workers suggested that on cooling the phase transformation of α to β-NiS, which is accompanied by a 4% volume increase, was responsible for the fracture of the thermally tempered plate glass [6,7]. A study of the glass with additions of nickel sulphide impurities [4] concluded that the fracture-initiating stones were not necessarily the NiS compound, and that the cause of fracture was the thermal expansion mismatch between the nickel sulphide phases and the glass matrix. For example, it is known [10] that pentlandite, $(Fe,Ni)_9S_8$, a naturally occurring mineral, has an unusually large coefficient of thermal expansion.

This work involved a transmission electron microscopy (TEM) microstructural and microchemical investigation of several samples of stones from glass. Samples of silicate glass

containing tiny nickel sulphide stones were supplied by Dr. M. Swain[1] and Dr. A. Mishra[2]. The samples from Swain were of two types. The first were stones recovered from fractured plate glass. These stones were observed to be at the fracture origins of the plate glass. The second were stones in bulk, unfractured plate glass. The samples supplied by Mishra were also unfractured bulk glass specimens. The chemistry and thermal processing of the glasses were unknown. Analysis of the stones was difficult due to their small size (80 - 250 μm). Normal X-ray diffraction methods were not applicable, and TEM sample preparation was not possible using conventional materials science techniques. Ultramicrotomy was used to prepare the TEM samples [11].

EXPERIMENTAL TECHNIQUES

The stones in bulk glass samples, just visible to the naked eye, were examined optically by polarised light microscopy using a Leco Neophot instrument. They were then removed from the glass by cutting thin slices of glass with a diamond saw, marking the glass with a diamond pen and carefully crushing the glass to release the stone. Several stones were lost or broken in the process. Two stones which adhered well to the surface of the fractured glass were prepared for scanning electron microscopy observation (SEM) by coating with vacuum-evaporated carbon.

To prepare samples for TEM the stones were embedded in Eponate 12 epoxy resin[3]. The embedding mixture formulation included 5.0 ml Eponate 12, 1.0 ml dodecanyl succinic anhydride, 4.0 ml nadic methyl anhydride and 0.2 ml *tri-[dimethyl amino ethyl] phenol*. Embedding the samples was accomplished by first polymerising shallow blanks of the mixture in a silicone mold, then placing the stone on the blank, filling the mold with the mixture and repolymerising for 48 hours. Using a razor blade, the casting was trimmed to a pyramid having an approximately 0.5 x 0.5 mm^2 square face, the center of which contained the embedded particle. Sections approximately 900Å thick were then cut using a Reichert OM U2 ultramicrotome equipped with a diamond knife. The cutting speed was 1mm/sec. The sections were recovered on to 400 mesh copper TEM grids, air-dried and coated with a thin film of vacuum-evaporated carbon in readiness for TEM. No conductive coating was applied to the sections cut from the stones supplied by Mishra. TEM was performed using a Philips EM 420 instrument at 120 keV, in conjunction with an EDAX 9900 system equipped with a SiLi X-ray detector. Single crystal and polycrystalline selected area diffraction patterns were obtained and analysed.

RESULTS

Figure 1 shows an inclusion within a bulk glass sample. This optical micrograph, taken with transmitted polarised light, clearly reveals the strain field associated with the particle. The stones were typically spherical with a rough surface and adhered strongly to the glass, as can be seen in figure 2, which is an SEM micrograph of a stone located at a fracture origin in broken plate glass.

Ultramicrotomy produced several artifacts in the TEM specimens cut from the stones. Figure 3a shows the typical 'chatter' morphology of the knife-damaged material, and figure 3b shows scratches (labelled 's') thought to be due to knife chips or abraded material. Fine lamellae (~10 nm) were seen, which may have been the result of stress-induced crystalline slip during cutting. Rare areas of relatively undamaged material were occasionally observed and several grain boundaries were seen (arrowed in figure 3b).

1. University of Sydney, NSW, Australia.
2. PPG Glass Industries, Pittsburgh, PA, USA.
3. Ted Pella Inc., Redding, CA, USA.

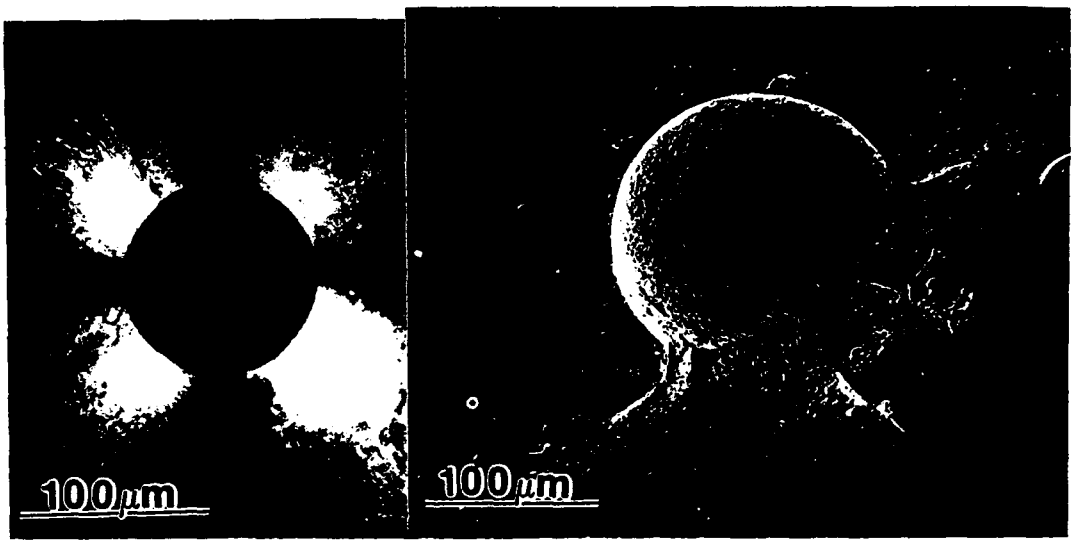

Figure 1. Polarised light micrograph of nickel sulphide stone in glass showing birefringence around the embedded stone.

Figure 2. Scanning electron micrograph of nickel sulphide stone at fracture origin in broken plate glass.

EDS analyses of the microtomed TEM samples showed only sulphur, nickel and occasionally traces of iron. Extensive analyses gave a range of Ni:S ratios from pure nickel to $Ni_{50}S_{50}$ (at. %). Most of the analyses lay between $Ni_{60}S_{40}$ and $Ni_{50}S_{50}$. Variation in Ni:S ratio was observed both within, as well as between samples. Few analyses showed equivalent amounts of nickel and sulphur.

Electron diffraction analysis was hampered by the damaged microstructure. However, selected area diffraction with a large aperture was a suitable technique because the microcrystalline ring patterns could be used for phase identification by analogy with X-ray powder diffraction patterns. Figure 4a shows a typical ring pattern obtained from a stone located at the fracture origin. This pattern corresponded to β-NiS. The ring pattern shown in figure 4b was obtained from the bulk glass stone supplied by Mishra. It showed α-NiS reflections. Other patterns, observed from the bulk glass sample of Swain, were more complex and not all the rings could be indexed as α-NiS reflections. However, no β-NiS was detected in these patterns. The unidentified rings may have been due to oxides of nickel and iron. A number of selected area diffraction patterns from single crystals (figure 5) gave results in agreement with the microcrystalline ring measurements. The results of the EDS and diffraction analyses are summarised in Table 1.

Table I: Detected Phases in NiS Stones.

Sample	Fracture Origin	Swain's Bulk Glass	Mishra's Bulk Glass
Phases identified	traces of α-NiS, β-NiS	probably α-NiS, no β-NiS, some nickel oxide or nickel	α-NiS, no β-NiS

Figure 3. Bright Field TEM images of ultramicrotomed nickel sulphide stone showing the microstructural damage. (a). 'Chatter' morphology; (b). Scratches ('s') from diamond knife. Grain boundaries are arrowed in (b).

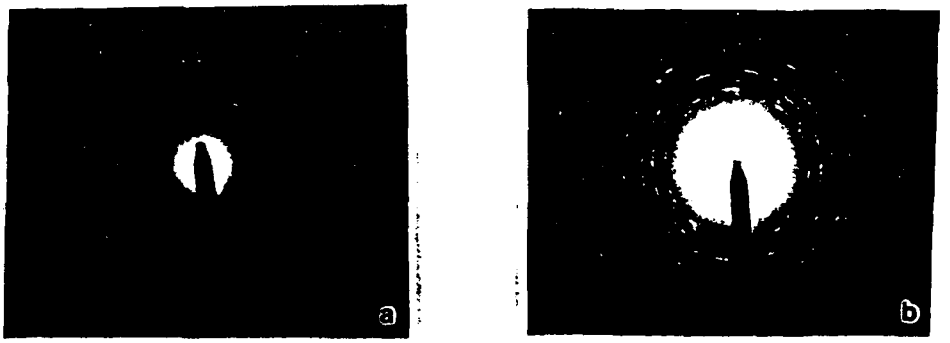

Figure 4. Microcrystalline ring diffraction patterns from ultramicrotomed nickel sulphide stones (a). α-NiS; and (b). β-NiS.

Figure 5. Selected area diffraction patterns from ultramicrotomed nickel sulphide stones. (a). [0001] α-NiS; and (b). [01 $\bar{1}$2] β-NiS

DISCUSSION

The use of ultramicrotomy to prepare the tiny stones for TEM observations was of mixed advantage. It enabled semi-quantitative microchemical analyses, which could not otherwise have been performed, but did not allow accurate observation of the microstructure of the stones. Ultramicrotomy induced permanent strain that produced streaks and distorted the diffraction patterns. Interpretation of microcrystalline ring patterns was not straightforward when several phases were present, as appeared to be the case for the bulk glass samples supplied by Swain.

EDS analysis, although not sufficiently quantitative to allow outright identification of phases, confirmed that the composition of the stones was nickel sulphide. The variation in Ni:S ratio observed both within and between samples was believed to indicate the presence of various nickel sulphide compounds, which strongly suggested that the stones were polycrystalline and not single phase. The identification of regions of pure nickel or nickel oxide by EDS supported this conclusion. This polycrystallinity was confirmed by bright field images (see figure 3b).

The microcrystalline ring diffraction patterns provided further evidence of the presence of various nickel sulphide phases in the stones from different glass samples. Analysis of the stones from bulk glass clearly showed that α-NiS was the major phase in this sample. The same type of results from the stone found at the fracture origin indicated just as clearly that β-NiS was the major phase present in these fracture-initiating stones. These results were consistent with the hypothesis that fracture of the glass occurred as a result of the α→β transformation in NiS.

There are several possible scenarios for the fracture of the glass as a result of phase transformation within the stone. The rough surface of the stone provided inhomogeneities at the particle / glass interface which would be the most likely sites for flaw nucleation. Flaws may have propagated radially or tangentially to the interface.

The stresses generated by the volume increase accompanying phase transformation are postulated as the driving force for flaw nucleation and propagation. Since the stones were polycrystalline, transformation was possible within each α-NiS grain. Transformation may have occurred grain by grain over time or, if the transformation was stress-inducible, the autocatalytic effect (as seen in zirconia [12]) may have caused essentially spontaneous transformation of the entire particle. If transformation was gradual, nucleation and growth of the critical flaw may have been gradual also, with each additional increment of transformation stress causing either a new nucleation event or propagation of the existing microcrack(s) [5,7]. On the other hand, if the transformation

of the particle was complete within a short space of time, the nucleation and propagation of the flaw to critical size may have been rapid.

Field observation [9] of the failure of the plate glass windows indicated a dependence on ambient temperature, with more window failures recorded from the warmer side of buildings. A time dependence of failure is also implied by the variable time to failure of the various windows. These observations would be consistent with either hypothesis for the role of the phase transformation. Calculation of the total stresses generated by complete transformation of particles [6] indicated that the stresses for particles above a critical size would be sufficient to cause failure of the glass matrix. However, gradual transformation of the polycrystalline stone combined with thermal cycling due to ambient temperature fluctuations seems a more likely mechanism of fracture.

CONCLUSION

Small, spherical, silver-coloured stones found in plate glass were analysed microchemically and were found to contain nickel and sulphur in ratios between Ni and $Ni_{50}S_{50}$ (at. %). The stones were polycrystalline and possibly polyphasic. Compositions appeared to vary from stone to stone, with some compositions being less harmful to the glass than others. Electron diffraction allowed the identification of α-NiS in unfractured glass and β-NiS in fractured glass. The results were consistent with the hypothesis that the $\alpha \rightarrow \beta$ transformation in NiS played a role in initiating fracture in plate glass containing nickel sulphide stones. No direct observations of the transformation were made.

ACKNOWLEDGEMENTS

This work was supported by the Air Force Office of Scientific Research under grant number AFOSR-89-0300. Use of the electron microscope facilities at the Center for Microanalysis of Materials in the Materials Research Laboratory and the Center for Electron Microscopy, both at the University of Illinois at Urbana-Champaign, are gratefully acknowledged. Thanks are due to Dr. M. Swain (University of Sydney, Australia) and Dr. A. Mishra (Pittsburgh Plate Glass Co. Pittsburgh, USA) for supplying the glass samples.

REFERENCES

1) Tabuchi, H.: 10th International Congress on Glass, (Ceram.Soc. Japan, Kyoto, Japan, July 1974).
2) Wagner, R.: Glastech. Berichte., (in Fre) 1977, 50, 296.
3) Merker, L.: Glastech. Berichte., (in Ger) 1974, 47, 116.
4) St. Gobain Glass Industries, France, Internal Report.
5) Bradt, R. C.: Alfred University Fractography Conference, August 1986.
6) Swain, M. V.: J. Mat. Sci., 1981, 16, 151.
7) Hsiao, C. C.: Fracture 1977 Vol. 3, (ICF4, Waterloo, Canada).
8) Evans, A. G.: J. Mat. Sci., 1974, 9, 1145.
9) Ballantyne, E. R.: CSIRO Division of Building Research Report, Melbourne, 1961.
10) Rajamani, V. and Prewitt, C. T.: Am.Mineral., 1974, 60, 39.
11) Popoola, O. O., Cooper, J. J., Jakstys, B. P. and Kriven, W. M. : MRS Symp.Proc., 1991, Boston, (in press).
12) Gupta, T. K., Lange, F. F. and Bechtold, J. H. : J. Mat. Sci., 1978, 13, 1464.

CERAMICS
adding the value

VOLUME 1

Editor: M.J. Bannister

AUSTCERAM 92

Proceedings of the International Ceramic Conference
Australia 1992

Volumes 1 and 2 – AUSTCERAM 92 manuscripts

"Microstructural Investigation of Fracture-Initiating Nickel Sulfide Inclusions in Glass," O. O. Popoola, J. J. Cooper and W. M. Kriven. Ceramic Science and Engineering Proceedings, (1993), in press.

"Microstructural Investigation of Fracture-Initiating Nickel Sulfide Inclusions in Glass".

O. O. Popoola, J. J. Cooper and W. M. Kriven,

Department of Materials Science and Engineering,
University of Illinois at Urbana-Champaign,
105 S. Goodwin Avenue, Urbana IL 61801

ABSTRACT

Transmission electron microscopy was used to investigate the microstructure and the microchemistry of nickel sulfide inclusions in plate glass. TEM samples from inclusions recovered from both fracture surfaces and bulk glass were prepared by ultramicrotomy. The inclusions were polycrystalline and contained predominantly $Ni_{1-x}S$ phases. Traces of Ni_3S_2 and Ni_7S_6 were also found. Electron diffraction analyses showed that the inclusions on the fracture surfaces were β-NiS while those from the unfractured bulk glasses were α-NiS. These results confirmed the hypothesis that the volume increase associated with the α to β transformation in NiS caused fracture. The glass processing conditions determined the microstructure of the inclusions.

INTRODUCTION

The spontaneous fracture of thermally-toughened plate glass has been attributed to the presence of nickel sulfide inclusions [1-3]. These inclusions, typically 150 μm in diameter, were formed as a result of the chemical reactions between sodium sulfate (Na_2SO_4) and a nickel compound in the presence of a reducing agent during glass manufacture. Their small size has limited the methods available for characterizing them. Using scanning electron microscopy (SEM) and energy dispersive spectroscopy (EDS), Bradt [4] found them to be composed of

nickel and sulfur and noted that it was probable that the stones were polycrystalline and not single phase. Hsiao [5] examined a small stone from a fracture surface and identified both α-NiS and β-NiS by X-ray diffraction, and similar findings were reported by Ballantyne [6]. A study of sulfide inclusions in plate glass by electron probe microanalysis (EPMA) [1] identified sulfide stones of various compositions, including Ni_3S_2 and $Ni_{1-x}S$. Two alternative explanations for the fracture-initiating behavior of the nickel sulfide stones have been proposed. Many workers suggested that on cooling, the phase transformation of the α to β-NiS, which is accompanied by a 4% volume increase, is responsible for the fracture of the thermally tempered plate glass [6]. The transformable phases that may produce significant volume changes in the Ni-S system (thereby causing fracture) are $Ni_{1-x}S$, Ni_3S_2, and Ni_7S_6 [8]. Table 1 below lists their characteristics, where $\Delta V = (V_2-V_1)/V_1$ and V_1 is the molar volume of the parent phase.

Table 1. Transformable Nickel Sulfur Compounds

Compound	Low Temp. Phase	High Temp. Phase	Transformation Temperature	ΔV (% Volume Change)
Ni_3S_2	Rhomb, R3m	Cubic, F43m	565 °C	+3 to -6.5
Ni_7S_6	Ortho, C222	Ortho, Bmmb	397 °C	~+30
$Ni_{1-x}S$	Rhomb, R3m	Hex, $P6_3/mmc$	282 to 379 °C	+2.3 to +4

In all cases the extent of volume change is dependent on the transformation temperature and the stoichiometry. The high temperature phases can be metastably retained down to low temperatures by stoichiometry offsets, impurity additions and rapid quenching. The metastably retained phases have been found to transform with time at room temperature [2, 5]. A detailed analyses of the strain field around the inclusions showed that a critical size of 60 μm was needed for fracture to occur [5, 7]. For an inclusion 200 μm in diameter, a partial α to β phase transformation

resulting in a 2% volume increase was found to generate sufficiently high internal stress to initiate fracture viscoelastically [5] in a fully tempered plate glass.

An alternative explanation was that the instantaneous fracture may be attributed to the thermal expansion mismatch between the particles and the glass matrix. A study of the glass with additions of nickel sulfide impurities [8] concluded that the fracture-initiating stones were not necessarily the NiS compound, and that the cause of fracture was the thermal expansion mismatch between the nickel sulfide phases and the glass matrix. For example, it is known [9] that pentlandite, $(Fe,Ni)_9S_8$, a naturally occurring mineral, has an unusually large coefficient of thermal expansion.

Although, some optical and scanning electron microscopy studies of these stones have been performed [2, 10, 11,12] the essential microstructural features (phase identification, grain sizes, twinning, etc.) needed to understand the nature of the phase transformations are yet to be determined. The inclusions are generally too small for X-ray analyses and analytical electron microprobe results are only indicative of overall compositions. The aim of this communication is to report the results of a transmission electron microscopy (TEM) investigation of these inclusions. Two sets of samples were studied. The first, supplied by Dr. M. Swain, consisted of fractured and bulk glasses obtained from the Commonwealth Scientific Investigation and Research Organization (CSIRO) in Melbourne, Australia. The second set, supplied by Dr. A. Mishra were bulk glasses made by the Pittsburgh Plate and Glass Company (PPG). The exact processing conditions of both sets of samples were unknown.

EXPERIMENTAL TECHNIQUES

The inclusions in bulk glass samples, just visible to the naked eye, were examined optically by polarized light microscopy using a Leco Neophot instrument. They were then removed from the glass by cutting thin slices of glass with a diamond saw, marking the glass with a diamond pen and carefully crushing the

glass up to them. Several inclusions were lost or broken in the process. Two inclusions which adhered well to the surface of the fractured glass were prepared for scanning electron microscopy observation (SEM) by coating with vacuum-evaporated carbon.

To prepare samples for TEM, the inclusions were embedded in Eponate 12 epoxy resin. The embedding mixture formulation included 5.0 ml Eponate 12, 1.0 ml dodecanyl succinic anhydride, 4.0 ml nadic methyl anhydride and 0.2 ml tri-[dimethyl amino ethyl] phenol. Embedding the samples was accomplished by first polymerizing shallow blanks of the mixture in a silicone mold, then placing the stone on the blank, filling the mold with the mixture and then, repolymerizing for 48 hours. Using a razor blade, the casting was trimmed to a pyramid having an approximately 0.5 x 0.5 mm^2 square face, the center of which contained the embedded particle. Sections approximately 900Å thick were then cut using a Reichert OM U2 ultramicrotome equipped with a diamond knife. The cutting speed was 1mm/sec. The sections were recovered on to 400 mesh copper TEM grids, air-dried and coated with a thin film of vacuum-evaporated carbon in readiness for TEM. TEM was performed using a Philips EM 420 instrument operated at 120 KeV, in conjunction with an EDAX 9900 system equipped with a Si-Li X-ray detector. Single crystal and polycrystalline selected area diffraction patterns (SAD) using a large objective aperture were obtained and analyzed.

EXPERIMENTAL RESULTS

Microstructures:

The results obtained on the samples from Dr. Swain are presented in Figures 1 to 3. Figure 1 shows an inclusion within a bulk glass. This transmitted polarized light optical micrograph revealed the strain field around the inclusion. In this particular case, no inhomogeneity with localized strain could be seen. Although the particle was about 250 μm in diameter, no cracks were observed around it, suggesting that the particle had not transformed or that the extent of transformation

was not sufficient to induce fracture. A scanning electron micrograph of an inclusion located at the fracture surface is shown in Figure 2. This inclusion, about 200 mm in diameter, adhered strongly to the glass matrix and could be readily seen at the fracture origin. Its surface was very rough and had numerous cracks

A low magnification, bright field TEM micrograph of the ultramicrotomed section is shown in Figure 3a. It consisted of many slivers separated by cracks. This indicated that extensive deformation occurred during ultramicrotomy. Other microstructural features are shown in Figure 3b to 3d. Figure 3b shows the characteristic chatter morphology of ultramicrotomed samples, readily identifiable by the absence of contrast variations across the boundaries. Figure 3c shows the polycrystalline nature of the inclusions. Apart from the fine chatter and knife scratches, the grain boundaries can readily be identified (see arrows). Figure 3d shows an internally twinned sliver. The twin width was about 0.01μm. Contrast variation across the twin boundaries was clearly visible. Some of the twin boundaries contained cracks. The microstructure of the inclusions recovered from the PPG glass is shown in Figure 4. These inclusions were also polycrystalline and extensively faulted.

Electron Diffraction Analyses:

Figure 5 summarizes the electron diffraction analyses from all the samples. The sample recovered from the fracture surface contained predominantly β-NiS (Figures 5a and 5b) with traces of α-NiS. A few grains of Ni_3S_2 and Ni_7S_6 were also observed as evidenced by the large aperture, selected area diffraction pattern shown in Figure 5c. Apart from Ni_3S_2 and Ni_7S_6 impurities, the inclusions in the unfractured bulk glasses contained the a-NiS phase. No β-NiS phase was identified in these samples. EDS analyses from all the samples showed Ni and S peaks, with occasional traces of Fe. Most of the analyses lay between $Ni_{60}S_{40}$ and $Ni_{50}S_{50}$. Compositional variations were observed both within and between samples. Table 2 below summarized the results obtained for all cases.

Table 2: Principal Phases Detected in Nickel Sulfide Inclusions.

Sample	Fracture Origin	Swain 's Bulk Glass	Mishra 's Bulk Glass
Phases identified	β-NiS , traces of α-NiS,	α-NiS, no β-NiS, nickel oxide or nickel	α-NiS, no β-NiS

DISCUSSION

The use of ultramicrotomy to prepare the tiny stones for TEM observations was of mixed advantage. It enabled semi-quantitative, microchemical analyses, which could not otherwise have been performed, and allowed the observation of the microstructure of the stones. However, it induced permanent strain damage which produced streaks and distorted the diffraction patterns, thus rendering their interpretation difficult. This investigation showed that the microstructure of the inclusions depended on the glass processing conditions. The samples supplied by Dr. Swain were polycrystalline with occasionally twinned grains, while those from PPG were highly faulted crystals. These microstructural differences could affect the transformability of the metastably retained α-NiS.

EDS analysis, although not sufficiently quantitative to allow outright identification of phases, confirmed that the composition of the stones was indeed nickel sulfide. The variation in Ni:S ratio observed both within and between samples was believed to indicate the presence of various nickel sulfide compounds, which strongly suggested that the stones were polycrystalline and not single phase. The identification of regions of pure nickel or nickel oxide by EDS supported this conclusion. This polycrystallinity was confirmed by TEM bright field images.

The micro crystalline ring diffraction patterns observed in large aperture selected are diffraction patterns provided further evidence of the presence of various nickel sulfide phases in the stones from different glass samples. Analysis of

the stones from bulk glass clearly showed that α-NiS was the major phase in this sample. The same type of results from the stone found at the fracture origin indicated just as clearly that β-NiS was the major phase present in these fracture-initiating stones. These results were consistent with the hypothesis that fracture of the glass occurred as a result of the α→β transformation in NiS. There are several possible scenarios for the fracture of the glass as a result of phase transformation within the stone. The rough surface of the stone provided inhomogeneities at the particle / glass interface which would be the most likely sites for nucleation at flaws.

The stresses generated by the volume increase (2 - 4%, depending on the precise composition and lattice parameters) accompanying the phase transformation are postulated to be the driving force for nucleation and propagation of the transformation. Since the stones were polycrystalline, transformation was possible within each α-NiS grain. Transformation may have occurred grain by grain over time depending on grain size, twin width and temperature. If transformation were gradual, nucleation and growth of the critical flaw may have been gradual also, with each additional increment of transformation stress causing either a new nucleation event or propagation of the existing microcrack(s). The α to β transformation in NiS does not appear to be stress inducible. Repeated mechanical polishing, under various loads, of both fine and coarse grained surfaces of the α phase did not produce any X-ray detectable β phase [13]. Instanteneous stress build up resulting from spontaneous transformation caused by autocatalysis could thus be ruled out.

It appeared unlikely that the fracture was caused by thermal expansion mismatch between the particles and the glass matrix. Studies of Al_2O_3 toughened glasses showed that for large particles, thermal expansion mismatch caused weakening, whereas for small particles strengthening occurred [14,15, 16]. The weakening / toughening transition, considering only thermal expansion mismatch was found to occur for an inclusion size of 40 μm. The calculations of Evans at al. [7] showed that the mechanical stresses generated as a result of the α to β

transformation in a 60 μm NiS inclusion were enough to cause spontaneous fracture of plate glass. The fact that particles larger than 150 μm randomly dispersed in the glass did not necessarily cause fracture negate the thermal expansion mismatch hypothesis.

Field observation [10] of the failure of the plate glass windows indicated a dependence on ambient temperature, with more window failures recorded from the hotter side of buildings. A time dependence of failure is also implied by the variable time to failure of the various windows. These observations would be consistent with either hypothesis for the role of the phase transformation. Calculation of the total stresses generated by complete transformation of particles [6] indicated that the stresses for particles above a critical size would be sufficient to cause failure of the glass matrix. However, gradual relaxation and residual stress activity in the glass matrix surrounding the polycrystalline stone, combined with thermal cycling due to ambient temperature fluctuations seems to be a likely mechanism of nucleation of the $\alpha \rightarrow \beta$ transformation leading to fracture.

CONCLUSION

Small, spherical, silver-colored stones found in plate glass were analyzed microchemically and were found to contain nickel and sulfur in ratios between Ni and $Ni_{50}S_{50}$ (at. %). The stones were polycrystalline and possibly polyphasic. Compositions appeared to vary from stone to stone, with some compositions being less harmful to the glass than others. Electron diffraction allowed the identification of α-NiS in unfractured glass and β-NiS in fractured glass. The results were consistent with the hypothesis that the $\alpha \rightarrow \beta$ transformation in NiS played a role in initiating fracture in tempered plate glass containing nickel sulfide stones.

ACKNOWLEDGMENTS

This work was supported by the Air Force Office of Scientific Research under Grant number AFOSR-89-0300. Use of the electron microscope facilities at the Center for Microanalysis of Materials in the Materials Research Laboratory at UIUC

are gratefully acknowledged. Thanks are due to Dr. M. Swain of the University of Sydney, Australia and Dr. A. Mishra of the Pittsburgh Plate and Glass Co. Pittsburgh, USA for supplying the glass samples.

REFERENCES

1) Tabuchi, H.: 10th International Congress on Glass, (Ceram. Soc. Japan, Kyoto, Japan, July (1974).

2) Wagner, R.: Glastech. Berichte., (in Fre) 1977, 50, 296.

3) Merker, L.: Glastech. Berichte., (in Ger) 1974, 47, 116.

4) Bradt, R. C.: Alfred University Fractography Conference, August 1986.

5) Hsiao, C. C.: Fracture 1977 Vol. 3, (ICF4, Waterloo, Canada).

6) Ballantyne, E. R.: CSIRO Division of Building Research Report, Melbourne, 1961.

7) Evans, A. G.: J. Mat. Sci., 1974, 9, 1145.

8) St. Gobain Glass Industries, France, Internal Report.

9) Rajamani, V. and Prewitt, C. T.: Am.Mineral., 1974, 60, 39.

10) Swain, M. V.: J. Mat. Sci., 1981, 16, 151.

11) Popoola, O. O., Cooper, J. J., Jakstys, B.P. and Kriven, W. M.: Mat. Res. Soc. Symp. Proc. 254 (1992), 271.

12) J. J. Cooper, O. O. Popoola and W. M. Kriven.: Proc. Int. Cer. Conf. Ed. J. M. Bannister, CSIRO Publications, 1992, 186.

13) J. J. Cooper: M. S. Thesis, University of Illinois, 1992.

14) Gupta, T. K., Lange, F. F. and Bechtol, J. H.: J. Mat. Sci., 1978, 13, 1464.

15) J. S. Nadeau and J. J. Dickerson; J. Am. Cer. Soc., (1980), 63, No 9-10, 517.

16) D. Bunis: Science of Ceramics, Vol 1, Ed. G. H. Stewart, Academic Press, New York, 1962, 315.

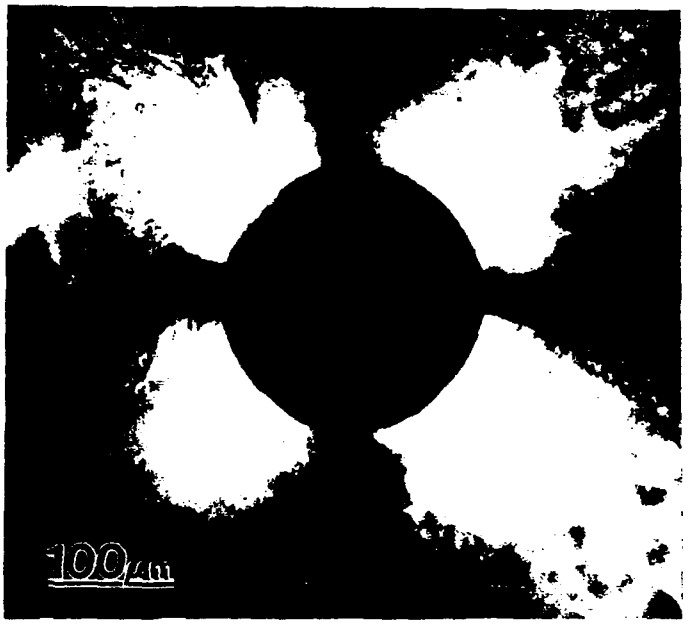

Figure 1.: Polarized light micrograph of a nickel sulfide stone embeddedin the bulk plate glass showing birefringence around the embedded stone.

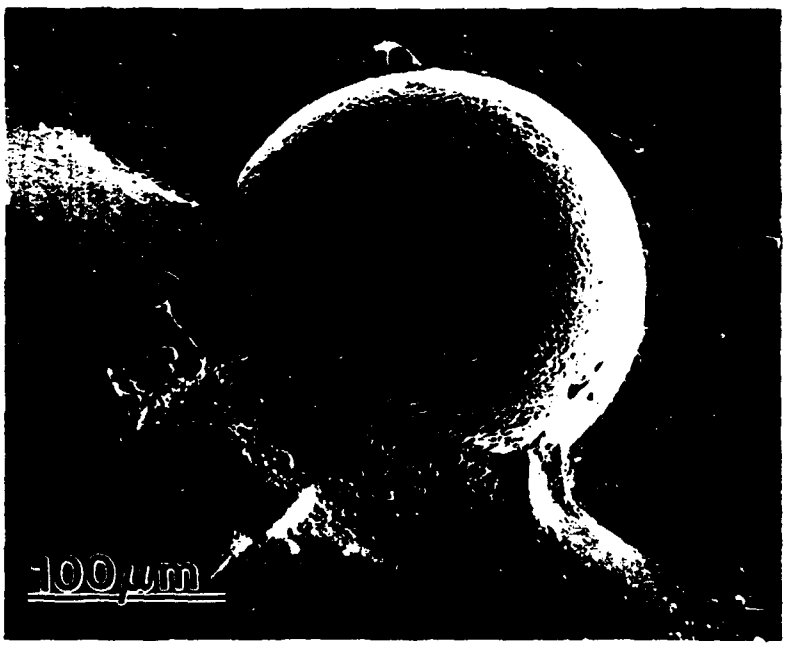

Figure 2.: Scanning electron electron micrograph (SEM) of an inclusion at the fracture origin of the tempered plate glass. The particles strongly adhered to the surface.

Figure 3.: (a) Transmission electron micrographs (TEM) of ultramicrotomed inclusion from CSIRO showing slivers of nickel sulfide. The sample underwent a significant deformation during specimen preparation.

Figure 3.: (b) Ultramicrotomy - induced chatter. Note that there was no contrast variation across the boundaries.

Figure 3.: (c) Microstructure showing the grain boundaries (arrowed), confirming the polycrystalline nature of the inclusions.

Figure 3.: (d) Internally twinned sliver.

Figure 4.: The microstructure of the inclusion from the PPG bulk glass specimen showing extensive faults. The sample was polycrystalline and the associated diffraction pattern (insert) showed streaks.

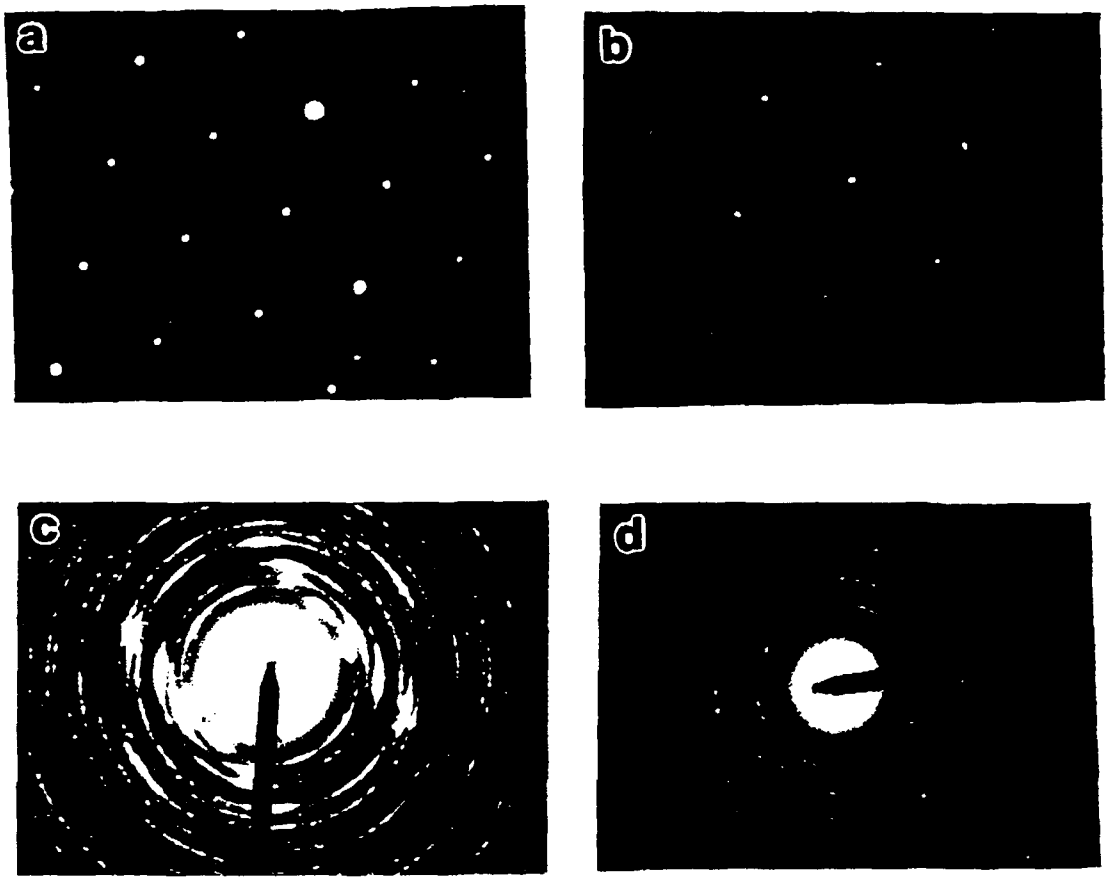

Figure 5.: Selected area diffraction (SAD) patterns from nickel sulfide inclusions in plate glass.

(a) [0001] α-NiS obtained from CSIRO bulk glass.

(b) [0001] β-NiS obtained from the inclusion at the fracture surface of CSIRO broken glass.

(c) β-NiS ring pattern obtained from the same inclusion as in (b).

(d) α-NiS polycrystalline ring pattern obtained from PPG bulk glass.

"Mechanical Properties and Microstructures of Ca_2SiO_4 - $CaZrO_3$ Composites"

by

Tien I Hou* ‡ and Waltraud M. Kriven*
Department of Materials Science and Engineering,
University of Illinois at Urbana-Champaign.

Submitted for publication in the Journal of the American Ceramic Society,
July, 1991.

manuscript number [#196499]

Presented at 92nd and 93rd Annual Meetings of the American Ceramic Society, held in Dallas, Texas in 1990 and in Cincinnati, OH in 1991, under abstract numbers [#8-SVI-90] and [#115-B-91], respectively.

---

* Member, the American Ceramic Society.
‡ Now at Chung-Shan Institute of Science and Technology, Tauyuan, Taiwan.

Abstract

Three types of composite Ca_2SiO_4 - $CaZrO_3$ microstructures were fabricated and their microstructures related to mechanical properties. In the first type, Ca_2SiO_4 was added as a minor phase. The second type consisted of a 50 vol% Ca_2SiO_4 - 50 vol% $CaZrO_3$ mixture, while the third type was a reverse of the first. Pure $CaZrO_3$ was also studied as a control and found to have a toughness dependent on its grain size. In composites with Ca_2SiO_4 as the minor phase, a toughness increase was observed which was also a function of matrix grain size. The composite with the second type of microstructure had the highest toughness of about 4.0 $MPa \cdot m^{1/2}$, which was about double that of the base material. No evidence was found for transformation toughening by Ca_2SiO_4. Crack deflection and microcracking were the main toughening mechanisms observed in this composite system. Microstructural observations indicated the existence of weak grain boundaries in $CaZrO_3$ agglomerates and weak interfaces between the two phases.

[Key words: Microstructure, matrix grain size, toughening particle size, toughness, strength, interfaces, crack deflection, microcracking].

I. Introduction

It has been shown that ceramics can be toughened by the incorporation of second phase particulates. The major toughening mechanisms include crack pinning, crack deflection, microcracking, transformation toughening, etc[1]. In particulate-reinforced ceramics, either the matrix or the second phase particles may be a transformable phase, which could be retained in a metastable state by suitable processing conditions. Zirconia (ZrO_2)-toughened ceramics are good examples. Through microstructural control, many such materials have been developed. Microstructurally, they can be divided into three groups: (i) single phase ZrO_2, e.g.TZP [2,3] (ii) ZrO_2 as a second phase embedded in other matrices, e.g., ZTA [4-9] and (iii) ZrO_2 as a matrix containing other minor second phase particulates, e.g., Al_2O_3 in TZP [10-12]. Toughening mechanisms in these materials are mainly due to transformation toughening and microcracking.

Recently, attention has been paid to more complicated zirconia-containing materials. For example, a duplex structure with ZrO_2 single crystals and TZP agglomerates added to the Al_2O_3 matrix has increased the toughness to about 12 $MPa{\cdot}m^{1/2}$, compared with 3 $MPa{\cdot}m^{1/2}$ for the Al_2O_3 matrix.[9] The simultaneous addition of SrO and Al_2O_3 to Ce-TZP resulted in a higher strength of 500-700 MPa as compared with 250 MPa for Ce-TZP alone and at the same time retained the high toughness of 14-15 $MPa{\cdot}m^{1/2}$ of Ce-TZP.[12]

Dicalcium silicate (Ca_2SiO_4) has five polymorphs, among which the orthorhombic (β) to monoclinic (γ) transformation is similar to the tetragonal to monoclinic transformation in ZrO_2.[13] However, differences exist between these two corresponding transformations. Firstly, in Ca_2SiO_4 the transformation occurs from a twinned β microstructure to an untwinned γ structure, while for ZrO_2 the transformation is the reverse, i.e. from a single crystal tetragonal to a twinned monoclinic structure. Secondly, unlike ZrO_2, the transformation from β to γ is irreversible. Thirdly, the volume increase associated with the phase transformation is 12 % for Ca_2SiO_4, while it is only 4.9%for ZrO_2 at room temperature. Some

Ca_2SiO_4 - $CaZrO_3$ composites containing Ca_2SiO_4 as a second phase have already been investigated.[14-16]

The objectives of the present work were to investigate the claim by Moya et al.(14) of transformation toughening in the Ca_2SiO_4 - $CaZrO_3$ system. Specifically, we proposed to fabricate Ca_2SiO_4 - $CaZrO_3$ composites having three types of microstructures. In addition to pure $CaZrO_3$ as a control, the first type was Ca_2SiO_4 added as a second phase to a $CaZrO_3$ matrix. The second consisted of a 50 vol% Ca_2SiO_4 - 50 vol% $CaZrO_3$ mixture, while the third was a reverse of the first one. Basically, the first was similar to ZTA while the second and third were similar to TZP + Al_2O_3 composites. The aim was to measure the mechanical properties and relate them to the microstructures.

II. Experimental Procedures

(1) Powder Preparation

The $CaZrO_3$ powder was commercially available,* and was attritor-milled[fl] to reduce the average particle size to about 1 μm. The Ca_2SiO_4 powder was made by a modified Pechini process.[17,18] The starting materials were $Ca(NO_3)_2$ solution, colloidal silica,[#] citric acid[‡] and ethylene glycol.[‡] The $Ca(NO_3)_2$ solution, the concentration of which was ~0.2 g/ml, was prepared by dissolving $Ca(NO_3)_2.4H_2O$[‡] in deionized water. The calcined powder was then attritor-milled to about 0.37 μm or sedimented to get different particle sizes. The average particle sizes obtained through sedimentation was 5.2 μm, 3.6 μm, 1.5 μm, 0.46 μm and 0.25 μm.

---

* Alfa Products, Danvers, MA

fl Attritor Type B, Size 01, Union Process Inc., Akron, OH.

\# Ludox HS-40, Du Pont, Wilmington, DE.

‡ Fisher Scientific, NJ.

‡ Fisher Scientific, NJ.

‡ Fisher Scientific, NJ.

(2) *Preparation of Dense Samples*

Powders of $CaZrO_3$ and Ca_2SiO_4 were mixed in isopropanol and dried. The mixtures were die-pressed and isostatically pressed at 25,000 psi before firing under the following different conditions.

(A) Pure $CaZrO_3$

Single phase $CaZrO_3$ samples were prepared either by sintering from 1450°C to 1600°C for 2 hrs, or by hot pressing at 1250°C for 40 min and for 1 hr under a pressure of 5,000 psi. Some of the hot pressed samples were further annealed in Ar atmosphere to obtain different grain sizes.

(B) Composites with 10 vol % Ca_2SiO_4.

Five composites with initial Ca_2SiO_4 particle sizes of 5.2 μm, 3.6 μm, 1.5 μm, 0.46 μm and 0.25 μm, respectively, were manufactured by sintering at 1550°C for 2 hrs. This group of composites corresponded to the first type of microstructure with Ca_2SiO_4 as a second phase.

(C) Composites with 10, 30 and 50 vol % $CaZrO_3$.

These composites using a Ca_2SiO_4 powder with a particle size of 0.37 μm, were sintered at 1500°C for 5 hrs. They constituted the second type of microstructure corresponding to the 50 vol% Ca_2SiO_4 - 50 vol% $CaZrO_3$ mixture and the third type, having $CaZrO_3$ as a minor phase.

(3) *Mechanical and Microstructural Characterization of Samples.*

Strength measurements were made with an Instron instrument† using the four-point flexure method, at a displacement rate of 0.5 mm/mm. The bend bar dimensions were about 2.5 mm (height) x 3.5 mm (width) x 15 mm (length) with an inner span of 6.35 mm and an outer span of 12.7 mm. The single-edge, notched-beam (SENB) method in three point loading with a 12.7 mm span, was used to measure the fracture toughness. The bend bar dimensions were about 2.5 mm (width) x 3.5 mm (height) x 15 mm (length),

---

† Model 4502, Instron Corp., Canton, MA.

with a displacement rate of 0.05 mm/min.† The notch width and depth were about 0.35 mm and 0.8 mm respectively. The toughness calculations were based on the equation specified in the ASTM.(19) The pulse echo technique¥ was used to measure the Young's modulus.(20) The thermal expansion coefficient of single-phase β-Ca_2SiO_4 was measured by thermo-mechanical analysis (TMA)*

The microstructures were studied by SEM§ and by TEM‡ operated at 120 KV. SEM specimens were polished to a 1μm grit finish and thermally etched to reveal grain sizes. TEM specimens were prepared by standard methods of mechanically grinding and polishing 3mm discs down to a 1μm diamond grit finish followed by ion beam milling. Vickers indents¶ under loads of 44N were made on as-polished or thermally etched samples in order to produce controlled cracks which were then examined by SEM and TEM.

III. Results

(1) Pure $CaZrO_3$

(A) Mechanical Properties

The toughness measurements for pure $CaZrO_3$ are plotted in Fig. 1 and are seen to be a function of grain size.With decreasing grain size, the toughness increased to a maximum value of about 2.6 MPa·$m^{1/2}$ and then decreased to about 2.0 MPa·$m^{1/2}$, corresponding to the intrinsic property of the material. In the plot of strength *vs* (grain size) $^{-1/2}$ for sintered $CaZrO_3$ as seen in Fig. 2, the strength increased with decreasing grain size. This was interpreted as being due to a combination of both strength and toughness effects. While toughness increased with decreasing grain size, larger grain sizes were associated with increasing flaw sizes, thereby reducing the strength. The overall result was a lower strength for the

---

† Model 4502, Instron Corp., Canton, MA.
¥ NDT-150, Nortec Inc., Kennewick, WA.
* Model 943 Thermomechanical Analyzer, DuPont Instruments, Wilmington, DE.
§ Model S-800 SEM, Hitachi, Tokyo, Japan.
‡ EM-400T, Philips Instruments, Inc., Mahwah, NJ.
¶ Zwick Model 3212, Mark V Laboratory, Inc., East Granby, Connecticut.

larger grain sized material. Fig. 3 shows that the Young's modulus also depended on grain size. The modulus was almost constant for grain sizes less than 5 μm, having a constant value of ~231 GPa, but for grain sizes greater than 5 μm, the E value began to decrease due to spontaneous microcracking.

(B) Microstructure

Specimens of pure $CaZrO_3$ sintered at 1600°C were ~95%-96% of theoretical density (TD) and had a range of grain sizes up to 30 μm, as indicated in Fig. 1. SEM observations showed that most of the pores were homogeneously dispersed and intergranular. A typical SEM micrograph of $CaZrO_3$ which was hot pressed at 1250°C for 40 min, having ~100% TD, is seen in Fig. 4. Hot pressed materials had a smallest grain size of ~ 2 μm (Fig. 1) and no microcracking was observed by TEM.

(2) Composites with 10 vol % Ca_2SiO_4

(A) Mechanical Properties

In Fig. 5(a), the toughness of composites sintered at 1550°C increased with decreasing Ca_2SiO_4 particle size from about 2.0 to 2.7 MPa·$m^{1/2}$, for a matrix grain size ranging from 8 μm to 12 μm. These fell within the range of maximum toughness of pure $CaZrO_3$ as seen in Fig. 1, although there was not much difference in toughness between 8 μm and 12 μm. On replotting the toughness of matrix and of composite as a function of corresponding matrix grain size (Fig. 5(b)), it was evident that the toughness of the composites was higher than that of the pure matrix. In order to obtain a corrected toughness increase (ΔK) by excluding the matrix grain size effect, an experimental assumption was made such that:

$$K_{Ic\ \text{composite with grain size A}} = K_{Ic\ \text{pure matrix with same grain size A}} + \Delta K.$$

These differences in pure *vs* composite toughness values for the same matrix grain size yielded a corrected toughness increase (ΔK). When this was plotted as a function of Ca_2SiO_4 particles size (Fig. 5(c)), it was seen that ΔK increased with decreasing Ca_2SiO_4 particle size.

The strength of composites was considered to be controlled both by toughness and flaw size. Since (i) the surface was polished to a 9 μm diamond grit finish, (ii) the minimum matrix grain size for all the composites was about 8 μm and (iii) the Ca_2SiO_4 particle sizes for all the composites were less than the matrix grain sizes, it could be assumed that the dominant flaw size was equal, in dimension, to the matrix grain size. Thus it was considered to be meaningful to have a plot of strength *vs* matrix grain size, as shown in Fig. 6 for composites sintered at 1550°C. There, it was seen that the strengths of the composites were again higher than those of the pure matrices of the same grain size, i.e., the same flaw size. Hence, both the toughness and strength were increased in the composites as compared to the pure matrices of corresponding grain size. For the purposes of subsequent theoretical predictions, the average thermal expansion coefficient of single-phase β-Ca_2SiO_4 was measured by TMA to be $4 \times 10^{-6}\ °C^{-1}$.

(B) Microstructure

SEM micrographs of Ca_2SiO_4 composites indicated a uniform microstucture with irregularly-shaped Ca_2SiO_4 particles intergranularly dispersed in the matrix. TEM observations (e.g. Fig. 7) often found cavities in the microstructure possibly due to the ejection of transformed γ particles. The transformation resulted in radial microcracking along matrix grain boundaries and within adjacent Ca_2SiO_4 particles. The residual crack openings (δ) of radial microcracks along grain boundaries were measured and related to the radius (r) of Ca_2SiO_4 particle cavity (Fig. 8). The result showed a random distribution of data points, probably due to the measurements depending on the tilted projections observed in the TEM. However, the average ratio of δ/r was about 0.9. Microcracking between twinned β-Ca_2SiO_4 and the matrix was also frequently observed in TEM specimens (Fig. 9), which could have been caused by local tensile stresses at the twin terminations.[21]

(3) *Composites with 10, 30 and 50 vol % $CaZrO_3$.*

(A) Mechanical Properties

Toughness and strength values for composites of 10, 30 and 50 vol % $CaZrO_3$ fired at 1500°C for 5 hrs both increased with increasing volume fraction of $CaZrO_3$ as shown in Fig. 10. Their densities were of the order of 95~96% TD. A plot of modulus *vs* $CaZrO_3$ content (Fig. 11) gave a straight line whose intercepts had values of E = 130 GPa for Ca_2SiO_4 and E = 210 GPa for $CaZrO_3$. These values compared with pulse echo measurements of elastic moduli for single phase materials. For single phase $CaZrO_3$ (also of ~95%-96% TD), it ranged from 131 GPa for matrix grain size 30 μm, to 174 GPa for grain size 8 μm. The measured Young's modulus for the fully dense, hot pressed, single phase $CaZrO_3$ of grain size < 5 μm was 231 GPa. The extrapolated value for Ca_2SiO_4 was in good agreement with the 110 GPa measured made on single phase materials[22].

(B) Microstructure

Composites of 10, 30 and 50 vol % $CaZrO_3$ sintered at 1500°C for 5 hrs were again ~95-96% of TD. While pores were still intergranular, they were larger and not as homogeneously distributed as in the pure $CaZrO_3$ phase, as expected in the sintering of two phase materials. Fig. 12 is an SEM micrograph of the 50 vol% $CaZrO_3$ composite. Each composite contained $CaZrO_3$ agglomerates whose sizes increased with increasing $CaZrO_3$ content. They were approximately 1, 2, and 4 μm for 10, 30 and 50 vol % $CaZrO_3$ composites, respectively. The corresponding Ca_2SiO_4 particle sizes were 12, 8 and 5 μm, respectively. Within a $CaZrO_3$ agglomerate, the grain size was 1~2 μm.

An interesting phenomenon was found on thermal annealing. Fig. 13 (a) is an as-polished SEM micrograph of a 50 vol % $CaZrO_3$ composite sintered at 1500°C for 5 hrs, showing no texture in Ca_2SiO_4 grains. After annealing at 1300°C for half an hour, the same area contained some lath structures as seen in Fig. 13 (b). These were similar to surface γ phase as identified by XRD[16] and were considered to be thermally induced γ phase.

Crack propagation profiles are illustrated in the SEM micrographs of Figs 14 and 15(a-c). In composites with 10 and 30 vol % $CaZrO_3$, cracks were deflected by small $CaZrO_3$ particles ~1-2 μm (Fig. 14). In the 50 vol %

$CaZrO_3$ composites, cracks propagated along Ca_2SiO_4 and $CaZrO_3$ interfaces or close to grain boundaries in a $CaZrO_3$ agglomerate as seen in Fig. 15(a). Secondary microcracking parallel to the main crack was also observed at Ca_2SiO_4 and $CaZrO_3$ interfaces as seen in the adjoining Fig. 15(b) and Fig. 15(c). These were believed to be induced by the stress intensity generated at the crack tip during propagation. Fig. 16 is a corresponding TEM micrograph of an indented specimen showing crack propagation along Ca_2SiO_4 and $CaZrO_3$ interfaces.

IV. Discussion

(1) Pure $CaZrO_3$.

As expected, the toughness of single phase, orthorhombic $CaZrO_3$ depended on its grain size. This was related to microcracking caused by anisotropy in thermal expansion coefficients. A toughness dependence on grain size has already been found in some non-cubic materials[23]. In $CaZrO_3$ the highest toughness was measured at grain size 5 μm, with the intrinsic toughness corresponding to grain size 2 μm (Fig. 1). This is close to the theoretical prediction that the grain size below which the toughness becomes constant is about 0.4 times the critical grain size for spontaneous microcracking[24].

The critical grain size for spontaneous microcracking can be calculated using the equation:[25]

$$\ell_c = 3.1\,(K_b / E\,\Delta\alpha\,\Delta T)^2 \qquad [1]$$

where E = Young's modulus
ΔT = temperature range over which the residual stress develops
$\Delta\alpha$ = anistropy in thermal expansion
K_b = fracture resistance of the boundary.

With $K_b = (\tau E)^{1/2}$, the above equation can be rewritten as:

$$\ell_c = 3.1\,\tau/E\,(\Delta\alpha\,\Delta T)^2 \qquad [2]$$

Since only the average thermal expansion coefficient of 9×10^{-6} °C^{-1} was available,[26] $\Delta\alpha$ was estimated using the crystallographic assumption that the thermal expansion coefficients along the three crystallographic axes were 2α, 2α and α. The α was then calculated to be 5.4×10^{-6} °C^{-1}, (since $2\alpha + 2\alpha + \alpha) / 3 = 9 \times 10^{-6}$. The $\Delta\alpha$ was taken as the difference between the maximum and minum thermal expansion coefficients, and hence equal to 5.4×10^{-6} °C^{-1}. Substituting this into equation [2] together with $\tau = 1$ J/m^2, $\Delta T = 1200$ °C and $E = 170$ GPa for a grain size of ~7 μm, the calculated critical grain size was about 4.3 μm which is in quite good agreement with experimentally observed 5 μm shown in Fig. 1.

(2) *Ca_2SiO_4 - $CaZrO_3$ Composites.*

(A) Composites with 10 vol % Ca_2SiO_4.

Since the matrix grain sizes in these composites fell within the range where toughness of the pure matrix depended on grain size, unlike ZTA, the toughening effect in this system was made more complicated. The critical grain size in alumina for maximum toughness is ~100μm.[23] The two-fold toughness increase in this system reported by Moya et al.[14] appeared to include the matrix grain size effect. A toughness of 1.2 MPa·m$^{1/2}$ was reported for pure $CaZrO_3$ with grain size 16 μm and 2.4 MPa·m$^{1/2}$ was reported for the composite with a matrix grain size of ~3μm.[14]

Since Ca_2SiO_4 particles were intergranular and the matrix was under large tensile stress due to the large volume increase of Ca_2SiO_4 particles upon transformation, radial microcracking from the particles tended to occur in the TEM specimens. The radial microcracking phenomenon observed in this system was similar to that occuring in ZrO_2 - Al_2O_3.[27] Compared with that for ZrO_2 in ZTA, it was found that the value of (δ/r) for Ca_2SiO_4 was about two times greater than that for ZrO_2.[27] This was considered to be reasonable in view of the ratios $E_{matrix} / E_{2nd\ phase}$ and $\Delta V_{Ca_2SiO_4} / \Delta V_{ZrO_2}$. The value of $E_{matrix} / E_{2nd\ phase}$ was about 2 for both the ZTA and the Ca_2SiO_4 - $CaZrO_3$ systems, while $\Delta V_{Ca_2SiO_4} / \Delta V_{ZrO_2}$ was about 2.5. If it occurred in the bulk, a larger crack opening would reduce the Young's modulus and result in a smaller toughness increase than that due to transformation toughening alone, without any attendant

microcracking.[28] It can be inferred, therefore, that it would not be suitable to add a toughener with a large volume increase on transformation to a matrix with a low modulus.

Microcracking between β-Ca_2SiO_4 and the matrix was often observed in the composites. It was first pointed out by Kriven et al.[15] However, the stress induced β to γ transformation did not appear to occur in the bulk composite, since no transformation product was detected by XRD on the fracture surface and since there was no marked increase in mechanical properties. One possible reason for the lack of transformation was that microcracking between β-Ca_2SiO_4 and the matrix might have occurred at a stress lower than that required to initiate transformation, by reducing the stress intensity at Ca_2SiO_4 particles. The dominant toughening mechanism therefore, was considered to be associated with microcracking between β-Ca_2SiO_4 and the $CaZrO_3$ matrix. Since the toughness increase was a function of particle size, a pure deflection mechanism was ruled out.[21]

Microcracking between β-Ca_2SiO_4 and the $CaZrO_3$ matrix could be attributed to (i) the thermal expansion mismatch between the two phases and (ii) to the twinned microstructure of the β-Ca_2SiO_4 particles. The critical particle size for spontaneous microcracking could be estimated from the following equation:[29]

$$D_s > (\tau_m) / (\Delta\varepsilon)^2 E \qquad [3]$$

where D_s = critical particle size for spontaneous microcracking
τ_m = fracture energy for microcracking
$\Delta\varepsilon$ = particle-matrix mismatch strain (~$\Delta\alpha\Delta T$), where $\Delta\alpha$ is thermal expansion mismatch and ΔT is the temperature difference over which the mismatch strains build up
E = Young's modulus

With $\gamma = 1$ J/m^2, $\Delta T = 1200$°C, $E = 170$ GPa and $\Delta\alpha = 9 - 4 \times 10^{-6}$ °C^{-1}, (being 9×10^{-6} °C^{-1} for $CaZrO_3$ [26] and 4×10^{-6} °C^{-1} for Ca_2SiO_4 as measured by thermomechanical analysis in this work), the calculated critical particle for spontaneous microcracking was about 1.4 μm. This compared reasonably with the optimum toughness values of 4μm reported by Moya et al.[14] and 2 μm reported by Barinek.[16]

(B) Composites with 10, 30 and 50 vol % of $CaZrO_3$.

The toughness measurements and Vickers indentations indicated that toughening was mainly due to crack deflection in these composites. In the 50 vol% $CaZrO_3$ composites, microcracking also contributed to the overall toughening. In all three types of composites, cracks were observed to have deflected around $CaZrO_3$ particles, indicating that the crack paths were independent of the$CaZrO_3$ particle sizes (1~4μm). In addition, the residual stress state in this composite system was favorable for crack deflection to occur, since the thermal expansion coefficient of $CaZrO_3$ was greater that that of β-Ca_2SiO_4.

Essentially, the toughness increased with increasing volume fraction of $CaZrO_3$ up to 50 vol%. The toughness increase of the 50 vol % $CaZrO_3$ composite (K_{IC} = 4.0 MPa·$m^{1/2}$) was about two fold that of a pure β- Ca_2SiO_4 material (K_{IC} = 2.0 MPa·$m^{1/2}$).[22] This was higher than that (1.4 ~ 1.75) predicted by a deflection mechanism for spherical second phase particles.[30] The additional toughness increase was believed to be derived from microcracking.

Secondary microcracking near the main crack was observed by SEM (Figs. 17(a) and (b)), in the 50 vol % $CaZrO_3$ composite. Applying equation[3] with γ = 1 J/m^2, ΔT = 1200°C, E = 154 GPa and $\Delta\alpha$ = (9 - 4) x 10^{-6}°C^{-1}, the critical particle size for microcracking is estimated to be ~1.5 μm. The $CaZrO_3$ grain size in the composites with 10, 30 and 50 vol % $CaZrO_3$ was about 1, 2 and 4 μm, respectively. Therefore, the Ca_2SiO_4-$CaZrO_3$ interfaces in the 50 vol% $CaZrO_3$ composite could be weak enough to have stress-induced microcracking as observed. Since the strength increased with increasing toughness for the 50 vol% $CaZrO_3$ composite, this indicated that the deflection mechanism was dominant and that the flaw size due to microcracking might be less that the critical flaw size. The cracks propagating along, or close to grain boundaries in the $CaZrO_3$ agglomerates confirmed the weakness of these grain boundaries. It was noted that the grain size in a $CaZrO_3$ agglomerate was 1 ~ 2 μm, which was close to the transition grain size of about 2 μm for pure $CaZrO_3$ (Fig. 1).

Transformation toughening did not appear to play a role in this system. No transformation product was detected by X-ray diffraction of fracture surfaces, implying that stress-induced transformation did not take

place on fracture. Furthermore, no evidence was found by TEM for transformation to the γ-phase adjacent to Vickers indentation cracks. The lack of transformation is interpreted as being due to the nucleation barrier being too high to achieve with the stress field of a propagating crack in this system .

The three types of microstructures fabricated and evaluated in the β-Ca_2SiO_4-$CaZrO_3$ system are schematically summarized in Fig. 17. In microstructure I, the second phase additions of twinned β-Ca_2SiO_4 were located at $CaZrO_3$ grain boundaries. Since the thermal expansion of β-Ca_2SiO_4 was lower than that $CaZrO_3$, β-Ca_2SiO_4 was under compression and $CaZrO_3$ was under tension on cooling from the sintering temperature. Microstructure III was the reverse of microstructure I so that the reverse residual stress state applied i.e., β-Ca_2SiO_4 was under tension while $CaZrO_3$ was under compression. In general, microstructure III was superior to microstructure I. In the former, the matrix was under compression and the cracking was circumferential around the second phase particles (intrinsically stable), while in the latter, the matrix was under tension and cracking would occur radially from the second phase (i.e., easier for crack linkage). The characteristics of microstructure II were that $CaZrO_3$ agglomerates were embedded in the β-Ca_2SiO_4 matrix and cracks not only propagated along interfaces, but also along grain boundaries within the $CaZrO_3$ agglomerates, thereby giving the highest toughness of all the three types of microstructures.

V. Summary and Conclusions

(1) Pure $CaZrO_3$.

The toughness and Young's modulus of single phase $CaZrO_3$ were a function of its grain size. The intrinsic value of toughness was ~2 MPa·$m^{1/2}$ observed at a grain size of 2 μm, while a maximum toughness of 2.5 μm was measured for a grain size of ~5 μm. This was due to thermal expansion anisotropy leading to stres induced microcracking. Microcracking in larger grain sized materials was responsible for decreases in both toughness and Young's modulus.

(2) 10 vol % Ca_2SiO_4 - $CaZrO_3$ Composites.

In 10 vol % Ca_2SiO_4 composites, matrix grain sizes fell within the range where the toughness of pure matrix depended on matrix grain size. An experimental assumption was made in order to obtain a corrected toughness increase (ΔK). A highest toughness increase ΔK of ~0.9 $MPa \cdot m^{1/2}$ respresenting a 45 % increase over the 2 $MPa \cdot m^{1/2}$ for pure $CaZrO_3$), was obtained for the composite fired at 1550°C containing Ca_2Si particle sizes of 2~3 μm. Observed microcracking between β-Ca_2SiO_4 and the matrix was considered to be the dominant mechanism. TEM thin foil measurements indicated that the ratio of residual crack openings (δ) to radius (r) of Ca_2SiO_4 was about twice that for ZrO_2 in ZTA.

(3) 10, 30 and 50 vol % $CaZrO_3$.

Amongst these, the 50 vol %$CaZrO_3$ composite fired for 5 hrs at 1500°C had the highest toughness values of about 4 $MPa \cdot m^{1/2}$, which was about twice that of the base material. In this composite, $CaZrO_3$ agglomerates were successfully incorporated into the Ca_2SiO_4 matrix. Microstructural observations indicated the existence of weak grain boundaries within $CaZrO_3$ agglomerates and weak interfaces between Ca_2SiO_4 and $CaZrO_3$. These were associated with (i) crystallographic anisotropy of orthorhombic $CaZrO_3$, (ii) thermal expansion mismatch between the two phases and (iii) the twinned structure of β-particles. Cracks propagated not only along β-Ca_2SiO_4 - $CaZrO_3$ interfaces but also along grain boundaries withing $CaZrO_3$ agglomerates. Thus toughening was derived mainly from crack deflection and microcracking mechanisms.

While a lath structure, considered to be thermally induced γ-Ca_2SiO_4 , was found in polished specimens, no evidence was found for transformation toughening by Ca_2SiO_4 in this system. This was attributed to too high a nucleation barrier to induce the transformation by a propagationg crack. Microcracking between β-Ca_2SiO_4 and the $CaZrO_3$ matrix occurred instead. Our study suggests that a potential toughener such as Ca_2SiO_4 with such a large 12 % volume increase on transformation would not be suitable to add to matrix with a low elastic modulus, since larger residual crack openings

would occur and any transformation toughening benefits would be reduced due to the attendant microcracking.

Finally, the claims of Moya et al[14] of transformation toughening cannot be substantiated. Instead our work has shown that the modest toughness increase reported by these authors may be attributed to a reduction in matrix grain size, crack deflection and microcracking mechanisms.

VI. Acknowledgements

This work was sponsored by the US Air Force Office of Scientific Research, through grant number AFOSR-89-0300. T.I. Hou gratefully acknowledges support from the Government of Taiwan, Republic of China. Use of the electron microscope facilities in the Center for Microanalysis of Materials in the MRL as well as the Center for Electron Microscopy, both at the University of Illinois at Urbana-Champaign, are acknowledged.

VII. References

1. R. W. Rice, "Mechanisms of Toughening in Ceramic Matrix Composites," *Ceram. Eng. Sci. Proc.*, **2** [7-8] 661-701 (1981)

2. T. K. Gupta, J. H. Betchtold, R. C. Kuzniki, L. H. Kadoff, and B. R. Rossing, "Stabilization of Tetragonal Phase in Polycrystalline Zirconia," *J. Mat. Sci.*, **12** [10-12] 2421-6 (1977)

3. T. Masaki, "Mechanical Properties of Y_2O_3-Stabilized Tetragonal ZrO_2 Polycrystals After Ageing at High Temperature," *J. Am. Ceram. Soc.*, **69** [7] 519-22 (1986)

4. N. Claussen, "Fracture Toughness of Al_2O_3 with an Unstabilized ZrO_2 Dispersed Phase" *J. Am. Ceram. Soc.*, **59** [1-2] 49-51 (1976)

5. N. Claussen and J. Jahn, "Mechanical Properties of Sintered and Hot-Pressed Si_3N_4-ZrO_2 Composites," *J. Am. Ceram. Soc.*, **61** [1-2] 94-95 (1978)

6. N. Claussen and J. Jahn, "Mechanical Properties of Sintered In Situ-Reacted Mullite-Zirconia Composites," *J. Am. Ceram. Soc.*, **63** [3-4] 228-229 (1980)

7. P. F. Becher, "Transient Thermal Stress Behavior in ZrO_2-Toughened Al_2O_3," *J. Am. Ceram. Soc.*, **64** [1] 37-39 (1981)

8. D. J. Green and M. G. Metcalf, "Properties of Slip-Cast Tranformation-Toughened β"-Al_2O_3/ ZrO_2 Composites," *J. Am. Ceram. Soc. Bull.*, **63** [6] 803-807 (1984)

9. J. Wang and R. Stevens, "Toughening Mechanisms in Duplex Alumina-Zirconia Ceramics," *J. Mat. Sci.*, **23**, 804-808 (1988)

10. K. Tsukuma, K. Ueda, and M. Shimada, "Strength and Fracture Toughness of Isostatically Hot-Pressed Composites of Al_2O_3 and

Y_2O_3-Partially-Stabilized ZrO_2," *J. Am. Ceram. Soc.*, 68 [1] C-4-C-5 (1985)

11. K. Tsukuma and T. Takahata, "Mechanical Property and Microstructure of TZP and TZP/Al_2O_3 Composite," *Advanced Structural Ceramics*, Vol. 78. Edited by P. F. Becher, M. V. Swain, and S. Somiya. Materials Research Society, Pittsburgh, PA, (1987)

1. R. A. Cutler, R. J. Mayhew, K. M. Prettyman and A. V. Virkar, "High-Toughness Ce-TZP/Al_2O_3 Ceramics with Improved Hardness and Strength," *J. Am. Ceram. Soc.*, 74 [1] 179-86 (1991)

13. W. M. Kriven, "Possible Alternatives Transformation Tougheners to Zirconia: Crystallographic Aspects," *J. Am. Ceram. Soc.*, 71 [12] 1021-30 (1988).

14. J. S. Moya, P. Pena, and S. De Aza, "Transformation Toughening in Composites Containing Dicalcium Silicate," *J. Am. Ceram. Soc.*, 68 [9] 259-262 (1985

15. W. M. Kriven, C. J. Chan and E. A. Barinek, "The Particle Size Effect of Dicalcium Silicate in a Calcium Zirconate Matrix," *Advances in Ceramics Vol. 24, Part A.* Science and Technology of Zirconia III. Edited by S. Somiya, N. Yamamoto and H. Yanagida. The American Ceramic Society, Westerville, OH; pp 145-155, (1988)

16. E. A. Barinek, "The Development of Dicalcium Silicate as a Transformation Toughener." M S Thesis, University of Illinois at Urbana-Champaign, 1988.

17. P. A. Lessing, "Mixed-Cation Oxide Powders via PolymericPrecursors," *Ceram. Bull.* 68 [5], 1002-1007 (1989).

18. "Chemical Preparation of Ca_2SiO_4 and Sr_2SiO_4 Powders," I. Nettleship, J. L. Shull and W. M. Kriven, to be published.

19. W. F. Brown and J. E. Srawley, "Plane strain Crack Toughness in High Strength Metallic Materials," *ASTM STP* **410**, Amer. Soc. for Testing and Materials, pp.13-15 (1966)

20. E. Schreiber, O. L.Anderson, and N. Soga, *Elastic Constants and Their Measurement*, Pub. McGraw Hill, New York (1974)

21. Y. Fu, A. G. Evans and W. M. Kriven, "Microcrack Nucleation in Ceramics Subject to a Phase Transformation," *J. Amer. Ceram. Soc.*, **67** [9] 626-630 (1984)

22. I. Nettleship, Y. J. Kim, K. G. Slavick and W. M. Kriven, "Preparation, Microstructures and Mechanical Properties of Pure β-Ca_2SiO_4," to be published.

23. R. W. Rice, S. W. Freiman, and P. F. Becher, "Grain-Size Dependence of Fracture Energy in Ceramics: I, Experiment," *J. Am. Ceram. Soc.*, **64** [6] 346-350 (1981)

24. Y. Fu and A. G. Evans, "Microcrack Zone Formation in Single Phase Polycrystals," *Acta Metall.*, **30**, 1619-1625 (1982)

25. A. G. Evans and Y. Fu, "Mechanical Behavior of Alumina: A Model Anisotropic Brittle Solid," *Advance in Ceramics*, Vol. **10**, 697-719, Edited by W. David Kingery. The American Ceramic Society, Columbus, OH (1983).

26. K. H. Hellwege and A. M. Hellwege, *LANDOLT-BORNSTEIN, Numerical Data and Functional Relationships in Science and Technology,* Spring-Verlag Berlin. Heidelberg. New York, Vol. **16**, p.81 (1981)

27. M. Ruhle, A. G. Evans, R. M. McMeeking, P. G. Charalambides and J. W. Hutchinson, "Microcracking Toughening in Alumina/Zirconia," *Acta Metall.*, **35** [11] 2701-2710 (1987)

28. A. G. Evans "Toughening Mechanisms in Zirconia Alloys " pp.193-212, *Advances in Ceramics, Vol. 12*, Science and Technology of Zirconia II Edited by N. Claussen, M. Ruhle, A. H. Heuer. The American Ceramic Society, Columbus, OH, 1984.

29. R. W. Rice, "Toughening in Ceramic Particulate and Whisker Composites," *Ceram. Eng. Sci. Proc.*, **11** [7-8] 667-694 (1990)

30. K. T. Faber and A. G. Evans, "Crack Deflection Process-I. Theory," *Acta Metall.*, **31** [4] 565-576 (1983)

Figure Captions

Fig. 1 Plot of toughness (K_{IC}) *vs* grain size for pure $CaZrO_3$.

Fig. 2 Plot of strength *vs* (grain size)$^{-1/2}$ for pure $CaZrO_3$.

Fig. 3 Plot of elastic modulus (E) *vs* grain size for pure $CaZrO_3$.

Fig. 4 SEM micrograph of pure $CaZrO_3$ hot pressed at 1250°C for 40 min, having an average grain size of 2 μm.

Fig. 5(a) Plot of toughness *vs* Ca_2SiO_4 particle size for 10 vol % Ca_2SiO_4 - $CaZrO_3$ composites sintered at 1550°C.

Fig. 5(b) Plot of toughness *vs* corresponding matrix $CaZrO_3$ grain size, and of pure $CaZrO_3$ for comparison.

Fig. 5(c) Corresponding plot of toughness increase (ΔK) corrected for the same matrix grain size *vs* Ca_2SiO_4 particle size.

Fig. 6 Plot of strength *vs* matrix grain size for 10 vol % Ca_2SiO_4 - $CaZrO_3$ composites sintered at 1550°C and compared to strengths of pure matrix grain sizes.

Fig. 7 TEM micrograph of 10 vol % Ca_2SiO_4 - $CaZrO_3$ composites sintered at 1550°C, showing a cavity from which a transformed γ-Ca_2SiO_4 particle was probably ejected. Microcracking resulted along adjoining matrix grain boundaries and within adjacent, twinned β-Ca_2SiO_4 particles.

Fig. 8 Plot of residual crack openings measured from TEM micrographs *vs* radius of corresponding Ca_2SiO_4 particles.

Fig. 9 TEM micrograph of Ca_2SiO_4 - $CaZrO_3$ composites sintered at 1550°C, showing microcracking between an untransformed, twinned β-Ca_2SiO_4 particle and matrix.

Fig. 10 Plot of toughness and strength *vs* volume fractions of $CaZrO_3$ additions for composites sintered at 1500°C for 5 hrs.

Fig. 11 Plot of Young's modulus *vs* volume fractions of $CaZrO_3$ for composites sintered at 1500°C for 5 hrs.

Fig. 12 SEM micrograph of general microstructure of 50 vol % $CaZrO_3$ composite sintered at 1500°C for 5 hrs.

Fig. 13 SEM micrograph of 50 vol % $CaZrO_3$ sintered at 1500°C for 5 hrs. (a) No lath structure was found on as-polished surfaces. (B) On annealing at 1300°C for 1/2 hr, lath structures, considered to be transformed γ-Ca_2SiO_4,[16] appeared.

Fig. 14 SEM micrograph of 10 vol % $CaZrO_3$ sintered at 1500°C for 5 hrs, showing crack deflection around $CaZrO_3$ particles.

Fig. 15 SEM micrograph of 50 vol % $CaZrO_3$ composite sintered at 1500°C for 5 hrs, showing (A) crack propagation along or close to grain boundaries in $CaZrO_3$ agglomerates and along $CaZrO_3$-Ca_2SiO_4 interfaces and (B) secondary microcracking (arrowed) along interfaces and withing Ca_2SiO_4 grains (adjoining micrograph). (C) Extensive crack deflection and microcracking aroung CaZrO3 agglomerates were evident.

Fig. 16 Corresponding TEM micrograph of Vickers indented crack in 50 vol % $CaZrO_3$ composite sintered at 1500°C for 5 hrs showing crack propagation along interfaces between Ca_2SiO_4 (C_2S) and $CaZrO_3$ (CZ). Note that the twinned β-Ca_2SiO_4 grains adjacent to the crack were still untransformed.

Fig. 17 Schematic summary of the three types of microstructures fabricated and evaluated. (A) $CaZrO_3$ with second phase additions of twinned β-Ca_2SiO_4. (B) 50 vol % Ca_2SiO_4 - 50 vol % $CaZrO_3$ mixture with $CaZrO_3$ agglomerate sizes comparable to Ca_2SiO_4 particle sizes. (C) Twinned β-Ca_2SiO_4 matrix with $CaZrO_3$ second phase additions.

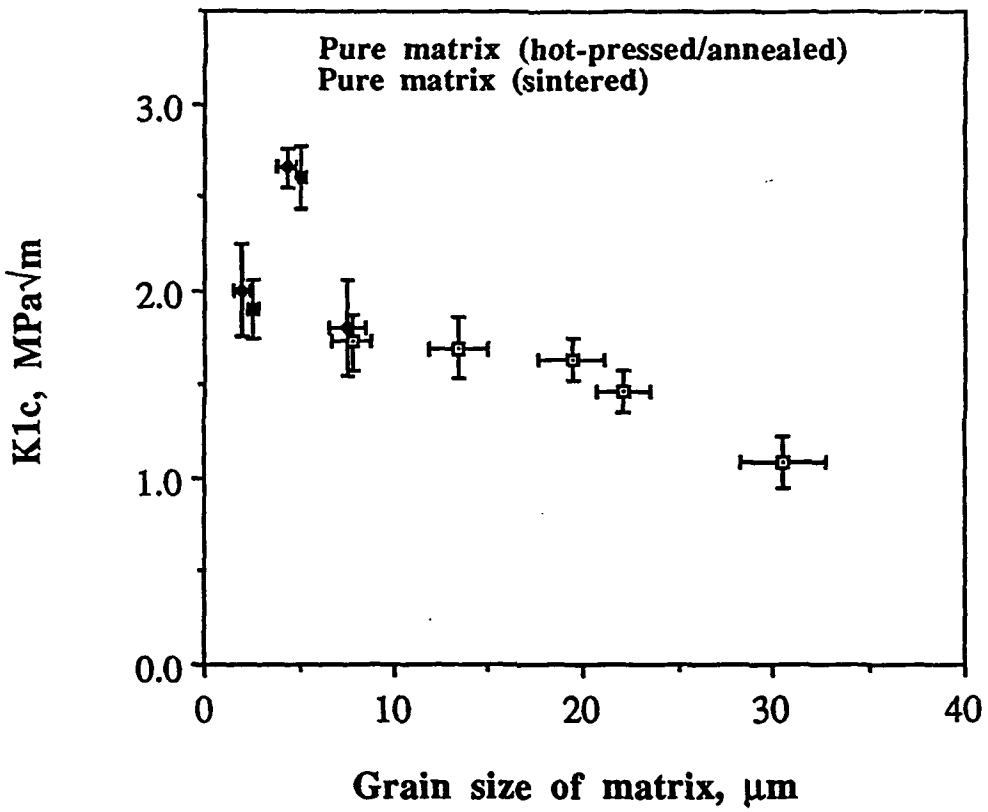

Fig. 1. Plot of toughness (K_{IC}) *vs* grain size for pure $CaZrO_3$.

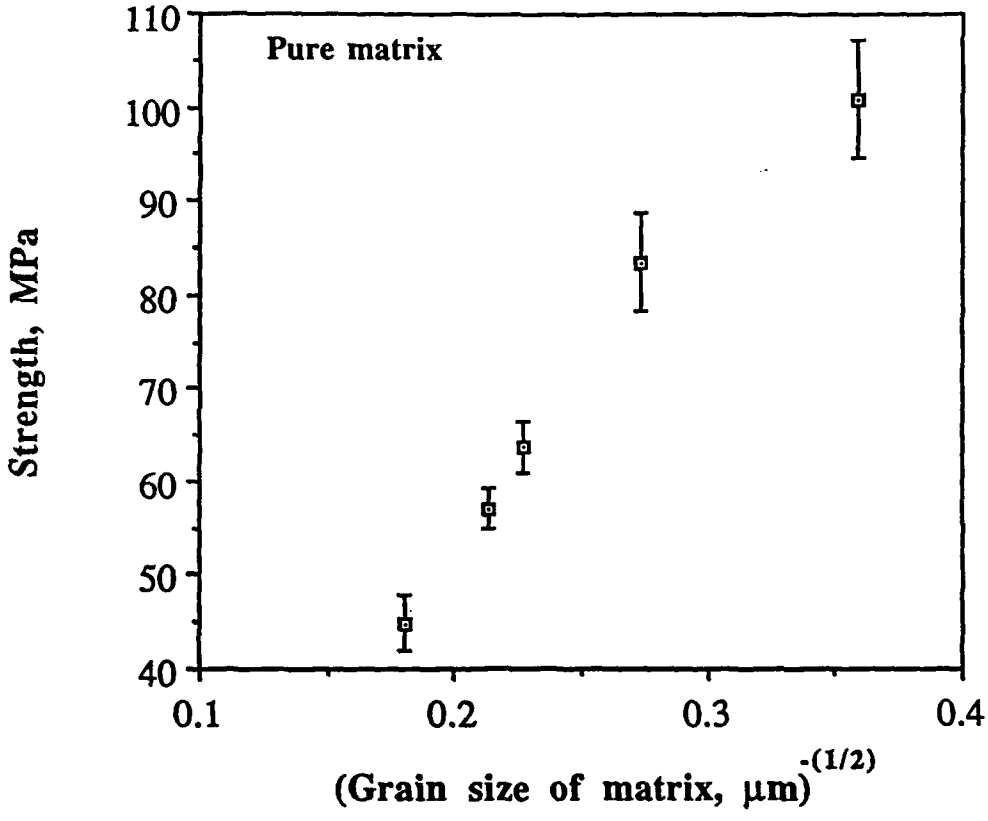

Fig. 2. Plot of strength *vs* (grain size)$^{-1/2}$ for pure $CaZrO_3$.

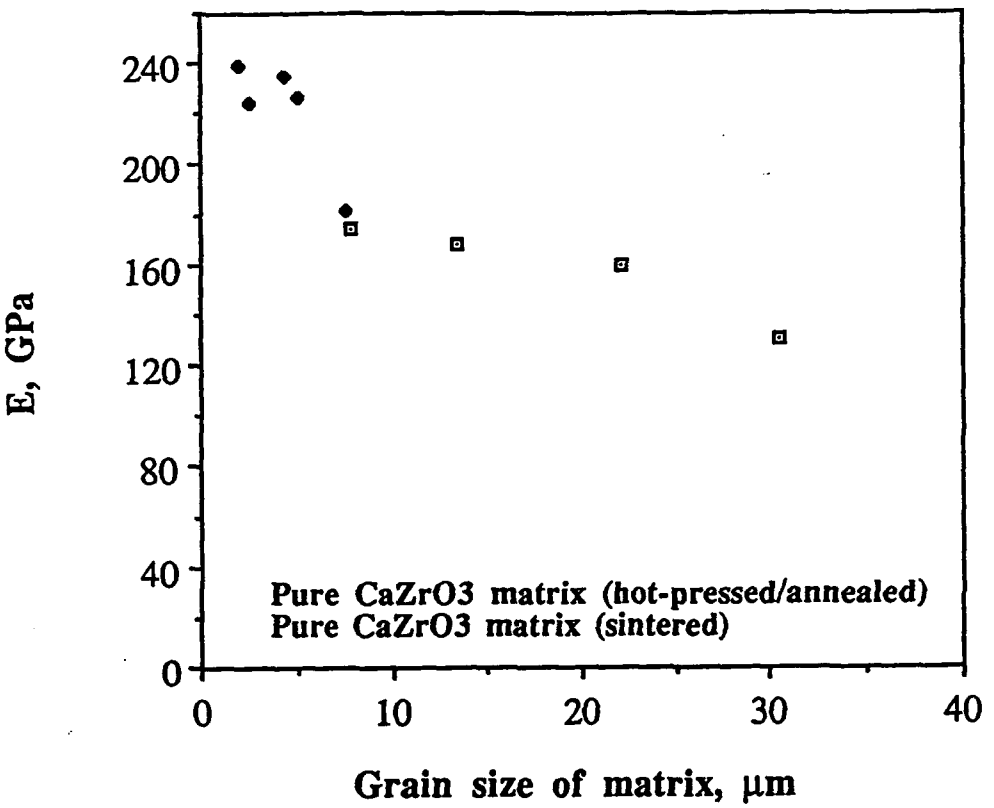

Fig. 3. Plot of elastic modulus (E) *vs* grain size for pure $CaZrO_3$.

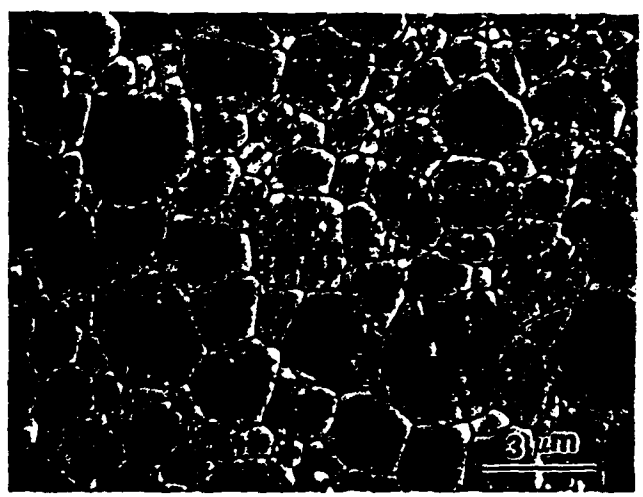

Fig. 4. SEM micrograph of pure $CaZrO_3$ hot pressed at 1250°C for 40 min, having an average grain size of 2 μm.

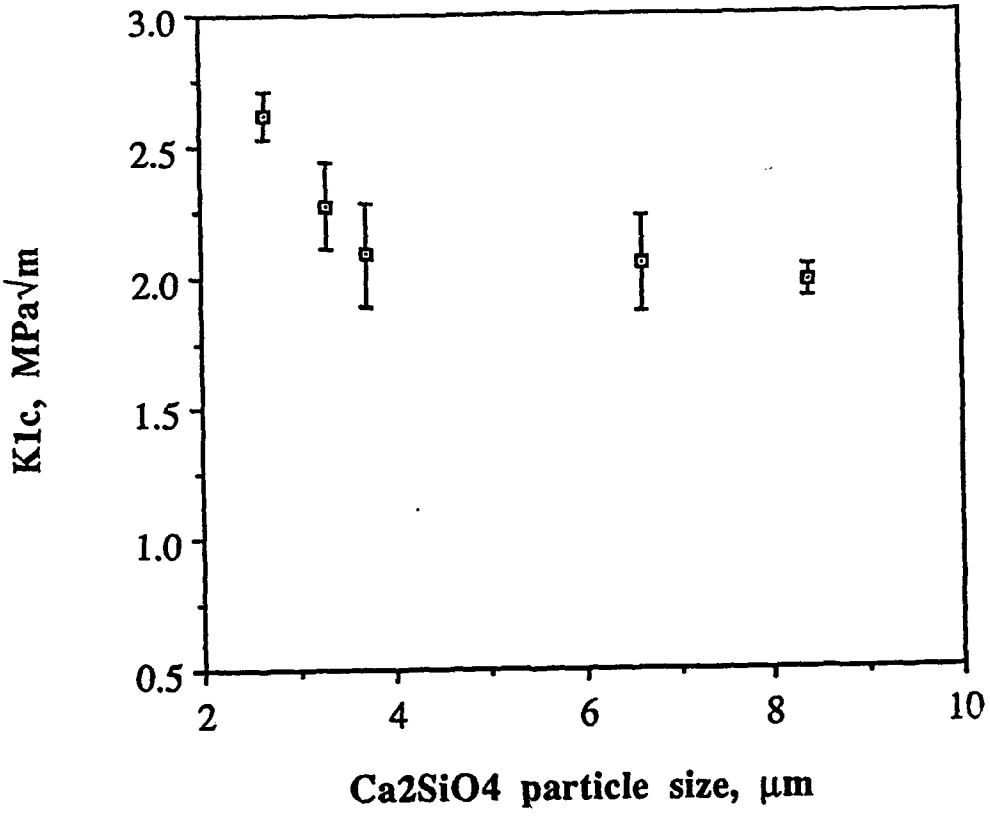

Fig. 5(A). Plot of toughness *vs* Ca_2SiO_4 particle size for 10 vol % Ca_2SiO_4 - $CaZrO_3$ composites sintered at 1550°C.

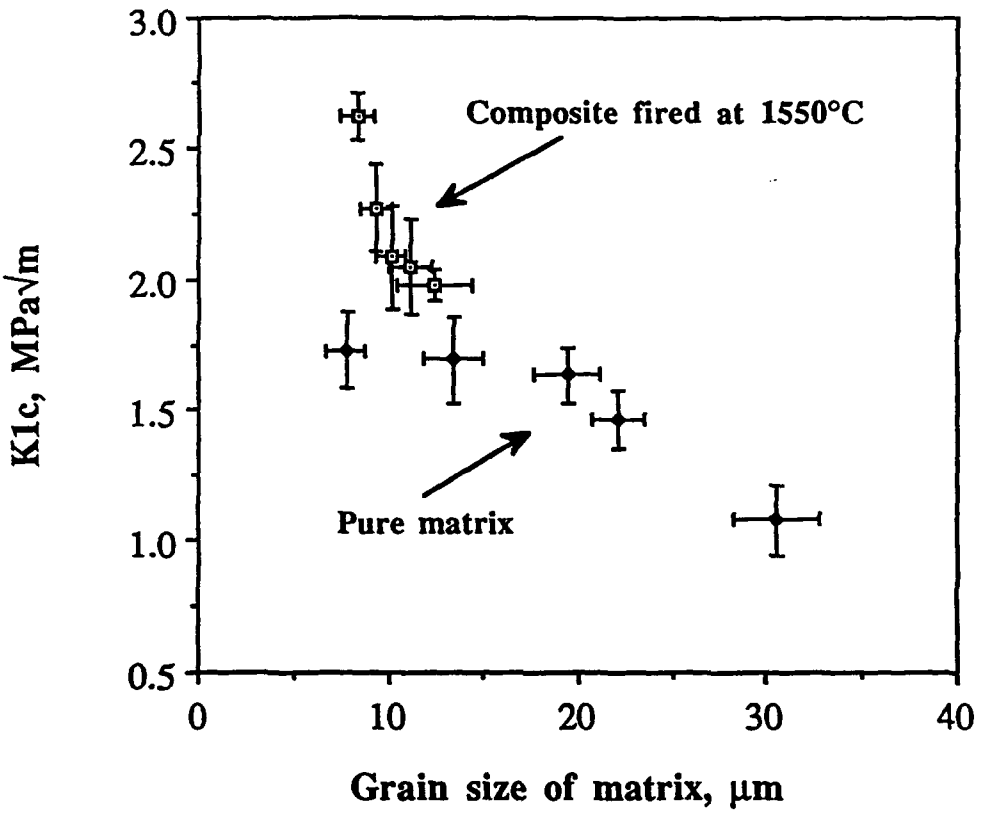

Fig. 5(B). Plot of toughness *vs* corresponding matrix $CaZrO_3$ grain size, and of pure $CaZrO_3$ for comparison.

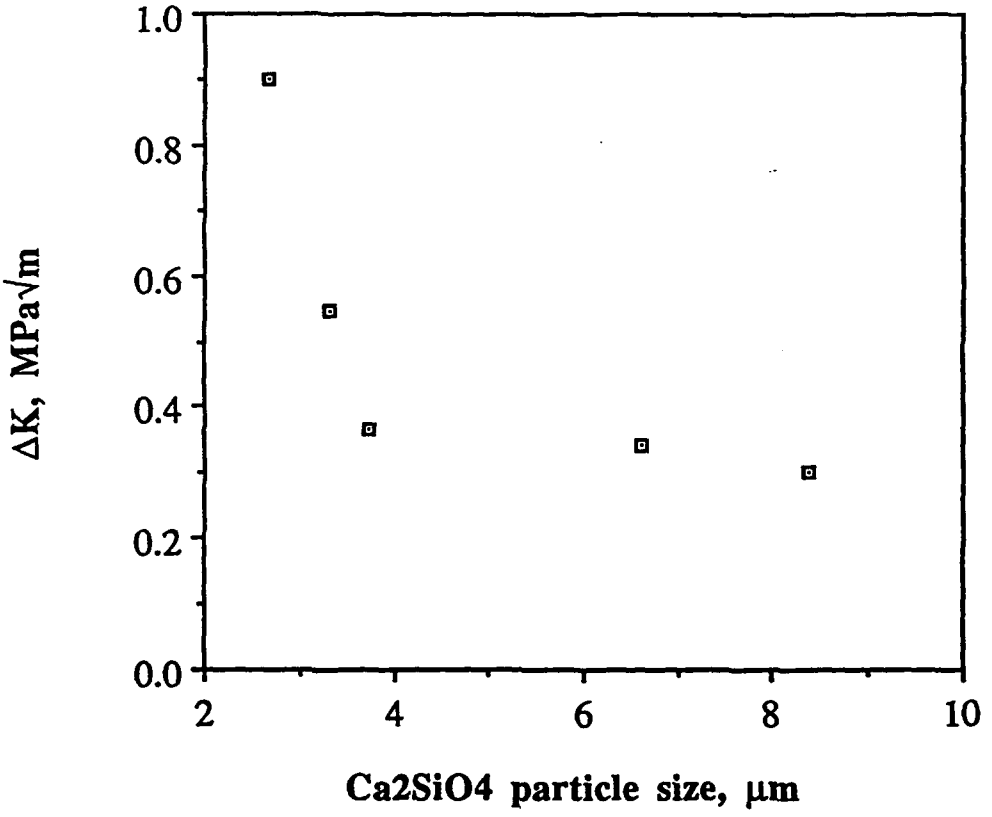

Fig. 5(C). Corresponding plot of toughness increase (ΔK) corrected for the same matrix grain size *vs* Ca_2SiO_4 particle size.

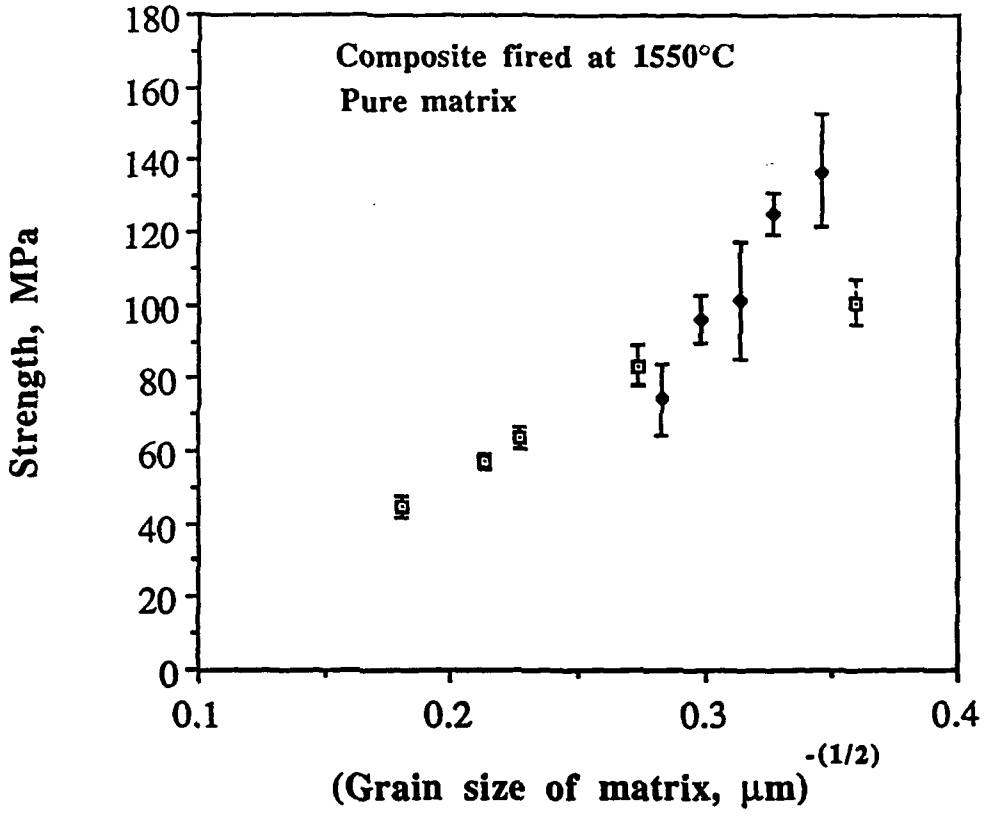

Fig. 6. Plot of strength *vs* matrix grain size for 10 vol % Ca_2SiC_4 - $CaZrO_3$ composites sintered at 1550°C and compared to strengths of pure matrix grain sizes.

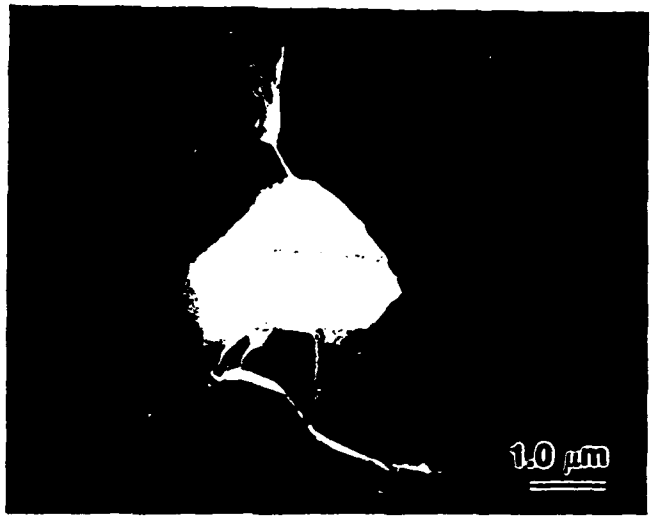

Fig. 7. TEM micrograph of 10 vol % Ca_2SiO_4 - $CaZrO_3$ composites sintered at 1550°C, showing a cavity from which a transformed γ-Ca_2SiO_4 particle was probably ejected. Microcracking resulted along adjoining matrix grain boundaries and within adjacent, twinned β-Ca_2SiO_4 particles.

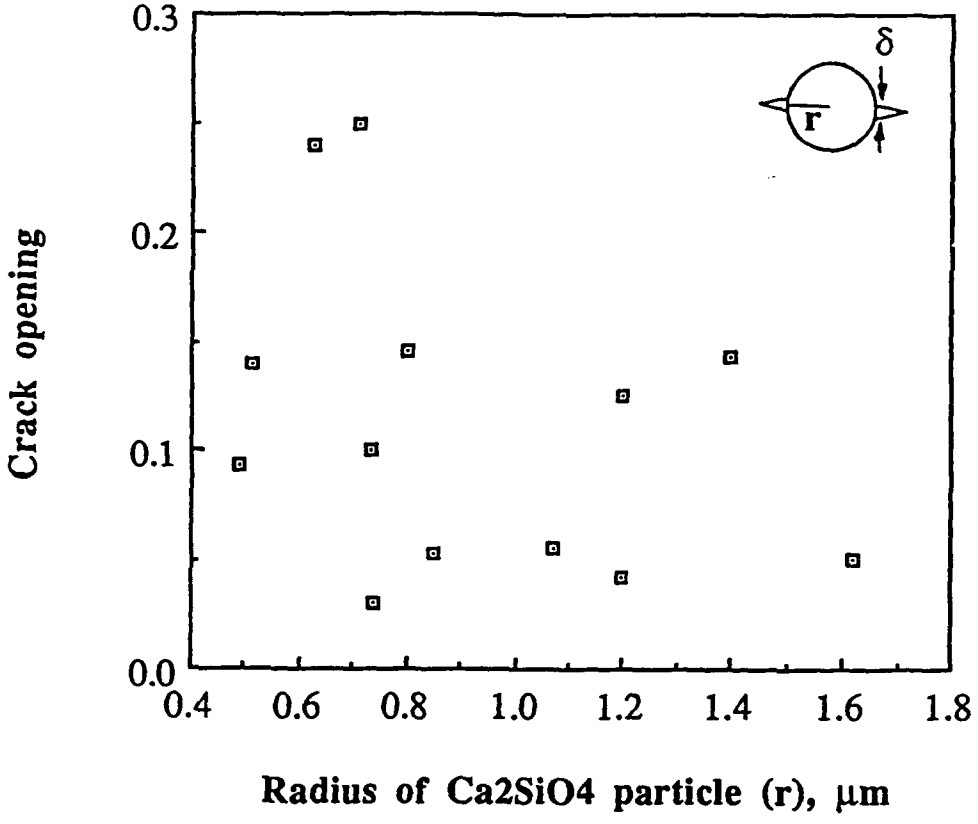

Fig. 8. Plot of residual crack openings measured from TEM micrographs *vs* radius of corresponding Ca_2SiO_4 particles.

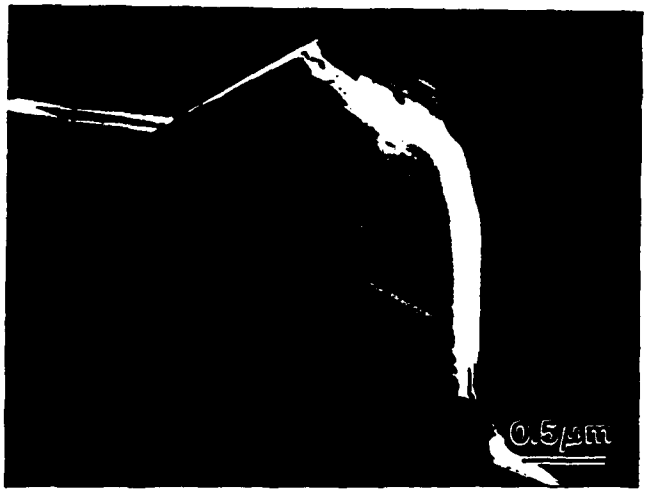

Fig. 9. TEM micrograph of Ca_2SiO_4 - $CaZrO_3$ composites sintered at 1550°C, showing microcracking between an untransformed, twinned β-Ca_2SiO_4 particle and matrix.

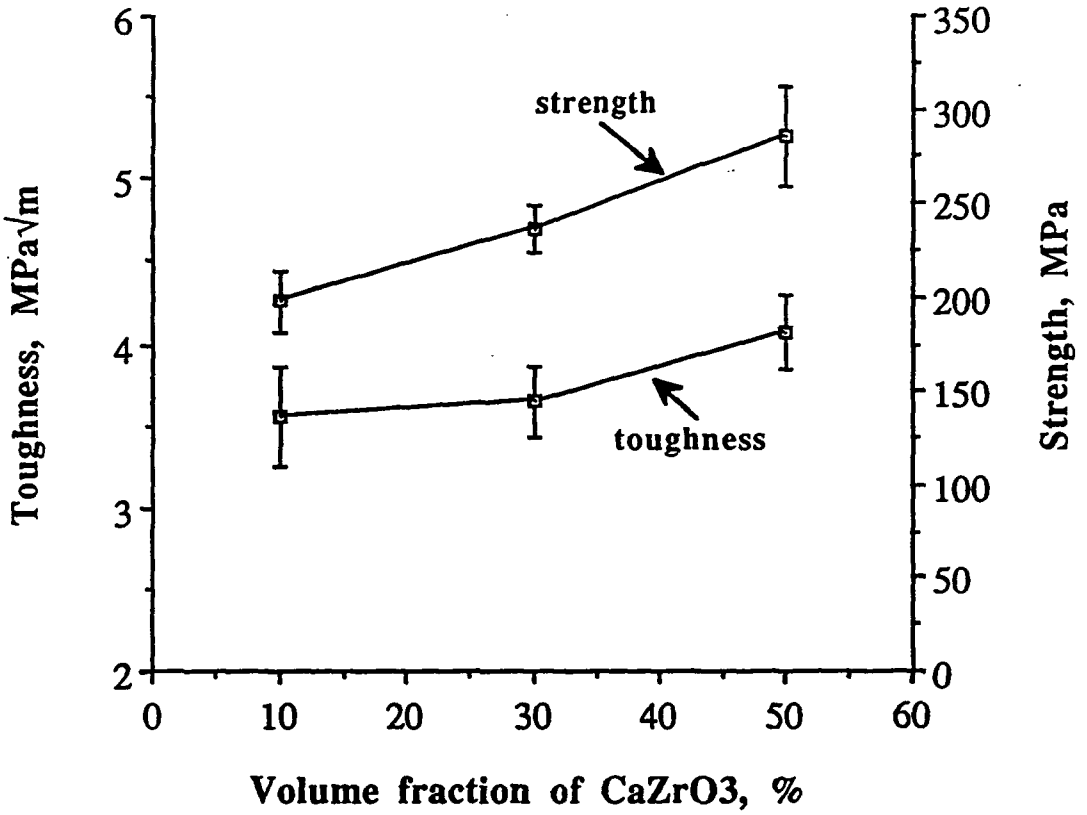

Fig. 10. Plot of toughness and strength *vs* volume fractions of $CaZrO_3$ additions for composites sintered at 1500°C for 5 hrs.

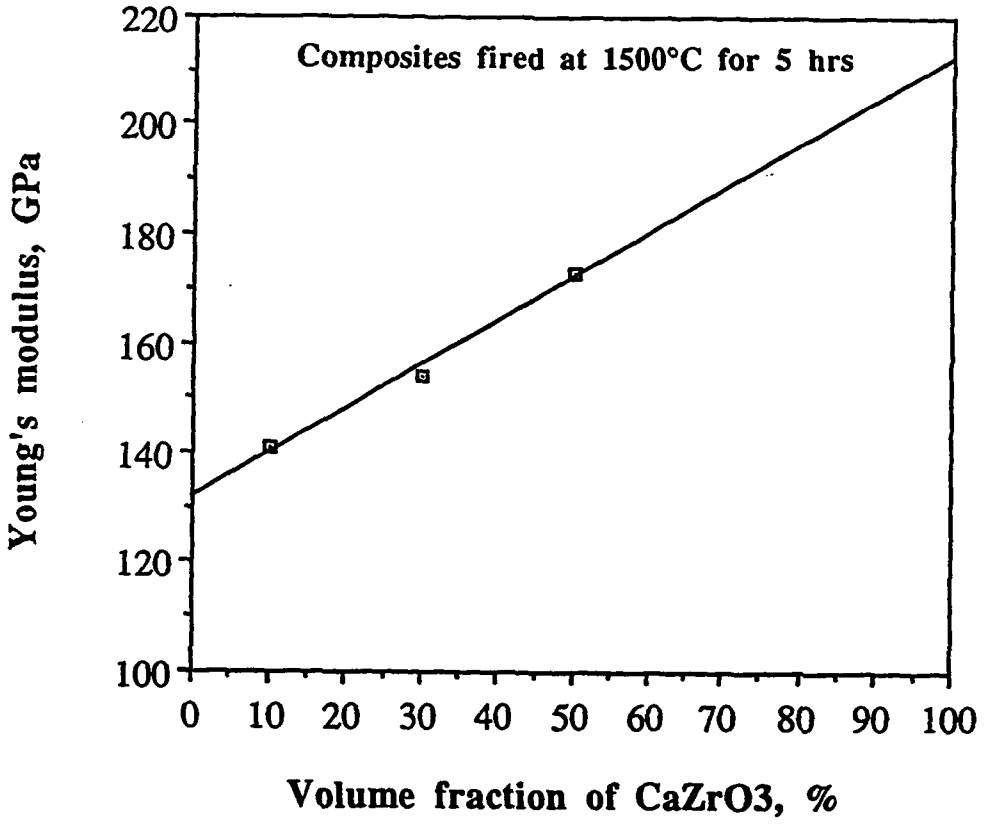

Fig. 11. Plot of Young's modulus *vs* volume fractions of $CaZrO_3$ for composites sintered at 1500°C for 5 hrs.

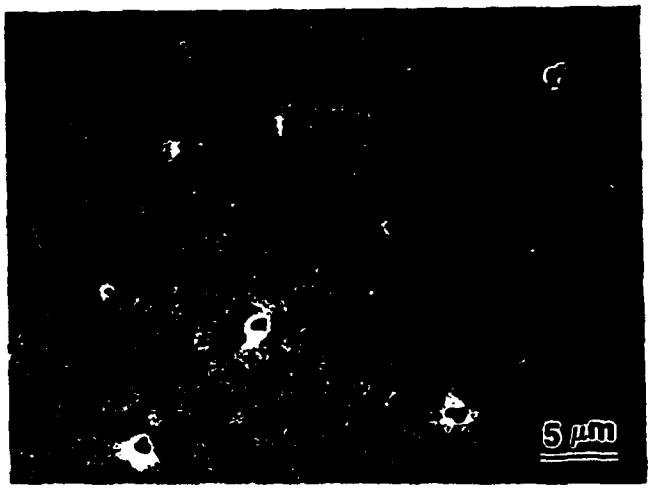

Fig. 12. SEM micrograph of general microstructure of 50 vol % $CaZrO_3$ composite sintered at 1500°C for 5 hrs.

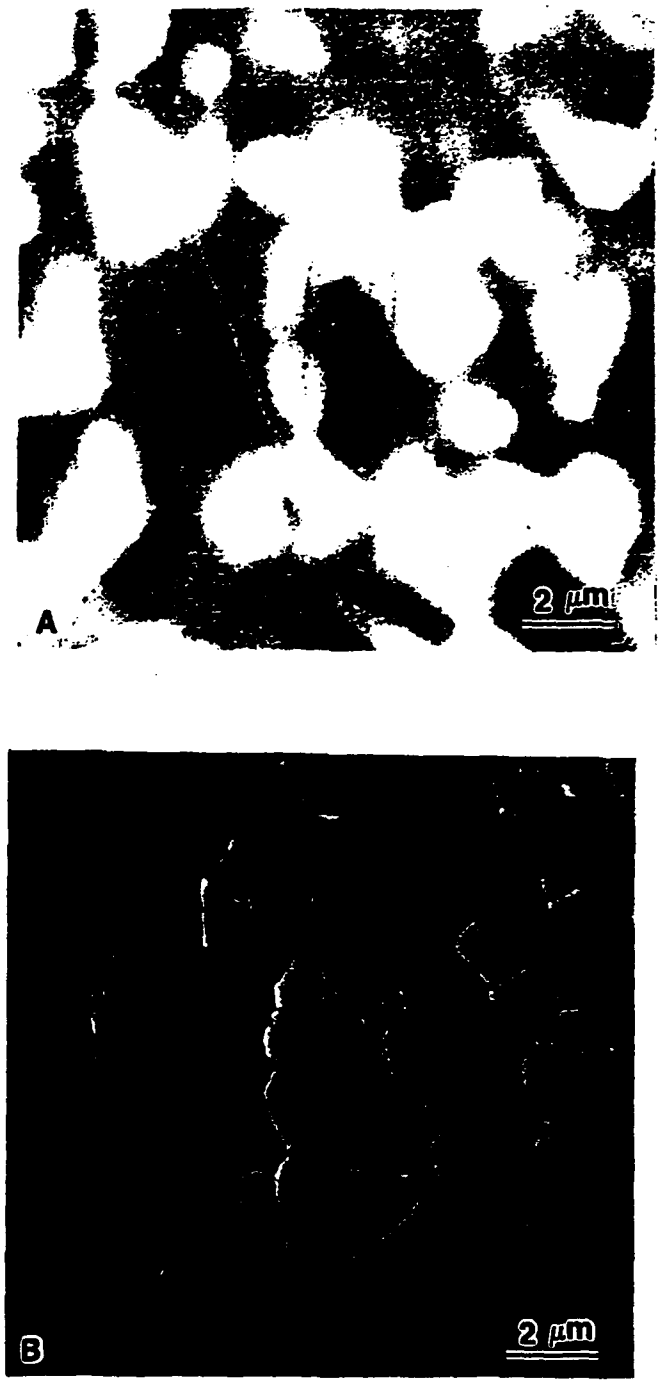

Fig. 13 SEM micrograph of 50 vol % $CaZrO_3$ sintered at 1500°C for 5 hrs. (A) No lath structure was found on as-polished surfaces. (B) On annealing at 1300°C for 1/2 hr, lath structures, considered to be transformed γ-Ca_2SiO_4,[16] appeared.

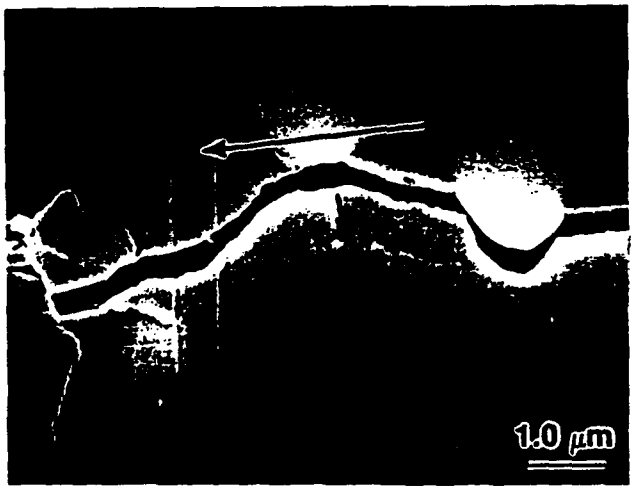

Fig. 14. SEM micrograph of 10 vol % $CaZrO_3$ sintered at 1500°C for 5 hrs, showing crack deflection around $CaZrO_3$ particles.

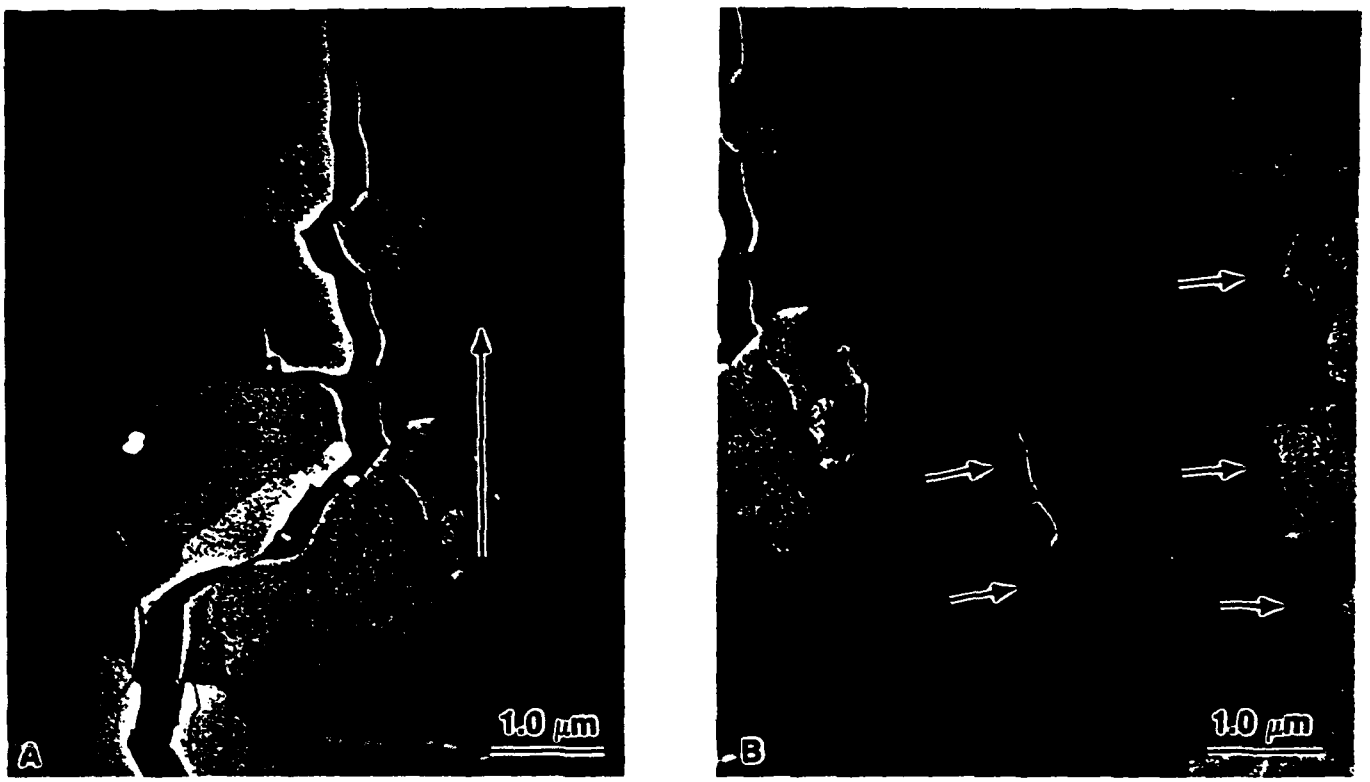

Fig. 15. SEM micrograph of 50 vol % $CaZrO_3$ composite sintered at 1500°C for 5 hrs, showing (A) crack propagation along or close to grain boundaries in $CaZrO_3$ agglomerates and along $CaZrO_3$-Ca_2SiO_4 interfaces and (B) secondary microcracking (arrowed) along interfaces and withing Ca_2SiO_4 grains (adjoining micrograph). (C) Extensive crack deflection and microcracking aroung $CaZrO_3$ agglomerates were evident.

Fig. 15. SEM micrograph of 50 vol % $CaZrO_3$ composite sintered at 1500°C for 5 hrs, showing (A) crack propagation along or close to grain boundaries in $CaZrO_3$ agglomerates and along $CaZrO_3$-Ca_2SiO_4 interfaces and (B) secondary microcracking (arrowed) along interfaces and withing Ca_2SiO_4 grains (adjoining micrograph). (C) Extensive crack deflection and microcracking aroung $CaZrO_3$ agglomerates were evident.

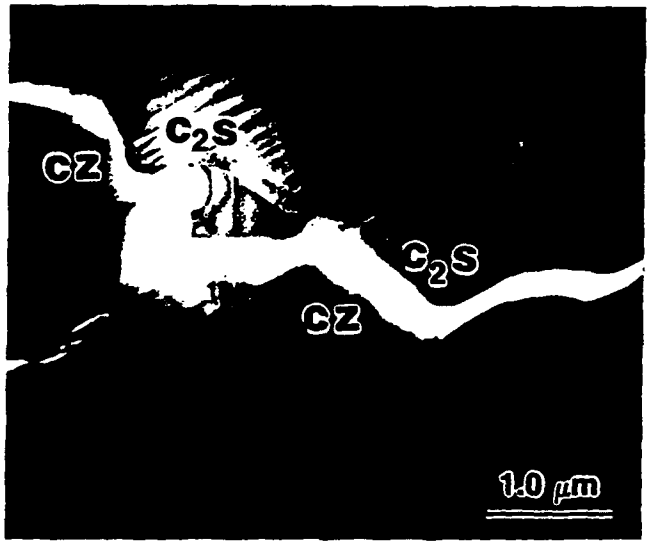

Fig. 16. Corresponding TEM micrograph of Vickers indented crack in 50 vol % $CaZrO_3$ composite sintered at 1500°C for 5 hrs showing crack propagation along interfaces between Ca_2SiO_4 (C_2S) and $CaZrO_3$ (CZ). Note that the twinned β-Ca_2SiO_4 grains adjacent to the crack were still untransformed.

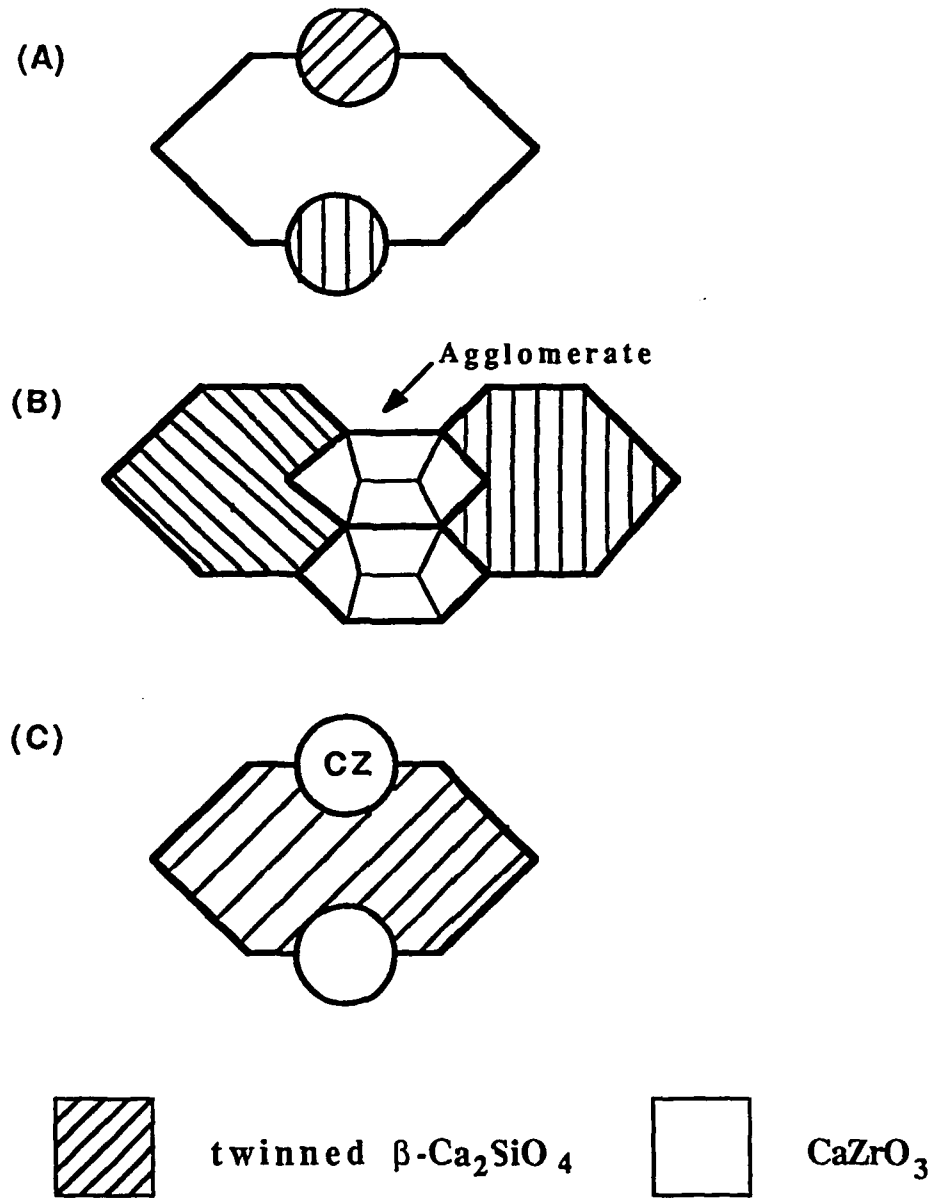

Fig. 17. Schematic summary of the three types of microstructures fabricated and evaluated. (a) $CaZrO_3$ with second phase additions of twinned β-Ca_2SiO_4. (b) 50 vol % Ca_2SiO_4 - 50 vol % $CaZrO_3$ mixture with $CaZrO_3$ agglomerate sizes comparable to Ca_2SiO_4 particle sizes. (c) Twinned β-Ca_2SiO_4 matrix with $CaZrO_3$ second phase additions.

"Preparation, Microstructure and Properties of Silicon Carbide - Dysprosia Composites"

Shin Kim* and Waltraud M. Kriven*,
Department of Materials Science and Engineering,
University of Illionis at Urbana-Champaign,
Urbana, IL 61801

In preparation for publication in the Journal of the American Ceramic Society, November 1991.

† (First Draft)

---

* Member, the American Ceramic Society

† Presented at the 91st, 92nd and 93rd Annual Meetings of the American Ceramic Society in Indianapolis, IN in April 1989 as abstract [#18-SI-89], in Dallas, TX in April 1990 as abstract [#72-SIV-90] and in Cincinnati, OH as abstract [#100-SVI-91], respectively.

ABSTRACT

Composites of silicon carbide with up to 30 vol% dysprosia (Dy_2O_3) were fabricated by hot pressing and hot isostatic pressing. The effects of Dy_2O_3 dispersions on the microstructure and on selected mechanical properties of the composites were investigated. With the dispersion of 10% to 15 vol% Dy_2O_3 in SiC matrix, the fracture toughness increased by ≈ 40%, while the flexural strength was comparable to that of unreinforced SiC. The increased fracture toughness was due to crack deflection in conjunction with crack-interface grain bridging and was not related to a phase transformation of Dy_2O_3 in the matrix. [Key words: silicon carbide, composites, dysprosium oxide, mechanical properties, hot pressing]

I. Introduction

Silicon carbide is a promising material because of its excellent chemical and physical properties. Good high temperature strength, sufficient thermal shock resistance, a low thermal expansion coefficient with good heat conductivity, as well as high hardness, abrasion resistance and low density, form the basis for the excellent mechanical properties of silicon carbide. However, its full potential has not been realized partially due to its tendency towards brittle behavior.

In SiC composites, particulate toughening of SiC has been realized by incorporating second phase particles like TiB_2[1-3] or TiC[4]. McMurtry et al.[1] have reported a 90% increase in fracture toughness and a 30% increase in flexural strength by TiB_2 additions to SiC. Wei and Becher[4] reported an

increase in both fracture toughness and strength by dispersing TiC particles into a SiC matrix.

Dysprosia (Dy_2O_3), one of the lanthanide sesquioxides, has high temperature thermodynamic stability and low volatility.[5] The lanthanide sesquioxides have been proposed as potential high temperature transformation tougheners.[6,7] On cooling, like other lanthanide sesquioxides in the series, dysprosia (Dy_2O_3) transforms from monoclinic (B) to cubic (C) symmetry with an 8% volume increase at about 1850 °C on cooling. The reverse transformation occurs at 1950°C on heating.[8] The nature of the transformation in lanthanide sesquioxides with atomic numbers higher than 65 (Tb_2O_3, Dy_2O_3, Ho_2O_3) appears to be displacive and possibly martensitic, like that of zirconia.[6,9]

Several workers have studied the effect of quenching on the metastable retention of high temperature phases.[10-12] Retention of pure Dy_2O_3 in the high temperature form (monoclinic) could be achieved by rapid cooling. McPherson[11] prepared metastable B phases of Sm_2O_3 through Dy_2O_3 by rapid cooling. Coutures et al.[12] reported forming the B phase of the oxides of Gd_2O_3 through Lu_2O_3 and Y_2O_3 by melting samples and quenching the resulting vapors on a bell jar. Lopato et al.[10] reported that quenched Dy_2O_3 was retained in the B form. They also reported a partial transformation B $\rightarrow$ C for Dy_2O_3 by grinding samples in an agate mortar.

An investigation of the lanthanide sesquioxides as transformation toughening agents[9] showed an increase in toughness by dispersing Tb_2O_3 into an MgO matrix. It was attributed to the B to C transformation at temperatures $\geq$ 1075°C. No previous work was conducted, however, to

disperse Dy_2O_3 into a ceramic matrix in order to investigate its effect on the toughness of a composite.

In the present work, composites of silicon carbides with up to 30 vol% dysprosia were fabricated. The chemical compatibility of the SiC - Dy_2O_3 composite system was investigated and the effects of dispersed dysprosia in SiC matrix on the physical and mechanical properties of the composites were evaluated.

II. Experimental Procedure

(1) Starting Powders

Silicon carbide powders from two different manufacturers were investigated in this study. Very fine β-silicon carbide powders (designated AL) with low oxygen content were obtained. Table I describes the characteristics of the powders. Both α and β phase submicron SiC powders# (designated ST) from another manufacturer were also purchased. SiC powders were sent to chemical analysis service laboratories for a determination of oxygen content by either the inert gas fusion method+ or neutron activation analysis.§ Particle sizes of some of powders were determined by the sedimentation method.‡ The Dy_2O_3 powders∞ had an average particle size of ≈ 2 μm. The purity of the powder was 99.9%.

Amorphous boron and carbon were used in some composites as sintering additives. Amorphous boron powders¶ had a particle size of 0.85 μm, BET specific surface area of 8 - 13 m^2/g and 96.2% purity. Two types of carbon sources were used. Most of the carbon additions were made

---

Grade A10 (α-SiC) and B10 (β-SiC), Herman C. Starck Inc., New York, NY

+ Model RO-116 Oxygen Determinator, Leco Corporation, St. Joseph, MI

§ Atomic Energy of Canada Limited, Whiteshell Nuclear Research Establishment, Pinawa, Manitoba, Canada

‡ Sedigraph 5000 ET, Micromeretics, Inc., Norcross, GA

∞ Molybdenum Corporation of America, Louviers, CO

¶ Amorphous boron, Grade I, Herman C. Starck Inc., New York, NY

Table I. SiC Powder Characteristics

Type of Powders (Grade)	AL β-SiC	ST α-SiC (A10)	ST β-SiC (B10)
Manufacturing method	Plasma synthesis	Acheson process	Carbothermic reduction
Chemical Analysis			
O (wt%)	0.1	0.70	0.74
Cl (wt%)	0.15		
B (wt%)	0.25 - 0.3		
Free C (wt%)	0.3 - 0.5		
Free Si (wt%)	< 0.1		
Fe (ppm)	< 50	150	250
Al (ppm)	< 50	400	800
Ca (ppm)	< 50	100	100
All Other Elements	Undetected		
Surface Area (m^2/g)	10	14.97	13.9
Phase	β	α	β
Particle Size Distribution			
Median (μm)	0.5	0.63	0.70
D_{90}/D_{10} Ratio*	10		

* D_{90}/D_{10} is the ratio of the particle diameters at 90% and 10% of the cumulative particle size distribution curve.

using polyphenylene resin.# Graphite powders† with -325 mesh size and 99.9% purity were used for some SiC materials. 10 % to 30 vol % of Dy_2O_3 were added to SiC powders. Most SiC - Dy_2O_3 powders were attrition milled in methanol for 1 - 3 hours. Attrition milling# was conducted in methanol using 5 mm diameter SiC balls as a grinding media to prevent contamination from the grinding media.

Boron and carbon, if used, were added to the attritor with the powders. After attrition milling, the powder mixtures were dried and pulverized using an agate mortar and pestle, and then were screened through a 425 μm aperture (No. 40) stainless steel sieve. Some powders were mixed in a vibratory mixer§ for 20 to 30 min. No binder was added to the powder mixtures in this experiment. Polyphenylene resin, if used, was added to the powder mixture as a benzene solution with a concentration of 5 mg/ml. The benzene was removed in an air stream. The mixtures were dried at ≈ 80°C and passed through a 425 μm aperture sieve.

(2) Densification

Hot pressing, hot isostatic pressing and pressureless sintering were used for densification of the composites. The powder compacts were hot

---

H-Resin, Hercules Incorporated, Wilmington, DE

† Cerac, incorporated, Milwaukee, WI

Attritor mill size 01, Union Process, Inc., Akron, OH

§ Spex mixer/mill, Spex Industries, Inc., Metuchen, NJ

pressed† at 2000 - 2050°C for 20 min to 1 h hold times. The dies and rams were made of graphite. Graphite spacers with 6.4 mm thickness were placed between samples or between samples and rams. Graphite foil§ (10 mils thick) was used between die walls and powder compacts to prevent adherence and diffusion between the specimen and graphite die.

After initial clean-up cycles in vacuum at 300°C, the hot press chamber was kept at 50.5 KPa (0.5 atmosphere) using static argon gas. Hot pressing temperatures were 2000°C or 2050°C and hold times ranged from 10 min to 1h. A pressure of 28 MPa (4060 psi) was applied to the powder compact when the temperature began to increase above 300°C and was released at the end of the hold time.

For hot isostatic pressing, the pre-pressed compacts were outgassed in a high vacuum furnace at 1000 °C for 5 hours. Tantalum metal was used as the encapsulation material. Use of SiO_2 glass as an encapsulation material for SiC - Dy_2O_3 composites was avoided because of the chemical reaction of SiO_2 with Dy_2O_3 to form silicates. Fig. 1 summarizes the hipping process. Hot isostatic pressing¶ was conducted at 2000°C with an applied argon gas pressure of 186 MPa (27,000 psi) for a 1 h hold. Pressure was applied when the temperature reached 500°C to 186 MPa and was maintained during holding and cooling periods. A post densification hot

---

† 30 ton vacuum hot press,Series 3600, GCA Corp., Vacuum Industries Division, Somerville, MA

§ ATJ grade carbon, Union Carbide, Carbon Products Division, Cleveland, OH

¶ Model QIH-3, AESA Pressure Systems, Inc., Columbus, OH

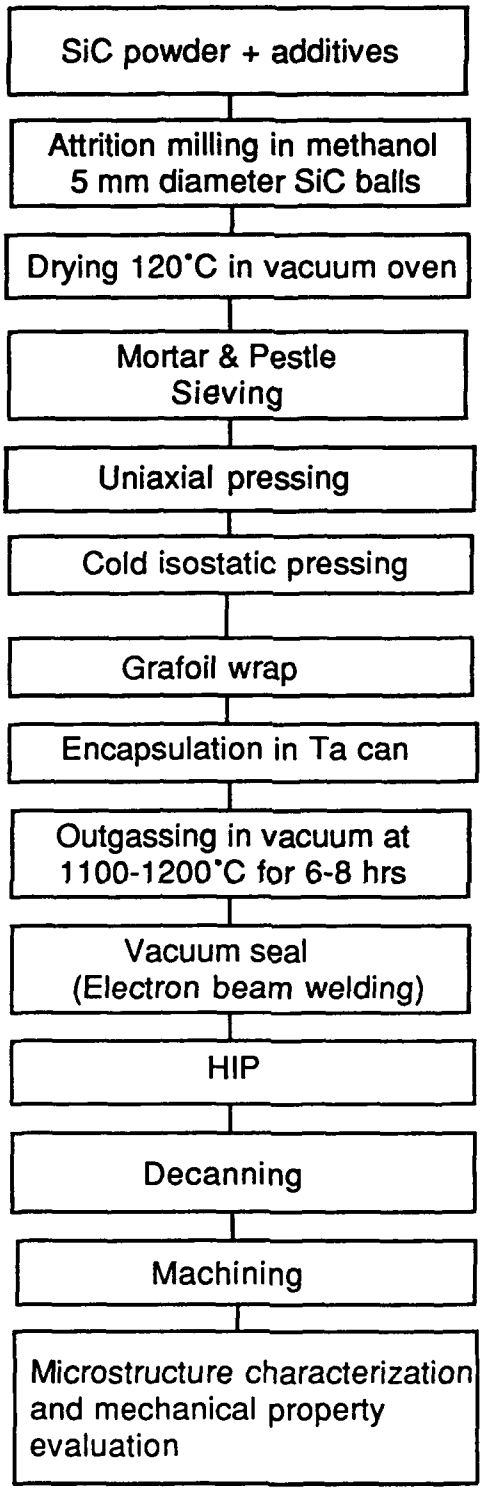

Fig. 1. Hot isostatic pressing process.

isostatic pressing treatment was conducted at 2000°C for 1 h for some hot pressed materials in an effort to increase the density of the composites.

Pressureless sintering of SiC - Dy_2O_3 composites was attempted using pre-pressed pellets of 12.7 mm diameter. A modified vacuum furnace§ with a tungsten heating element and heat shields was used. The furnace could be operated with a partial pressure of argon up to 50.1 KPa (0.5 atmosphere) as well as in high vacuum. Either vacuum or an argon atmosphere at 50.1 KPa (0.5 atmosphere) was used. Heating was conducted in vacuum up to ≈ 900°C and argon gas was introduced at ≈ 900°C. Heating rates ranging from 20°C/min to 100°C/min were employed. Sintering temperatures up to 2050°C were used. Hold times at sintering temperatures ranged from 2 min to 30 min. To prevent volatilization of Dy_2O_3 phase during sintering, some samples were sintered within a closed graphite crucible (threaded graphite cap and body).

(3) Thermal Treatment

Attempts were made to retain the high temperature form of Dy_2O_3 in a SiC matrix by rapid cooling. Because the cooling rates from the hot press or the hot isostatic press was slow (≈ 25°C/min), samples were heated up to 2050°C in a controlled atmosphere furnace which was capable of very rapid heating and cooling. An argon gas pressure of 50.5 KPa (0.5 atmosphere) was used above about 900°C. Samples were heated at 1900°, 1950°, 2000° and 2050°C. After a hold time of 15 min, the power was turned off. A very fast

---

§ Model 300, Richard D. Brew and Co., Inc., Concord, NH

cooling rate could be obtained. In 10 seconds, the temperature dropped by more than 200°C (from 1950°C to 1730°C).

In order to study the effect of long term, high temperature annealing on the phase stability and microstructures of SiC - Dy_2O_3 composites, annealing heat treatments were conducted by heating selected samples up to 1500 °C for 50 h in a programmable furnace[¶] (for static air) or in a programmable tube furnace[§] (for argon gas atmosphere). Both furnaces used molybdenum disilicide heating elements. Annealing temperatures were 1500°, 1250°, 1200°, and 1150 °C. Annealing was conducted in static air and flowing argon gas atmospheres at 1500°C and in static air at other temperatures.

(4) Characterization and Mechanical Property Evaluation

The density of bulk samples was measured by immersion in hexachloro-1,3–butadiene which wets ceramics much better than water, leading to a more accurate volume measurement. Selected specimens were examined in the SEM[§] , TEM[†], where selected area diffraction (SAD) and energy-dispersive x-ray spectrometer (EDS)[#] were applied where

---

¶ Teresco, Champaign, IL

§ Furnace Type 55434, Lindberg Co., Watertown, WI

§ Model S-800, Hitachi, Tokyo, Japan and Model ISI DS-130, International Scientific Instruments, Inc., Santa Clara, CA

† EM 420T (120 kV) and EM 430 (300 kV), Phillips Electronic Instr., Inc., Mount Vernon, NY

EDAX International, Inc., Prairie View, IL

appropriate. X-ray diffractometry[¶] was used to determine the phase composition of the samples.

Elastic modului were determined by the ultrasonic pulse-echo technique[187] with a commercial ultrasonic testing system[‡]. Vickers indentation hardness was determined using a commercial microhardness tester.[§] Samples were polished up to 1μm diamond grit finish. Most hardness values were determined at loads below the threshold for cracking. The fracture strength was measured in four-point flexure on bars ground to a 600 grit finish with bevelled edges. The inner and outer span lengths for the flexure tests were 10.5 mm and 19 mm, respectively. The crosshead speed was 0.5 mm/min. Flexure testing was accomplished using an Instron[§] testing machine. Recommended practices by Baratta,[13]Newnham[14] and the Military Standard[15] were followed. The fracture toughness of selected samples was measured in three-point flexure on notched bars or by the microindentation technique. The notch depth was kept to about 40 % of the bar depth. The samples were notched using a thin (≈ 300μm) diamond wafering blade on a high speed saw. The notch width varied from about 360 μm at the base of the notch to 380 μm at the surface of the sample. The Vickers microindentation method was used to determine the fracture toughness of selected composites with small

---

[¶] Model R400, Rigaku U.S.A., Danvers, MA

[‡] NDT-150, Nortec Corporation, Kennewick, WA

[§] Zwick 3212 microhardness tester, MarkV Laboratory, Inc., East Granby, CT

[§] Model 4502, Instron Corp., Canton, MA

dimensions. Loads ranging from 20 N (2 Kg) to 30 N (3 Kg) were used. An impact rate of ≈ 5 mm/min with a dwell time of 20 s was used for most tests. The equation proposed by Anstis et al.[16] was used to calculate the fracture toughness of the composites. The fracture toughness was given by the following equation:

$$K_{IC} = \S \left(\frac{E}{H}\right)^{1/2} \left(\frac{P}{c^{3/2}}\right)$$

where § is a calibration constant, approximately 0.016, P is the applied load, and 2c is the crack length.

The $\left(\frac{H}{E}\right)$ ratio was obtained by two different techniques. The first technique was the in situ determination of $\left(\frac{H}{E}\right)$ by first indenting with a Knoop pyramid indenter. Knoop indentations were made and the changes in short diagonal to long diagonal ratio due to elastic recovery were measured to calculate the hardness to elastic modulus ratio $\left(\frac{H}{E}\right)$ as proposed by Marshall, et al.[17]

$$\frac{H}{E} = \frac{1}{0.45}\left(\frac{b}{a} - \frac{b'}{a'}\right)$$

where a / b and a'/ b' are the ratios of diagonal dimensions before and after elastic recovery, respectively. Another method for the determination of the H / E was the calculation of the H / E ratio from direct measurements of both the Vickers hardness and the Young's modulus. All indents which

did not produce well-defined radial cracks were rejected. A minimum of 6 indents were used for calculation of the fracture toughness of a material.

III. Results

(1) Density of Composites

Table II shows the densities of the composites after hot pressing. The theoretical density was calculated assuming no chemical reaction between SiC and Dy_2O_3. By hot pressing or hot isostatic pressing, SiC - Dy_2O_3 composites could be densified to high densities. However, SiC with 10% or more Dy_2O_3 additions always showed lower % theoretical density (%TD) than samples without any Dy_2O_3 additions when hot pressed under the same conditions. Specimens densified by hot isostatic pressing using tantalum encapsulation consistently showed higher densities as shown in Table III. Densities above 97 %TD were obtained without sintering additives. A post-densification, hot isostatic pressing treatment of some materials increased the density by ≈ 1 %. Specimens made by pressureless sintering did not sinter to high densities. The highest density (measured by the weight divided by dimensions method) obtained by pressureless sintering in this experiment was ≈ 80 %TD. The green density of specimen 103 was 59.6 %TD. The density increased only by ≈ 5 %. Samples covered with SiC powders within a closed graphite container (sample 103) showed a weight loss of ≈ 5 % after sintering, while samples sintered without a closed crucible showed a weight loss of ≈ 14% after sintering.

(2) Phases Identification

All as-hot pressed or as-hot isostatically pressed SiC - Dy_2O_3 composites always contained cubic (C) Dy_2O_3 in SiC matrices as

Table II. Densities of Hot Pressed SiC Materials

ID No.	Specimen	Densification	Density (g/cm^3)	%TD*
001	ST α-SiC	HP 2050°C/30 min (1% B and 1% C)	3.16	98.6%
012	ST α10D	HP 2050°C/30 min (0.5% C)	3.53	96.2%
012.5	ST α10D	HP followed by HIP 2000°C/1h	3.55	96.7%
013	ST α10D	HP 2050°C/30 min with 1%C	3.52	96.0%
013.5	ST α10D	HP followed by HIP 2000°C/1h	3.56	97.1%
951	ST α10D	HE 2050°C/10 min HF treated SiC powders	3.43	93.6%
952	ST α10D	HE 2050°C/10 min HF treated SiC (1% B and 1% C)	3.58	97.6%
911	ST α15D	HP 2000°C/20 min	3.47	89.1%
912	ST β15D	HP 2000°C/20 min	3.48	89.3%
104	AL β-SiC	HP 2000°C/1h	3.16	98.4%
104.5	AL β-SiC	HP followed by HIP at 2000°C/1h	3.19	99.4%
105	AL β15D	HP 2000°C/1h	3.53	90.4%
105.5	AL β15D	HP followed by HIP at 2000°C	3.57	91.7%
107	AL β-SiC	HP 2000°C/1h, out-gassed at 1000°C	3.05	95.0%
108	AL β15D	HP 2000°C/1h, 1h attrition out-gassed at 1000 °C	3.64	93.3%
109	AL β15D	HP 2000°C/1h, 2h attrition out-gassed at 1000 °C	3.64	93.4%

* % TD = % of the theoretical density

Notations: ST α10D denotes α-SiC Starck powder with 10 vol % Dy_2O_3.
AL β15D denotes β-Alcoa powder with 15 vol % Dy_2O_3.

Table III. Densities of Hot Isostatically Pressed SiC Composites

ID No.	Specimen	Densification	Density (g/cm^3)	%TD
70.1	AL 15D	HIP 2000°C/1h, 1 hr attrition, grafoil	3.82	98.0%
70.2	AL 15D	HIP 2000°C/1h, 1 hr attrition, no grafoil wrap	3.77	96.6%
71	AL 15D	HIP 2000°C/1h, 2 hr attrition, grafoil	3.83	98.1%
921	ST β15D	HIP 2000°C/1h, no grafoil wrap	3.85	98.8%
80	ST α15D	HIP 2000°C/1h, vibratory mixing, grafoil (0.6 % B and 4 % C)	3.81	97.7%
941	ST α30D	HIP 2000°C/80 min (1% C and 1% B)	4.82	>99.9%
942	ST β30D	HIP 2000°C/80 min (1% C and 1% B)	4.36	95.1%

Notation: AL 15D denotes Alcoa SiC powder with 15 vol % Dy_2O_3.
ST α30D denotes Starck α-SiC powder with 30 vol % Dy_2O_3.

determined by X-ray diffraction analysis. After the rapid cooling heat treatment from the monoclinic phase region, it was possible to retain monoclinic Dy_2O_3 in a SiC matrix. Fig. 2 compares X-ray diffraction patterns of the hot pressed AL 15D composite (specimen: 105) before and after the rapid cooling heat treatment. The as-hot pressed composite (bottom curve) contained C-Dy_2O_3 only. After rapid cooling (top curve), B-Dy_2O_3 was identified. As-hot isostatically pressed composites, like as-hot pressed composites, contained C-Dy_2O_3 only. After the rapid cooling heat treatment, both C and B-Dy_2O_3 were present in the hot isostatically pressed composites. The surfaces of the ST α10D composite (specimen 951) was ground with a 220 grit diamond grinding wheel in the as-hot-pressed and rapidly cooled state and the Dy_2O_3 phases were identified by X-ray diffractometry. Fig. 3. shows the diffraction patterns of the composite. The as-hot-pressed composite contained C-Dy_2O_3 and the rapidly cooled specimen contained B-Dy_2O_3. Grinding of the specimen containing C-Dy_2O_3 could not induce a phase transformation of Dy_2O_3 in the matrix. Grinding of the specimen containing B-Dy_2O_3 could not induce a phase transformation, either.

Trace amounts of Dy_2SiO_5 were detected by the X-ray diffraction technique in hot pressed composites densified with as-received ST SiC powders . In SiC - Dy_2O_3 composites densified using SiC powders treated by hydrofluoric acid, no other phases such as dysprosium silicates or carbides were detected. Trace amounts of $DySi_2$ were detected in hot isostatically pressed AL 15D specimens.

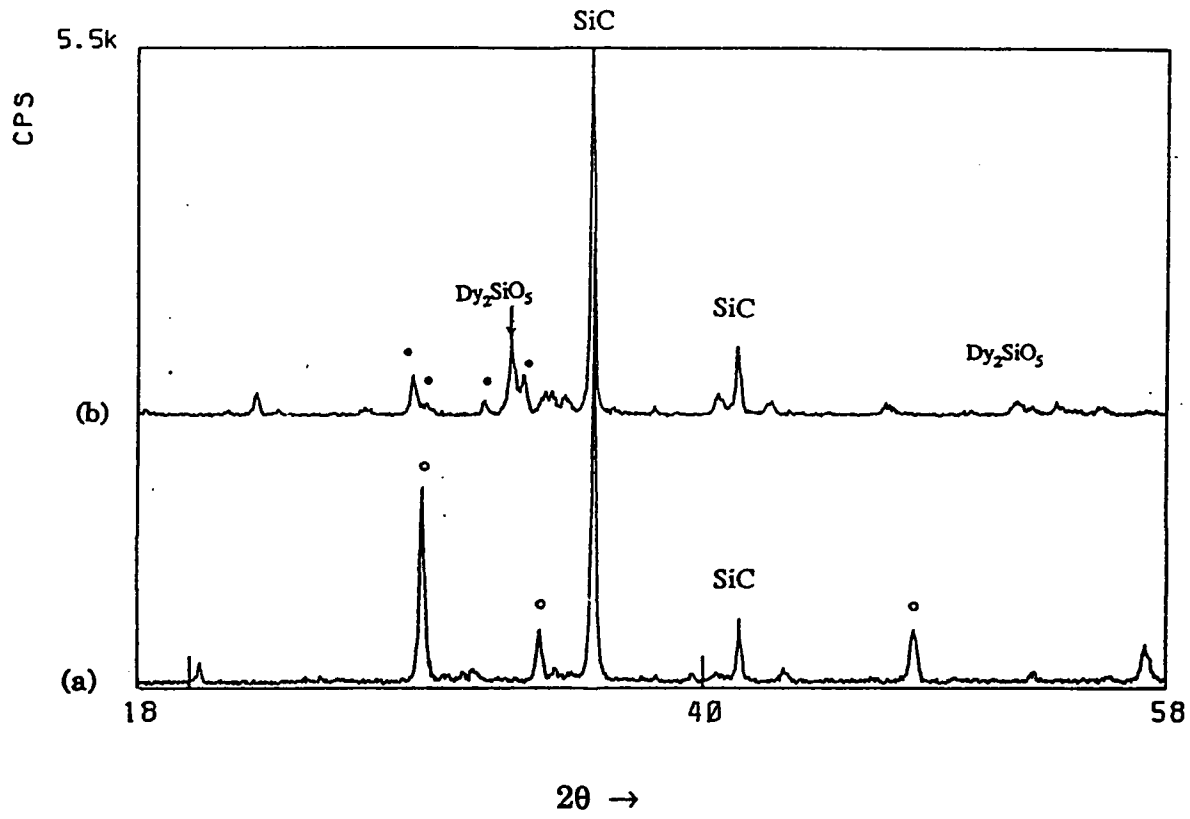

Fig. 2. X-ray diffraction patterns of hot pressed AL 15D composite (specimen 105) (a) before and (b) after the rapid cooling heat treatment. Solid dots (•) represent B-dysprosia and open dots (◦) represent C-dysprosia.

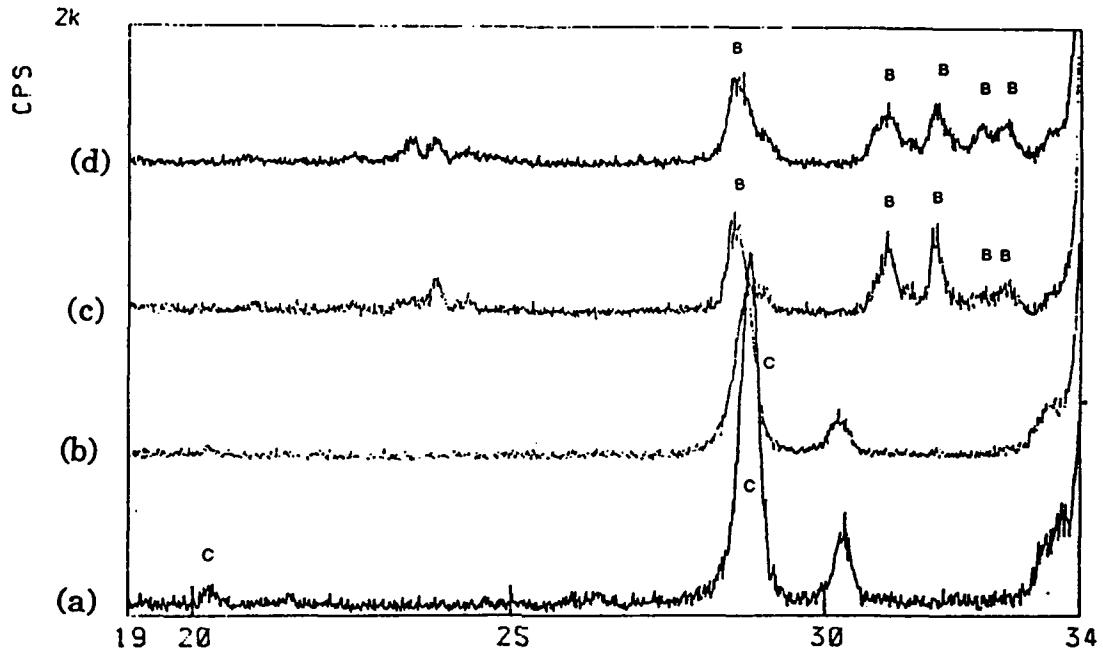

Fig. 3. X-ray diffraction patterns of hot pressed AL 10D composite (specimen 951). From bottom to top, (a) as-hot-pressed; (b) ground surface of as-hot-pressed composite; (c) rapidly cooled from 2050°C; (d) ground surface of rapidly cooled composite. B = B-Dy_2O_3, C = C-Dy_2O_3

(3) Microstructure

Fig. 4 shows the microstructures of hot pressed SiC without Dy_2O_3 additions. Thermal etching revealed the the grain boundaries. SiC grains were equiaxed and the average grain size of ST α-SiC was ≈ 5.7 μm while that of AL SiC was ≈ 2.2 μm. Fig. 5 shows the SEM micrograph of hot pressed AL β15D (specimen 105). Due to atomic number contrast, heavy Dy_2O_3 phases appeared bright and light SiC grains appeared dark. In the TEM micrograph shown in Fig. 6, Dy_2O_3 phases appeared dark , while light SiC grains appeared bright. The morphology of Dy_2O_3 phases suggested that a liquid phase has formed during hot pressing. The dark Dy_2O_3 phase wet SiC grains and often contained small light crystals (Fig. 6 b), suggesting precipitation of some SiC crystallites. TEM EDS spectra of the Dy_2O_3 phase and small crystallites in the Dy_2O_3 phase are shown in Fig. 7. The Dy_2O_3 phase contained some Si in it (Fig. 7 a) and the light crystallite inside the Dy_2O_3 phase showed only Si (Fig. 7 b). Selected area electron diffraction patterns indicated that the Dy_2O_3 phases were crystalline. SiC grains in the composites were equiaxed and had a grain size ≤ 3 μm.

When 30 vol% Dy_2O_3 was added to the SiC, the Dy_2O_3 phases completely surrounded the SiC grains and microcracks were frequently observed as shown in Fig. 8. The microcracks usually occurred in Dy_2O_3 phases. These microcracks were observed only in composites containing large amounts (30 vol%) of Dy_2O_3. It was observed after some months later that both hot isostatically pressed ST α30D (specimen 941) and ST β30D (specimen 942) had completely disintegrated into powders spontaneously.

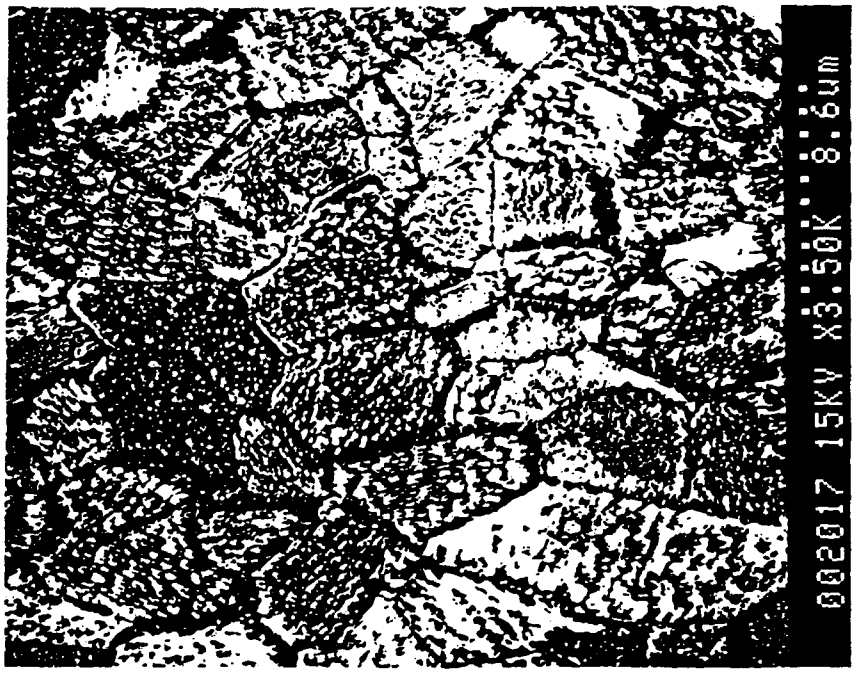

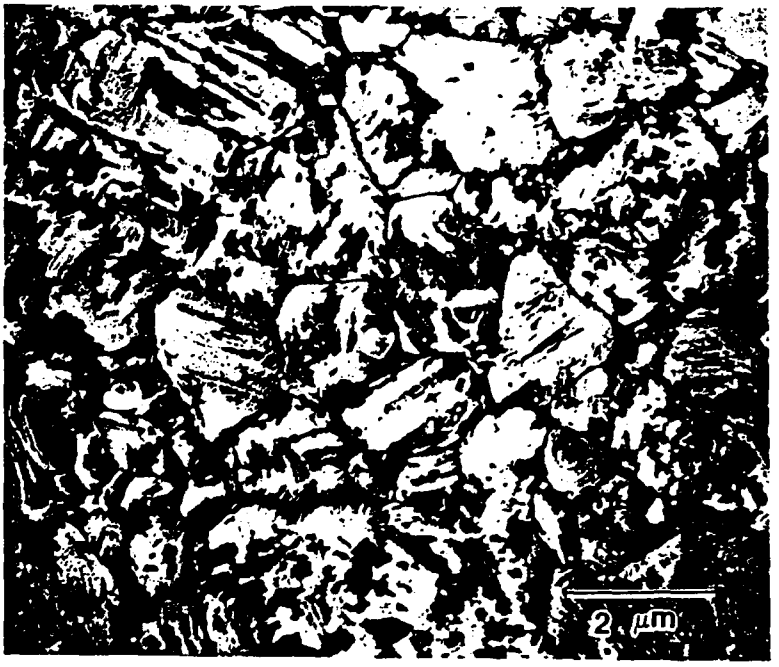

(b)

Fig. 4. SEM micrographs of hot pressed ST SiC (specimen 001). (a) ST α-SiC (specimen 001) (b) AL SiC (specimen 104). Thermally etched, 1500°C/15 min in vacuum.

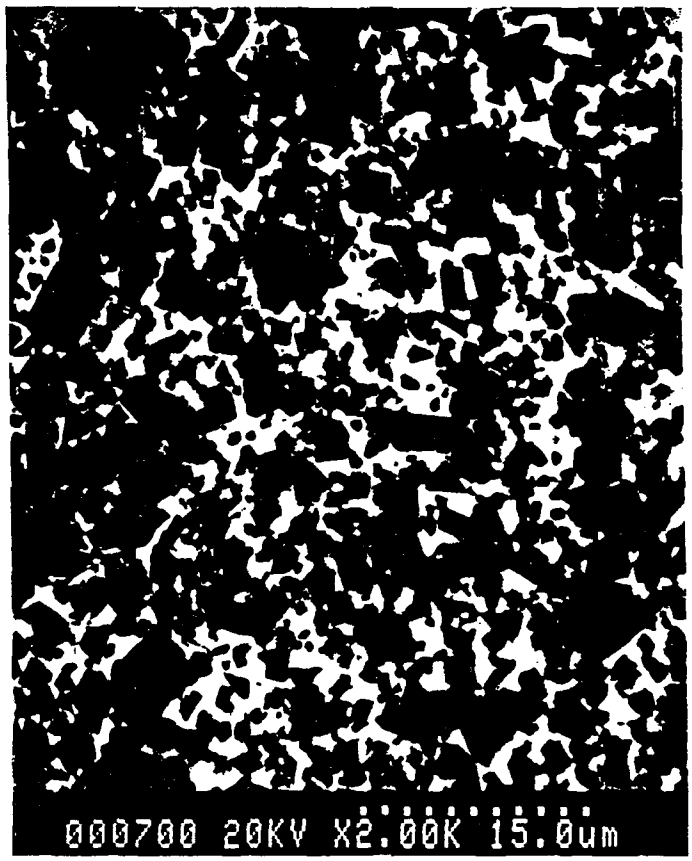

Fig. 5. SEM micrograph of hot pressed AL β15D (specimen 105). Polished and unetched surface.

(a)

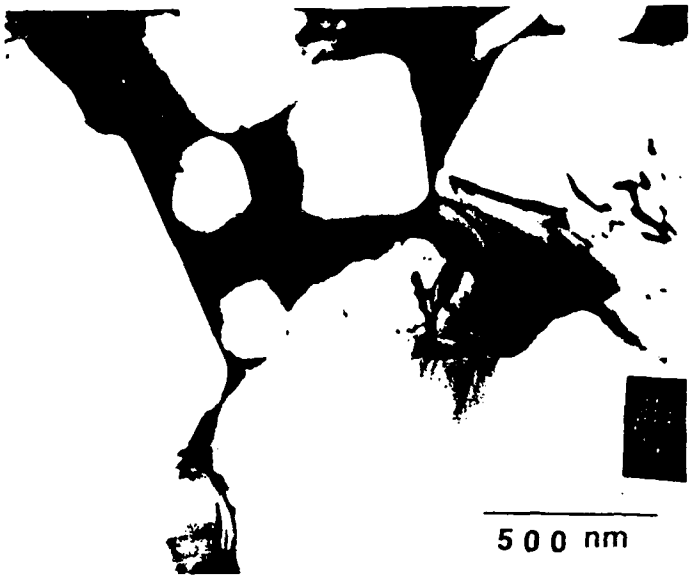

(b)

Fig. 6. Bright field TEM micrographs of hot pressed composites. (a) AL β15D (specimen 105) (b) ST α15D.

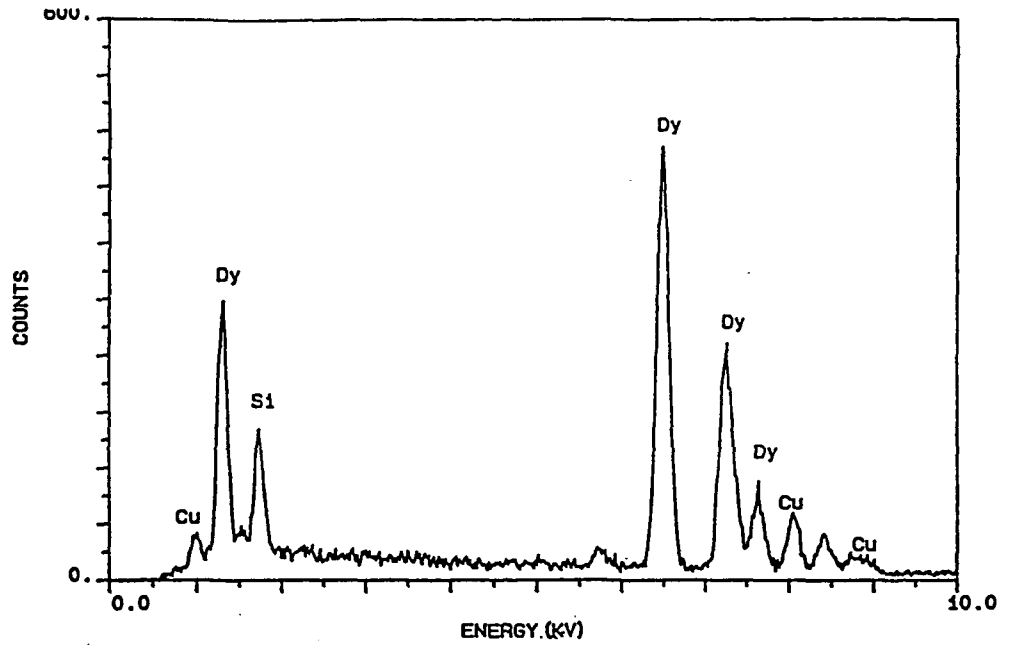

(a)

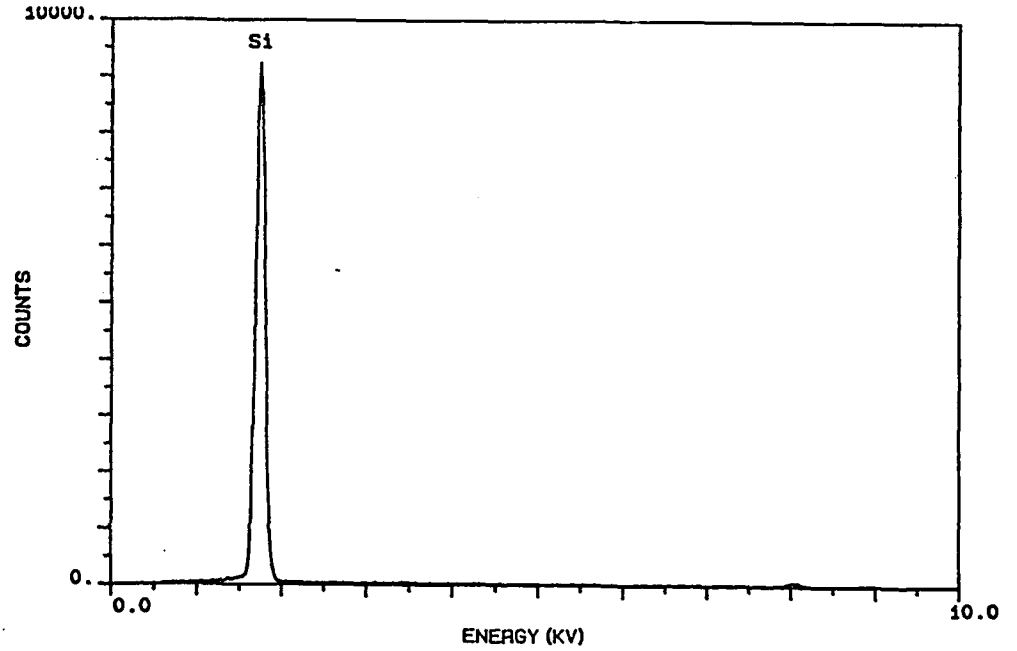

(b)

Fig. 7. TEM EDS spectra of (a) Dy_2O_3 phase and (b) light crystallite inside Dy_2O_3 phase in SiC - Dy_2O_3 composites.

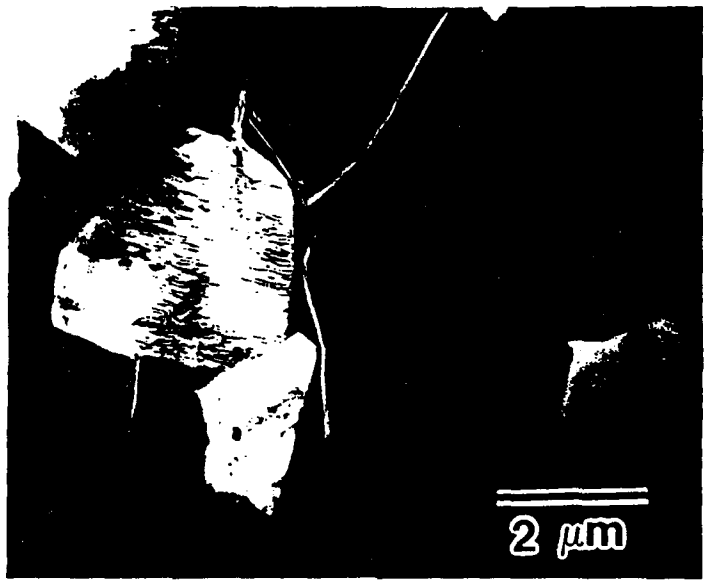

(a)

(b)

Fig. 8. Bright field TEM micrographs of hot isostatically pressed ST α30D (specimen 941). Microcracks were frequently observed.

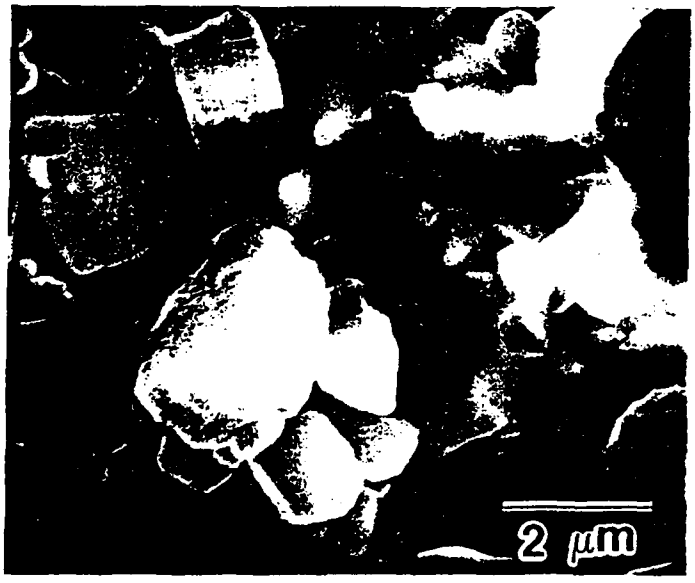

(a)

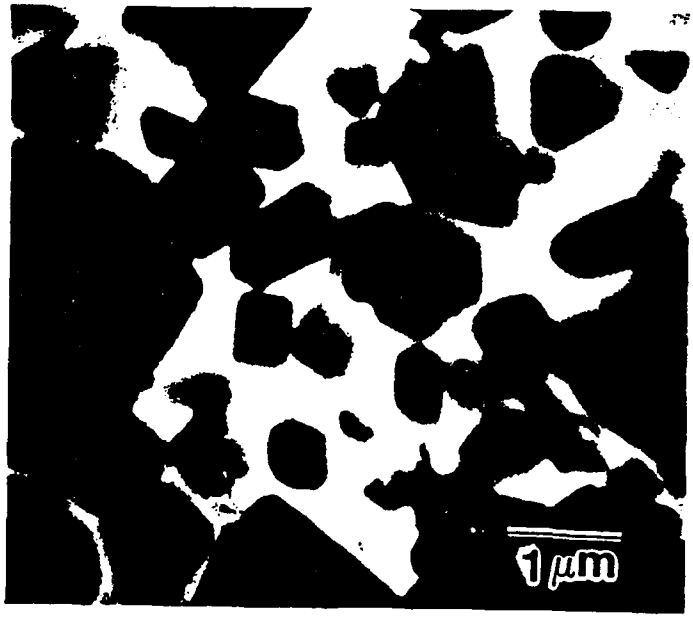

(b)

Fig. 9. SEM micrographs of hipped ST β15D (specimen 921) after annealing in air 1500°C/50h.
(a) as-annealed surface; (b) polished surface (interior region)

Fig. 9 shows the microstructures of hot isostatically pressed ST β15D (specimen 921) after annealing in air at 1500°C for 50h. The grain size remained almost unchanged after annealing at 1500 C for 50 hours. The air annealed surface (Fig. 9 a) shows evidence of evaporation of Dy_2O_3 phase during annealing. TEM/EDS was used in order to determine the Si content in dysprosia grains. Several measurements were made on different dysprosia grains and the average Si content is listed in Table IV. Little difference in Si content was observed after the annealing treatments.

(4) Physical and Mechanical Properties

Table V lists the elastic properties of selected hot pressed materials and they are plotted as a function of Dy_2O_3 content in Fig. 10. The Young's modulus and shear modulus both decreased with increasing Dy_2O_3 content. The post-densification hot isostatic pressing treatment increased the moduli slightly. Table VI shows the Vickers hardness of selected composites. As expected, the hardness of the composite was lower than that of the hot pressed SiC.

The hardness/modulus ratios and fracture toughness values of materials are shown in Table VII. Hot pressed AL β-SiC showed an average K_{IC} value of 2.96 $MPa\sqrt{m}$, while Dy_2O_3 - dispersed SiC composites showed an average K_{IC} value of 4.15 $MPa\sqrt{m}$. An increase of fracture toughness by ≈ 40% was observed when 15 vol % Dy_2O_3 was added to SiC. The rapidly cooled material (monoclinic (B) phase of Dy_2O_3 in SiC matrix) exhibited the same fracture toughness as the as-hot pressed material (cubic phase of Dy_2O_3 in the composite). This suggested that the toughening

ST β30D denotes Starck β-SiC powders with 30 vol % Dy_2O_3.

Table IV. Average Si Content in Dy_2O_3 Grain in Hipped Samples

ID No.	Material	Average Si Content (at%)
921	As-hipped ST β15D	5.1%
921	Air annealed ST β15D 1500°C/50h	6.6%

Table V. Elastic Properties of SiC Materials

ID No.	Specimen	Young's Modulus (GPa)	Shear Modulus (GPa)	Poisson's Ratio
001	ST α-SiC	458	193	0.18
012.5	ST α10D (0.5%C) HIP treated	391	166	0.18
013.5	ST α10D (1% C) HIP treated	411	160	0.29
104	AL β-SiC	414	178	0.17
104.5	AL β-SiC HIP treated	426	180	0.18
105	AL 15D	348	143	0.21
105.5	AL 15D HIP treated	361	153	0.18
109	AL 15D outgassed at 1000 °C	369	156	0.18

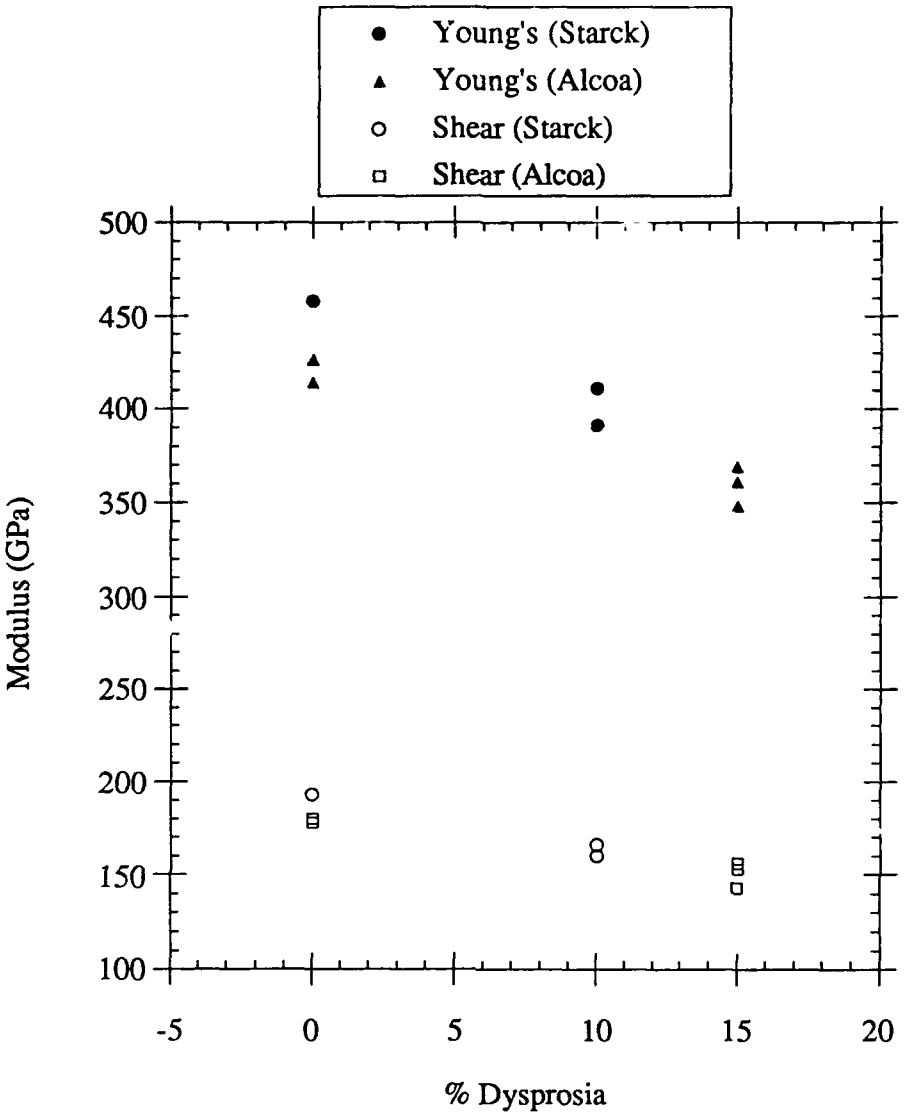

Fig. 10. Elastic properties of SiC composites as a function of Dy_2O_3 content.

Table VI. Vickers Hardness Values of Hot Pressed Materials

ID No.	Specimen	VHN (kgf/mm^2)	GPa	Number of indents
104	AL SiC - HP	2896 ± 51	28.4 ± 0.5	7
105	AL 15D - HP	2299 ± 181	22.6 ± 1.8	7
105.2	AL 15D -HP Rapidly cooled from 1950°C	1709 ± 424	16.8 ± 4.2	6

Table VII. Hardness/Modulus (H/E) Ratios and Indentation Toughness of Hot Pressed SiC Materials

ID No.	Material	H / E Ratio	H / E Method*	Vickers load (N)	K_{IC} ($MPa\sqrt{m}$)
104	AL β-SiC	0.0686	Indep*	20	3.16 ± 0.18
104	AL β-SiC	0.0901 ± 0.0100	Knoop	20	2.76 ± 0.16
105	AL β15D	0.0670	Indep*	20	4.26 ± 0.32
105	AL β15D	0.0699 ± 0.0058	Knoop	20	4.17 ± 0.31
105	AL β15D	0.0670	Indep*	30	4.13 ± 0.22
105	AL β15D	0.0699 ± 0.0058	Knoop	30	4.04 ± 0.22
105.2	AL β15D Rapid cooled from 1950°C	0.083 ± 0.007	Knoop	20	4.08 ± 0.81

* Indep = Calculated from independent measurements of Vickers hardness and Young's modulus

mechanism in this composite was not related to a martensitic phase transformation of the Dy_2O_3 phase in the composite.

The flexural strength (MOR) and notched beam fracture toughness of hot pressed ST SiC composites are shown in Table VIII. As observed by the Vickers microindentation method for AL materials, here the SiC - Dy_2O_3 composite showed a higher fracture toughness than SiC without Dy_2O_3 additions. An increase of ≈ 38% in fracture toughness was observed. The flexural strengths of both materials were almost the same.

(5) Crack Microstructure Interaction

Fig. 11 shows the Vickers microindentation impressions of hot pressed AL SiC (specimen 104) and AL β15D (specimen 105). Well-developed, penny-like radial cracks are clearly seen in this material. The development of well-defined, penny-like cracks from Vickers microindentations on these materials made it possible to employ the Vickers microindentation technique to evaluate the fracture behavior of the composites.

The crack-propagation profiles produced by indentation on AL SiC materials are shown in Fig. 12. The crack path was nearly straight with negligible deflection in hot pressed AL SiC (Fig. 12 a). The crack propagated in a transgranular mode. With the addition of Dy_2O_3, the crack propagation profiles shown in Fig. 12 (b) showed more crack deflection compared to SiC hot pressed without Dy_2O_3 addition. Often the cracks cut through the Dy_2O_3

Table VIII. Flexural Strength and Notched Beam Fracture Toughness of Hot Pressed ST SiC Materials

ID No.	Material	Flexural strength (MPa)	K_{IC} ($MPa\sqrt{m}$)
001	ST α-SiC (98.6% TD)	387 ± 53 (6)*	4.0 ± 0.8 (5)
013.5	ST α10D (HIP treated to 97.1%TD)	379 ± 18 (6)	5.5 ± 0.6 (7)

* The numbers in parentheses represent the number of specimens tested.

Table IX. The Predicted and Experimentally Determined Young's Moduli of SiC Composites

ID number	Material	Paul's upper bound (GPa)	Paul's lower bound (GPa)	Experimentally determined (GPa)
012.5	ST α10D	429	391	391
013.5	ST α10D	429	391	411
105	AL β15D	377	340	348
105.5	AL β15D-Hipped	388	346	361

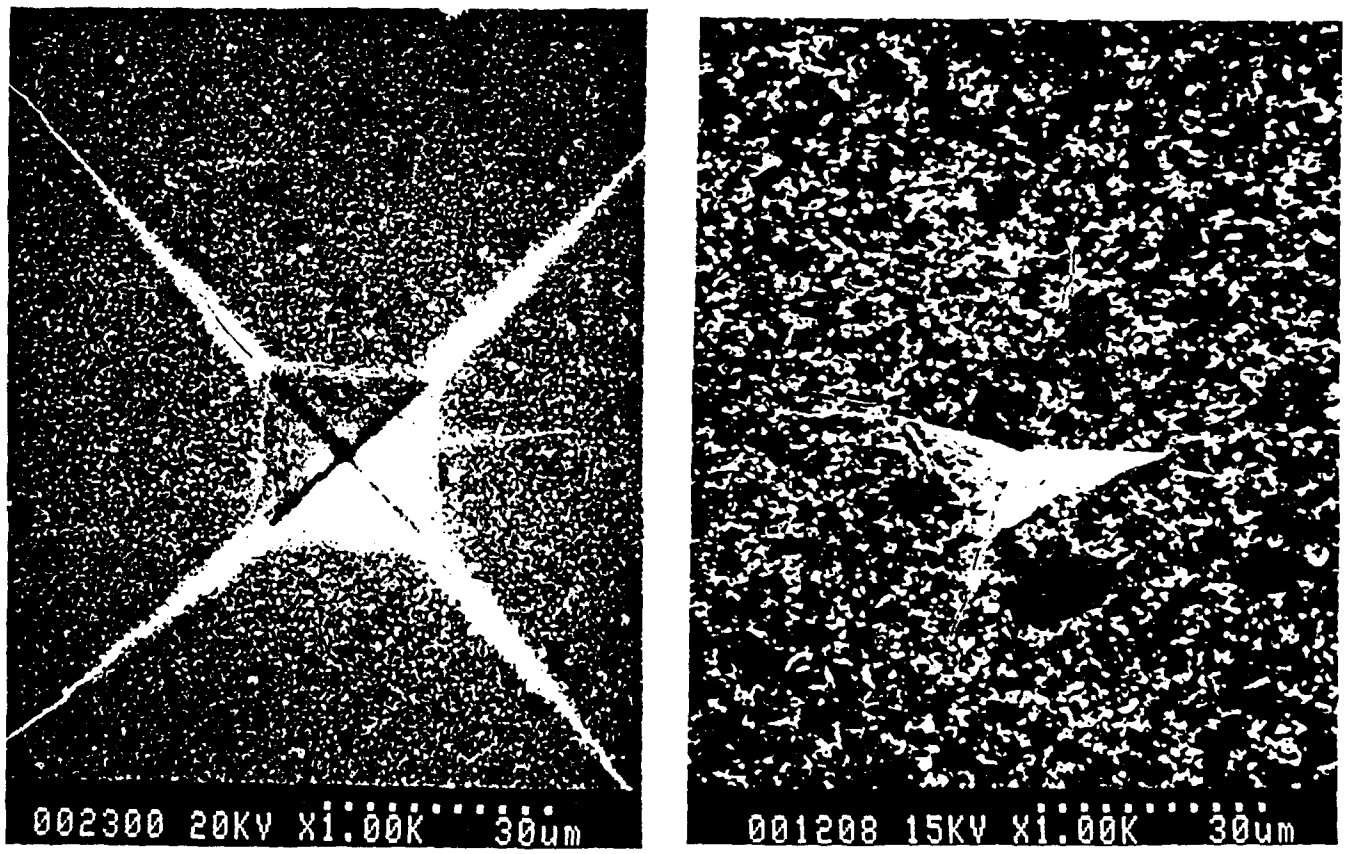

Fig. 11. SEM micrograph of a Vickers impressions.
(a) AL β-SiC at 20 N (2 kg) load (specimen 104)
(b) AL β15D at 20 N (2 kg) load (specimen 105). Indentation was made on thermally etched specimen to reveal grain boundaries.

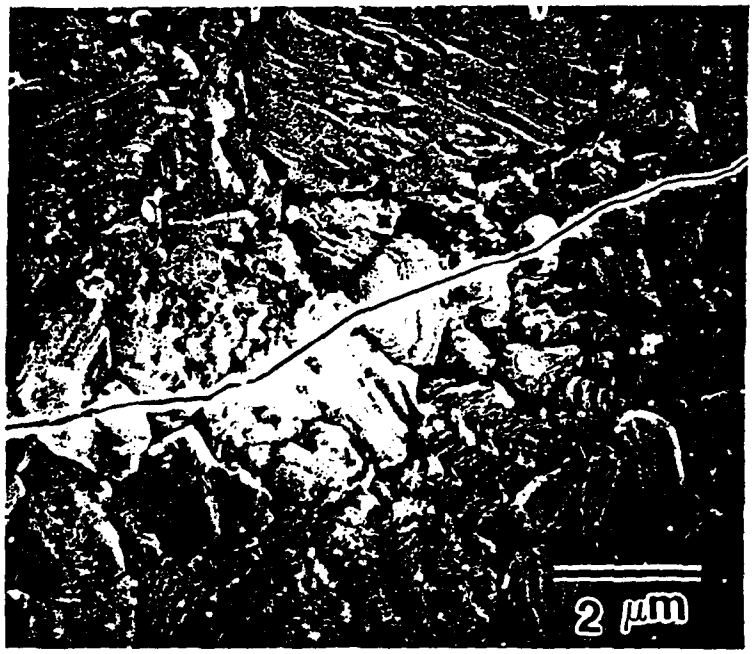

(a)

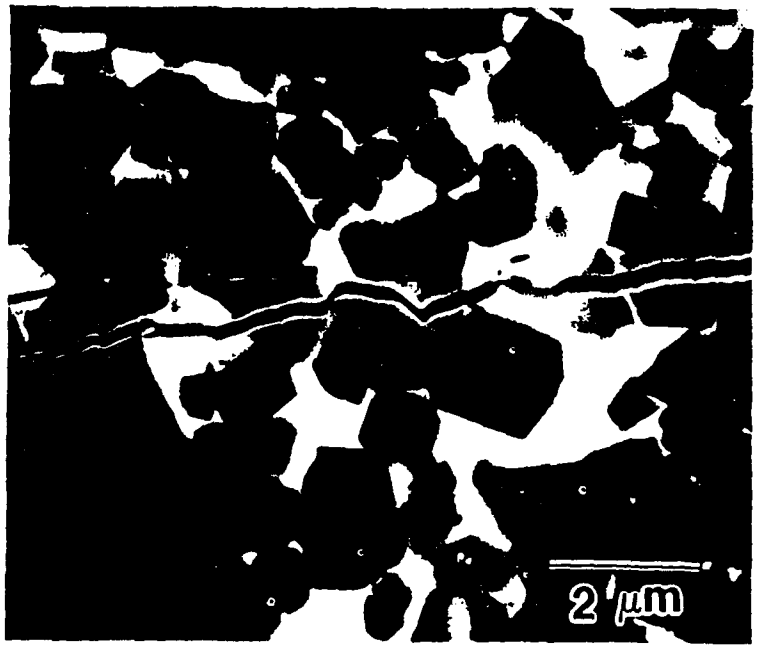

(b)

Fig. 12. Crack propagation of Vickers indentation cracks.
(a) hot pressed AL β-SiC (specimen 104)
(thermally etched 1500°C/15min, average grain size: 2.2 μm)
(b) hot pressed AL β15D (unetched, specimen 105).

particles. The crack-propagation profiles on ST SiC materials are shown in Fig. 13. Hot pressed ST SiC, like hot pressed AL SiC, showed planar crack path with no deflection. With 10 vol% Dy_2O_3 addition, the crack deflection in ST α10D (specimen 013.5) is obvious as shown in Fig. 13 (b). In this composite, cracks propagated mainly by intergranular mode, whereas in AL β15D the cracks propagated predominantly in a transgranular mode.

Fig. 14 (a) shows a grain along the crack path which served as a physical contact restraint to increase the crack resistance of the composite. Fig. 14 (b) shows a possible site for bridges across the crack interface as proposed by Swanson and et al.[18] to be the major mechanism for crack resistance. Fig. 15 shows a bridging grain almost separated from adjacent crack walls.

Fig. 16 shows the fracture surfaces of hot pressed composites. The fracture in hot pressed SiC without Dy_2O_3 additions (specimen 001) was trasgranular whereas the fracture surface in ST α10D (specimen 013.5) showed considerable amount of intergranular fracture. The fracture surface of hot pressed SiC without Dy_2O_3 additions was rather smooth compared with the fracture surface of the hot pressed composite with Dy_2O_3 additions which showed rougher surface with more deflection. Notice also the fine scale of the microstructure of the composite compared with hot pressed SiC without Dy_2O_3 additions. Fine SiC grains were also observed within Dy_2O_3 phases.

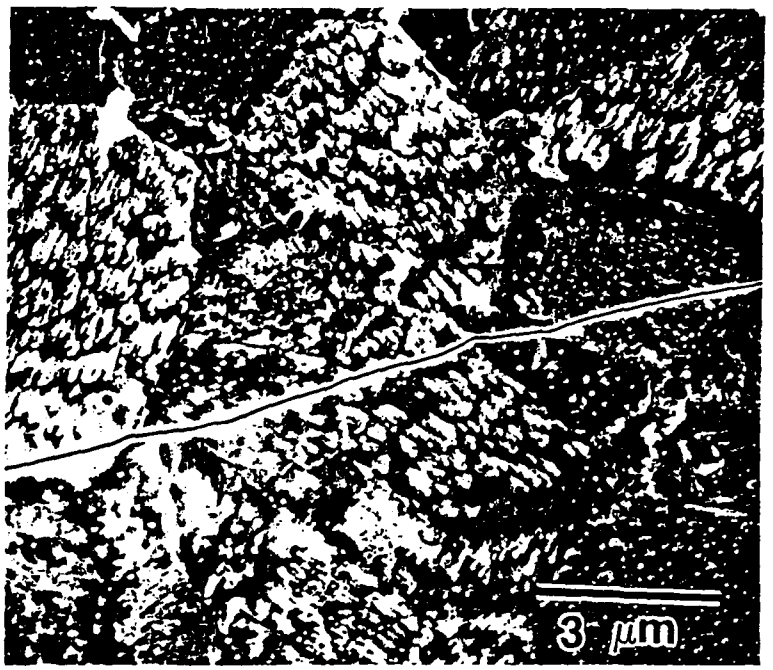

(a)

(b)

Fig. 13. Crack propagation of Vickers indentation cracks.
(a) hot pressed ST α-SiC (specimen 001)
(thermally etched 1500°C/15min, average grain size: 5.7 μm)
(b) hot pressed ST α10D (specimen 013.5).

Fig. 14. Scanning electron micrograph of (a) an indentation crack showing frictional interlocking at a grain bridging site (specimen 105) and (b) a segmented fracture trace at the surface and the possible bridging site behind the tip of an extended radial crack (specimen 105).

Fig. 15. Scanning electron micrograph showing the bridging grain broken away from crack walls (specimen 105).

(a)

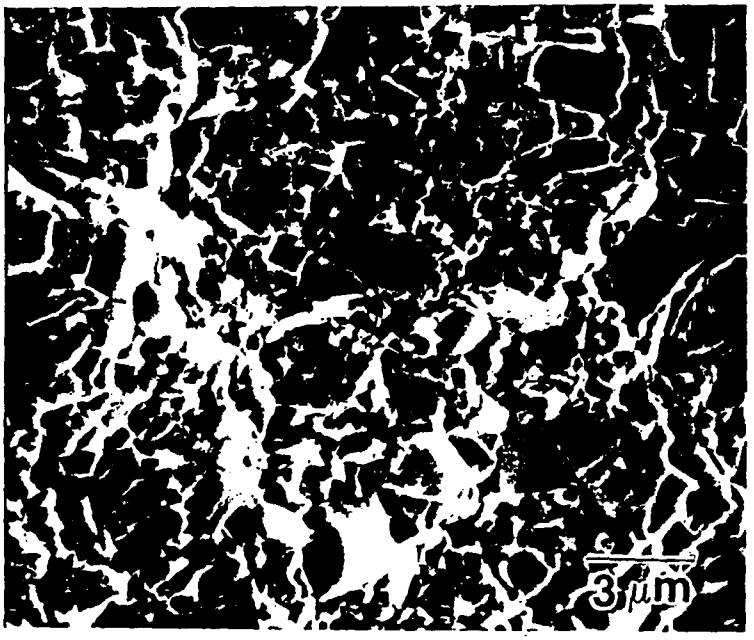

(b)

Fig. 16. Fracture surfaces of hot pressed composites.
(a) hot pressed ST α-SiC (specimen 001)
(b) hot pressed ST α10D (specimen 013.5).

IV. Discussion

(1) Chemical Compatibility of the SiC - Dy_2O_3 System

One of the most important requirements for particulate toughened ceramics is that the dispersed phase should be chemically compatible with the matrix material. It should not chemically react with the matrix material to form a second phase and should remain stable after densification. Preliminary thermodynamic calculations based on the free energy considerations predicted that the criterion of chemical compatibility of lanthanide sesquioxides with SiC could be satisfied.[19] X-ray diffraction analysis revealed no second phase formation except trace amounts of Dy_2SiO_5 in hot pressed composites densified with as-received ST SiC powders or $DySi_2$ in hot isostatically pressed AL 15D specimens. In SiC - Dy_2O_3 composites densified using SiC powders treated with hydrofluoric acid, no other phases were detected. The microstructures (both SEM and TEM) showed no chemical reaction products at grain boundaries between SiC and Dy_2O_3. Furthermore, no decomposition of SiC occurred. It can be concluded, therefore, that Dy_2O_3 is chemically compatible with SiC. This study confirmed Negita's prediction from free energy consideration of reactions, that lanthanide sesquioxides did not decompose SiC in the sintering process.[20]

(2) Densification of the SiC - Dy_2O_3 Composites

It was shown from this study that densification of SiC - Dy_2O_3 composites was difficult without the assistance of an applied pressure. Pressureless sintered specimens showed weight losses from 3 % to 14%. The ST α30D specimen sintered at 1950°C for 30 min (specimen 945) showed a 12% weight loss while the same material sintered at 1850°C for 30 min (specimen 947) showed only a 3% weight loss. The increased evaporation of Dy_2O_3 at higher temperatures accounted for this large weight loss at higher temperatures. The only available literature concerning the vaporization rate of Dy_2O_3[182] reported a vaporization rate of 0.2×10^{-5} at 1600°C and 5×10^{-5} at 2200°C in vacuum. The highest density that could be obtained by pressureless sintering in this study was 80% TD. It appears that a vapor phase transport mechanism dominated the mass transport and therefore no appreciable shrinkage occurred. When sintered at 2050°C for 2 min in a closed graphite container to reduce vaporization (specimen 103), a 5 % weight loss was observed. Further work to minimize the vaporization and to optimize the sintering schedule can improve the densities of the pressureless sintered composites.

By hot pressing or hot isostatic pressing, SiC - Dy_2O_3 composites could be densified to high densities. However, SiC with Dy_2O_3 additions showed lower % theoretical density (%TD) than samples without any Dy_2O_3 additions when hot pressed under the same conditions. This behavior was contrary to the initial expectation that the addition of Dy_2O_3 would promote the densification of the composite through the formation of liquid phase by reaction with silica present as impurities on the surface of SiC powders.

Evaporation of Dy_2O_3 at high hot pressing temperatures, the highly refractory nature of Dy_2O_3 and high liquid formation temperature may account for the reduced sinterability. In Si_3N_4 systems densified with rare earth oxide additives, it has been reported that the sinterability decreased as the melting temperature of the additive became higher.[22]

The beneficial effect of C and B additions on densification was confirmed. Hot pressed ST α10D without C and B additives (specimen 951) had a density of 93.6 % TD, while the addition of 1% C and 1% B (specimen 952) increased the density to 97.6 %TD. The ST 15D composites (specimens 911 and 912) which were hot pressed without C or B additives showed densities of only ≈ 89% TD. AL β-SiC (specimens 104) could be hot pressed to high density without additional C or B additives due to the presence of doped C (0.25 to 0.3 wt %) and B (0.3 to 0.5 wt%) in the plasma synthesized SiC powders.

(3) Microstructure and Phases

One of the characteristic features of all SiC - Dy_2O_3 composites was the morphology of the Dy_2O_3 phases within the SiC matrix. The SiC grains were equiaxed but the Dy_2O_3 grains were not equiaxed and they wetted SiC grains and frequently encompassed individual SiC grains, suggesting that they had been a liquid phase at the densification temperature.

Pure Dy_2O_3 has a melting temperature of ≈ 2310°C and does not melt at hot pressing temperatures of 2000°C. However, when Dy_2O_3 is incorporated into a SiC matrix, a liquid phase can be expected to form because of the presence of SiO_2 on the surface of SiC powders. Industrial

SiC powders are invariably contaminated with oxygen (0.5 to 15 wt %) which is present as oxides (primarily silicon dioxide (SiO_2)) as a result of the production method (carbothermal reduction of SiO_2) or of surface oxidation of the powders during mechanical grinding.

The as-received ST SiC powders contained ≈ 0.88 mole % (0.7 wt%) oxygen. In SiC - 15 vol% Dy_2O_3 (4.6 mole% Dy_2O_3), the mole % of SiO_2 in the system corresponds to 0.84%. When only the Dy_2O_3 - SiO_2 binary system is considered (by excluding SiC), the mole % of Dy_2O_3 in the Dy_2O_3 - SiO_2 binary system is 84.6%, and that of SiO_2 is 15.4%. The binary phase diagram for the Dy_2O_3 - SiO_2 system in Fig. 17 shows that above the eutectic temperature of 1790°C, a liquid phase forms and at the composition of 15.4 mole % SiO_2 at 2000°C (hot pressing temperature), the equilibrium phases are ≈ 68 mole % of liquid phase and ≈ 32 mole % of solid Dy_2O_3. The distribution of equilibrium phases in the SiC - Dy_2O_3 system corresponds to ≈ 94.6 mole % free SiC (solid), ≈ 1.7 mole % free Dy_2O_3 (solid) and ≈ 3.7 mole % liquid phase. The composition of the liquid phase at 2000°C is ≈ 78 mole % Dy_2O_3 and ≈ 22 mole % SiO_2. The liquid phase formed at the densification temperature can account for the the small crystallites (SiC grains) often observed in SiC - Dy_2O_3 composites. They are considered to result from the dissolution of SiC into the liquid phase and then subsequent reprecipitation of the SiC grains. Some SiC grains that protruded into the Dy_2O_3 phase had curved interfaces indicating that they were wetted by the Dy_2O_3 - SiO_2 liquid phase. The binary phase diagram in Fig. 5.1 does not indicate any solid solution between Dy_2O_3 and SiO_2. This study showed, however, that some Si can be dissolved into Dy_2O_3 at the elevated densification temperatures used in this study.

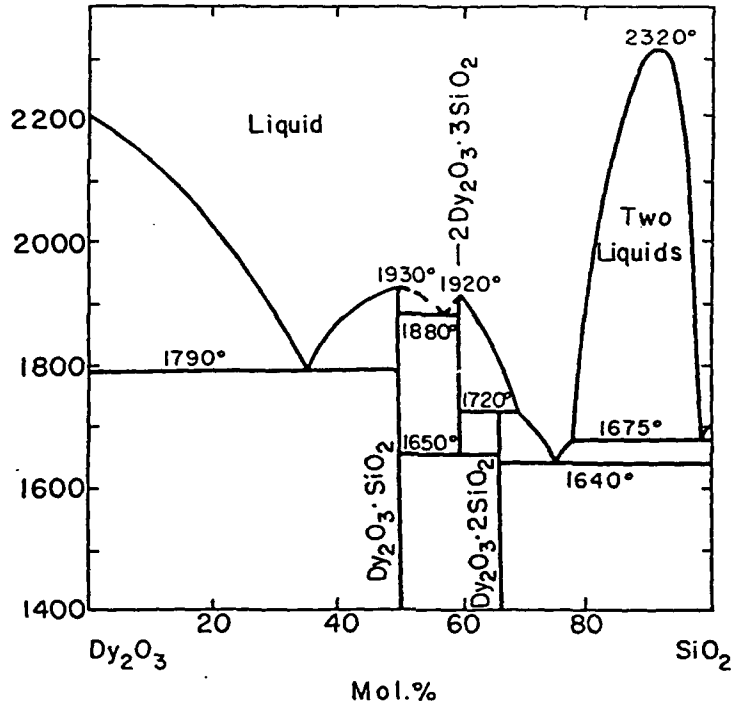

Fig. 17. The Dy_2O_3 - SiO_2 binary phase diagram.[202]

Another characteristic feature of the SiC - Dy_2O_3 composites was the crystalline nature of the Dy_2O_3 phase in the SiC matrix. Although the Dy_2O_3 phase formed a liquid phase at the densification temperatures, it crystallized into crystalline Dy_2O_3 upon cooling to room temperature. The smaller amount of glass-forming SiO_2 in the liquid may account for the absence of glassy phase upon cooling.

In AL SiC, the largest grain size of SiC in the SiC - Dy_2O_3 composites investigated in this work was ≈ 4 μm and the average grain size was ≈ 2 μm. This was similar to the grain size of hot pressed AL β-SiC densified without Dy_2O_3 additions. However, the average grain size of SiC in hot pressed ST SiC without Dy_2O_3 additions was larger (≈ 5.7 μm) and the largest grain size was ≈ 15 μm. The larger particle size of ST powders (≈ 1μm) compared to that of AL powders (≈ 0.5 μm) and the higher hot pressing temperature (2050°C rather than 2000°C) contributed to the larger grain size of SiC in ST SiC compared with AL SiC.

In ST SiC - Dy_2O_3 composites, the addition of Dy_2O_3 inhibited the grain growth of the SiC in the composite. The liquid phase present during hot pressing separated the grains to prevent them from growing during the coalescence stage of densification. Exaggerated grain growth of SiC reported in hot pressed β-SiC even at a lower hot pressing temperature of 1950°C[111] was not observed in any of the hot pressed SiC or SiC - Dy_2O_3 composites.

The discrete Dy_2O_3 phases observed in C and B added composites (specimen 952) compared to wetting grain boundary Dy_2O_3 phases in composites hot pressed without C and B additives (specimen 951) can be

explained by the deoxidative role of the carbon. Carbon removes the silica on the surface of SiC by the reaction:

$$SiO_2 + 3\,C = SiC + 2\,CO\uparrow$$

Dy_2O_3 is much more stable than SiO_2 at high temperatures; for example, the free energy of formation of Dy_2O_3 and SiO_2 at 1700°K are as follows:

$$\Delta G^\circ_f, Dy_2O_3 = -221 \text{ Kcal/mole } O_2,$$
$$\Delta G^\circ_f, SiO_2 = -146 \text{ Kcal/mole } O_2$$

Therefore, carbon attacks SiO_2 preferentially, and Dy_2O_3 remains thermodynamically stable.

In SiC with 30 vol% Dy_2O_3 (specimen 941 and 942), the instant macrocracking was retarded due to the presence of SiC grains. The SiC grains were considered to have constrained the Dy_2O_3 phase from macrocracking. Only microcracking was observed in the Dy_2O_3 phases. However, because the Dy_2O_3 phases were continuous, the high residual stresses that had been developed due to volume change caused the specimen to disintegrate gradually into powders. This microcracking was not observed in any of the SiC - Dy_2O_3 composites containing 10 to 15 vol% Dy_2O_3 where the Dy_2O_3 phases were not continuous.

As reported in the literature concerning the rapid cooling effect on the retention of the monoclinic phase of pure Dy_2O_3 (not in a matrix), this work confirmed the importance of the rapid cooling on the retention of the B - Dy_2O_3 in a matrix. However, the cooling rates employed in this work

were slower than those in the literature, suggesting that the matrix constraint effect by the SiC also operated in the retention of the B - Dy_2O_3.

Mechanical grinding could provide sites of high free energy by producing damaged particles in the form of twins, dislocations, cracks, and sharp edges. These high energy sites could serve as nucleation sites for the phase transformation. Hot pressed composites (specimen 951), either with cubic Dy_2O_3 (as-hot pressed) or with monoclinic Dy_2O_3 (rapidly cooled from 2050°C), did not exhibit any transformation of the Dy_2O_3 phase by mechanical grinding. This behavior was in contrast to the reported B to C transformations by grinding of Dy_2O_3 samples obtained by quenching,[10] or the C to B transformation of monolithic Dy_2O_3 (not in a matrix) by grinding.[9] The failure of the Dy_2O_3 phases in a SiC matrix to exhibit any transformation by mechanical grinding suggested that there was a large nucleation barrier to transformation in the SiC matrix at room temperature.

(4) Mechanical Property Evaluation

The Young's modulus values of hot pressed SiC were in good agreement with the literature values. Ruh et al.[23] reported a zero porosity Young's modulus of 437 GPa by the resonant sphere technique, and Srinivasan et al.[24] reported a zero porosity value of 419 GPa for sintered α-SiC. Coblenz[25] determined the modulus on sintered and hot pressed materials and a zero porosity value of 469 GPa was reported. Schreiber and Soga[26] reported a zero porosity of 458 GPa for a hot pressed SiC. The Young's modulus of AL β-SiC (414 GPa; specimen 104) was in good

agreement with the value (410 GPa) reported by Baumgartner and Rossing[27] who used the same plasma synthesized powders. The slightly increased moduli (≈ 3 to 4%) of post-densification hot isostatic pressed composites were due to the reduced porosity by the hot isostatic pressing treatment.

The dispersion of Dy_2O_3 into a SiC matrix caused the Young's modulus to decrease because of the low modulus of Dy_2O_3. Addition of 10 vol% Dy_2O_3 caused the Young's modulus to decrease by ≈ 10 to 14 % and addition of 15 vol% Dy_2O_3 resulted in ≈ 12 to 15 % decreases in the Young's modulus. Notice, however, that the Dy_2O_3 - dispersed composites contained more porosity than those densified without Dy_2O_3 additions. Therefore, the zero porosity values of the composites could be higher than those reported here.

The Young's moduli of the composites were within the two limits predicted by Paul[28] assuming uniform stress and uniform strain:

$$E_{UB} = E_{SiC} V_{SiC} + E_{Dy_2O_3} V_{Dy_2O_3} \qquad \text{(uniform strain)}$$

$$\frac{1}{E_{LB}} = \frac{V_{SiC}}{E_{SiC}} + \frac{V_{Dy_2O_3}}{E_{Dy_2O_3}} \qquad \text{(uniform stress)}$$

where E_{UB} and E_{LB} are the Paul's upper and lower limits, E is the Young's modulus of pure phase, and V represents the volume fraction of each phase in the composite.

Table 9 lists the predicted and experimentally determined Young's moduli of SiC composites. Fig. 18 shows the experimentally determined Young's moduli values as well as the Paul's upper and lower bounds as a function of Dy_2O_3 volume fraction. All experimentally determined Young's moduli values were within the limits predicted by the theory. There was no dramatic decrease in the moduli values observed in microcracked materials such as Al_2O_3 - ZrO_2 composite,[29] indirectly proving that there was no formation of microcracks in the composites.

The Vickers hardness of hot pressed AL β-SiC (28.4 GPa; specimen 104) was close to the value of 27.4 GPa reported by Baumgartner and Rossing[27] who used the the same plasma synthesized powders. The dispersion of 15 vol% Dy_2O_3 in the same AL SiC matrix (specimen 105) caused the Vickers hardness to decrease by ≈ 20% to 22.6 GPa. Two factors contributed to this reduced hardness of the composite. The lower hardness of the Dy_2O_3 was primarily responsible for the decrease. As in the case of Young's modulus, the higher porosity of the composite also contributed to the lower hardness.

The fracture toughness values of hot pressed AL β-SiC or its composite determined by the Vickers indentation method were lower than those of hot pressed ST α10D determined by the three-point, single edge notched beam (SENB) method. This may be related to the different testing methods rather than to the different material properties. Srinivasan and Seshadri[30] compared the single edge notched beam (SENB) and Vickers indentation techniques to determine the fracture toughness of sintered

Table VIII. Flexural Strength and Notched Beam Fracture Toughness of Hot Pressed ST SiC Materials

ID No.	Material	Flexural strength (MPa)	K_{IC} (MPa$\sqrt{m}$)
001	ST α-SiC (98.6% TD)	387 ± 53 (6)*	4.0 ± 0.8 (5)
013.5	ST α10D (HIP treated to 97.1%TD)	379 ± 18 (6)	5.5 ± 0.6 (7)

* The numbers in parentheses represent the number of specimens tested.

Table IX. The Predicted and Experimentally Determined Young's Moduli of SiC Composites

ID number	Material	Paul's upper bound (GPa)	Paul's lower bound (GPa)	Experimentally determined (GPa)
012.5	ST α10D	429	391	391
013.5	ST α10D	429	391	411
105	AL β15D	377	340	348
105.5	AL β15D-Hipped	388	346	361

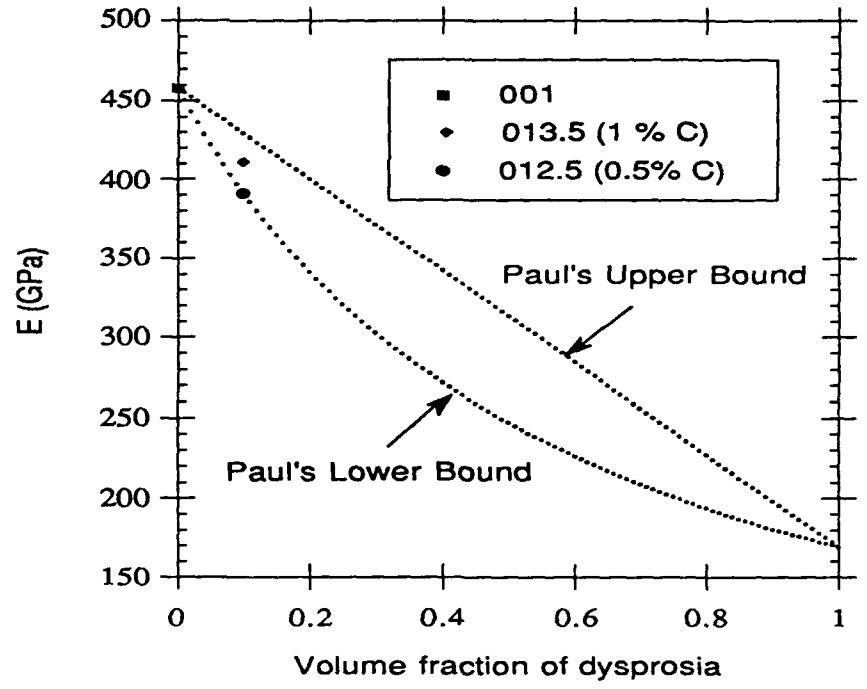

(a)

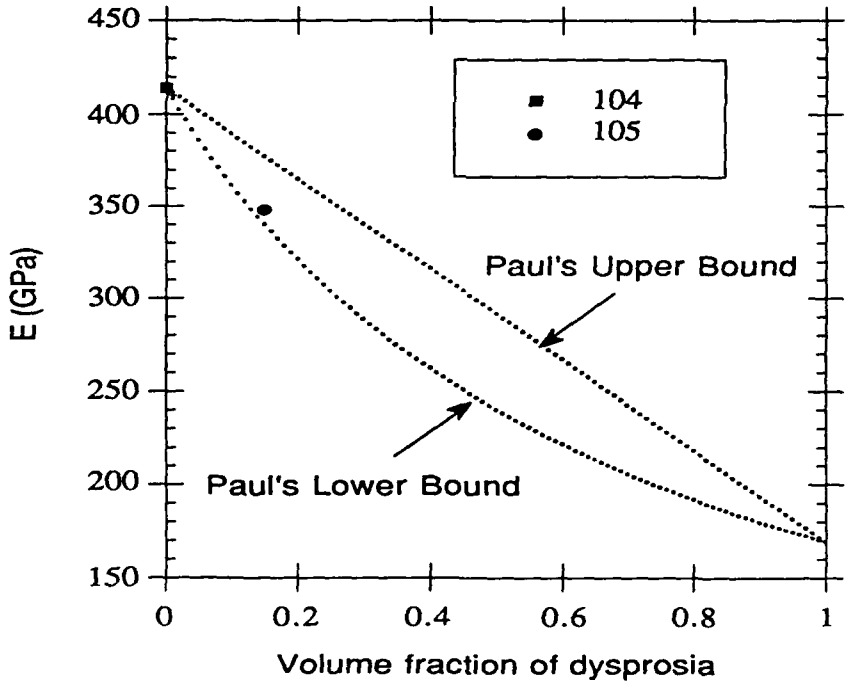

(b)

Fig. 18. Comparison of the predicted and experimentally determined Young's elastic moduli of SiC materials.
(a) ST materials (b) AL materials.

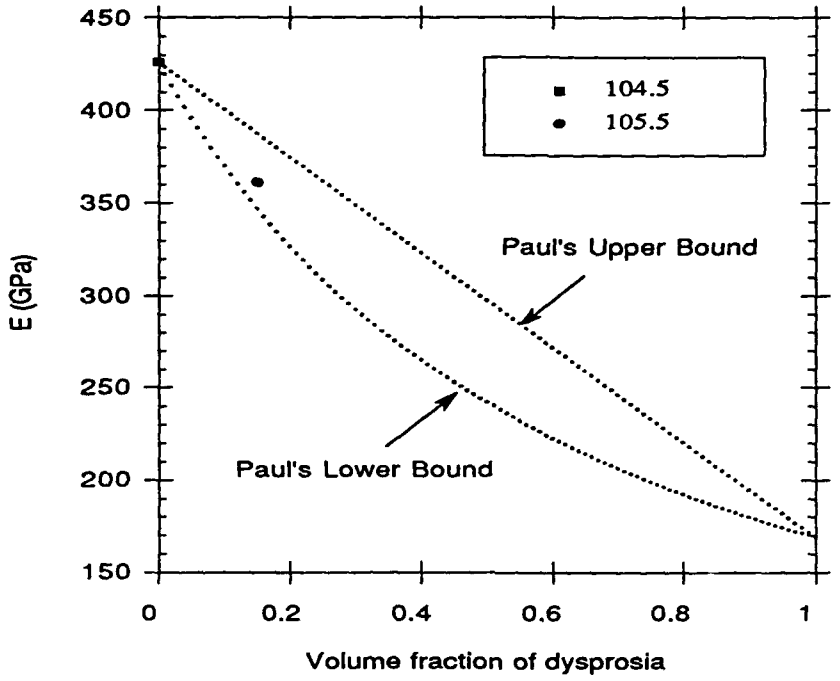

(c)

Fig. 18. (continued) Comparison of the predicted and experimentally determined Young's elastic moduli of SiC materials.

(c) Hip treated AL materials.

α-SiC and found that the toughness values obtained using the Vickers indentation technique were on average 30 % lower than most obtained from SENB. These differences arose from the different analytical solutions used for the computation of K_{IC} as well as the experimental procedures employed. For example, recent interest in the indentation behavior of ceramic materials had produced about 13 equations proposed for calculation of K_{IC} from the Vickers indentation technique.[31]

Moussa et al.[32] have determined the K_{IC} values for SiC using the Vickers indentation technique and five formulas had been used and applied to loads ranging from 0.5 kg to 10 kg. The five relations gave five completely separate sets of values as a function of load. They observed a large difference in K_{IC} values calculated at one load value. The lowest and highest values were in a ratio of 2. This was undoubtedly due to the way in which the various expressions had been calibrated. Moussa et al.[32] suggested that the constants needed to be calibrated over a narrower range of K_{IC} values. The equation used in this work for the determination of the K_{IC} values of SiC - Dy_2O_3 composites by the Vickers indentation method was the one proposed by Anstis et al.[16] The results of Moussa et al.[32] showed that the K_{IC} values obtained using this equation were among the lowest of the values obtained from the five equations. The equation used in this work was chosen primarily because it had been most widely used. The constants in the equation had been calibrated by averaging over a wide range of materials (15 different materials including a commercial SiC, monocrystalline, polycrystalline, and amorphous solids) with K_{IC} values ranging from 0.7 to 12 MPa$\sqrt{m}$. However, as pointed out by Anstis et al.,[16] the Vickers indentation technique for the determination of K_{IC} is ideally

suited to toughness evaluation on a comparative basis. If the constants are calibrated over a narrower range of K_{IC} values for silicon carbides rather than for many different materials and if the K_{ic} values are determined for varying loads, then more reliable K_{IC} data for SiC can be obtained using the Vickers indentation method.

The use of different methods for the determination of the H / E ratio caused relatively small differences in the Vickers indentation toughness values. In AL β15D (specimen 105), the difference in the K_{IC} values was only ≈ 2%. In AL β-SiC (specimen 104), the difference was ≈ 13%. In both materials, use of in-situ Knoop indentation for the determination of the H / E ratio resulted in a lower Vickers indentation toughness values.

The effect of different Vickers loads (20 and 30 N) was examined in hot pressed AL β15D (specimen 105). The slightly lower value of K_{IC} at a Vickers load of 30 N was in contrast to the results of Moussa et al.[32] on aluminum doped, hot pressed SiC where the Vickers indentation K_{IC} values increased with the Vickers loads up to ≈ 40 to 50 N (Fig. 5.2). However, the difference in K_{IC} values (0.13 $MPa\sqrt{m}$) was less than one standard deviation (≈ 0.22 to 0.32), so that the difference could be ignored. The negligible difference in the K_{IC} values at increasing loads suggested that this material might not exhibit a rising R-curve behavior, though obviously more work is required to confirm this.

The improved fracture toughness of Dy_2O_3 - dispersed SiC composites was confirmed in both hot pressed AL and ST composites. An increase in fracture toughness by ≈ 40% was observed in AL β15D composites, and an increase in fracture toughness by ≈ 38% was observed in ST α10D.

The similar flexural strengths of Dy_2O_3 dispersed composite (ST α10D: specimen 013.5) compared with hot pressed SiC without Dy_2O_3 additions (specimen 001) could be due to the finer grain size of SiC in the composite. In spite of the lower strength of Dy_2O_3, the addition of Dy_2O_3 contributed to the finer SiC grain size which could have contributed to the strengthening of the composite. The flexural strengths of hot pressed SiC (≈ 390 MPa) were in the lower range of the literature values which ranged from 300 MPa to 800 MPa.[33] The dry processing method employed in this work rather than the slurry processing could partly be responsible for the lower values.

(5) Crack Microstructure Interaction

The deflection of cracks in Dy_2O_3 - dispersed SiC composites was observed in both AL and ST composites. The deflection of cracks in Dy_2O_3 - dispersed SiC composites compared with the planar fracture path throughout the crack propagation in hot pressed SiC appeared to be partly responsible for the increased fracture toughness of the composite. This deflection was also confirmed in SEM examination of the fracture surface where hot pressed SiC exhibited smooth fracture surface, suggesting little deflection of the crack, while Dy_2O_3 - dispersed SiC composites exhibited rougher fracture surfaces. Similar crack deflection behavior was observed in a ZrO_2 - dispersed Si_3N_4,[34] an Al_2O_3-fluxed hot pressed SiC, and SiC with additions of Y_2O_3 and Al_2O_3.[35]

SEM examination of indentation crack propagation profiles suggested crack bridging as another possible toughening mechanism in the Dy_2O_3 - dispersed SiC composites. Grains along the crack path which could have served as a physical contact restraint to increase the crack resistance were observed. Possible sites for bridges across the crack interface, as proposed by Swanson et al.[18] to be the major mechanism for crack resistance, were also observed (Fig. 4.38). In hot pressed SiC without Dy_2O_3 additions, no such crack - microstructure interactions were observed. If a crack was allowed to propagate (by applying a higher load, for example), then these sites, well behind the advancing crack tip, might act as a source of crack interface bridging, thereby increasing the resistance to crack propagation. Swanson et al. showed through in-situ observations, that as the crack front advanced, the grain bridging sites were left behind and provided a restraining force that must be overcome for failure to occur. The SEM observations in this work were conducted after the cracking. Thus, the crack bridging mechanism in the Dy_2O_3 - dispersed SiC composites could not be directly observed. Crack bridging, as one of the wake toughening mechanisms, could show a rising R-curve behavior. R-curve measurements, therefore, would be appropriate in order to properly evaluate the fracture toughness of the composites.

The microcrack toughening might not have contributed to the toughening in the composites. The presence of the microcrack induces a nonlinear material response, by virtue of the effect of the microcracks on the elastic modulus.[36] The stress - strain curve that occurs in a material subject to microcracking shows a decreased modulus above the critical stress for microcracking. The stress - strain curve of the composites (as

well as SiC without Dy_2O_3 additions) showed linear elastic behavior up to fracture, suggesting no formation of stress induce microcracks.

V. Conclusions

Composites of SiC with 10 to 15 vol% dispersed Dy_2O_3 were fabricated by hot pressing and encapsulated hot isostatic pressing techniques. High vaporization rates of Dy_2O_3 in the SiC - Dy_2O_3 system prohibited normal pressureless sintering. The phase analysis and microstructures (both SEM and TEM) showed that Dy_2O_3 was chemically compatible with SiC matrix. The SiC grains in the SiC - Dy_2O_3 composites were equiaxed and had a relatively small grain size. The average grain size of SiC in the composite was ≈ 2 μm. Hot pressed AL β-SiC without Dy_2O_3 additions exhibited a similar average SiC grain size (≈ 2.2 μm). Hot pressed ST α-SiC without Dy_2O_3 additions, however, exhibited a larger average SiC grain size (≈ 5.7 μm). The Dy_2O_3 grains were not equiaxed and they wetted SiC grains and frequently encompassed individual SiC grains, suggesting that a liquid phase formed at the densification temperature.

As-hot-pressed or as-hipped composites always contained cubic Dy_2O_3 in a SiC matrix. Rapid cooling from the monoclinic region was necessary to retain the monoclinic Dy_2O_3 phase. The failure of the Dy_2O_3 phases in a SiC matrix to exhibit any transformation by mechanical grinding suggested that there was a large nucleation barrier to transformation in the SiC matrix at room temperature.

With the addition of 10% to 15 vol% Dy_2O_3, the hardness and Young's modulus of the composites decreased. The Young's modulus values of the composites were within the limits predicted by the theory and supported the absence of microcracks in the composites which were confirmed by TEM.

The fracture toughness of Dy_2O_3 - dispersed SiC composites increased by ≈ 40% and the flexural strength was comparable to that of unreinforced SiC. This increase in fracture toughness was not related to a phase transformation of Dy_2O_3 in the matrix.

Hot pressed SiC without Dy_2O_3 additions showed typical brittle crack propagation behavior with a planar crack path throughout propagation. It appeared from examination of crack propagation behavior and fracture surfaces that the possible toughening mechanisms in the Dy_2O_3 - dispersed SiC composites could be crack deflection in conjunction with crack-interface grain bridging.

References

1 C. H. McMurtry, W. D. G. Boecker, S. G. Seshadri, J. S. Zanghi, and J. Garnier, "Microstructure and Material Properties of SiC-TiB_2 Particulate Composites," *Am. Ceram. Soc. Bull.*, **66**, [2] 325-29 (1987).

2 H. Cai, W.-H. Gu, and K. T. Faber, "Microcrack Toughening in a SiC-TiB_2 Composite," Proceedings of the American Society for Composites: Fifth Technical Conference on Composite Materials, 892-901, (1990).

3 A. G. Evans, "Perspective on the Development of High-Toughness Ceramics," *J. Am. Ceram. Soc.*, **73**, [2] 187-206 (1990).

4 G. C. Wei and P. E. Becher, "Improvements in Mechanical Properties in SiC by the Addition of TiC Particles," *J. Am. Ceram. Soc.*, **67**, [8] 571-574 (1984).

5 L. Eyring, "The Binary Rare Earth Oxides"; pp. 337-399 in Non-Metallic Compounds, Handbook on the Physics and Chemistry of Rare Earths, Vol. 3. Edited by K. A. Gschneidner Jr. and L. Eyring. North-Holland Publishing Company, Amsterdam, 1979.

6 W. M. Kriven, "Possible Alternative Transformation Tougheners to Zirconia: Crystallographic Aspects," *J. Am. Ceram. Soc.*, **71**, [12] 1021-1030 (1988).

7 W. M. Kriven, "Martensitic Toughening of Ceramics," *J. Mater. Sci. & Eng. A*, **A 127**, [2] 249-255 (1990).

8 O. Sudre, "Investigation of the Monoclinic (B) to Cubic (C) Transformation of Dysprosium Sesquioxide (Dy_2O_3)"; M.S. Thesis. University of Illinois, Urbana, IL, 1988.

9 P. Jero, "Investigation of the lanthanide Sesquioxides as High Temperature Transformation Toughening Agents"; Ph. D. Thesis. University of Illinois, Urbana, IL, 1988.

10 L. M. Lopato, B. S. Nigmanov, Z. A. Zaitseva, and A. Shevchenko, "Influence of Cooling Rate on the Phase Ratios in Lanthanaid Oxide - Yttrium Oxide System," *Applied Solar Energy*, **21**, [2] 58-61 (1985).

11 R. McPherson, "Formation of Metastable Monoclinic Rare Earth Sesquioxides from the Melt," *J. Mater. Sci.*, **18**, 1341-1345 (1983).

12 J. P. Coutures, J. Coutures, R. Renard, and G. Benezech, "Vaporization en atmosphere controlee des oxydes de lanthanides liquides. Etude des phases obtenues par trempe des vapeurs," *Comptus. Rendus Acad. Sc. Paris*, **275C**, 1203-1206 (1972).

13 F. I. Baratta, "Requirements for Flexure Testing of Brittle Materials"; pp. 194-222 in Methods for Assessing the Structural Reliability of Brittle Materials, ASTM STP 844, Edited by S. W. Freiman and C. M. Hudson. Am. Soc. Testing and Materials, Philadelphia, PA, 1984.

14 R. C. Newnham, "Strength Tests for Brittle Materials," *Proc. Brit. Ceram. Soc.*, **25**, 281-293 (1975).

15 "MIL-STD-1942 (MR): Flexural Strength of High Performance Ceramics at Ambient Temperature", Department of the Army, Washington, DC, 1983.

16 G. R. Anstis, P. Chantikul, B. R. Lawn, and D. B. Marshall, "A Critical Evaluation of Indentation Techniques for Measuring Fracture Toughness: I, Direct Crack Measurements," *J. Am. Ceram. Soc.*, **64**, [9] 533-38 (1981).

17 D. B. Marshall, T. Noma, and A. G. Evans, "A Simple Method for Determining Elastic-Modulus- to-Hardness Ratios using Knoop Indentation Measurements," *J. Am. Ceram. Soc*, **65**, [10] c-175-c-176 (1982).

18 P. L. Swanson, C. J. Fairbanks, B. R. Lawn, and Y.-W. Mai, "Crack-Interface Grain bridging as a Fracture Resistance Mechanism in Ceramics: I, Experimental Study on Alumina," *J. Am. Ceram. Soc.*, **70**, [4] 279-89 (1987).

19 W. M. Kriven, "High Temperature Toughening and Creep Studies in Composite Ceramics", Annual Report to AFOSR University of Illinois at Urbana-Champaign (July1st 1985 through June 30th 1986)

20 K. Negita, "Effective Sintering Aids for Silicon Carbide Ceramics: Reactivities of Silicon Carbide with Various Additives," *J. Am. Ceram. Soc.*, **69**, [12] C-308-C-310 (1986).

21 V. L. Balkevich, Y. M. Mosin, and I. A. Kuznetsova, "Certain Properties of Ceramic Obtained from Dy and Yb Oxides," *Inorg. Mater.*, **12**, [1] 122 (1976).

22 N. Hirosaki, A. Okada, and K. Matoba, "Sintering of Si_3N_4 with the Addition of Rare-Earth Oxides," *J. Am. Ceram. Soc.*, **71**, [3] C-144-C-147 (1988).

23 R. Ruh, A. Zangvil, and J. Barlowe, "Elastic Properties of SiC, AIN, and Their Solid Solutions and Particulate Composites," *Am. Ceram. Soc. Bull.*, **64**, [10] 1368-73 (1985).

24 M. Srinivasan, S. G. Seshadri, and G. W. Weber, "Microstructural Effects on the Mechanical Properties of Sintered Alpha Silicon Carbide," *Am. Ceram. Soc. Bull.*, **59**, [3] 364 (1980).

25 W. S. Coblenz, "Elastic Moduli of Boron-Doped Silicon Carbide," *J. Am. Ceram. Soc.*, **58**, [11-12] 530-531 (1975).

26 E. Schreiber and N. Soga, "Elastic Constants of Silicon Carbide," *J. Am. Ceram. Soc.*, **49**, [6] 342 (1966).

27 H. R. Baumgartner and B. R. Rossing, "Pressureless Sintering and Properties of Plasma Synthesized SiC Powder"; pp. 3-16 in Silicon Carbide '87, Ceram. Trans., Vol. 2. Edited by J. Cawley and C. Semler. The Am. Ceram. Soc., Westerville, OH, 1989.

28 B. Paul, "Prediction of Elastic Constants of Multiphase Materials," *Trans. AIME*, **218**, 36-41 (1960).

29 D. J. Green, "Critical Microstructures for Microcracking in Al_2O_3 - ZrO_2 Composite," *J. Am. Ceram. Soc.*, **65**, [12] 610-614 (1982).

30 M. Srinivasan and S. G. Seshadri, "Application of Single Edge Notched Beam and Indentation Techniques to Determine Fracture Toughness of Alpha Silicon Carbide"; pp. 46-68 in Fracture Mechanics Methods for Ceramics, Rocks, and Concrete, ASTM STP, Vol. 745. Edited by S. W. Freiman and E. R. Fuller. Am. Soc. for Testing and Materials, Philadelphia, PA, 1981.

31 I. J. McColm, Ceramic Hardness, Plenum Press, New York, 1990.

32 R. Moussa, I. Coppolani, and F. Osterstock, "Indentation Techniques Applied to Silicon Carbides," *Proc. Br. Ceram. Soc.*, **32**, 237-247 (1982).

33 N. Hecht and D. McCullum, "Investigation of Selected Silicon Nitride and Silicon Carbide Ceramics," *Ceram. Eng. Sci. Proc.*, **9**, [9-10] 1313-1332 (1988).

34 K. Terao, Y. Miyamito, and M. Koizumi, "Characteristics of ZrO_2 - dispersed Si_3N_4 without Additives Fabricated by Hot Isostatic Pressing," *J. Am. Ceram. Soc.*, **71**, [3] C-167-C-169 (1988).

35 D. H. Kim and C. H. Kim, "Toughening Behavior of Silicon Carbide with Additions of Yttria and Alumina," *J. Am. Ceram. Soc.*, **73**, [5] 1431-1434 (1990).

36 B. Budianski and R. J. O'Connell, "Elastic Moduli of a Cracked Solid," *Int. J. Solids Struct.*, **12**, 81-97 (1976).

The Monoclinic (B) to Cubic (C) Phase Transformation of Dysprosia (Dy_2O_3)

Part I: Experimental studies

by

O. Sudre*, K.R. Venkatachari†, W.M. Kriven.
Department of Ceramic Engineering
University of Illinois at Urbana-Champaign
Urbana, Il 61801.

First Draft

*Present adress: Materilas Department, Engineering III,
University of California, Santa Barbara, CA 93106.

†Present adress: Institute Materilas Processing,
Michigan Tech. University, Houghton, MI 49931

ABSTRACT

The monoclinic (B) to cubic (C) phase transformation of Dy_2O_3 exhibits a positive volume change (~+5%) on cooling at ~1950°C (~+8.9% when extrapolated at room temperature). By analogy ~~to~~ with zirconia, dysprosia is considered ~~as~~ to be a potential transformation toughener. However, the monoclinic high-temperature (B) phase is difficult to retain at room temperature and its transformation to the cubic (C) phase is poorly understood. The first part of this series of two papers presents experimental studies on this compound. A laser-melting/roller-quenching technique was used to stabilize the high-temperature monoclinic phase down to room temperature. The flakes resulting from this processing route had a monoclinic crystal structure. The thermodynamics and kinetics of the transformation to the cubic stable phase were subsequently studied by D.T.A., T.G.A. and X-ray diffraction. Results suggested that the transformation is thermally controlled at low temperatures (<600°C) but appears displacive at higher temperatures. In the companion paper (Part II), the crystallography of the two phases is detailed and a mechanism for the transformation is proposed.

INTRODUCTION

The first examples of high-toughness ceramics relied upon the monoclinic (m) to tetragonal (t) phase transformation occurring in ZrO_2. The increase in fracture resistance was correlated to the crystal volume expansion and shear deformation taking place in the wake of a crack tip. The transformation characteristics of zirconia are now well understood. Kriven[Kriven ~~1987~~ 1988] reviewed in detail the crystallographic aspects of other potential transformation toughener materials. That study included dicalcium silicate as well as some of the ~~rare-earth-oxides~~ lanthanide sesquioxides (rare earth oxides). The transformation of the former is now relatively well understood. ~~documented and has shown promising characteristics as transformation toughener.~~ The rare-earth oxides alternative system on the other hand, need to be further investigated.

The monoclinic (B) to cubic (C) phase transformation of the rare-earth oxides exhibits characteristics similar to that of zirconia. Of particular interest, the transformation of dysprosia has been reported to occur at around 1950°C with a positive volume expansion which led to the shattering on cooling of ceramic pieces. Most of the literature dealing with the rare-earth oxides dates from the 1960's. The rare-earth sesquioxides exhibit five different polymorphs depending on temperature and cation radius. Figure 1 shows the temperature phase stability temperature range for each element of the series as determined by Foex and Traverse. These five polymorphs can be divided in two groups: the B, A, H and X phases which exhibit a characteristic layer structure and the cubic (C) phase which is best described as a fluorite structure with one quarter of the anion sites left vacant. The crystallography of these phases is well known and has already been reviewed [Kriven 1987, Kriven, Kim, Fleming 199?]. The companion paper will describe more thoroughly the

crystallography of the monoclinic (B) and the cubic (C) phases with an emphasis on the phase transformation.

The work on the B-C phase transformation of the rare-earth sesquioxides has been extensive but results were often inconsistent and led to many interpretations. The main factors affecting the stability of the high temperature monoclinic (B) phase as well as the phase transformation to the room temperature cubic (C) phase are the temperature, the pressure, some chemical additions, the environment, the cooling rate and possibly the anisotropic surface energy.

The temperatures of the polymorphic transformations of dysprosia are estimated as follows:

$$\text{Melt} \xrightarrow{2360^\circ C} \text{H} \xrightarrow{2175^\circ C} \text{B} \underset{1950^\circ C}{\overset{1860^\circ C}{\rightleftharpoons}} \text{C}$$

The B-C transformation temperature showed some discrepancies in the literature[Brauer, 1968]. The conditions of the experiments were often different and the preparation of the specimen or the atmospheric conditions seemed to affect the transformation temperature [Brauer1968, Boulesteix 1982]. An hysteresis phenomenon with a temperature range of 200°C was reported by two groups [Foex and traverse 1966, Rudenko and Boganov 1970]. Because of the very high temperatures involved, these transformation temperatures are not well established.

Pressure is known to induce polymorphic transformations. Applying pressure to the room temperature cubic phase was able to stabilize the high temperature monoclinic phase or to lower its transformation temperature[](37)to(39)]. For instance, the transformation temperature of Dy_2O_3 was lowered to 1020°C at 30 kbar. The stabilizing effect of the pressure

is thought to originate from the large volume contraction of the (C) to (B) transformation. In the same register, grinding experiments have shown the potential of transforming the cubic phase to the monoclinic phase[(40)]. Work of Jero[unpublished/thesis?] showed that grinding of Sm_2O_3, Gd_2O_3, Tb_2O_3, Dy_2O_3 could transform the room temperature cubic phase to the metastable monoclinic phase. The reverse transformation for Dy_2O_3 was reported by Lopato and co-workers[(42)]. These grinding experiments probably involve a complex stress and temperature state on the crystals but could potentially be interpretated as a shear mechanism associated with the transformation.

Another recognized method for the stabilization of the monoclinic phase is the addition of impurities. On one hand, calcia and strontia are known to stabilize the high-temperature phase leading to a decrease of the transformation temperature. On the other hand, additions of ZrO_2, HfO_2 or Y_2O_3 stabilized the low temperature cubic phase and raised the transformation temperature. Addition of lithia activated the reversibility of the Gd_2O_3 transformation usually considered as very sluggish[xx]. In that case, Gd_2O_3 could even be cycled through the transformation temperature until the lithium content was insufficient due to evaporation. In addition, the addition of impurites allow to broaden the B+C field. This effect was used to investigate a partially stabilized Dy_2O_3 (PSD) as an analog to the partially stabilized zirconia (PSZ) [Kriven,Kim,Fleming199?]. The important effect of impurities on the phase stabilization might be one of the reasons for the discrepancies in the results reported in the literature.

Another source for these discrepancies concerns the effect of environment on the phase transformation. The rare-earth sesquioxides are often prone to oxygen non stochiometry. It is often reported that the ceramic

pieces made from these oxides turn from white to black upon high temperature heat treatment. Furthermore, studies of Rudenko and Boganov have shown that, depending on the rare-earth cation, the transformation might be a function of the oxygen stochiometry or hydroxide content. They showed with the lower rare-earth oxide of the lanthanide series (up to Tb_2O_3??) that the transformation temperature decreases with a more reducing atmosphere and that hydrothermal conditions could reverse the transformation from the monoclinic to the cubic phase. This effect could be attribuated to the hydroxide ions which stuffed the layer structure of the monoclinic phase and pressured the structure form within inducing the transformation to the more open cubic phase.

A common means of stabilization of the high temperature phase consisted in quenching the oxide from the melt. Strong quenching are always required to stabilize the high-temperature monoclinic phase for the oxides in the lanthanide series above Gd_2O_3.[(7), (47)]. Quenching of Dy_2O_3 from the melt stabilized the monoclinic phase when water-quenched but produced the cubic phase when done in air. Warshaw and Roy showed that annealing with subsequent quenching could also retain the high temperature phase but to a lesser extent. Experiments of Mc Pherson and Venkatachari showed that an almost pure monoclinic phase could be retained down to room temperature by plasma spraying. Eyring and Homlberg[xx] showed similar results using a similar technique (splat cooling?). In situ beam heating T.E.M. experiments also showed that microcrystals of the C phase led to large B grains which could be retained when the beam was removed (e.g., quenching)[xx]. This was possible for specimens with thicknesses less than 0.1 μm. Stabilization was explained by the effect of the low surface energy (20-1)B plane which was parallel to the specimen surface.

Little is known on the particle size effect on the stabilization of the monoclinic phase. This effect has to be correlated with the low energy (20-1)B plane of the monoclinic phase since the particle size effect is related to the volume to surface energy ratio of the grain. Work on vapor deposition of the rare-earth sesquioxides led to the direct stabilization of the monoclinic phase[(50-51)]. Coutures and Renard[(50)] stabilized the phase as a stochiometric oxide. The particle size was about 50 Å and the faces of the crystal were believed to correspond to the face of the tetrahedron of Caro's model which is considered as the building block of these oxide structures. On the opposite, crystals obtained by Andreeva and Gil'man had a size above 300Å and were cubic for the yttric rare-earth oxides (e.g., rare-earth oxides of the series above Tb_2O_3). Plasma spraying experiments were able to retain the monoclinic phase [Mc Pherson, Venkatachari] without a very strong prefferred orientation. The grain size was reported of the order of 3 μm[Venkatachari]. These results suggested a combined effect of the grain size and crystal anisotropy.

Eventhough a lot of work has been done with these materials, there is no clear cut understanding on the C to B transformation of the rare-earth oxides. One aspect of the problem concerns the reversibility of the transformation. The C to B transformation was reported early on as irreversible for the oxides in the series below Gd_2O_3 whereas it was very rapid for Tb_2O_3, Dy_2O_3 and Ho_2O_3. In fact, even the lower rare-earth oxides can, in certain conditions, be brought back to the cubic phase. This type of transformation often involves an hydroxide[xx] or a non-stochiometric intermediate phase[xx] or some grinding prior to annealing[xx]. Chemical additions are also able to favor the reversibility as for lithium oxide for Gd_2O_3[xx]. On the other hand, for the higher rare earth oxides stabilization of

the high temperature monoclinic phase is the main problem. Consistent studies on the reverse B to C transformation are scarce. Hoekstra was able to convert the monoclinic back to the cubic phase of ???? after several hours of annealing at 950°C. In addition, Ho_2O_3, initially stabilized by pressure, did retansform to the cubic phase at 400°C after prolonged annealing. Coutures and Renard retransformed their monoclinic crystallites prepared from vapor phase deposition in 5 minutes at 1400°C or in 2 to 3 hours at 1000°C. The reversibility when using calcia chemical addition seemed to originate from the decomposition of the addition[Kriven, Kim, Fleming]. As for Dy_2O_3, it is only reported that the ceramic pieces shatter on cooling due to the reverse transformation.

From this review on the factors affecting the B to C transformation of the rare-earth oxides, it appears that (1) there is no certainty on the type of the transformation, (2) a number of the observations are similar to those done on ZrO_2. In order to assess the usefulness of this transformation for transformation toughening, further characterization of the transformation is required. This study is primarily focussed on the transformation of Dy_2O_3 which seems to be the best analog to that of ZrO_2. In the first paper of this series of two papers, the retention of the monoclinic phase of dysprosia was pursued. Subsequent work was aimed at the study of the reverse transformation under controlled conditions, allowing to draw some insights on the type of the transformation. In the second paper, the crystallography of the transformation was studied and a mechanism proposed.

EXPERIMENTAL

The retention of the monoclinic phase was performed using a melting/quenching technique. Bars of pure dysprosium oxide 2 mm x 2mm x

12 mm were prepared by uniaxially pressing powder[1]. Melting of these refractory compounds is difficult due to their high melting point (above 2400°C). A CO_2 laser was used for this purpose as shown in Figure 2. Only a few kilowatts were necessary when using a F-18 telescope. The localized point of focus allowed to lower the tip of the bar in the laser beam as the power was increased, leading to a good control of the drop formation at the tip of the bar. In order to quench the specimen, a titanium twin-roller quencher was placed under the bar at a distance of about 15 cm. The distance between the roller was minimized such as to obtain a tight contact between them. The quenching rate of this type of apparatus is thought to be of the order of 10^7 °C/sec. and was able to produce flakes of monoclinic Dy_2O_3. The same technique was also applied to ZrO_2, HfO_2 and Gd_2O_3 as a matter of comparison.

The flakes were characterized first at room temperature, then as a function of annealing temperature. Techniques used included quantitative X-ray diffraction, optical and electronic microscopy, differential thermal analysis and thermogravimetry. The flakes and the powder resulting from crushing the flakes were mounted on double-sticky tape for the X-ray diffraction analysis. The scanning speed was 5° 2θ/min. , the sampling step was 0.02. The scan was added seven times to increase the intensity of the pattern and therefore, the resolution of the measurements. In order to calculate the lattice parameters, a diffraction pattern was recorded from 20°-60° 2θ scanning range. A refinement of the lattice parameters was realized using a U.S.G.S. program[2]. The quantitative analysis of the ratio between the

---

Molycorp corp.

[1] Molycorp, corp.

[2] U.S.G.S.C. Cell Refinement and Indexing Program (USGSCRIP) by Appleman and Evans (1973).

cubic and the monoclinic phases was determined from the characteristic patterns in the 25°-35° 2θ range: the cubic phase has two major peaks whereas the monoclinic has six as shown in Figure 3 (A). For a mixture of the two phases, the amount of each phase is proportional to the integrated intensity of its peaks:

$$I_C = K_C \times \%C \qquad I_B = K_B \times \%B.$$

where I_C and I_B are the integrated intensity of a peak and K_C and K_B are constants related to the structure factor of the plane. Peak overlaps and preferred orientation may have given erroneous results when using calculated constants. Hence, a calibration curve was used since almost pure monoclinic could be obtained by the laser-melting/roller quenching method. This method allowed to consider several peaks in both phases reducing any preferred orientation problems or errors due to measurements of peak areas. The peaks used were (111)m+(222)c, (401)m, (40-2)m, (310)m, (11-2)m and (400)c as shown in Figure 3(A). The ratio was:

$$R = \frac{I_M}{I_M + I_{(111)_B} + I_{(222)_C} + I_{(400)_C}}$$

where

$$I_M = I_{(401)_B} + I_{(40\bar{2})_B} + I_{(310)_B} + I_{(11\bar{2})_B}$$

This ratio can also be expressed by

$$R = \frac{k_B^1 (\%B)}{\left[\left(k_B^2 - k_C\right)(\%B) + k_C\right]}$$

where $k_B{}^1, k_B{}^2, k_C$ are constants related to the structure of the two crystals. The calibration curve was done using lightly ground as-quenched flakes for

the pure monoclinic phase and as-received powder or fully transformed flakes for the cubic phase. Figure 3(B) shows the calibration curve.

Scanning electron microscopy (S.E.M.) and transmission electron microscopy (T.E.M.) were performed on the flakes to characterize grain size and the defects in the microstructure. For T.E.M. observations, the flakes were manually cut and mounted on a copper grid and then, ion-milled directly owing to their small thickness. In addition, some in-situ T.E.M. transformations were attempted in the microscope. Heating the specimen was performed by removing the apertures and focussing the beam. After this heat treatment the region was observed for any transformed grains. Similarly, a hot stage experiment was performed in a 1 M.e.v. high-voltage electron microscope (H.V.E.M.) to follow the microstructure as the specimen was gradually heated from room temperature to 600°C over a two-hour period.

Additional characterization was performed by differential thermal analysis (D.T.A.)[3] and thermogravimetry (T.G.A.)[4]. The experiments were run with 30 to 40 mg of crushed flakes at 5°C/min. up to 1000°C which was enough for fully transforming the monoclinic phase to the cubic phase. Platinum crucibles were used and cubic dysprosium powder was chosen as a reference in the D.T.A. experiment.

Kinetic study of the B to C transformation

Molycorp corp.

[3]Dupont Model 910 High-temperature D.T.A. with 1090 Thermal Analyser, E.I. Dupont de Nemours, Inc., Wilmington, DE.

[4]Dupont Model 951 T.G.A. with 1090 Thermal Analyser, E.I. Dupont de Nemours, Inc., Wilmington, DE.

The kinetic study of a transformation could give useful indications as to the mechanism of the transformation. Different annealing treatments of the flakes allowed quantitative characterization of the transformation following an analysis used earlier by Whitney[(65)] for the tetragonal to cubic transformation in zirconia.

An Avrami-type equation was used:

$$f(t)=e^{-kt^n}$$

where f(t) is the fraction of the monoclinic phase left untransformed after a certain time t, n is the kinetic law constant or also called order of the transformation. This constant is related to the growth mechanism of a the cubic nuclei in the monoclinic matrix. The other constant, k, is related to the number of potential cubic nuclei as well as to the rate of formation and growth of the cubic nuclei. This constant k carries the thermal activation of the transformation:

$$k=k_0 \exp(-E_a/RT)$$

The annealing experiments were conducted in air with powder obtained from the ground flakes. Specimens were up-quenched to the annealing temperature and quenched back to room temperature in air after a suitable annealing time. The amount of monoclinic phase left was then quantitavely measured by X-ray diffraction. In order to find n and E_a as a function of temperature, Ln(Ln[1/(1-f(t)]) was plotted as a function of Ln(time) at constant temperature (slope=n and intercept=Ln(k)) while Ln k was plotted as a function of 1/T(°K) such that the slope gave E_a.

RESULTS

1. Characterization of the flakes

Flakes obtained by the laser-melting/roller-quenching technique are shown in Figure 4. A chemical analysis showed that the Dy_2O_3 flakes were 99.9% pure[M.S. thesis]. They were in general 1 to 2 cm in length, 40 to 100 μm thick, and generally curved. The technique was difficult to control which, in turn, resulted in a variable batch to batch quality of the flakes. The best batches were obtained when a large drop was melted at the tip of the bar with the laser. The color of the flakes was generally yellowish. The same technique applied to HfO_2, ZrO_2 and Gd_2O_3 led to white flakes.

The fast quenching rate effectively retained the high-temperature monoclinic phase of dysprosia down to room temperature. Figure 5 shows the full diffraction pattern for some crushed flakes. The X-ray diffraction A.S.T.M. card was found to be incomplete for monoclinic dysprosia and therefore, the monoclinic gadolinia data were used to index the planes of the pattern. The strongest peak of the cubic phase corresponding to the (222) plane, could be detected which was an indication of the presence of a very small amount of cubic phase. It was however assumed that the flakes were essentially monoclinic. The refinement of the lattice parameters gave good agreement with values found in the literature as shown in Table 1 and 2. X-ray diffraction made directly on the flakes showed a significant prefferred orientation parallel to the (20-1) monoclinic plane as shown in Figure 6. Gd_2O_3 flakes were also found to be fully monoclinic **(Is the cubic peak detected??)**. On the other hand, the high-temperature cubic or tetragonal phases of ZrO_2 and HfO_2 were not found: it was fully monoclinic.

Figure 7 (A to C) shows different S.E.M. micrographs of the surface of the Dy_2O_3 flakes. Different surface features could be observed including

cracks. The macro features reminded of a material that had been solidified from the melt (Figure 7A). At higher magnifications, the individual grain could be observed in some areas (Figure 7 Band C). Figure 8 shows an histogram of the grain size observed on the surface of the flakes. The mean grain size was found to be of the order of 2.4 μm. Some wavy features on the surface could be observed in some cases as shown in Figure 7C. ZrO_2 and HfO_2 had a completly different aspect (Figure 7D). The surface was extensively twinned.

T.E.M. observations showed different types of defects within the microstructure. The monoclinic crystals were often twinned and contained many dislocations (Figure 9). Some of these dislocations were very mobile since they were moving under the beam.

2. Characterization of the B to C transformation

Miscellaneous experiments were made on the flakes. The transformation could not been detected after neither grinding nor undercooling at liquid nitrogen temperature.

On the other hand, annealing of the flakes rapidly transformed them to the cubic phase. Microstructural observations showed that the surface of the flakes became rougher with increasing temperature with in particular appearence of a step-like morphology as shown in Figure 10 A and B. T.E.M. observations showed that most defects were annealed at 400°C-500°C. The transformation followed on an hot stage optical microscope showed that the flakes warped as they were heated. Around 580°C -600°C, the flakes are craking and shattering as observed in hot stage microscopy (optical and H.V.E.M.). Figure 10 C shows the powder resulting from the shattering of the

flakes at 600°C and Figure 10 D the crack formation in the flake as observed in hot-stage H.V.E.M..

The D.T.A. and T.G.A. analyses are shown in Figure 11. These runs were reproduced several times. The D.T.A. did not show any precise peak but rather indicated an exothermic reaction occurring on a large range of temperature above 400°C. The T.G.A. curve showed a slight weight increase of the specimen of about 0.325%. If this weight gain was only due to oxygen intake to recover the stochiometry of the sesquioxide, the corresponding formula of the starting oxide would be Dy_2O_{3-x}, x=0.075. This hypothesis is further supported by the color change from yellow to white. The weight gain occurred in two steps. At first, the rate is slow starting at 300°C, then, the rate increases above 600°C. At the end of the runs at 1000°C, the monoclinic phase has been completely transformed into the cubic phase. The atmosphere did not seem to affect the transformation. Runs in air or under inert gas (i.e., N_2) resulted in a similar transformation.

Furthermore, the transformation was also achieved in the high vacuum environment of a T.E.M. and a H.V.E.M. . The transformation by beam heating on some grains could be observed (Figure 12). However, the transformation was inconsistent and could not be controlled. In the hot stage, at around 600°C the flakes started to crack. The transformation was so violent that no crystallographic orientation relations could be obtained.

The kinetic study further characterized the transformation. The results of the transformation of the monoclinic phase as a function of temperature and time are shown in Figure 13 and 14. In Figure 13, the amount of monoclinic left at a given temperature is plotted as a function of time. For sake of clarity, only part of the experiments are reported on the graph. These experiments were consistent within a same batch of powder (e.g., crushed

flakes). However, differences in the amount transformed occurred from batch to batch. The accuracy of the X-ray quantitative analysis was poor below 15% of monoclinic phase due to the small integrated peak to background ratio. Figure 14 shows the Ln(Ln(1/1-f)) vs Ln(time) plot with f the volume fraction of monoclinic still present. The sets of points have been extrapolated to a straight line eventhough the behavior seemed more complex. Nevertheless, the plot of Ln k and the order of the transformation vs temperature showed a definite trend (Figure 15). In these plots, all the data from different batches were reported. The good correlation could,may be, be explained by the Ln-Ln scale used in the model. These results showed that the transformation starts below 500°C. At 600°C the rate of transformation is large (i.e., 60% of monoclinic has been transformed at 600°C after an hour). This temperature corresponds to the temperature at which the flakes are shattering. Above 600°C, the transformation became very fast. This double regime of the transformation was even clearer in Figure 15. First, the order of the transformation, n, decreased from one to almost zero. Second, the activation energy decreased from about 396 KJ/mole (94 Kcal/mole) to about 30 KJ/mole (7.4 Kcal/mole). Two competing mechanisms seemed to take place.

DISCUSSION

The laser-melting/roller-quenching technique was effective in retaining the high temperature monoclinic phase of Dy_2O_3. Conversely, ZrO_2 and HfO_2 could not be retained by this method. These refractory compounds have a similar melting point and if a similar crystallization temperatureis assumed, all of them should have crystallized in one of their high temperature crystal structure. Then, the thermodynamics of these

compounds must have been affected by other factors since only dysprosia high temperature phase was retained. A number of parameters can be responsible.

First, the stochiometry of the compound could be a stabilizing factor. The monoclinic phase is denser, therefore, any missing ions would produce a more relaxed state. This free-energy gain would essentially reduce the strain energy in the crystal. This hypothesis implies that the further the monoclinic phase is from stochiometry, the more stable it becomes. On one hand, the change of color with temperature and the weight increase on heating of the monoclinic powder would support this fact. Futhermore, on heating cubic dysprosia at its transformation temperature around 1950°C clearly induces a non-stochiometric product. The oxygen deficiency in the rare-earth oxides is well-known. The diffusion of oxygen in these materials is rapid and was indicated to start around 300°C[Eyring(1) in the cubic phase?]. This corresponds to the first weight increase in the T.G.A. experiment. Furthermore, as the transformation occurs, the diffusion of oxygen in the less dense cubic phase is certainly more rapid, inducing a higher rate of weight gain. This hypothesis would correlate well with the action of hydroxide ions inducing the transformation[xx]. On the other hand, the transformation was still occurring when no oxygen was available as shown in the T.E.M. and H.V.E.M. experiments. It seems therefore that the two occurences could simply be fortuitous or that the free-energy gain due to the non-stochiometry is not critical. In any case, zirconia and hafnia seemed to be stochiometric as evidenced by their white color and therefore could not profit of such stabilizing effect.

A second hypothesis would involve the defects in the microstructure. The monoclinic phase of the rare-earth is very plastic. Differents modes of

deformations are possible in the form of twins or dislocations. As the micrographs in Figure 9 have shown, the grains contained a certain amount of dislocations, twins and low angle grain boundary. These defects could have several origins. They could have been formed during the crystallization as Boulesteix et al. have shown in their in-situ crystallization experiments. Another possible origin comes from the mechanical effect of the rollers on the monoclinic phase. A third possibility is the lowering of the strain energy accumulated upon cooling which instead of producing the transformation to the cubic phase, promotes the deformation of the crystal by plastically deforming. The formation of these defects have also been found in plasma-sprayed monoclinic dysprosia[Venkatachari]. Upon annealing, it is therefore possible that these defects disappeared and allow the transformation to proceed. This type of stabilization was not possible in zirconia and hafnia since the plastic phase is, in this case, the low temperature monoclinic phase.

A third hypothesis involves the stabilizing effect of the surface energy. One aspect of the stabilization of the zirconia tetragonal phase involves the grain size or in other words, the surface to volume ratio. In the case of dysprosia, the grain size obtained through the laser-melting/roller-quenching technique is relatively large (~3 μm). Similar grain size magnitude was reported in plasma-sprayed dysprosia[Venkatachari]. Such a grain size in zirconia or hafnia would not be sufficiently small for stabilization. This also may explained the transformation of these latter oxides. In addition, as was shown in dicalcium silicate, the effective grain size controlling the transformation may well be the lath size[C.J. Chan]. On the other hand, the anisotropy of the crystal structure may be a stabilizing factor. This hypothesis is supported by the in-situ T.E.M. crystallization of Boulesteix et al.. The crystals in their experiment as well as in this study had a prefferred

orientation parallel to the layer plane of the structure. As the temperature is raised during annealing, the effective grain size may increase.

All these different factors combined may well produce enough free-energy gain to stabilize the monoclinic phase and are schematically depicted in Figure 16. The total free-energy difference can be written:

$$\Delta G = G_B - G_C$$

$$= (g_B V_B - g_c V_C) + \left(\sum_i \gamma^s_{iB} A_B - \sum_i \gamma^s_{iC} A_C \right)$$

$$+ \Delta G_{stochio.} + \Delta G_{plastic} - \frac{1}{2} \int_V \sigma_{ij} \varepsilon_{ij} \, dV$$

The terms include the crystal structure volume free-energy difference which is negative, the surface energy difference, the chemical energy due to the non stochiomatry, the free-energy gain by relieving the strain energy by plastic deformation and the negative remaining strain energy in the crystal. Upon annealing, all these terms evolve with temperature and could finally provide the necessary driving force for the transformation.

Once the thermodynamics aspect of the transformation has been clarified, the kinetics of the transformation is a concerned. The results seemed to indicate two competing mechanism and a clear thermally activated process. At low temperature, the transformation has a high activation energy and could therefore be considered thermally activated. The high order and activation energy of the transformation recalled the findings of Stecura on the C to B transformation of Gd_2O_3. At higher temperature, above 600°C, the transformation is rapid and violent. This result would indicate a displacive component to the transformation. The temperature activated process could have several origin. First, the thermal energy could alter the thermodynamic driving force by reducing some of the terms described earlier. For example, annealing of the defects such as dislocations or low angle grain boundaries

could reduce the plastic energy term and increase the grain size. In this case, the transformation is only thermodynamically limited and the mechanism of the transformation is essentially displacive. On the other hand if the stoechiometric effect is important or if the shuffling of the oxygen ions is necessary for the transformation to occur, the rate controlling factor could be the diffusion kinetics of the oxygen ions inside the crystal structure. The stochiometry is probably not a critical proble since the transformation still occur in high vacuum. The second hypothesis will be developped in the companion paper which deals with the crystallography of the transformation.

Finally, it is interesting to compare this transformation with the transformation of other inorganic compounds. Table 3 summarizes the characteristics of the martensitic tetragonal to monoclinic transformation of ZrO_2, the reconstructive anastase-rutile transformation of TiO_2 and the monoclinic to cubic transformation of Gd_2O_3 and Dy_2O_3. The two first compounds illustrate the possibility of a displacive or reconstructive mechanism as defined by Buerger[xx] and leading to a volume expansion of the crystal. The displacive mechanism involves only stretching or the re-orientation of bonds around an atomic site, whereas a reconstructive mechanism involves the breaking and reforming of bonds. The kinetics of the transformation of Dy_2O_3 indicate a potential displacive transformation. However, the study remains inconclusive. A second approach is taken in the following paper by considering the crystallography of the two structures, their relations and potential crystallographic transformation path.

It is too early to say if dysprosia can be used as a potential transformation toughener. It seems that more parameters are involved in controlling the transformation than in zirconia. The big challenge would be in the processing of the ceramic to be able to retain the monoclinic phase in a

metastable form. From this study, the transformation may be useful above a given temperature. For example, above 600°C the monoclinic phase could be maintain metastable. In addition, it could allow twin toughening at room temperature due to the plasticity of the monoclinic phase.

CONCLUSION

In this first paper, the stabilization of the high-temperature monoclinic phase of Dy_2O_3 was obtained via a laser-melting/roller-quenching technique. Microstructural characterization of the product as well as its transformation to its stable cubic phase were performed. The kinetic study of the transformation seems to indicate two competing mechanisms. Several factors can affect the transformation. The transformation can be either thermodynamically or kinetically limited. More experimental data would be necessary if more controlled processing route could be found. In the following paper, an atomistic approach is taken. The crystallography of the two phases is related and a possible mechanism for the transformation presented.

REFERENCES

TABLES

Table 1: Indexation of the monoclinic Dy_2O_3 at room temperature after grinding of the flakes.

No.	2Θ	d-spacing (Observed)	d-spacing (Calculated)	I/I0	(hkl)	
1	22.44	3.959	3.944	9	$20\bar{2}$*	
2	26.50	3.361	3.363	15	202	
3	28.63	3.115	3.115	66	111	
4	28.97	3.080		16		222C
5	29.72	3.004	3.005	85	401	
6	30.42	2.936	2.937	100	$40\bar{2}$	
7	30.81	2.900		13	?	
8	31.49	2.839	2.839	54	003	
9	32.07	2.789	2.787	72	310	
10	32.92	2.719	2.718	75	$11\bar{2}$	
11	39.35	2.288	2.288	19	600	
12	39.58	2.275		11	?	
13	40.40	2.231	2.229	9	$11\bar{3}$	
14	41.34	2.182	2.182	12	$60\bar{2}$	
15	41.55	2.172	2.170	20	$51\bar{1}$	
16	42.91	2.106	2.105	48	$31\bar{3}$	
17	48.09	1.891	1.890	41	313	
18	52.00	1.757	1.757	23	020	
19	52.46	1.743	1.743	17	$80\bar{1}$	
20	52.91	1.729	1.731, 1.726	9	$71\bar{1}$*, $20\bar{5}$*	
21	54.55	1.681	1.682, 1.681	39	404, $71\bar{2}$	
22	54.85	1.672		12	?	
23	55.45	1.656	1.655	9	221	
24	55.79	1.646	1.646, 1.645	26	$40\bar{5}$, 603	
25	56.14	1.637	1.635	19	$51\bar{4}$*	
26	56.37	1.631	1.631, 1.627	34	711, 801*	
27	56.92	1.616	1.616, 1.611	12	513, 022*	
28	57.46	1.603	1.605	9	$22\bar{2}$*	
29	57.96	1.590	1.589	10	205	
30	59.58	1.550	1.551, 1.557	20	$11\bar{5}$, 222*	
31	60.57	1.527	1.528	8	$31\bar{5}$	
32	61.05	1.517	1.517	20	421	
33	61.43	1.508	1.508	24	$42\bar{2}$	
34	61.80	1.500	1.502	18	802*	
35	62.08	1.494	1.494, 1.497	17	023,115*	
36	62.37	1.488	1.489	10	$22\bar{3}$*	

* plane rejected in the refinement calculation.

37	63.28	1.468	1.468	16	$80\bar{4}$
38	63.38	1.460		8	?
39	64.73	1.439	1.439	9	$\bar{5}15$

a= 13.946±0.002Å b= 3.5145±0.0005Å c= 8.653±0.001Å

and β= 100° 8.8'± 0.7'

considering 29 planes in the refinement of the lattice parameters.

Table 2: Comparison of the lattice parameters of dysprosia.

Method	a(Å)	b(Å)	c(Å)	β(°)	Authors
pressure	13.97	3.519	8.661	100.20	Hoekstra[17]
distillation H_2	13.93	3.520	8.631	100.20	Coutures[50]
distillation N_2	13.94	3.520	8.656	100.25	"
quenching	13.95	3.52	8.66	100.22	Coutures[47]
quenching	13.97	3.519	8.661	100.20	Nigmanov[69]
quenching	13.946	3.5145	8.653	100.24	This study

Table 3: Comparison of the transformation characteristics for different inorganic compounds.

Compound	ZrO_2	TiO_2[1],[58-60]	Gd_2O_3	Dy_2O_3
Structure[2]	mono.-tet.	tet.-tet. Anastase-Rutile	cub.-mono. C - B	
Temperature[3]	1175-950°C	610°C (min.)	1200°C	1950-1860°C
Reversibility	yes	no	difficult	yes
Volume change[1]	-3% to -5%	-8%	~-8%	
Quenching effect	possible	*N.A.*	*N.A.*	yes
Chemical effect	CaO, Y_2O_3	SO_4^{2-}	CaO, SrO/HfO_2, ZrO_2	
Pressure effect[1]	yes		yes	
Grinding effect	yes[4]	yes[1]	yes[1]	
Oxygen vacancy	yes(cubic)	yes	Possible	
Particle size/ Surface area	yes	little	yes	
Mechanism	martensitic	reconstructive with shear	reconstructive?	
	topotaxic	topotaxic	epitaxic-topotaxic?	
Coordination[5,4]	8 to 7		~7 to 6	
Thermodynamic ΔH.(Kcal/mole)	1.4	~0.1	~2	
Kinetic "speed"	fast	sluggish	sluggish	fast
order n	0.14-0.7	first	first(C to B)	?
activation energy (Kcal/mole)	17-138	~90	≥100	?

[1] γ to α Fe_2O_3 transformation has comparable characteristics.
[2] low to high temperature phase
[3] on heating-on cooling
[4] high to low temperature phase.
[5] cation

FIGURES

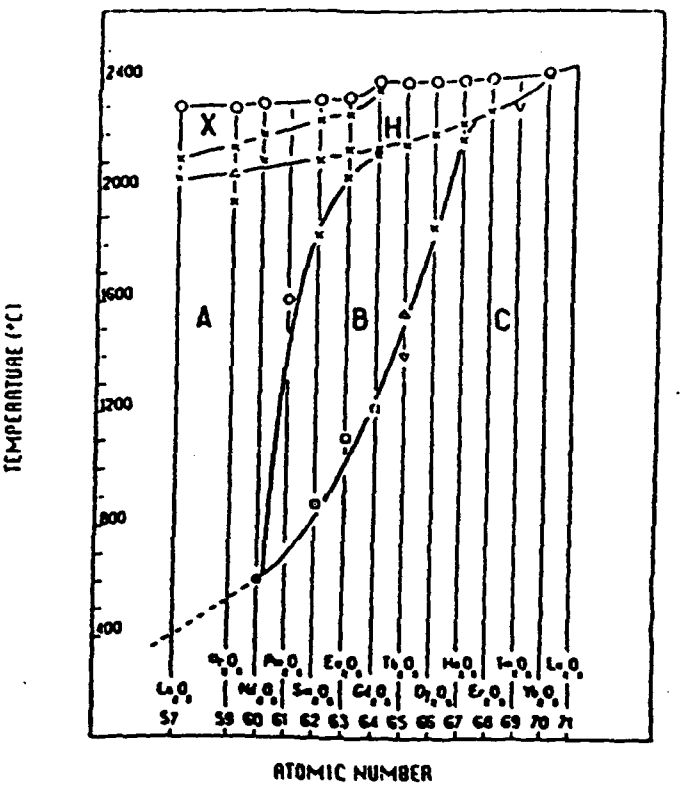

Figure 1: Polymorphs of the rare-earth sesquioxides as a function of temperature and ionic radius[7].

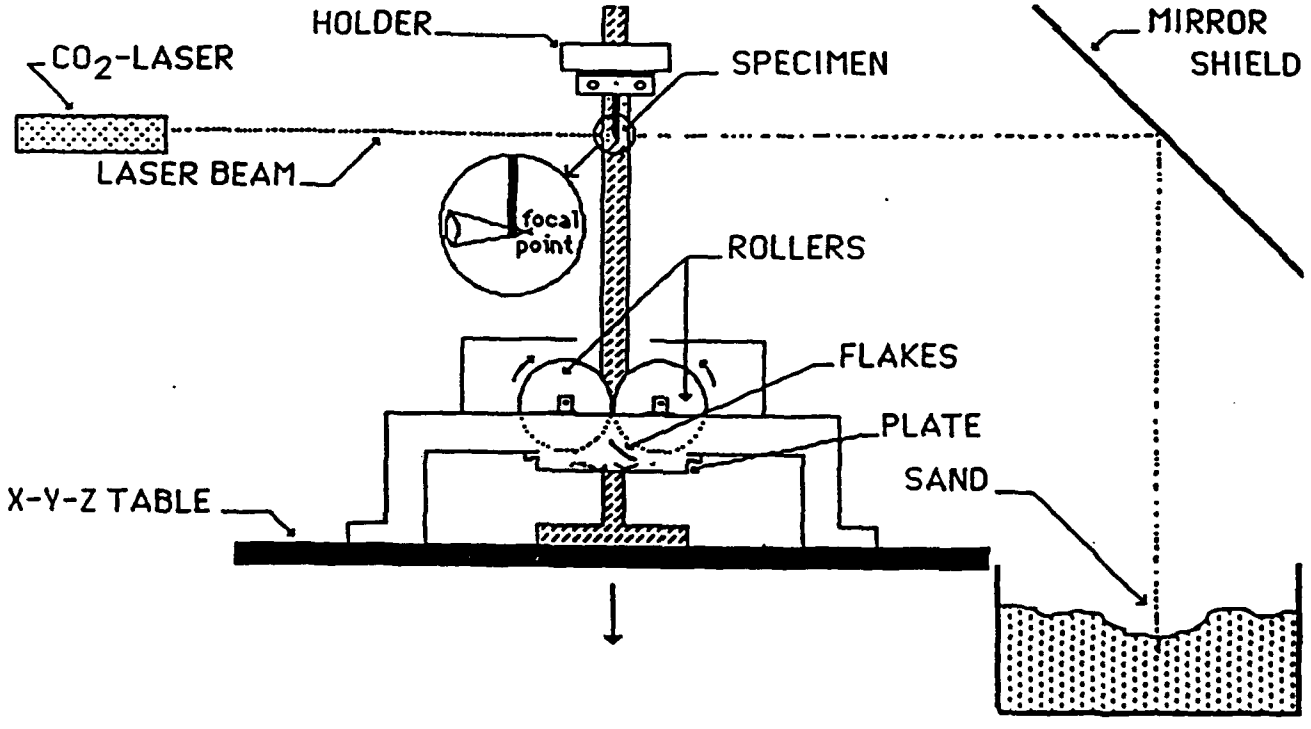

Figure 2 The laser-melting/roller-quenching experimental apparatus.

(A)

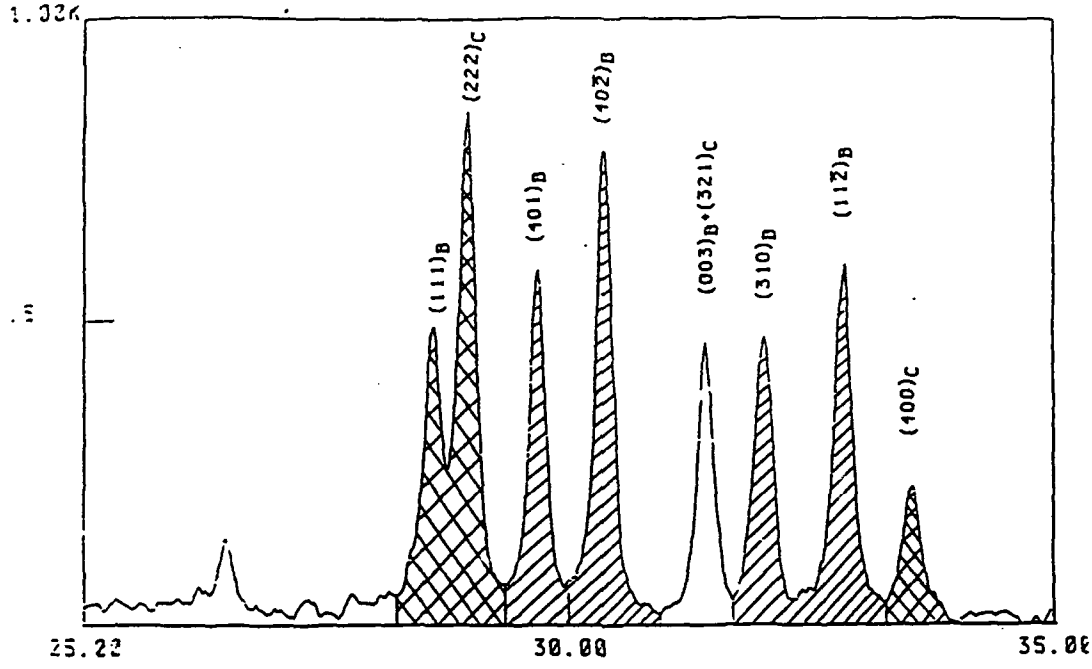

(B)

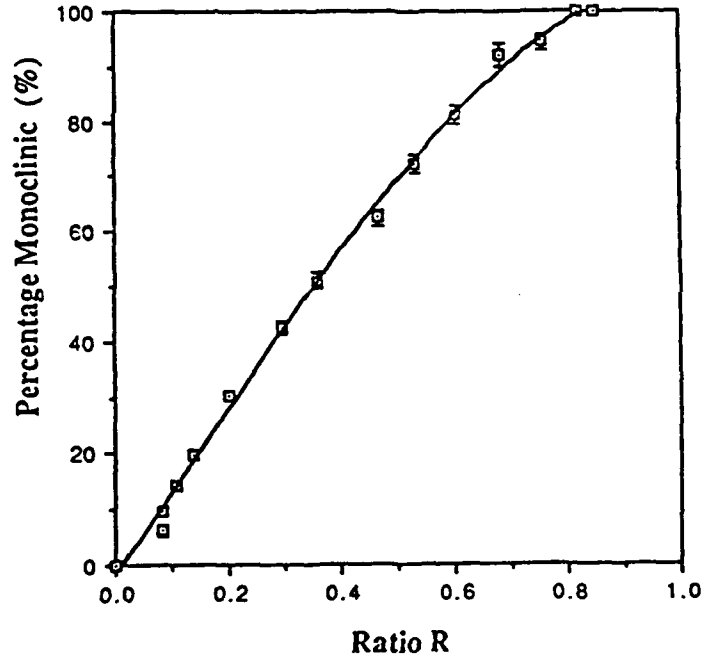

%m = - 1.7476 + 146.2348 R + 24.1544 R^2 - 63.8026 R^3 R = 1.00

Figure 3: (A) The X-ray diffraction pattern of a cubic and monoclinic mixture, (B) The calibration curve.

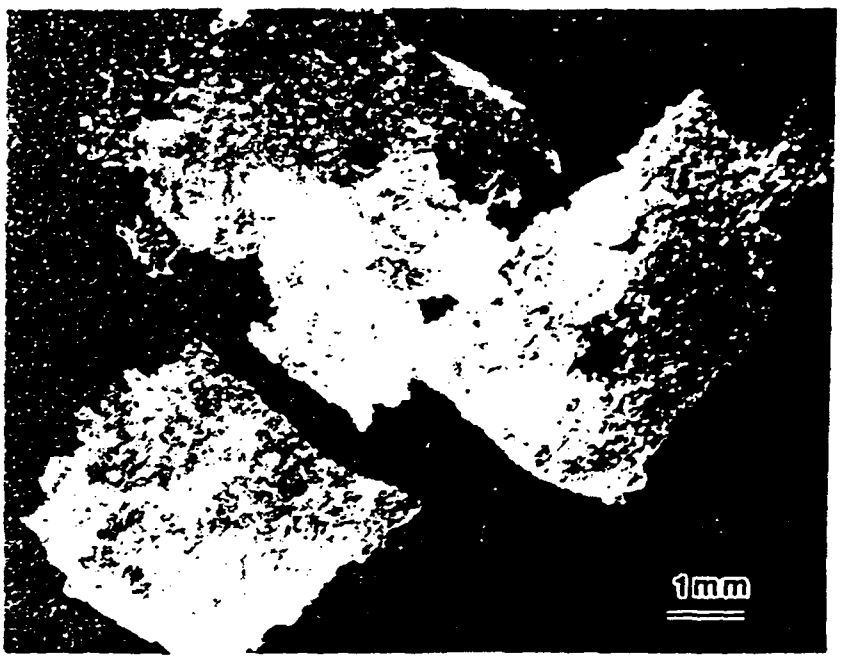

Figure 4 Optical micrograph of as-quenched flakes.

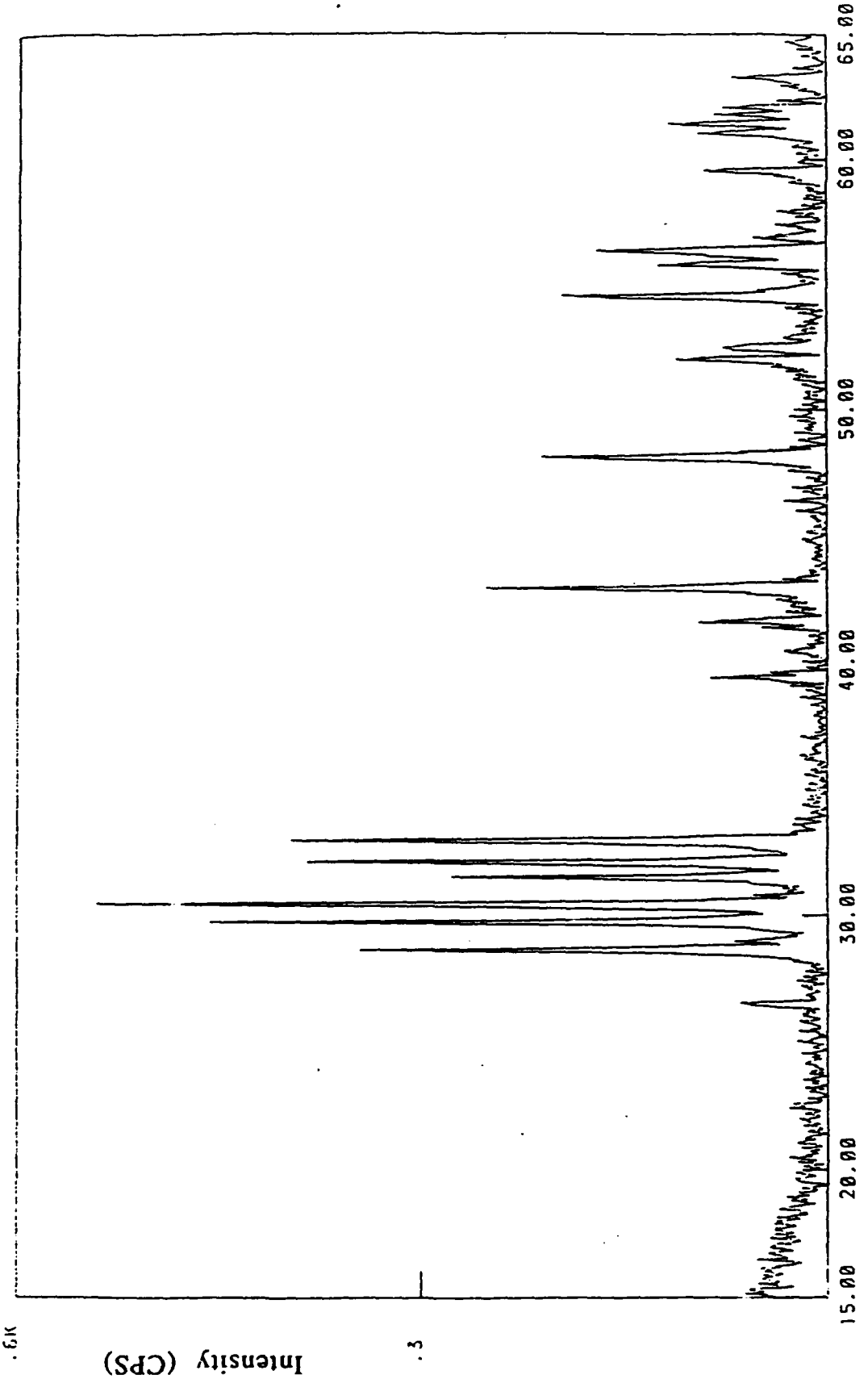

Figure 5: X-Ray diffractometry of monoclinic dysprosia.

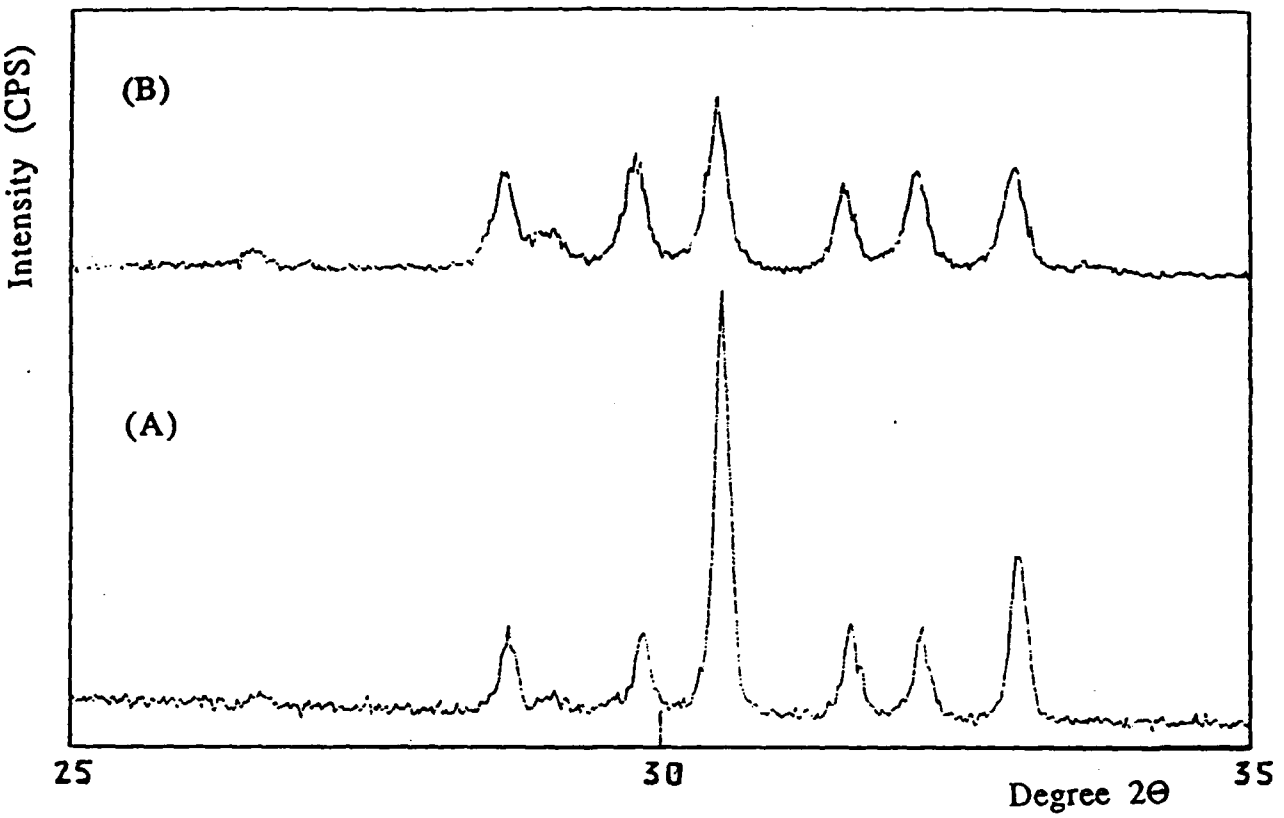

Figure 6: X-ray diffraction patterns from (A) the surface of the flakes, (B) powder from crushed flakes.

Figure 7

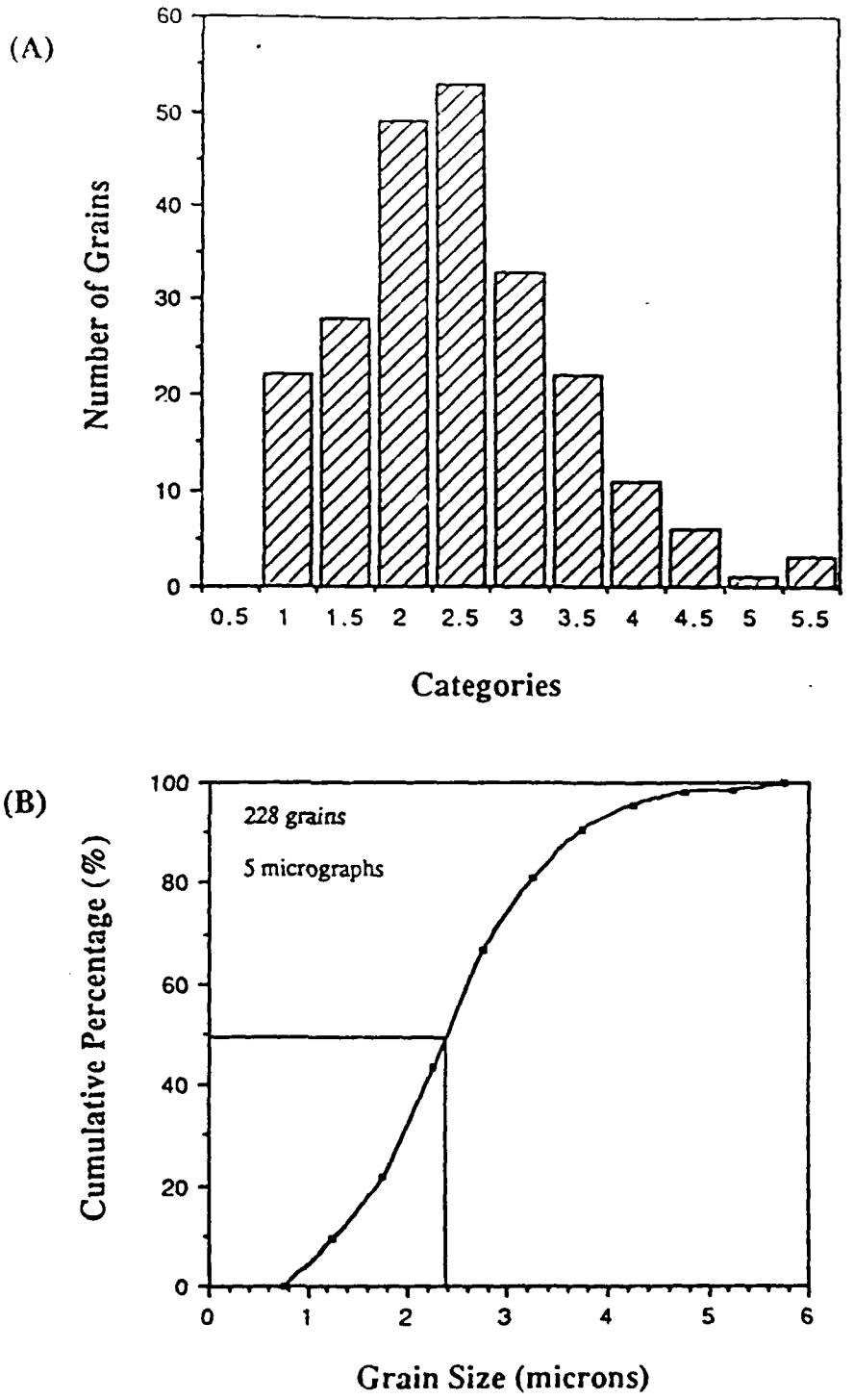

Figure 8: Particle size analysis on the surface of as-quenched flakes (A) Histogram, (B) Distribution curve.

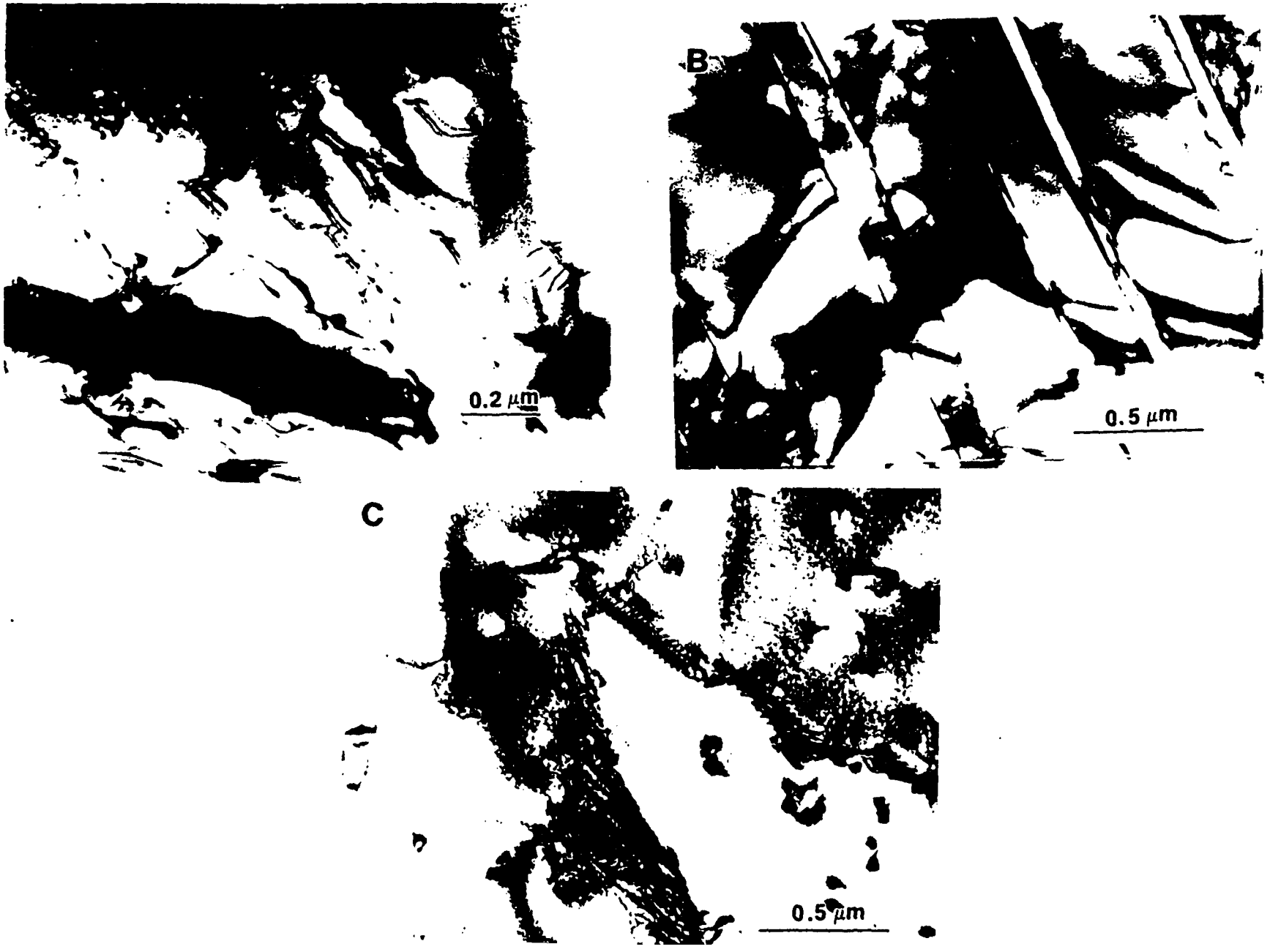
B
0.2 μm
0.5 μm
C
0.5 μm

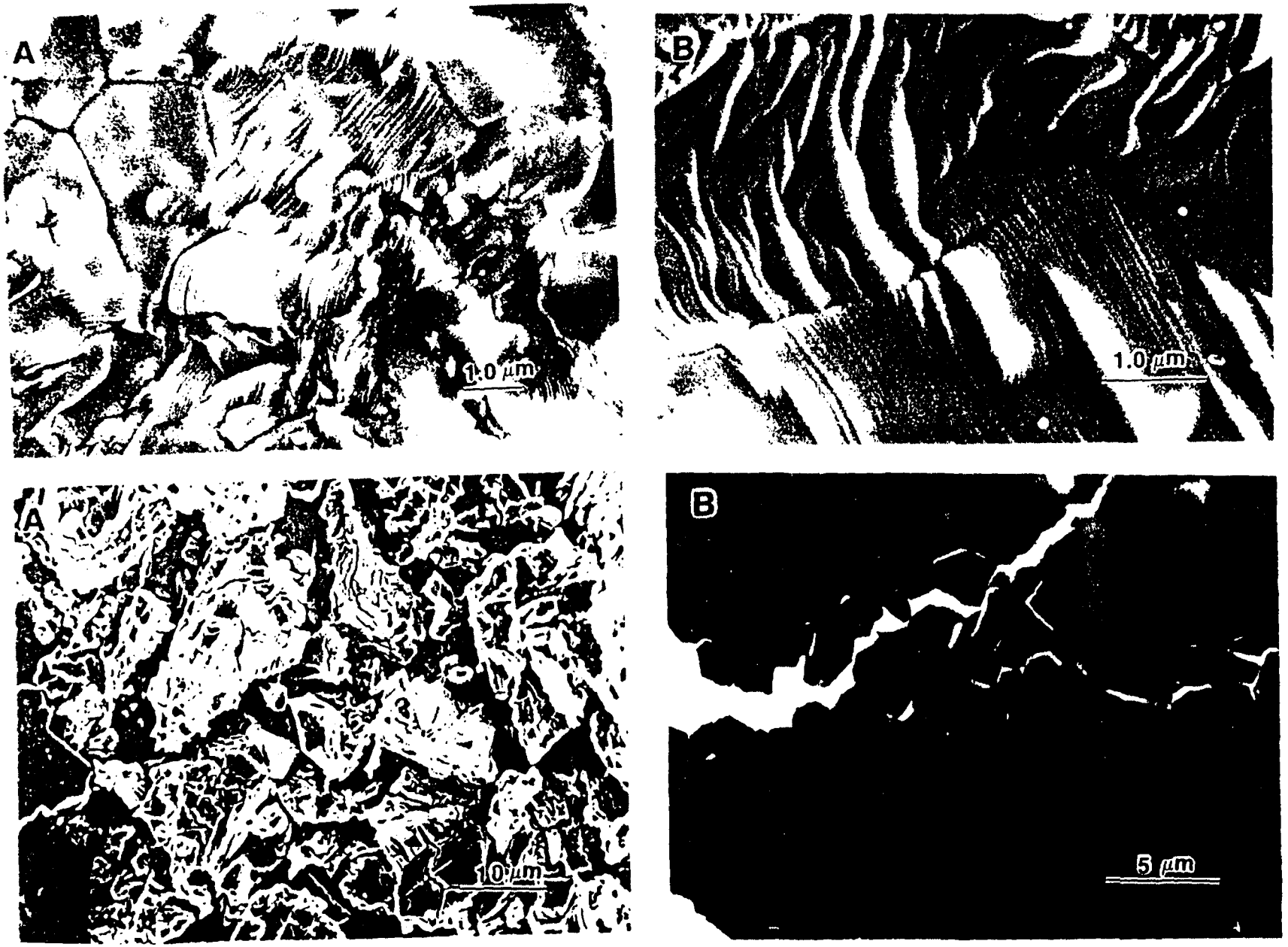
A
1.0 μm
B
1.0 μm
A
10 μm
B
5 μm

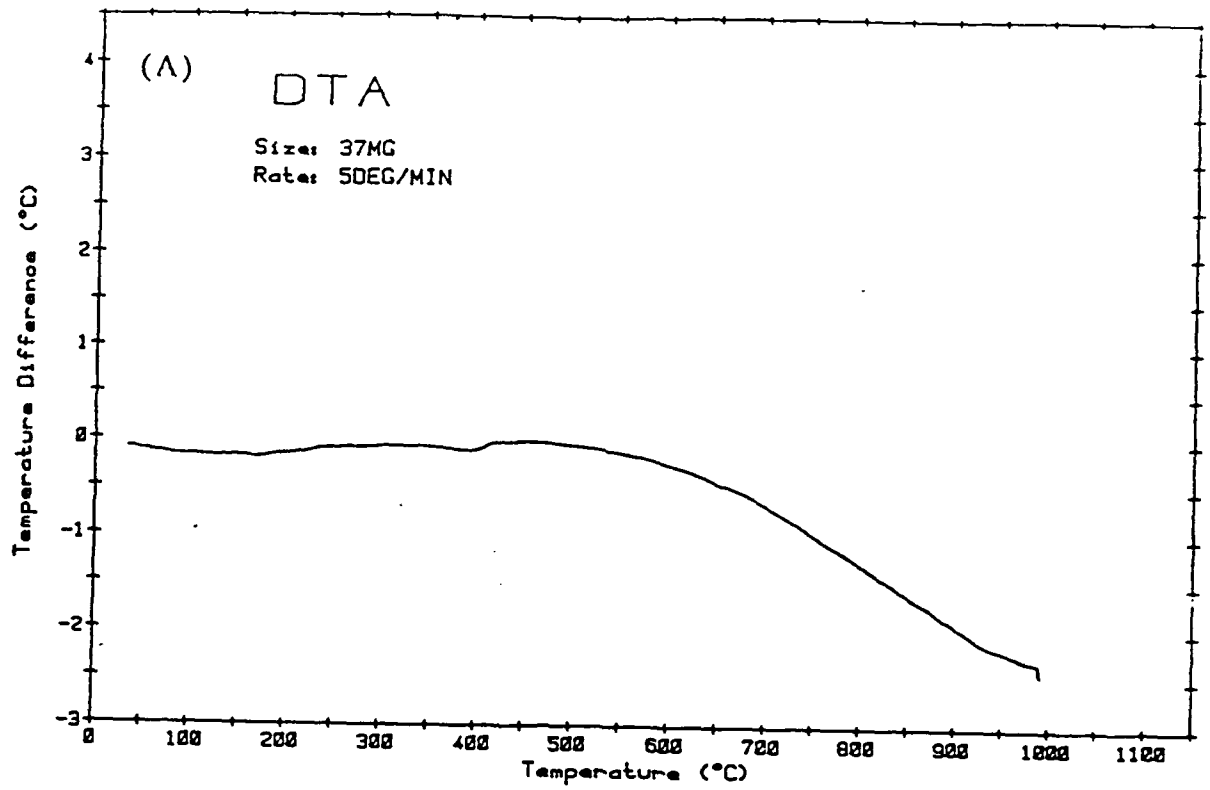

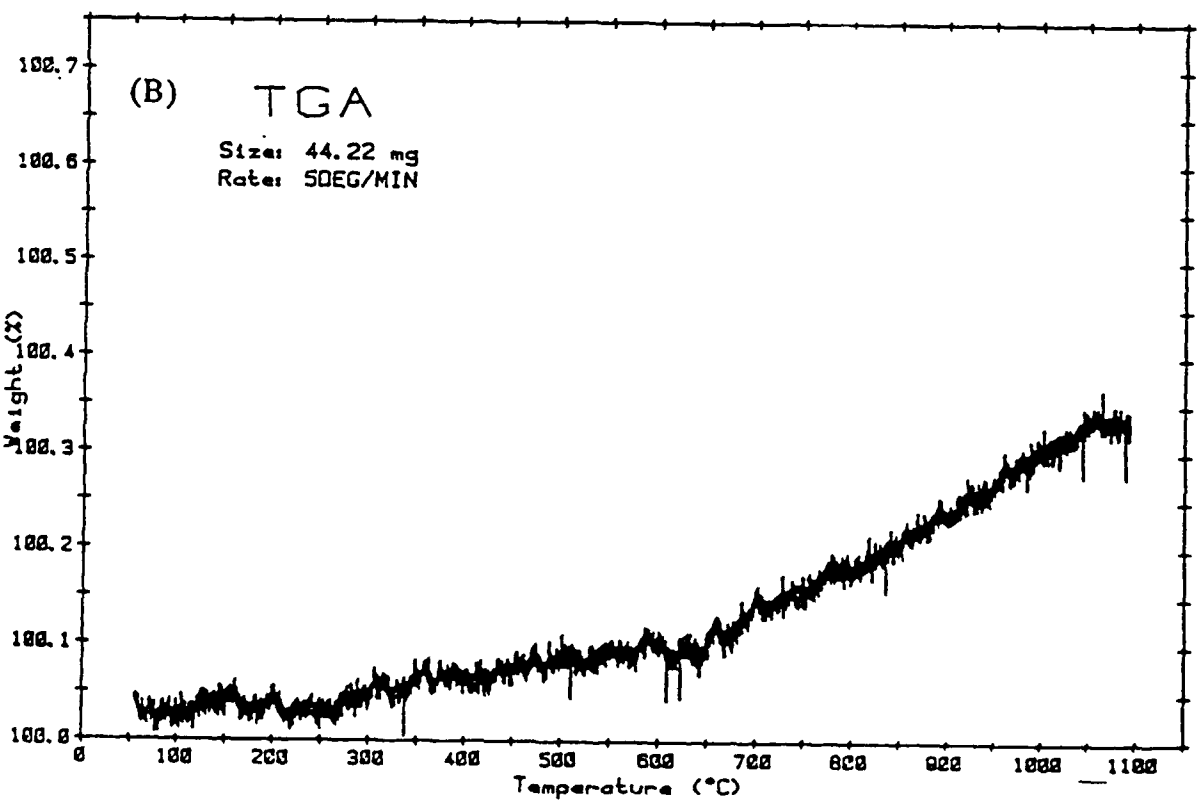

Figure 11: Thermal analysis: (A) D.T.A., (B) T.G.A..

Figure 12 Grain which is believed to have undergone the B to C transformation (A) before, (B) after.

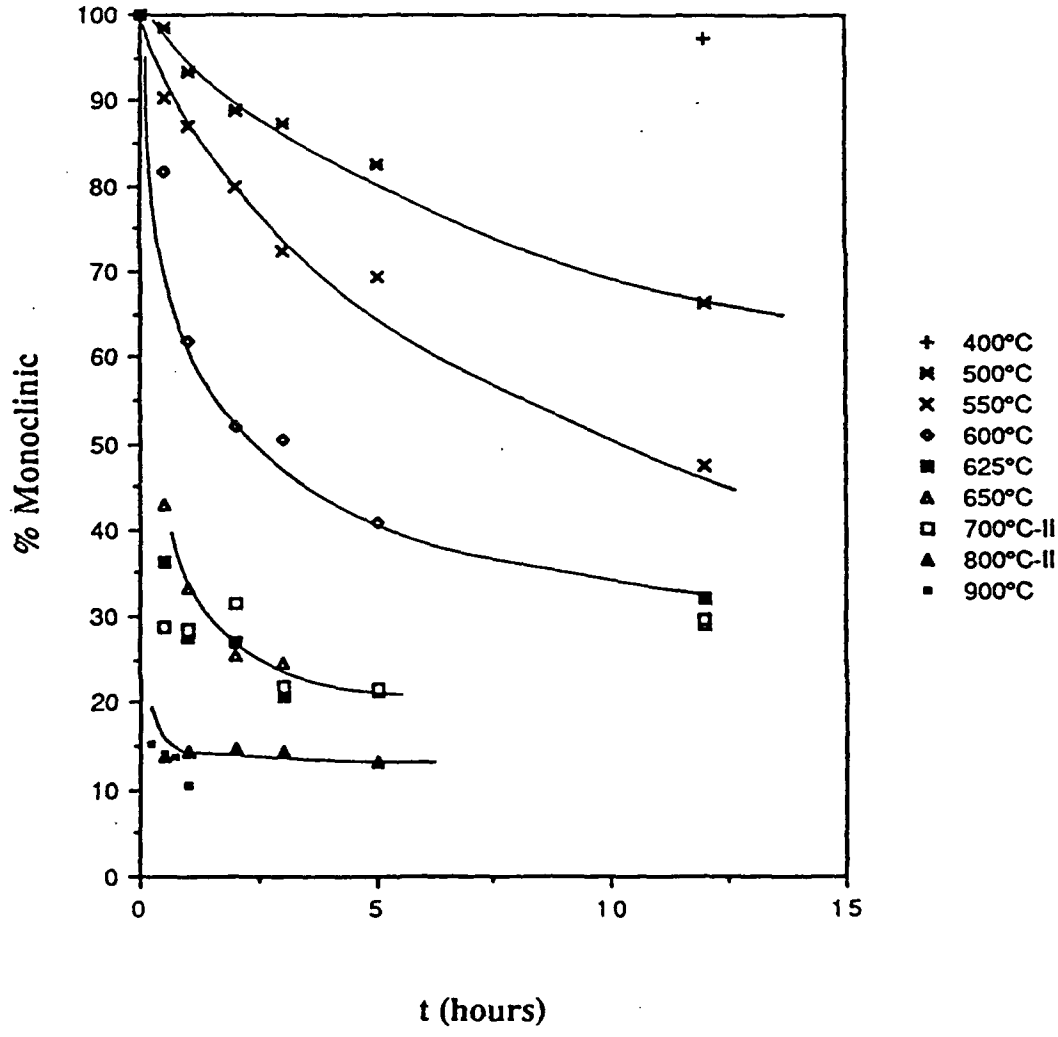

Figure 13: Kinetic study, % monoclinic phase left untransformed as a function of time.

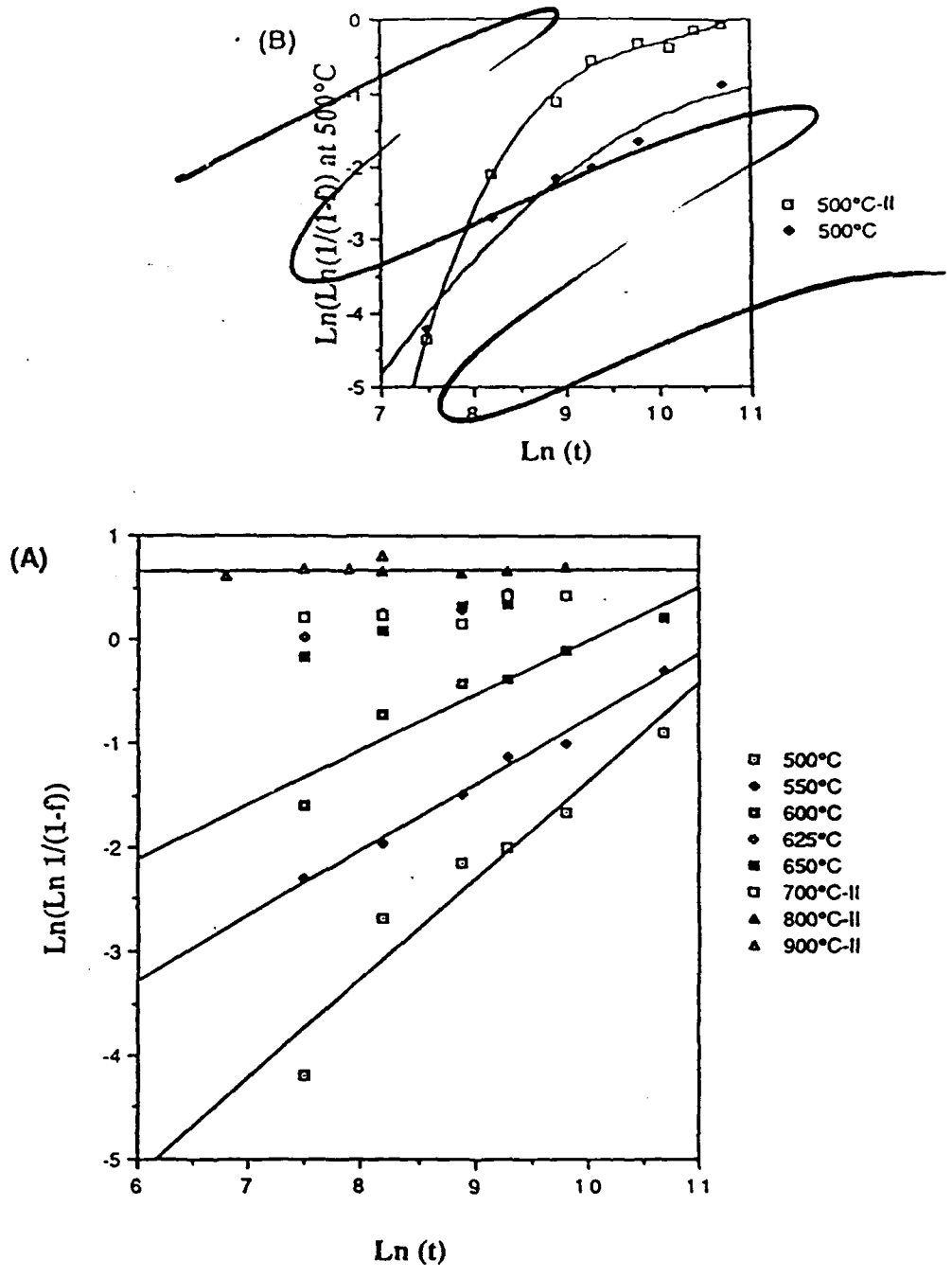

Figure 14: Kinetic study, $Ln(Ln(\frac{1}{1-f}))$ as a function of Ln(t) at different temperature of annealing. (A) General data, (B) Data for a experiment at 500°C showing the change in slope and intercept with time.

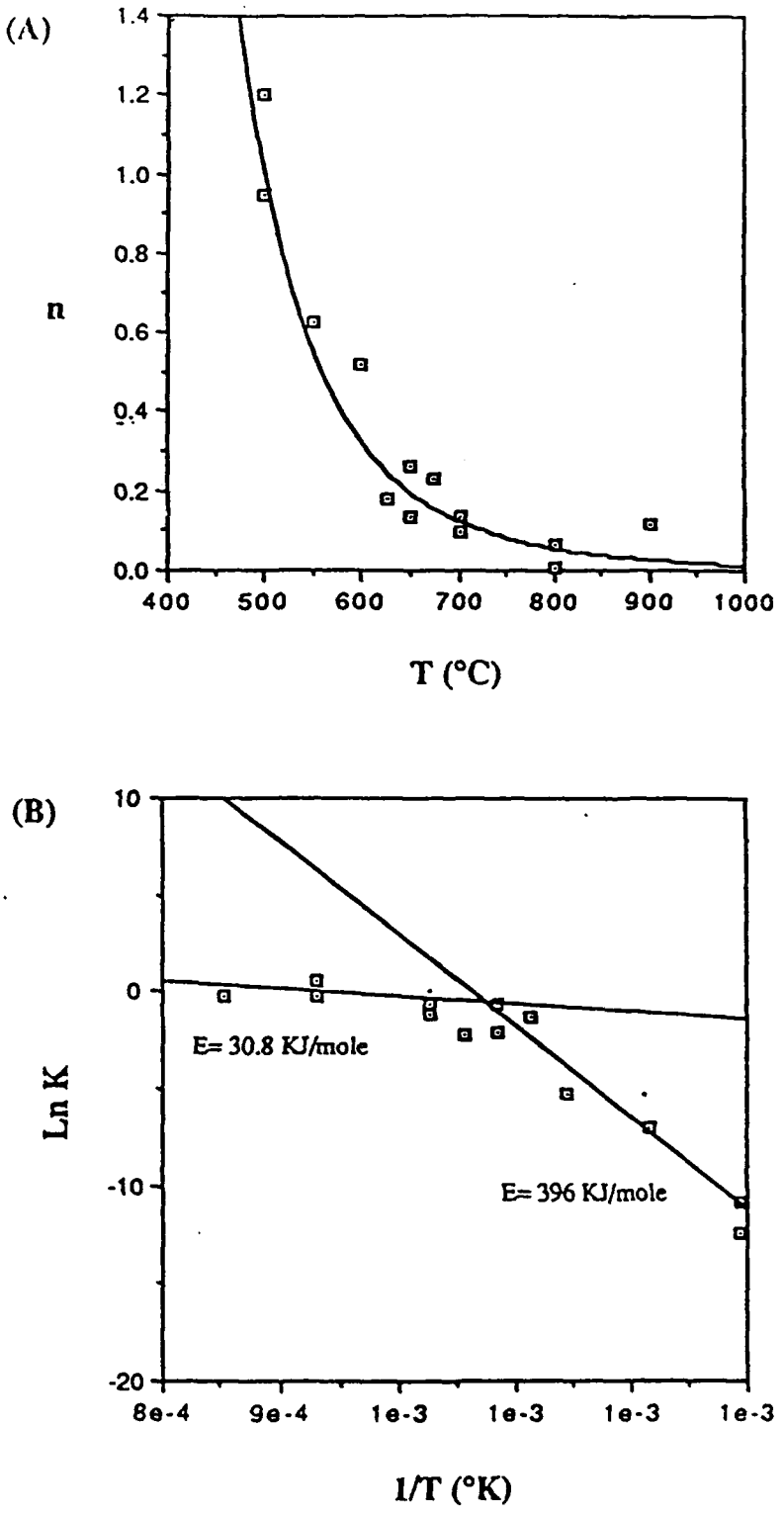

Figure 15: Kinetic study (A) Order of transformation n as a function of temperature, (B) Ln k as a function of 1/T(K).

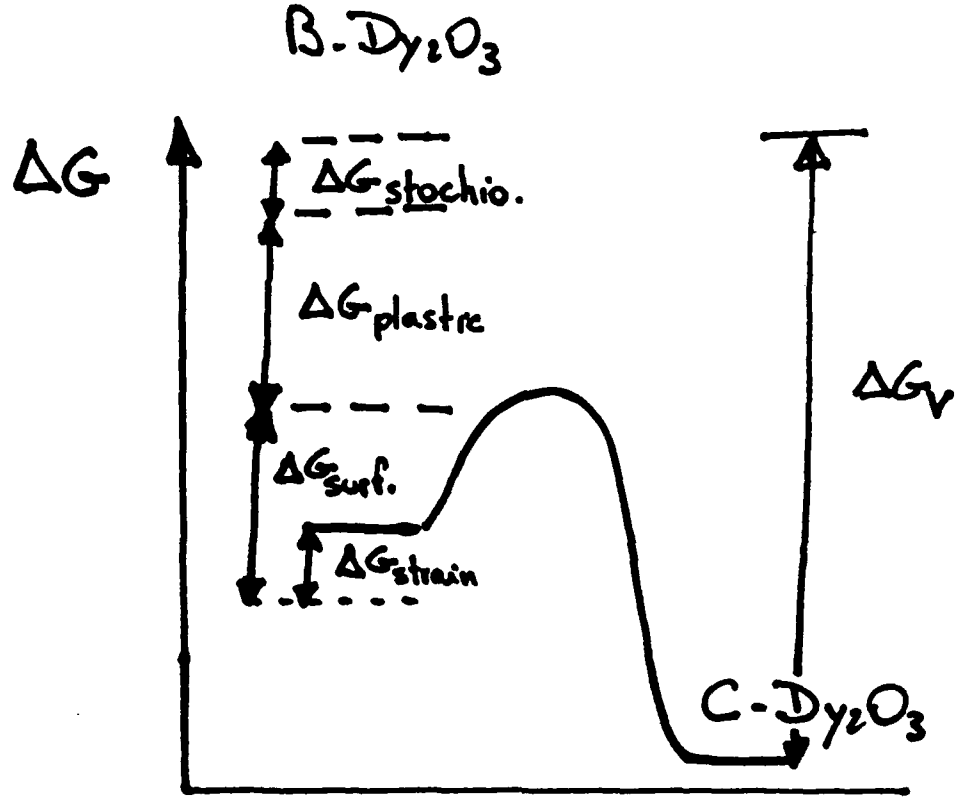
B-Dy_2O_3
ΔG
$\Delta G_{stochio.}$
$\Delta G_{plastic}$
$\Delta G_{surf.}$
ΔG_{strain}
ΔG_V
C-Dy_2O_3

Fig. 16.